This is a preprint of: "Quadratic differential systems with a finite saddle-node and an infinite saddle-node (1,1) SN - (B)", Joan Carles Artés, Marcos C. Mota, Alex Carlucci Rezende, *Internat. J. Bifur. Chaos Appl. Sci. Engrg.*, vol. 31(9), 2130026 (110 pages), 2021.
DOI: [10.1142/S0218127421300263]

QUADRATIC DIFFERENTIAL SYSTEMS WITH A FINITE SADDLE–NODE AND AN INFINITE SADDLE–NODE $(1,1)SN$ - (B)

JOAN C. ARTÉS
Departament de Matemàtiques, Universitat Autònoma de Barcelona, 08193 Bellaterra, Barcelona, Spain
E–mail: artes@mat.uab.cat

MARCOS C. MOTA
Instituto de Ciências Matemáticas e de Computação, Universidade de São Paulo, 13566–590, São Carlos, São Paulo, Brazil,
E–mail: coutinhomotam@gmail.com

ALEX C. REZENDE
Departamento de Matemática, Universidade Federal de São Carlos, 13565–905, São Carlos, São Paulo, Brazil,
E–mail: alexcr@ufscar.br

Our goal is to make a global study of the class $\mathbf{QsnSN_{11}}$ of all real quadratic polynomial differential systems which have a finite semi–elemental saddle–node and an infinite saddle–node formed by the coalescence of a finite and an infinite singularities. This class can be divided into two different families, namely, $\mathbf{QsnSN_{11}(A)}$ phase portraits possessing a finite saddle–node as the only finite singularity and $\mathbf{QsnSN_{11}(B)}$ phase portraits possessing a finite saddle–node and also a simple finite elemental singularity. Each one of these two families is given by a specific normal form. The study of family $\mathbf{QsnSN_{11}(A)}$ was done in [Artés *et al.*, 2020b] where the authors obtained 36 topologically distinct phase portraits for systems in the closure $\overline{\mathbf{QsnSN_{11}(A)}}$. In this paper we provide the complete study of the geometry of family $\mathbf{QsnSN_{11}(B)}$. This family modulo the action of the affine group and time homotheties is three–dimensional and we give the bifurcation diagram of its closure with respect to a specific normal form, in the three–dimensional real projective space. The respective bifurcation diagram yields 631 subsets with 226 topologically distinct phase portraits for systems in the closure $\overline{\mathbf{QsnSN_{11}(B)}}$ within the representatives of $\mathbf{QsnSN_{11}(B)}$ given by a specific normal form. Some of these phase portraits can be proven to have at least 3 limit cycles.
Keywords: Quadratic differential systems; finite saddle–node; finite elemental singularity; infinite saddle–node; phase portraits; bifurcation diagram; algebraic invariants.

1. Introduction, brief review of the literature and statement of the results

Here we call *quadratic differential systems*, or simply *quadratic systems*, differential systems of the form

$$\begin{array}{rcl} \dot{x} & = & p(x,y), \\ \dot{y} & = & q(x,y), \end{array} \tag{1}$$

where p and q are polynomials over $\mathbb{R}$ in x and y such that the $\max\{\deg(p), \deg(q)\} = 2$. To such systems one can always associate the quadratic vector field

$$\xi = p\frac{\partial}{\partial x} + q\frac{\partial}{\partial y}, \tag{2}$$

as well as the differential equation

$$q\,dx - p\,dy = 0. \tag{3}$$

Along this paper we will use indistinctly the expressions *quadratic systems* and *quadratic vector fields* to refer to either (1), or (2) or (3).

The class of all quadratic differential systems will be denoted by **QS**.

We can also write systems (1) as

$$\begin{array}{rcl} \dot{x} & = & p_0 + p_1(x,y) + p_2(x,y) \equiv p(x,y), \\ \dot{y} & = & q_0 + q_1(x,y) + q_2(x,y) \equiv q(x,y), \end{array} \tag{4}$$

where p_i and q_i are homogeneous polynomials of degree i in the variables x and y with real coefficients and $p_2^2 + q_2^2 \neq 0$.

Even after hundreds of studies on the topology of real planar quadratic vector fields, it is kind of impossible at this point to outline a complete characterization of their phase portraits, and attempting to topologically classify them, which occur rather often in applications, is quite a complex task. This family of systems depends on twelve parameters, but due to the action of the group $\mathrm{Aff}(2,\mathbb{R})$ of real affine transformations and time homotheties, the class ultimately depends on five parameters, but this is still a large number.

The main goal of this paper is to present the study of the class of all quadratic systems possessing a finite saddle–node $\overline{sn}_{(2)}$ located at the origin of the plane and an infinite saddle–node of type $\binom{\overline{1}}{1}SN$. We denote this class by $\mathbf{QsnSN_{11}}$. We recall that a finite saddle–node is a semi–elemental singular point whose neighborhood is formed by the union of two hyperbolic sectors and one parabolic sector. By a semi–elemental singular point we mean a point with zero determinant of its Jacobian matrix with only one eigenvalue equal to zero. These points are known in classical literature as semi–elementary, but we use the term *semi–elemental* introduced in [Artés *et al.*, 2013a] as part of a set of new definitions more deeply related to singularities, their multiplicities and, especially, their Jacobian matrices. In addition, an infinite saddle–node of type $\binom{\overline{1}}{1}SN$ is obtained by the coalescence of a finite antisaddle (respectively, finite saddle) with an infinite saddle (respectively, infinite node).

Whenever one wants to study a specific family of differential systems sharing a common property, it is necessary to select one (or several) normal form which contains all the phase portraits sharing the desired property. However, except in some trivial cases, it is impossible that the normal form does not contain other phase portraits, normally more degenerate than the cases under study. These other phase portraits are very important to understand the bifurcations that take place inside the chosen normal form. This is why we always study not just the family of systems that have the desired property, but the closure of the normal form which contains that family. That is, we study all the parameter space of the selected normal form, whether if it leads to the desired property or not. However, it is possible that a different normal form could have been chosen and in that case, the generic elements of the family under study should be the same, but the elements in the border might not be. That is, some phase portraits in the border of one normal form could be common or not, with elements in the border of the second normal form.

Inside the class $\overline{\mathbf{QsnSN_{11}}}$ where generically the origin is a saddle–node $\overline{sn}_{(2)}$ and we have an infinite singularity of type $\binom{\overline{1}}{1}SN$, we may have or not another simple finite elemental singularity. Then, we split this class into two different families: $\mathbf{QsnSN_{11}(A)}$ of phase portraits possessing the finite saddle–node as the only finite singularity and $\mathbf{QsnSN_{11}(B)}$ of phase portraits possessing the finite saddle–node and also a simple finite elemental singularity. The study of class $\overline{\mathbf{QsnSN_{11}(A)}}$ was done in [Artés *et al.*, 2020b] where the authors have considered for the first time a four–dimensional bifurcation diagram described by a specific normal form and they got 36 topologically distinct phase portraits for systems in $\overline{\mathbf{QsnSN_{11}(A)}}$. Here we

study the closure of family $\mathbf{QsnSN_{11}(B)}$.

We observe that there is another type of infinite saddle–node denoted by $\binom{\overline{0}}{2}SN$ which is given by the coalescence of an infinite saddle with an infinite node and which will appear in some of the phase portraits obtained in the class $\overline{\mathbf{QsnSN_{11}(B)}}$. We point out that by considering a specific normal form, the family of quadratic differential systems possessing a finite saddle–node $\overline{sn}_{(2)}$ and an infinite singularity $\binom{\overline{0}}{2}SN$ was completely studied in [Artés *et al.*, 2015].

For this analysis we follow the pattern set out in [Artés *et al.*, 2015] and, in order to avoid repeating technical sections which are the same for both papers, we refer to the mentioned paper for more complete information.

We recall that all the phase portraits are drawn in the Poincaré disc (for its definition we refer to [Dumortier *et al.*, 2006, Artés *et al.*, 2015]) and in what follows we present the notion of *graphics*, which play an important role in obtaining limit cycles when they are due to connection of separatrices, for example.

A *(nondegenerate) graphic* as defined in [Dumortier *et al.*, 1994] is formed by a finite sequence of singular points $r_1, r_2, \ldots, r_n$ (with possible repetitions) and non–trivial connecting orbits γ_i for $i = 1, \ldots, n$ such that γ_i has r_i as α–limit set and r_{i+1} as ω–limit set for $i < n$ and γ_n has r_n as α–limit set and r_1 as ω–limit set. Also normal orientations n_j of the non–trivial orbits must be coherent in the sense that if γ_{j-1} has left–hand orientation then so does γ_j. A *polycycle* is a graphic which has a Poincaré return map.

A *degenerate graphic* is formed by a finite sequence of singular points $r_1, r_2, \ldots, r_n$ (with possible repetitions) and non–trivial connecting orbits and/or segments of curves of singular points γ_i for $i = 1, \ldots, n$ such that γ_i has r_i as α–limit set and r_{i+1} as ω–limit set for $i < n$ and γ_n has r_n as α–limit set and r_1 as ω–limit set. Also normal orientations n_j of the non–trivial orbits must be coherent in the sense that if γ_{j-1} has left–hand orientation then so does γ_j. For more details, see [Dumortier *et al.*, 1994].

In [Artés *et al.*, 1998] the authors proved the existence of 44 topologically different phase portraits for the structurally stable quadratic planar differential systems modulo limit cycles, also known as the codimension–zero quadratic systems. Roughly speaking, these systems are characterized by having all singularities, finite and infinite, simple, no separatrix connection, and where any nest of limit cycles is considered as a single point with the stability of the outer limit cycle.

In [Artés *et al.*, 2018] the authors classified the structurally unstable quadratic systems of codimension one modulo limit cycles which have one and only one of the simplest structurally unstable objects: a saddle–node of multiplicity two (finite or infinite), a separatrix from one saddle point to another, or a separatrix forming a loop for a saddle point with its divergence nonzero. All the phase portraits of codimension one are split into four groups according to the possession of a structurally unstable element: (A) possessing a finite semi–elemental saddle–node, (B) possessing an infinite semi–elemental saddle–node $\binom{\overline{0}}{2}SN$, (C) possessing an infinite semi–elemental saddle–node $\binom{\overline{1}}{1}SN$, and (D) possessing a separatrix connection. The study of the codimension–one systems was done in approximately 20 years and finally it was obtained at least 204 (and at most 211) topologically distinct phase portraits of codimension one modulo limit cycles. Some recent studies (already at preprint level) have shown two mistakes in that book and have reduced (and confirmed) the number of cases to 202 (and a most 209).

The next step is to study the structurally unstable quadratic systems of codimension two, modulo limit cycles. The approach is the same as used in the previous two works [Artés *et al.*, 1998, Artés *et al.*, 2018]. One must start by looking for all the potential topological phase portraits of codimension two, and then try to realize all of them or show that some of them are impossible. So, it is also very convenient to have studied a bifurcation diagram that helps us in the realization problem. In many papers of this last type where families of phase portraits have been studied, it is quite common that the authors have missed one or several phase portraits, as we discuss in Appendix A. This may happen either because they have not interpreted correctly some of the bifurcation parts, or they have missed the existence of some nonalgebraic bifurcation, or there may exist some small "island" as they are described in Sec. 5. However when one does the study of all the potential topological phase

portraits and produces a list in a systematic way which is free of errors, then there is no possibility of missing a realizable case. It is just a problem of finding examples of realization or producing irrefutable proofs of the impossibility of realization of phase portraits.

The study of the codimension–two systems is already in progress. In [Artés *et al.*, 2020c] the authors have considered the group (AA) obtained by the existence of a cusp point, or two saddle–nodes or the coalescence of three finite singular points forming a semi–elemental singularity, yielding either a triple saddle, or a triple node. They obtained all the possible topological phase portraits of group (AA) and proved their realization. In their study, they got 34 new topologically distinct phase portraits in the Poincaré disc modulo limit cycles. Moreover, they proved the impossibility of one phase portrait among the 204 phase portraits presented in [Artés *et al.*, 2018].

Moreover, as we have already said, the bifurcation diagram for the class of the quadratic systems possessing a finite saddle–node $\overline{sn}_{(2)}$ and an infinite saddle–node $\binom{\overline{0}}{2}\,SN$ has been studied in [Artés *et al.*, 2014, Artés *et al.*, 2015], in which all the phase portraits obtained belong to the closure of the group (AB).

The present study is part of this attempt of classifying all the codimension–two quadratic systems and all the phase portraits obtained here belong to the group (AC). In [Artés *et al.*, 2020b], the authors started the study of this group by analyzing the closure of family $\mathbf{QsnSN_{11}(A)}$ (as mentioned before) and here we continue with this group by studying the closure of family $\mathbf{QsnSN_{11}(B)}$.

In the normal form (5), see page 14, the class $\overline{\mathbf{QsnSN_{11}(B)}}$ is partitioned into 631 parts: 112 three–dimensional ones, 265 two–dimensional ones, 203 one–dimensional ones and 51 points. This partition is obtained by considering all the bifurcation surfaces of singularities, one related to the presence of invariant straight lines, one related to connections of separatrices and one related to the presence of a double limit cycle, modulo "islands" (see Sec. 5).

We point out that we cannot have a global result about the number of limit cycles that a phase portrait may have. But we can assure that, in some places of the bifurcation diagram, the corresponding phase portraits have a specific number of limit cycles or even a quantity with identical parity (taking into account the multiplicity of limit cycles). More precisely, as we may find an island inside the parameter space for which in its border there exists a double limit cycle and inside the island there are two more limit cycles, all the claims regarding limit cycles always must be formulated with respect to the minimum number of limit cycles (proved to exist), but always having the possibility of the existence of "more" limit cycles, keeping the parity.

Theorem 1.1. *There are* 226 *topologically distinct phase portraits for the closure of the family of quadratic vector fields having a finite saddle–node* $\overline{sn}_{(2)}$*, a finite elemental singularity and an infinite saddle–node of type* $\binom{\overline{1}}{1}\,SN$*, and given by the normal form* (5) *(class* $\overline{\mathbf{QsnSN_{11}(B)}}$*). The bifurcation diagram for this class is given in the parameter space which is the projective three–dimensional space* $\mathbb{RP}^3$*. All these phase portraits are shown in Figs. 1 to 7. Also the following statements hold:*

(a) there are 148 *topologically distinct phase portraits in* $\mathbf{QsnSN_{11}(B)}$*;*

(b) there are 32 *phase portraits possessing exactly one simple limit cycle (or an odd number of them taking into account their multiplicity), and they are in the parts* V_{25}*,* V_{48}*,* V_{52}*,* V_{57}*,* V_{60}*,* V_{72}*,* V_{75}*,* V_{78}*,* V_{101}*,* V_{104}*,* V_{106}*,* $2S_{11}$*,* $2S_{13}$*,* $4S_{38}$*,* $4S_{64}$*,* $4S_{67}$*,* $5S_{13}$*,* $5S_{20}$*,* $5S_{23}$*,* $5S_{26}$*,* $5S_{32}$*,* $5S_{34}$*,* $7S_{15}$*,* $7S_{23}$*,* $9S_{16}$*,* $9S_{17}$*,* $9S_{18}$*,* $2.5L_5$*,* $4.5L_{13}$*,* $4.5L_{15}$*,* $5.7L_8$*,* $5.9L_3$*;*

(c) there are three phase portraits with exactly two simple limit cycles (or an even number of them taking into account their multiplicity) surrounding the same focus, and they are in the parts V_{107}*,* V_{110}*,* $7S_{24}$*;*

(d) there is one phase portrait with exactly three simple limit cycles (or a greater odd number of them taking into account their multiplicity) surrounding the same focus, and it is in the part V_{109}*;*

(e) there are two phase portraits possessing one double limit cycle (and no signs of other limit cycles) surrounding the same focus, and they are in the parts $10S_1$*,* $10S_3$*;*

(f) there is one phase portrait possessing one double limit cycle and one simple limit cycle (and no signs of other limit cycles) both surrounding the same focus, and it is in the part $10S_2$;

(g) there are 45 phase portraits with exactly one nondegenerate graphic surrounding a focus. These phase portraits are in the parts V_{26}, V_{49}, V_{53}, V_{102}, $4S_{65}$, $5S_{14}$, $5S_{15}$, $5S_{16}$, $5S_{17}$, $5S_{18}$, $5S_{19}$, $5S_{33}$, $7S_3$, $7S_4$, $7S_6$, $7S_7$, $7S_8$, $7S_{11}$, $7S_{13}$, $7S_{14}$, $7S_{22}$, $9S_{21}$, $2.5L_4$, $2.7L_1$, $4.4L_{12}$, $4.5L_8$, $4.5L_9$, $4.5L_{14}$, $5.7L_2$, $5.7L_3$, $5.7L_4$, $5.7L_5$, $5.7L_6$, $5.7L_7$, $5.7L_{11}$, $5.9L_4$, $5.9L_5$, $7.7L_1$, $7.9L_5$, $7.9L_7$, P_7, P_{14}, P_{20}, P_{49}, P_{50}. We highlight that phase portrait $7S_{14}$ is topologically equivalent to phase portrait corresponding to the part P_{27} of the bifurcation diagram (see Table 21), and for this last phase portrait the weak focus is of order two;

(h) there is one phase portrait, namely $7S_{23}$, which possesses one nondegenerate graphic and one simple limit cycle, both surrounding the same focus. This phase portrait is topologically equivalent to phases portraits corresponding to the parts $3.7L_4$ and $3.7L_5$ of the bifurcation diagram (see Table 21), and for each one of these two phase portraits the weak focus is of order one;

(i) there is one phase portrait, namely $7S_{24}$, which possesses one nondegenerate graphic and two simple limit cycles, all of them surrounding the same focus;

(j) there is one phase portrait, namely $7.10L_1$, which possesses one nondegenerate graphic and a double limit cycle, both surrounding the same focus;

(k) there are 31 phase portraits having an infinite family of nondegenerate graphics. More precisely:

(k_1) there are 20 phase portraits possessing an infinite family of nondegenerate graphics and all of the phase portraits have no singularities inside the graphics. These phase portraits are in the parts $9S_3$, $9S_5$, $9S_7$, $9S_{10}$, $9S_{11}$, $9S_{16}$, $9S_{17}$, $9S_{29}$, $9S_{30}$, $9S_{33}$, $9S_{35}$, $9S_{36}$, $2.9L_1$, $2.9L_3$, $2.9L_4$, $4.9L_1$, $4.9L_6$, $4.9L_7$, $7.9L_1$, $7.9L_8$;

(k_2) there are eight phase portraits possessing an infinite family of nondegenerate graphics (with no singularity inside) and also another type of graphic which surrounds a focus. These phase portraits are in the parts $9S_{19}$, $9S_{20}$, $9S_{22}$, $4.9L_4$, $4.9L_5$, $7.9L_3$, $7.9L_4$, $7.9L_6$;

(k_3) the remaining three phase portraits possess an infinite family of nondegenerate graphics and also another type of graphic, and the three phase portraits have no singularities inside the graphics. These phase portraits are in the parts $9S_1$, $9S_{27}$, $9S_{28}$;

(l) there are seven phase portraits with degenerate graphics, and they are in the parts $8S_1$, $4.8L_1$, $5.8L_1$, $9.9L_1$, P_3, P_{29}, P_{36}.

Proposition 1.2. *There are 40 topologically distinct phase portraits of codimension two, modulo limit cycles, in the family $\mathbf{QsnSN_{11}(B)}$.*

Corollary 1.3. *In Table 1 we give the numbers of phase portraits of both families $\mathbf{QsnSN_{11}(B)}$ and its closure for special types of phase portraits.*

Table 1. Comparison between the set $\mathbf{QsnSN_{11}(B)}$ and its border (the numbers represent the absolute values in each subclass)

	$\mathbf{QsnSN_{11}(B)}$	Border of $\mathbf{QsnSN_{11}(B)}$
Distinct phase portraits	148	78
Phase portraits with exactly one simple limit cycle	25	7
Phase portraits with exactly two simple limit cycles	3	0
Phase portraits with exactly three simple limit cycles	1	0
Phase portraits with exactly one double limit cycle	2	0
Phase portraits with one double limit cycle and one simple limit cycle	1	0
Phase portraits with exactly one nondegenerate graphic	39	9
Phase portraits with an infinite family of nondegenerate graphics	0	31
Phase portraits with degenerate graphics	0	7

Corollary 1.4. *There are two topologically dis-*

tinct phase portraits which appear simultaneously in both classes $\overline{\mathbf{QsnSN_{11}(A)}}$ *(described in [Artés* et al.*, 2020b]) and* $\overline{\mathbf{QsnSN_{11}(B)}}$*. The correspondences are indicated in Table 2 and the phase portraits in each row are topologically equivalent.*

Table 2. Topological equivalence between phase portraits from classes $\overline{\mathbf{QsnSN_{11}(A)}}$ and $\overline{\mathbf{QsnSN_{11}(B)}}$

$\overline{\mathbf{QsnSN_{11}(A)}}$	$\overline{\mathbf{QsnSN_{11}(B)}}$
$2.8S_2$	$4.8L_1$
$2.8.9L_1$	P_3

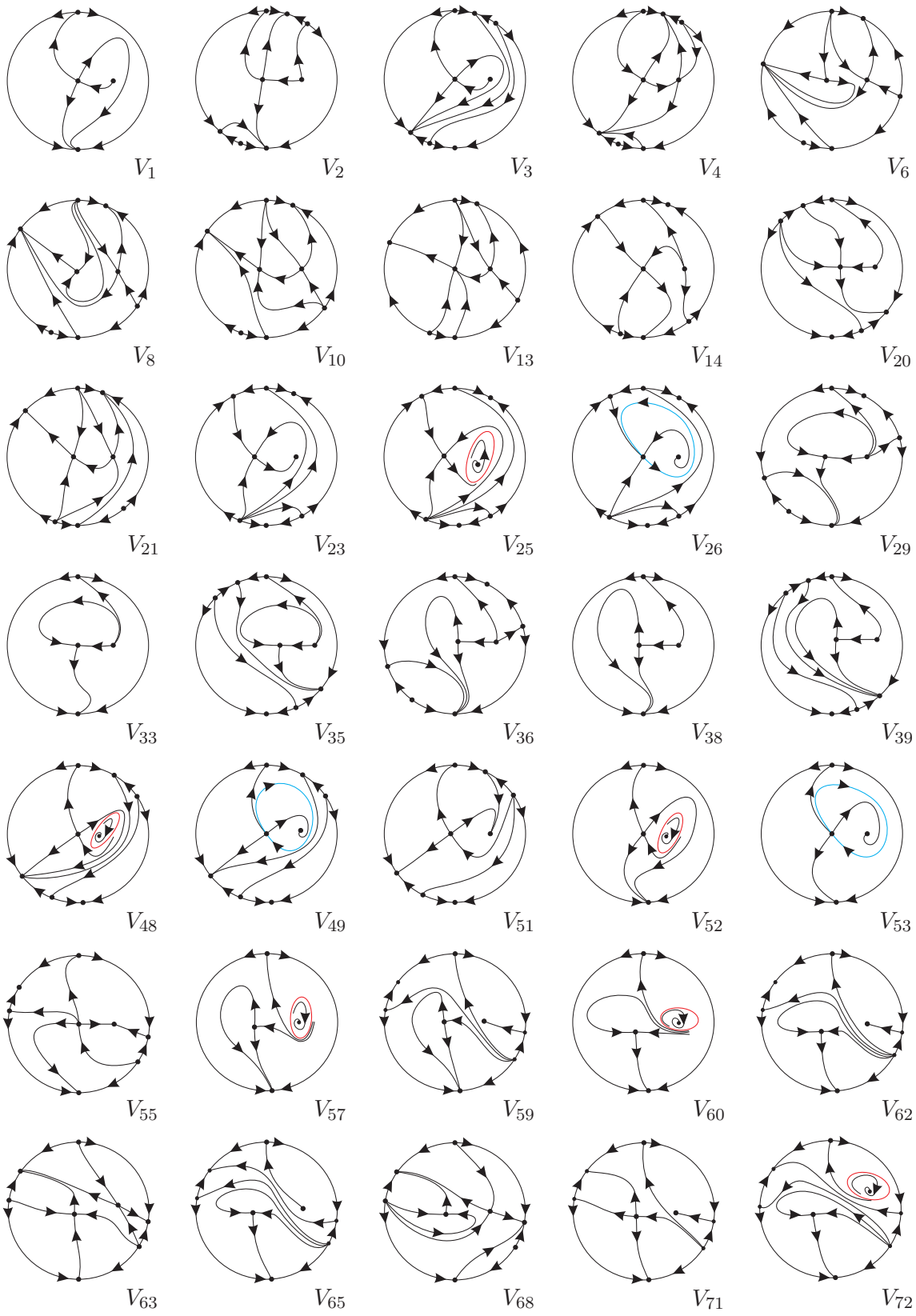

Fig. 1. Phase portraits for quadratic vector fields with a finite saddle–node $\overline{sn}_{(2)}$, a finite elemental singularity and an infinite saddle–node of type $\overline{\binom{1}{1}}SN$, from class $\overline{\mathbf{QsnSN_{11}(B)}}$

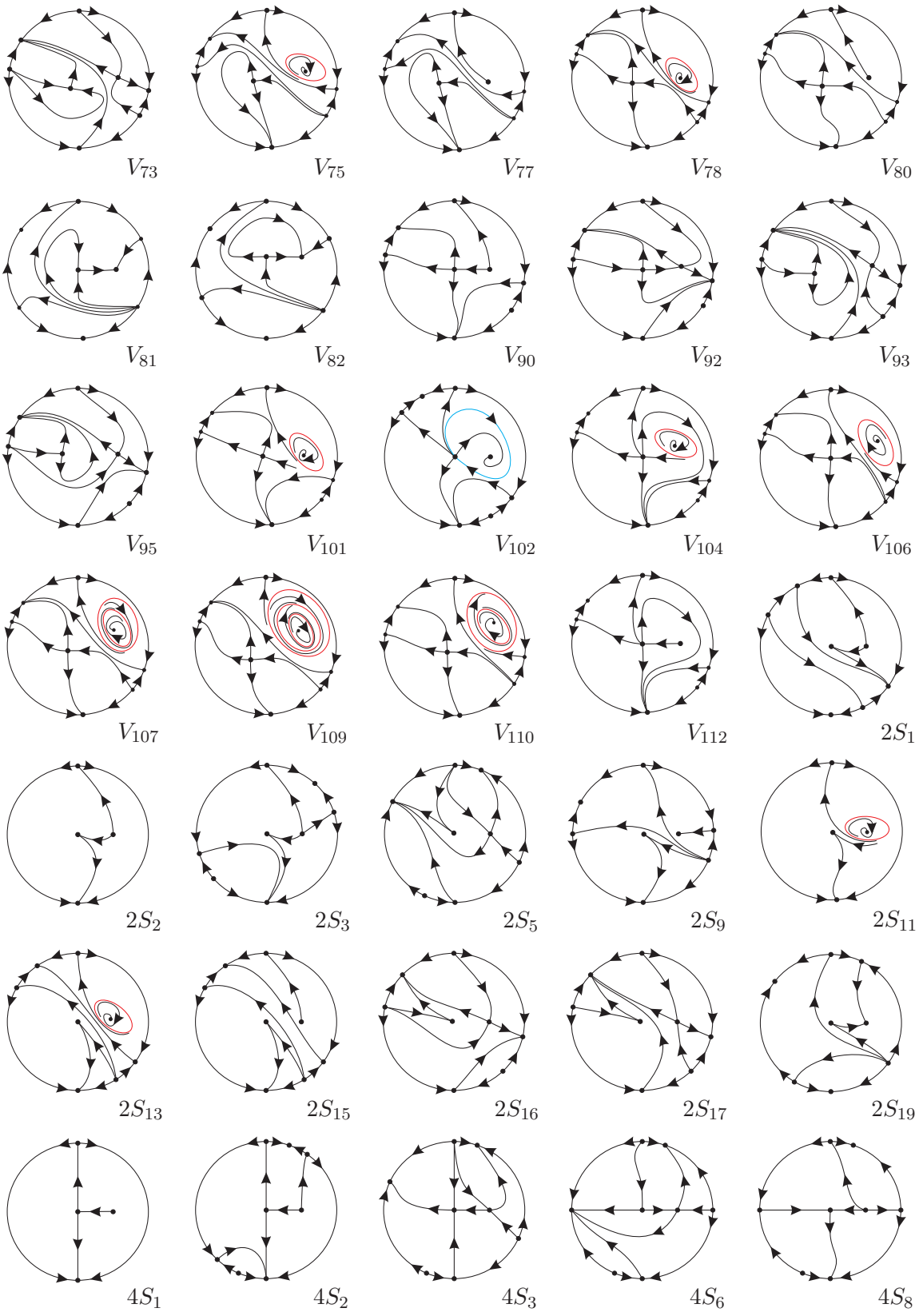

Fig. 2. Continuation of Fig. 1

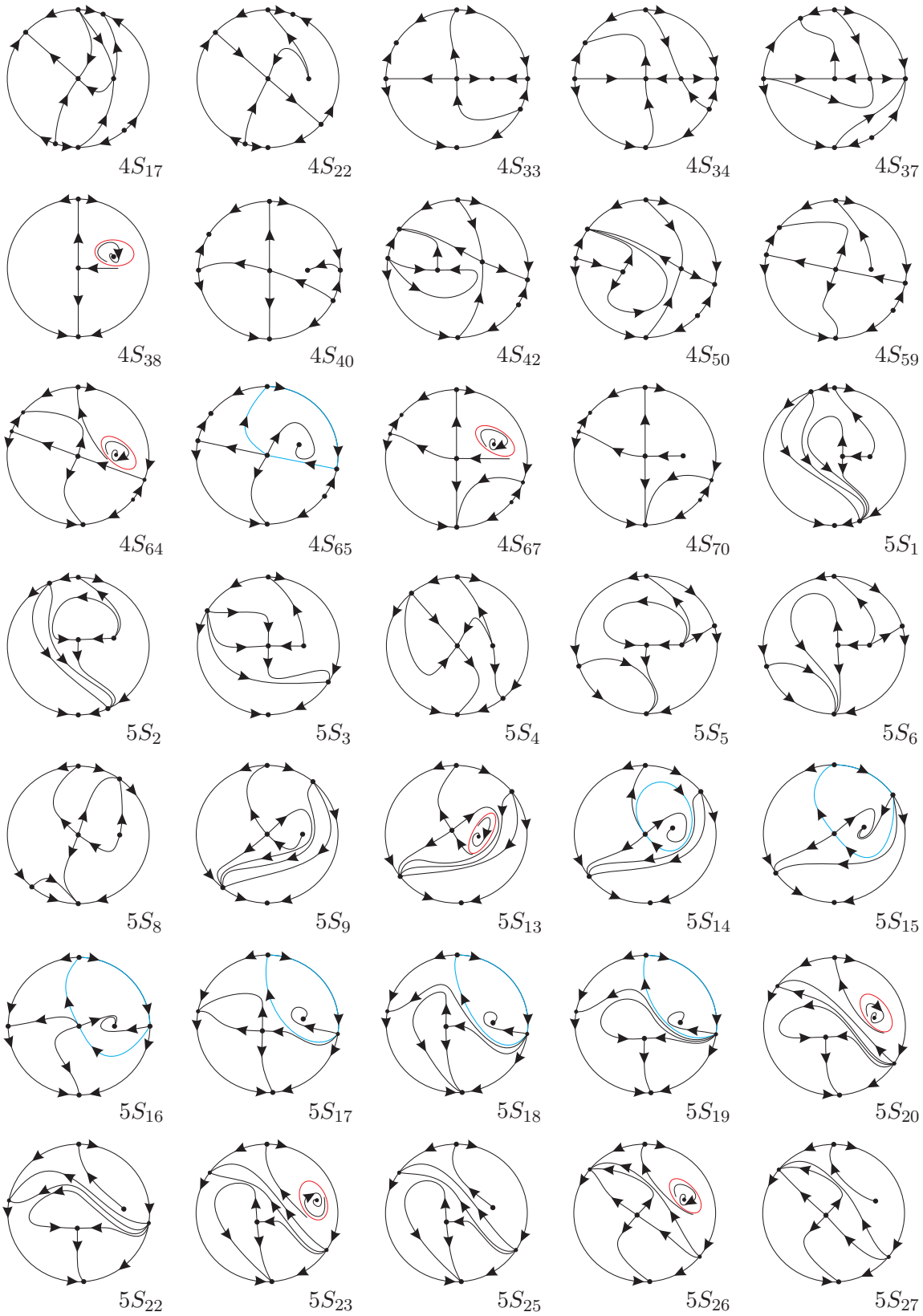

Fig. 3. Continuation of Fig. 2

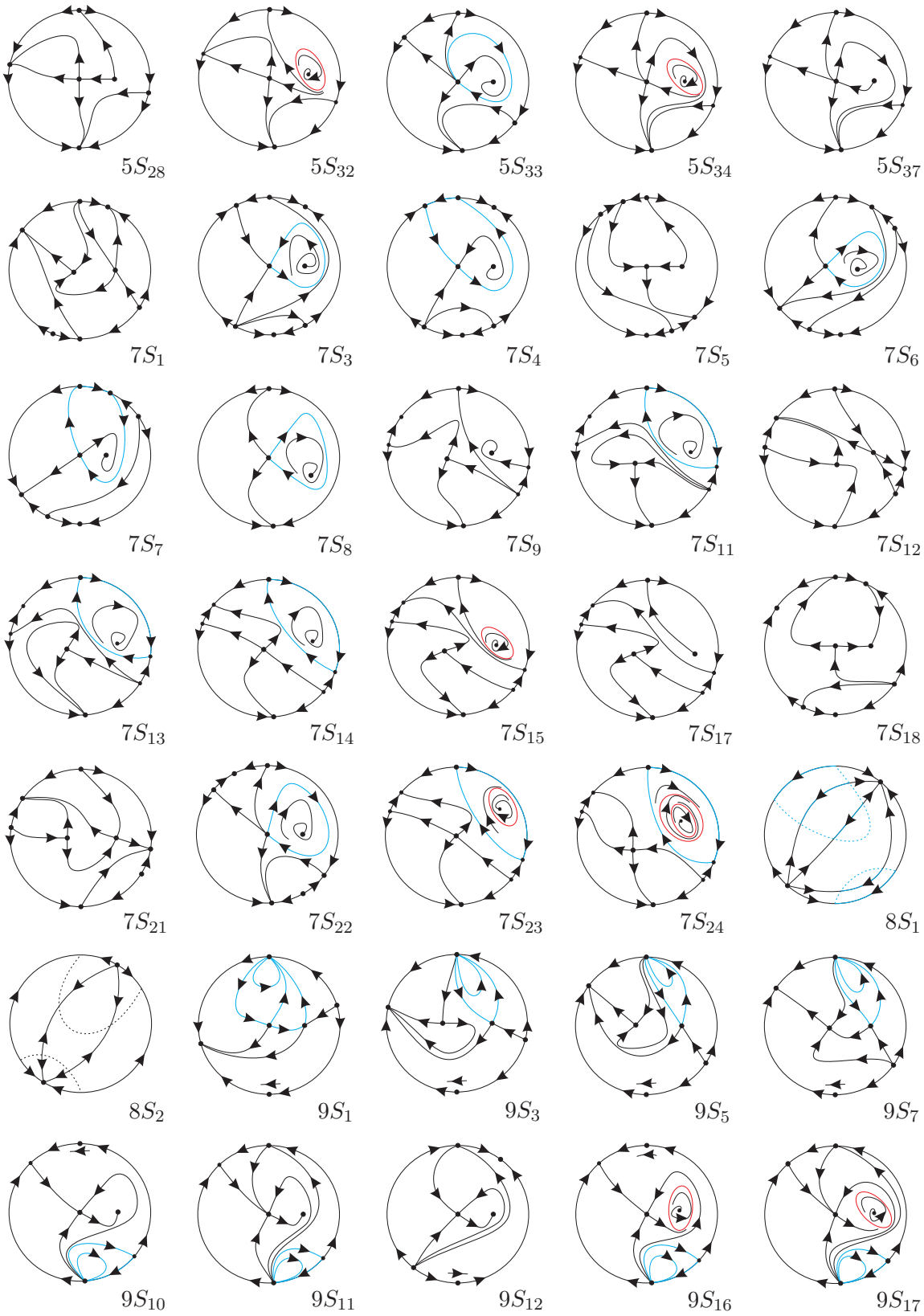

Fig. 4. Continuation of Fig. 3

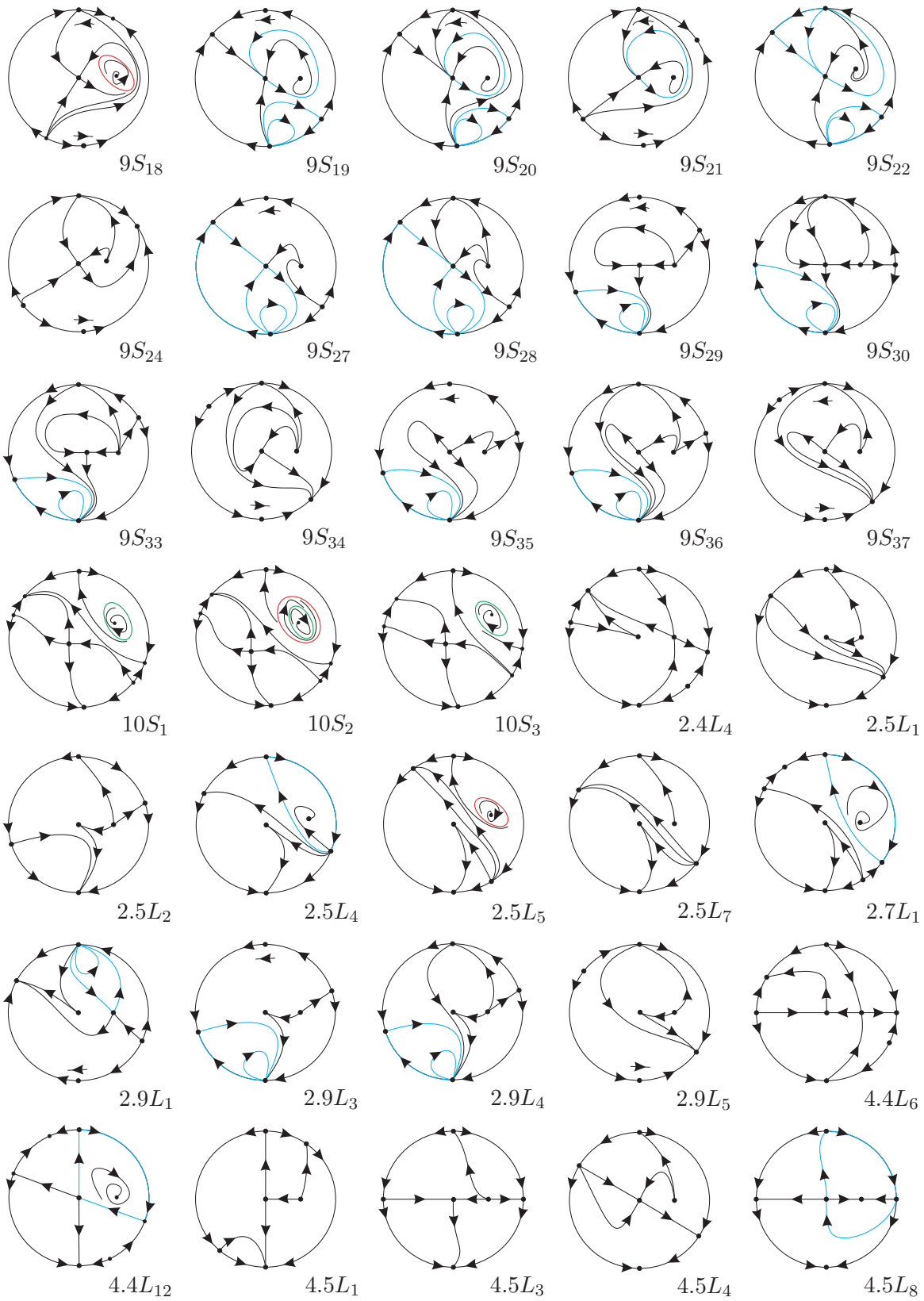

Fig. 5. Continuation of Fig. 4

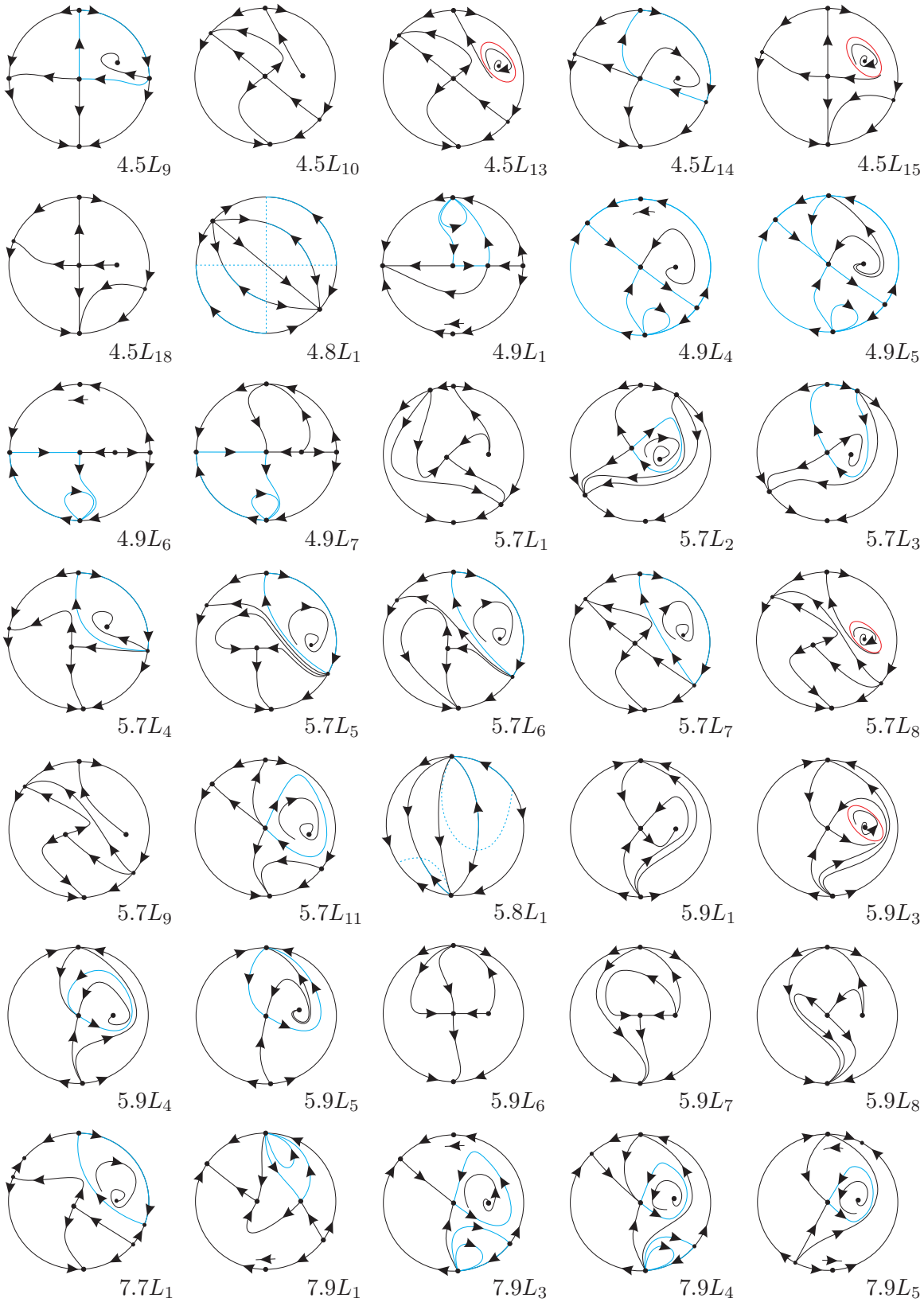

Fig. 6. Continuation of Fig. 5

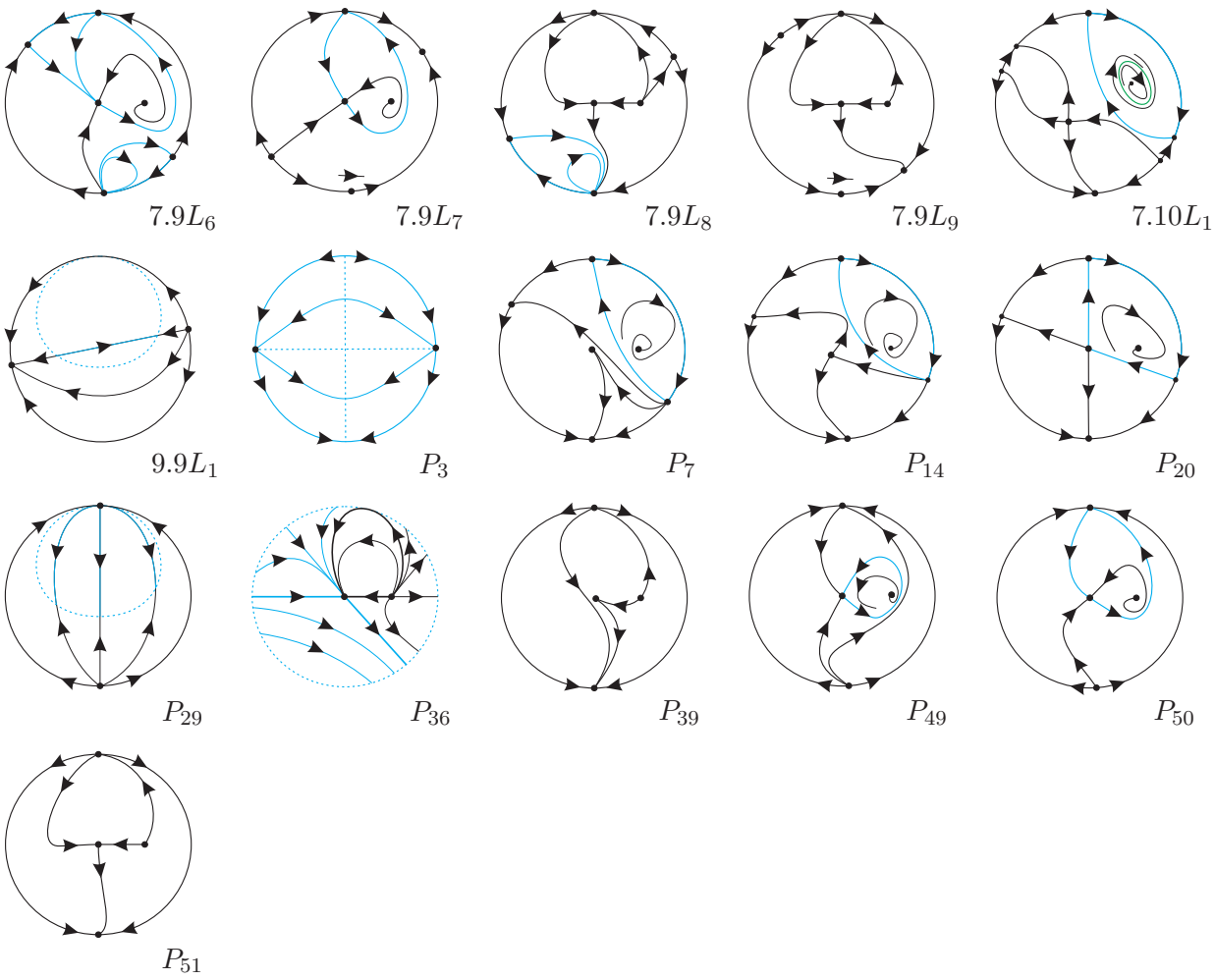

Fig. 7. Continuation of Fig. 6

For family $\mathbf{QsnSN_{11}(B)}$, from its 148 topologically different phase portraits, 54 occur in three–dimensional parts, 67 in two–dimensional parts, 24 in one–dimensional parts and three occur in a zero–dimensional parts.

For the border of $\mathbf{QsnSN_{11}(B)}$, from its 78 topologically different phase portraits, 37 occur in two–dimensional parts, 34 in one–dimensional parts and seven occur in zero–dimensional parts.

In Figs. 1 to 7 we have illustrated all the singularities with a small disc. In case of degenerate systems we have also illustrated the infinite singular point belonging to the degenerate set with a small disc only if this point is an infinite singularity of the reduced system. We have drawn with thicker curves the separatrices and we have added some thinner orbits to avoid confusion in some cases.

We have drawn all the limit cycles (and loops) possessing a convex shape (see Lemma 3.31 from [Artés *et al.*, 2018]). The limit cycle is colored in red if it is simple (as in [Artés *et al.*, 2015], for instance) and it is colored in dark green if it is double. In addition, all the graphics are colored in blue. We notice that, as the weak foci are graphics reduced to a point, the weak foci could be included in the definition of graphics and then we should have colored them in blue. However, in order to follow the same pattern as in previous similar papers and according to our definition of graphics we keep all of them in black.

Remark 1.5. We label the phase portraits according to the parts of the bifurcation diagram where they occur. Here we call *volumes* (V) the three–dimensional parts of the bifurcation diagram, *surfaces* (S) the two–dimensional ones, *curves* (L) the one–dimensional ones, and *points* (P) the zero–dimensional ones. These labels could be different for two topologically equivalent phase portraits occurring in distinct parts. Some of the phase portraits in three–dimensional parts also occur in some lower dimensional parts bordering these three–dimensional parts. An example occurs when a node turns into a focus. An analogous situation happens for phase portraits in two–dimensional or one–dimensional parts, coinciding with some phase portraits situated on their border. Moreover, as in [Artés *et al.*, 2006, Artés *et al.*, 2015], we use the same pattern in order to indicate the elements (V), (S), (L) and (P) in the bifurcation diagram.

This paper is organized as follows. In Sec. 2 we describe the normal form for the family of quadratic systems having a finite saddle–node and an infinite saddle–node of type $\binom{1}{1}SN$.

In Sec. 3 we list some basic properties of quadratic systems related with this study.

In Sec. 4 we mention some algebraic and geometric concepts that were introduced in [Artés *et al.*, 2006] involving T–comitants and invariants for quadratic systems as used by the Sibirsky's School. Moreover, using the mentioned concepts as tools, we construct the bifurcation surfaces for the class $\overline{\mathbf{QsnSN_{11}(B)}}$.

In Sec. 5 we discuss about the possible existence of "islands" in the bifurcation diagram.

In Sec. 6 we introduce a global invariant denoted by $\mathcal{I}$, which classifies completely, up to topological equivalence, the phase portraits that we have obtained for the systems in the class $\overline{\mathbf{QsnSN_{11}(B)}}$. Theorem 6.15 shows clearly that they are uniquely determined (up to topological equivalence) by the values of the invariant $\mathcal{I}$.

In Appendix A we present some incompatibilities found in previous classifications of phase portraits possessing specific properties on its singularities.

2. Quadratic vector fields with a finite saddle–node $\overline{sn}_{(2)}$, a finite elemental singularity and an infinite saddle–node of type $\binom{1}{1}SN$

In [Artés *et al.*, 2008] the authors have constructed the normal form for quadratic systems possessing one double and one simple real finite singularities. In what follows we present an idea of such a construction.

Proposition 2.1. *Every nondegenerate quadratic system with a finite semi–elemental double saddle–node $\overline{sn}_{(2)}$, a finite elemental singularity and an infinite saddle–node of type $\binom{1}{1}SN$ can be brought via affine transformation to the following normal form*

$$\begin{aligned} \dot{x} &= cx + cy - cx^2 + 2hxy, \\ \dot{y} &= ex + ey - ex^2 + 2mxy, \end{aligned} \tag{5}$$

where c, e, h, m are real parameters and $eh \neq cm$.

Proof. We know that a quadratic system (1) can always be written into the form

$$\dot{x} = p_0 + p_1(x,y) + p_2(x,y) \equiv p(x,y),$$
$$\dot{y} = q_0 + q_1(x,y) + q_2(x,y) \equiv q(x,y)$$

with homogeneous polynomials p_i and q_i $(i = 0,1,2)$ of degree i in x, y:

$$p_0 = a_{00}, \quad p_1(x,y) = a_{10}x + a_{01}y,$$
$$p_2(x,y) = a_{20}x^2 + 2a_{11}xy + a_{02}y^2,$$
$$q_0 = b_{00}, \quad q_1(x,y) = b_{10}x + b_{01}y,$$
$$q_2(x,y) = b_{20}x^2 + 2b_{11}xy + b_{02}y^2.$$

We start supposing that such systems possess four real finite distinct singularities. Assume that one finite singularity has gone to infinity. Then the quadratic polynomials $p_2(x,y)$ and $q_2(x,y)$ have a linear common factor of the form $\alpha x + \beta y$. So this infinite singularity is of the form $N[-\beta : \alpha : 0]$ and via a rotation we can assume that this point is located on the direction $x = 0$, i.e. x will be a factor of $p_2(x,y)$ and $q_2(x,y)$. Then, for the above systems we can take $a_{02} = b_{02} = 0$. Now, since these systems possess three real finite distinct singularities, we can apply a translation in such a way that one of these singularities can be moved to the origin, i.e. we can assume $a_{00} = b_{00} = 0$. Therefore we obtain the systems:

$$\begin{aligned} \dot{x} &= a_1x + b_1y + c_1x^2 + 2d_1xy, \\ \dot{y} &= a_2x + b_2y + c_2x^2 + 2d_2xy, \end{aligned} \tag{6}$$

which, besides the point $M_1(0,0)$, have two other distinct real singularities $M_i(x_i, y_i)$ for $i \in \{2,3\}$. We observe that for systems (6), if $x_{2,3} = 0$ then we obtain

$$p(0, y_{2,3}) = b_1y_{2,3} = 0, \quad q(0, y_{2,3}) = b_2y_{2,3} = 0,$$

and since $y_{2,3} \neq 0$ (otherwise we would have a triple point at the origin) we have $b_1 = b_2 = 0$. This implies that systems (6) are degenerate. So we can assume $x_2 \neq 0$. Performing the linear transformation

$$\bar{x} = \frac{x}{x_2}, \quad \bar{y} = y, \quad \text{if} \quad y_2 = 0,$$

and

$$\bar{x} = \frac{x}{x_2}, \quad \bar{y} = x - \frac{x_2}{y_2}y, \quad \text{if} \quad y_2 \neq 0,$$

we keep the form (6) and clearly we locate the point $M_2(x_2, y_2)$ at the point $M_2(1,0)$. Imposing that $M_2(x_2, y_2) = (1,0)$ we obtain $a_1 = -c_1$ and $a_2 = -c_2$. These equalities allow us to write systems (6) into the form

$$\begin{aligned} \dot{x} &= a_1x + b_1y - a_1x^2 + 2d_1xy, \\ \dot{y} &= a_2x + b_2y - a_2x^2 + 2d_2xy, \end{aligned} \tag{7}$$

which have three finite singularities: $M_1(0,0)$, $M_2(1,0)$ and $M_3(x_3, y_3)$. Calculations show that M_3 has the coordinates

$$x_3 = \frac{d_{23}}{2d_{45}}, \quad y_3 = \frac{d_{23}(2d_{45} - d_{23})}{4d_{35}d_{45}},$$

where

$$d_{23} = a_2b_1 - a_1b_2, \quad d_{35} = b_1d_2 - b_2d_1,$$

$$d_{45} = a_2d_1 - a_1d_2,$$

verifying $d_{23}d_{35}d_{45}(2d_{45} - d_{23}) \neq 0$ (i.e. the points are finite and distinct).
For systems (7), we observe that $a_1^2 + a_2^2 \neq 0$, otherwise $d_{23} = 0 = d_{45}$, what contradicts the previous condition. Finally, in order to have a double finite singularity at the origin, i.e. forcing the point $M_1(0,0)$ to be double, without loss of generality we can make $d_{23} = 0$ by taking $b_1 = a_1$ and $b_2 = a_2$. Therefore, by renaming the coefficients $a_1 \to c$, $d_1 \to h$, $a_2 \to e$, $d_2 \to m$, we arrive at normal form (5) that we were looking for. Moreover, since $d_{35}d_{45} = -(eh - cm)^2 \neq 0$, we conclude that such systems are nondegenerate if and only if $eh - cm \neq 0$. ■

In order to complete the study the closure of family $\mathbf{QsnSN_{11}(B)}$ within the set of representatives of $\mathbf{QsnSN_{11}(B)}$ in the parameter space of normal form (5) it is necessary to consider also the case $h = 0$.

The next result assures the existence of invariant straight lines under certain conditions for systems (5).

Lemma 2.2. *A nondegenerate system* (5) *possesses the following invariant straight line if and only if the corresponding condition is satisfied:*

(i) $\{x = 0\} \Leftrightarrow c = 0$;

(ii) $\{y = 0\} \Leftrightarrow e = 0$;

(iii) $\{x = 1\} \Leftrightarrow h = -c/2$;

(iv) $\{y = -x\} \Leftrightarrow h = -(c + e + 2m)/2$.

Proof. We consider the algebraic curves

$$\begin{aligned} f_1(x, y) &\equiv x = 0, \\ f_2(x, y) &\equiv y = 0, \\ f_3(x, y) &\equiv x - 1 = 0, \\ f_4(x, y) &\equiv x + y = 0, \end{aligned}$$

and we show that the polynomials

$$\begin{aligned} K_1(x, y) &= 2hy, \\ K_2(x, y) &= 2mx, \\ K_3(x, y) &= -c(x + y), \\ K_4(x, y) &= -(c + e)(x - 1), \end{aligned}$$

are the cofactors of $f_1 = 0$, $f_2 = 0$, $f_3 = 0$ and $f_4 = 0$, respectively, after restricting systems (5) to the respective conditions. ■

We observe that systems (5) depend on four real parameters, namely, c, e, h and m. Then, the corresponding bifurcation diagram is actually the four–dimensional Euclidean space $\mathbb{R}^4$. Since the case $c = e = h = m = 0$ corresponds to the null system and it does not belong to our family, we can consider the real projective space $\mathbb{RP}^3$. In what follows we describe how we do this study.

Systems (5) depend on the parameter $\lambda = (c, e, h, m) \in \mathbb{R}^4$. We consider systems (5) which are nonzero, i.e. $\lambda = (c, e, h, m) \neq 0$. In this case, systems (5) can be rescaled with the time rescaling $(x, y, t) \to (x, y, t/\alpha)$, $\alpha \neq 0$. In fact, applying this transformation we obtain

$$\begin{aligned} \dot{x} &= \alpha' cx + \alpha' cy - \alpha' cx^2 + 2\alpha' hxy, \\ \dot{y} &= \alpha' ex + \alpha' ey - \alpha' ex^2 + 2\alpha' mxy, \end{aligned}$$

for $\alpha' = 1/\alpha$, $\alpha \neq 0$. Then, this transformation takes the systems with parameters (c, e, h, m) to systems with parameters $(\alpha' c, \alpha' e, \alpha' h, \alpha' m)$, with $\alpha' = 1/\alpha$. Hence, instead of considering as a parameter space the set $\mathbb{R}^4$ we may consider the real projective space $\mathbb{RP}^3$. The three–dimensional projective space $\mathbb{RP}^3$ can be viewed as the quotient space $\mathbb{S}^3/_\sim$ of $\mathbb{S}^3$ by the equivalence relation: (c, e, h, m) is equivalent to itself or to $(-c, -e, -h, -m)$. So, our parameter is $[\lambda] = [c : e : h : m] \in \mathbb{RP}^3 = \mathbb{S}^3/_\sim$. Since for $\alpha' = -1$ the signs of all the parameters change, we may consider $h \geq 0$ in $[c : e : h : m]$. Since $c^2 + e^2 + h^2 + m^2 = 1$, then $h = \sqrt{1 - (c^2 + e^2 + m^2)}$, where $0 \leq c^2 + e^2 + m^2 \leq 1$.

We can therefore view the parameter space as a ball: $\overline{\mathcal{B}} = \{(c, e, m) \in \mathbb{R}^3;\ c^2 + e^2 + m^2 \leq 1\}$ where on the equator two opposite points are identified. When $m = 0$, we identify the point $[c : e : h : 0] \in \mathbb{RP}^3$ with $[c : e : h] \in \mathbb{RP}^2$. So, this subset $\{m = 0\} \subset \overline{\mathcal{B}}$ can be identified with $\mathbb{RP}^2$, which can be viewed as a disc with two opposite points on the circumference (the equator) identified (see Fig. 8).

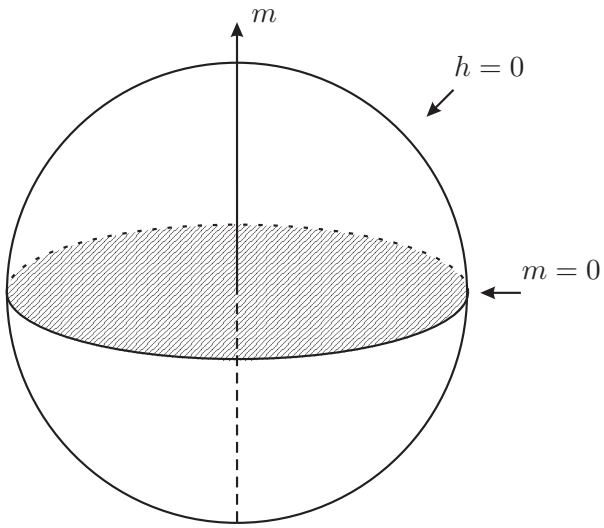

Fig. 8. The parameter space

For $h \neq 0$, we get the affine chart:

$$\begin{aligned} &\mathbb{RP}^3 \setminus \{h = 0\} \leftrightarrow \mathbb{R}^3 \\ &\quad [c : e : h : m] \to \left(\frac{c}{h}, \frac{e}{h}, \frac{m}{h}\right) = (\overline{c}, \overline{e}, \overline{m}) \\ &\quad [\overline{c} : \overline{e} : 1 : \overline{m}] \leftarrow (\overline{c}, \overline{e}, \overline{m}). \end{aligned}$$

The plane $h = 0$ in $\mathbb{RP}^3$ corresponds to the equation $c^2 + e^2 + m^2 = 1$ (the full sphere $\mathbb{S}^2$) and the line $h = m = 0$ in $\mathbb{RP}^3$ corresponds to the equation $c^2 + e^2 = 1$ (the equator $m = 0$ of $\mathbb{S}^2$).

We now consider planes in $\mathbb{R}^3$ of the form $\overline{m} = m_0$, where m_0 is a constant. The projective completion of such a plane in $\mathbb{RP}^3$ has the equation $m - m_0 h = 0$. So we see how the slices $\overline{m} = m_0$ need to be completed in the ball (see Fig. 9). We note that when $h = 0$ necessarily we must have $m = 0$ on such a slice, and thus the completion of the image

of the plane $\overline{m} = m_0$, when visualized in $\mathbb{S}^3$, must include the equator.

The specific equations of the correspondence of the points in the plane $\overline{m} = m_0$ of $\mathbb{R}^3$ (m_0 a constant) onto points in the interior of $\mathbb{S}^2$ ($\mathcal{B} = \{(c, e, m) \in \mathbb{R}^3;\ c^2 + e^2 + m^2 < 1\}$) follows from the bijection:

$$\mathbb{R}^3 \leftrightarrow \mathcal{B}$$
$$(\overline{c}, \overline{e}, \overline{m}) \leftrightarrow \left(\frac{\overline{c}}{r}, \frac{\overline{e}}{r}, \frac{\overline{m}}{r}\right),$$

with $r = \sqrt{\overline{c}^2 + \overline{e}^2 + \overline{m}^2 + 1}$. That is, for each plane $\overline{m} =$ constant in $\mathbb{R}^3$, there corresponds an ellipsoid $c^2 + e^2 + m^2(1 + m_0)^2/m_0^2 = 1, m \geq 0$ (see Fig. 9).

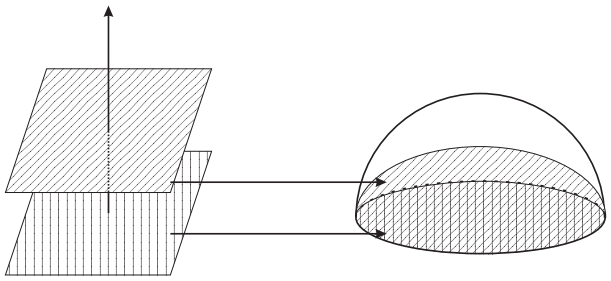

Fig. 9. Correspondence between planes and ellipsoides

Proposition 2.3. *By a rescaling in the variables, we may assume $h = 0$ or $h = 1$ in the normal form* (5).

Proof. If $h \neq 0$, by the reparametrization theorem we get that systems (5) are equivalent to

$$\dot{x} = Cx + Cy - Cx^2 + 2xy,$$
$$\dot{y} = Ex + Ey - Ex^2 + 2Mxy,$$

where $C = c/h, E = e/h$ and $M = m/h$. By renaming the coefficients $C \to c$, $E \to e$ and $M \to m$, we obtain systems (5) with $h = 1$. Moreover, we must also consider the case when $h = 0$. ■

3. A few basic properties of quadratic systems relevant for this study

The following results hold for any quadratic system. We present a reference where one can find their proofs.

(i) If a quadratic system has a limit cycle, then it surrounds a unique singular point, and this point is a focus; see [Coppel, 1966].

(ii) A quadratic system with an invariant straight line has at most one limit cycle; see [Coll & Llibre, 1988].

(iii) A quadratic system with more than one real invariant straight line has no limit cycle; see [Bautin, 1954].

We shall also recall the following specific results for quadratic systems having a weak focus of second and third order, respectively:

(iv) In quadratic systems there is at most one limit cycle surrounding a weak focus of second order and when it exist it is hyperbolic, see [Pingguang, 2001].

(v) There are no limit cycles in quadratic systems surrounding the weak focus of third order, see [Li, 1986].

The proof of the next result can be found in [Artés *et al.*, 1998].

Proposition 3.1. *Any graphic or degenerate graphic in a real planar polynomial differential system must either*

1) surround a singular point of index greater than or equal to +1, or

2) contain a singular point having an elliptic sector situated in the region delimited by the graphic, or

3) contain an infinite number of singular points.

4. The bifurcation diagram of the systems in $\overline{\mathbf{QsnSN_{11}(B)}}$

In this paper we intend to perform a complete study of a bifurcation diagram. So this is a global work and as such it uses global methods. In particular it uses algebraic and topological invariants. The algebraic invariants make results independent of specific normal forms. They also distinguish the phase portraits as the topological invariants also do. In this paper we use the concepts of algebraic invariant and T–comitant as formulated by the Sibirsky's School

for differential equations. For a quick summary of the general theory of these polynomial invariants and their precious relevance in working with polynomial differential systems we recommend Sec. 7 of [Artés *et al.*, 2006].

In this section we present the value of the algebraic invariants and T–comitants (with respect to normal form (5)) which are relevant in our study.

4.1. Algebraic bifurcation surfaces at the affine part of $\mathbb{RP}^3$

From Sec. 7 of [Artés *et al.*, 2008] and [Vulpe, 2011] we get the formulas which give the bifurcation surfaces of singularities in $\mathbb{R}^{12}$, produced by changes that may occur in the local nature of finite singularities. From [Schlomiuk & Vulpe, 2005] we get equivalent formulas for the infinite singular points. All of these formulas were lately compiled and improved in the book [Artés *et al.*, 2021].

Bifurcation surface in $\mathbb{RP}^3$ due to degeneracy of system

$(\mathcal{S}_8)$ Since for systems (5) we have an infinite saddle–node of type $\overline{\binom{1}{1}}SN$ we have that $\mu_0 = 0$. Moreover, since

$$\mu_1 = -4(eh - cm)^2 x, \quad \mu_2 = -4(eh - cm)^2 xy,$$

and

$$\mu_3 = \mu_4 = 0,$$

we define $(\mathcal{S}_8)$ as a surface whose equation is given by $\mu_1 = 0$, i.e.

$$(\mathcal{S}_8)\colon eh - cm = 0,$$

and therefore on this surface we have that $\mu_i = 0$, $i = 0, 1, 2, 3, 4$, i.e. systems (5) are degenerate (see [Artés *et al.*, 2021]). We point out that our aim is to construct a coherent and continuous bifurcation diagram. Although the phase portraits possessing a double finite saddle–node $\overline{sn}_{(2)}$, a finite elemental singularity and an infinite saddle–node $\overline{\binom{1}{1}}SN$, are located in open sets in this bifurcation diagram, in order to have these properties for this diagram, we also need to consider the borders of such sets. In particular, surface $(\mathcal{S}_8)$ borders open sets in this bifurcation diagram. In Fig. 10 we present the surface $(\mathcal{S}_8)$ in the three–dimensional affine space which is the hyperplane $h = 1$ in $\mathbb{R}^4$.

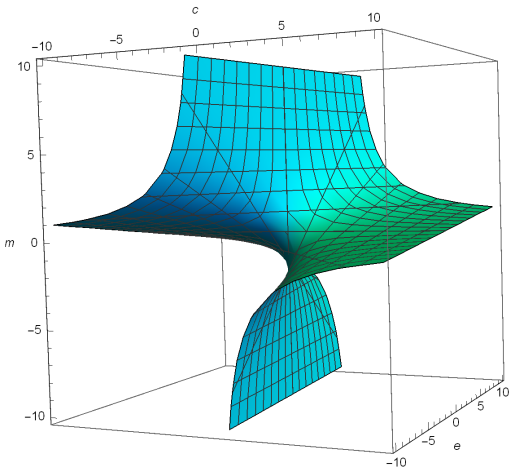

Fig. 10. Surface $(\mathcal{S}_8)$ for $h = 1$

Remark 4.1. In the equations of the following surfaces the factor $eh - cm$ is also present. This confirms that the systems on surface $(\mathcal{S}_8)$ are indeed degenerate (possessing curves of singularities) because many geometrical features happens at the same time when $eh - cm = 0$. However, we are interested in the other geometrical features that the following surfaces can provide. In this way, we assume, without loss of generality, that $eh - cm \neq 0$.

Bifurcation surface in $\mathbb{RP}^3$ due to the change of topological type of the origin

$(\mathcal{S}_2)$ This is the bifurcation surface due to the change of topological type of the origin. On this surface the origin becomes a cusp–type singularity. This phenomenon occurs when two separatrices of a saddle–node coalesce and, according to [Artés *et al.*, 2021], for normal form (5) this phenomenon is described by the invariant E_1 which in this case is given by

$$E_1 = -8(c + e)(-eh + cm)^4.$$

Taking into consideration Remark 4.1, we define surface $(\mathcal{S}_2)$ by

$$(\mathcal{S}_2)\colon c + e = 0.$$

Geometrically, such a surface is a plane on the projective space $\mathbb{RP}^3$ with projective coordinates c, e and m.

The surface of C^∞ bifurcation points due to a strong saddle or a strong focus changing the sign of their traces (weak saddle or weak focus)

$(\mathcal{S}_3)$ This is the bifurcation surface due to weak finite singularities, which occurs when the trace of a finite singular point is zero. According to [Vulpe, 2011], if the invariant polynomials $\mathcal{T}_4$ and $\mathcal{T}_3$ verify the conditions $\mathcal{T}_4 = 0$ and $\mathcal{T}_3 \neq 0$ then systems (5) have exactly one weak singularity. Indeed, for normal form (5) the previous conditions are equivalent to

$$\mathcal{T}_4 = -8h(c+e)^2(c-e-2m)(-eh+cm)^2 = 0,$$

$$\mathcal{T}_3 = -8h(c+e)(c-3e-4m)(-eh+cm)^2 \neq 0.$$

Taking into consideration Remark 4.1 we define surface $(\mathcal{S}_3)$ as

$$(\mathcal{S}_3)\colon c-e-2m=0.$$

We highlight that this bifurcation can produce a topological change if the weak point is a focus or just a C^∞ change if it is a saddle, except when this bifurcation coincides with a loop bifurcation associated with the same saddle, in which case, the change may also be topological (see for instance [Artés *et al.*, 2015; p. 50]).
We clearly have that such a surface is a plane on the projective space $\mathbb{RP}^3$ with projective coordinates c, e and m.

Bifurcation surface in $\mathbb{RP}^3$ due to the presence of invariant straight lines

$(\mathcal{S}_4)$ This surface will contain the points of the parameter space there appear invariant straight lines (see Lemma 2.2). This surface is split into some regions. Depending on these regions, the straight line may contain connections of separatrices from different points or not. So, in some cases, it may imply a topological bifurcation and, in others, just a C^∞ bifurcation. According to [Artés *et al.*, 2021], the equation of this surface is given by the invariant B_1. It is worth mentioning that $B_1 = 0$ is only a necessary condition for the existence of an invariant straight line, but it is not sufficient (see Corollary 4.6 from [Schlomiuk & Vulpe, 2004]), i.e. we may find some component of $B_1 = 0$ that does not represent an invariant straight line. For normal form (5) the invariant B_1 is given by

$$B_1 = -8c^2e^2(c+2h)(c+e+2h+2m)(-eh+cm)^3.$$

Taking into consideration Remark 4.1, we define surface $(\mathcal{S}_4)$ by the equation

$$(\mathcal{S}_4)\colon ce(c+2h)(c+e+2h+2m)=0.$$

In Fig. 11 we present the surface $(\mathcal{S}_4)$ in the three–dimensional affine space which is the hyperplane $h = 1$ in $\mathbb{R}^4$.

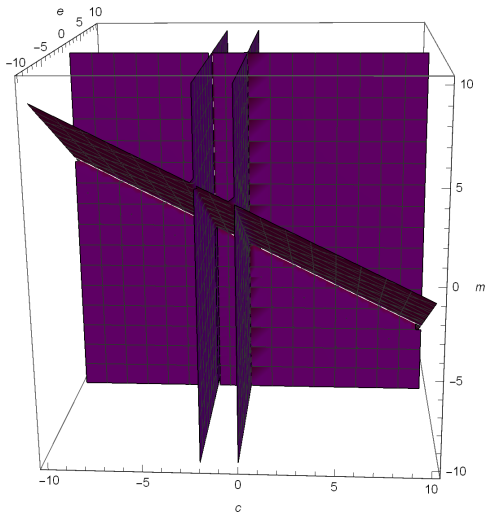

Fig. 11. Surface $(\mathcal{S}_4)$ for $h = 1$

The bifurcation surfaces above are all algebraic and they, except $(\mathcal{S}_4)$, are the bifurcation surfaces of finite singularities of systems (5) in the parameter space. We shall detect other two bifurcation surfaces not necessarily algebraic. On one of them the systems have global connection of separatrices different from that given by $(\mathcal{S}_4)$ and on the other the systems possess a double limit cycle. The equations of these bifurcation surfaces can only be determined approximately by means of numerical tools. Using arguments of continuity in the phase portraits we can prove the existence of these components not necessarily algebraic in the part where they appear, and we can check them numerically. We shall name them surfaces $(\mathcal{S}_7)$ (connection of separatrices) and $(\mathcal{S}_{10})$ (double limit cycles).

Remark 4.2. On surface $(\mathcal{S}_{10})$ the respective systems have at least one double limit cycle. Although this surface is obtained numerically, we can predict in which portion of the bifurcation diagram it can be placed. It must be in the neighborhood of the points of the bifurcation diagram corresponding to a weak focus $f^{(2)}$ of order two.

So, according to [Vulpe, 2011; Main Theorem, item (b_2)], the necessary condition for the existence of weak points of order two or higher is governed by $\mathcal{T}_4 = \mathcal{F}_1 = 0$. Taking into account Remark 4.1, for normal form (5) the expression of $\mathcal{F}_1$ is given by $\mathcal{F}_1 = c^2 + 2cm + 3ce + 2e$. For $h = 1$, calculations yield $\mathcal{T}_4 = \mathcal{F}_1 = 0$ if and only if

$$c - e - 2m = 2c^2 + (1 - 2m)c - 2m = 0. \qquad (8)$$

Such a quadratic equation has discriminant

$$\Delta = 4m^2 + 12m + 1,$$

which is zero if and only if

$$m = \frac{1}{2}\left(\pm 2\sqrt{2} - 3\right).$$

Therefore, for the equation $\mathcal{T}_4 = \mathcal{F}_1 = 0$ we have:

- one double real root if $\Delta = 0$, i.e. $m = \left(\pm 2\sqrt{2} - 3\right)/2$;
- two simple real roots if $\Delta > 0$, i.e. $m < \left(-2\sqrt{2} - 3\right)/2$ or $m > \left(2\sqrt{2} - 3\right)/2$;
- two complex roots if $\Delta < 0$, i.e. $m \in \left(\left(-2\sqrt{2} - 3\right)/2, \left(2\sqrt{2} - 3\right)/2\right)$.

These roots indicate the existence of weak singularities of order two or higher.
On the other hand, for nondegenerate systems (5) with $h = 1$ we have that

$$\mathcal{T}_4 = \mathcal{F}_1 = \mathcal{F}_2 = 0$$

if and only if $c = -6/5, e = 36/5$ and $m = -21/5$, and calculations show that $\mathcal{F}_3\mathcal{F}_4 \neq 0$. Then, according to [Vulpe, 2011; Main Theorem, item (b_3)], we have a third order weak singularity for $m = -21/5$.

Bifurcation surface in $\mathbb{RP}^3$ due to multiplicities of infinite singularities

$(\mathcal{S}_5)$ This is the bifurcation surface due to multiplicity of infinite singularities. This phenomena is detected by the invariant η (see Lemma 6.1 from [Artés *et al.*, 2021]), which, for normal form (5) is given by

$$\eta = -4h^2(-c^2 + 8eh - 4cm - 4m^2) = 0.$$

We define surface $(\mathcal{S}_5)$ by the equation

$$(\mathcal{S}_5)\colon h(c^2 - 8eh + 4cm + 4m^2) = 0.$$

In Fig. 12 we present the surface $(\mathcal{S}_5)$ in the three–dimensional affine space which is the hyperplane $h = 1$ in $\mathbb{R}^4$.

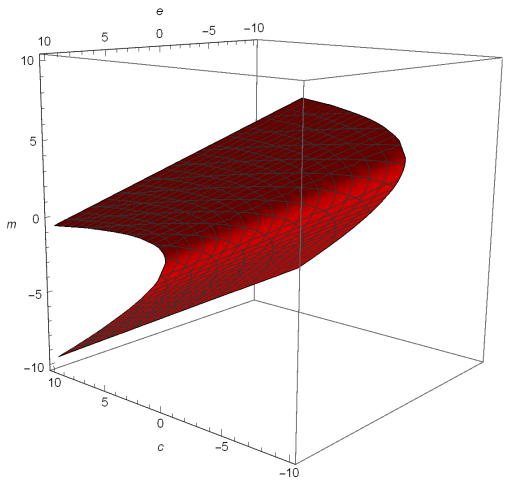

Fig. 12. Surface $(\mathcal{S}_5)$ for $h = 1$

The surface of C^∞ bifurcation due to a node becoming a focus

$(\mathcal{S}_6)$ This surface will contain the points of the parameter space where a finite node of the systems turns into a focus. This surface is a C^∞ but not a topological bifurcation surface. In fact, when we only cross the surface $(\mathcal{S}_6)$ in the bifurcation diagram, the topological phase portraits do not change. However, this surface is relevant for isolating the regions where a limit cycle surrounding an antisaddle cannot exist. Using the results of [Artés *et al.*, 2008], we must consider the invariant W_4. For normal form (5), W_4 is given by the polynomial

$$64h^2(c+e)^4(-eh+cm)^4(c^2-2ce+e^2-8eh)+ \\ +64h^2(c+e)^4(-eh+cm)^4(4cm+4em+4m^2).$$

Taking into consideration Remark 4.1 and the fact that W_4 can be considered only when $E_1 \neq 0$, i.e. $c + e \neq 0$ (see [Artés *et al.*, 2021; Table 6.2]), we define surface $(\mathcal{S}_6)$ as

$$(\mathcal{S}_6)\colon h(c^2-2ce+e^2-8eh+4cm+4em+4m^2) = 0.$$

In Fig. 13 we present the surface $(\mathcal{S}_6)$ in the three–dimensional affine space which is the hyperplane $h = 1$ in $\mathbb{R}^4$.

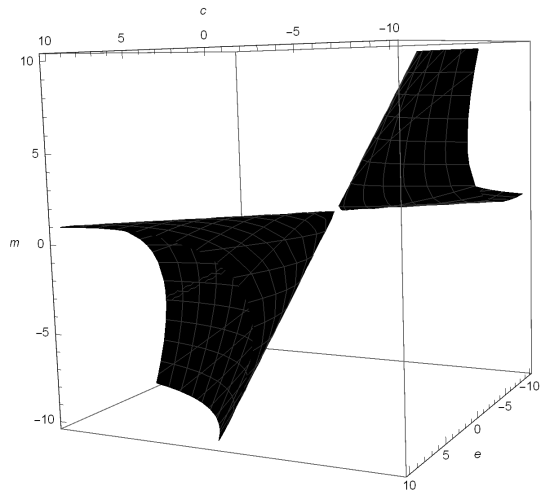

Fig. 13. Surface $(\mathcal{S}_6)$ for $h = 1$

We also must consider the invariant polynomial W_2, which for normal form (5) is described by the equation

$$W_2 = 64h^2(eh - cm)^4(3c^2 + 2ce + 3e^2 - 8eh) + \\ + 64h^2(eh - cm)^4(4cm + 4em + 4m^2).$$

This invariant polynomial, according to [Artés *et al.*, 2021; Table 6.2], can only be considered when $E_1 = c + e = 0$, and W_2 is zero when (for normal form (5)) $G_9 = h^2(eh - cm) \neq 0$, i.e. $h \neq 0$. Taking into consideration Remark 4.1 and the inclusion $\{E_1 = 0\} \subseteq \{\mathcal{T}_4 = 0\}$ we observe that, for normal form (5), the solutions of the equation $W_2 = 0$ are indeed the solutions of the system formed by the equations

$$c + e = 0, \quad h(c - e - 2m) = 0, \\ 3c^2 + 2ce + 3e^2 - 8eh + 4cm + 4em + 4m^2 = 0.$$

So, calculations yield $W_2 = 0$ as a set with coordinates (c, e, h, m), and such a set is given by

$$\{(-h, h, h, -h); h \in \mathbb{R}\}.$$

In what follows we work at the chart of $\mathbb{RP}^3$ corresponding to $h \neq 0$, and we take $h = 1$. Therefore, $W_2 = 0$ with coordinates (c, e, m) is given by $\{(0, 0, 0), (-1, 1, -1)\}$. We will denote this two–point set by $(\mathcal{S}_{6.2})$. More precisely, $(\mathcal{S}_{6.2})$=$\{\mathcal{S}_{6.21}, \mathcal{S}_{6.22}\}$, where $\mathcal{S}_{6.21}$=$\{(-1, 1, -1)\}$ and $\mathcal{S}_{6.22}$=$\{(0, 0, 0)\}$.

Remark 4.3. As we mentioned before, surface $(\mathcal{S}_6)$ is relevant for isolating the regions where a limit cycle surrounding an antisaddle cannot exist. Then, according to Remark 4.2 it is interesting to determine the intersection $\mathcal{T}_4 = \mathcal{F}_1 = 0$ with $W_4 = 0$. For normal form (5), calculations yield

$$W_4\Big|_{\mathcal{T}_4=\mathcal{F}_1=0} = \frac{4c^2(3 + 2c)}{1 + c},$$

and then W_4 intercepts the curve given by $\mathcal{T}_4 = \mathcal{F}_1 = 0$ at $c = 0$ and $c = -3/2$ (which is equivalent to $m = 0$ and $m = -3$, respectively). We observe that W_4 has a relative minimum at $m = 0$, since

$$\frac{\partial W_4}{\partial m}\Big|_{\mathcal{T}_4=\mathcal{F}_1=0|_{c=0}} = 0, \quad \frac{\partial^2 W_4}{\partial m^2}\Big|_{\mathcal{T}_4=\mathcal{F}_1=0|_{c=0}} = 8,$$

and, moreover, W_4 is decreasing at $m = -3$ because

$$\frac{\partial W_4}{\partial m}\Big|_{\mathcal{T}_4=\mathcal{F}_1=0|_{c=-3/2}} = -12.$$

As a result we conclude, respectively, that:

- if for $m > 0$ we do not have a weak focus of order two (or higher), then for every $m > 0$ we will not find such a kind of singularity, since we will not be "crossing" surface $(\mathcal{S}_6)$;
- if for $m < -3$ we have a weak focus of order two (or higher), then for every $m < -3$ we will find such a kind of singularity.

Remark 4.4. Even though we can draw a two–dimensional picture of the algebraic bifurcation surfaces of singularities in affine parts of $\mathbb{RP}^3$ as we did before, it is pointless to see a single two–dimensional image of all these bifurcation surfaces together in an affine part of $\mathbb{RP}^3$. As we shall see later, the full partition of the parameter space obtained from these bifurcation surfaces has 631 parts.

Due to the last remark we shall foliate the three–dimensional bifurcation diagram in $\mathbb{RP}^3$ by the planes $m = m_0$, with m_0 constant, plus the open half sphere $h = 0$ and we shall give pictures of the resulting bifurcation diagram on these planar sections on a disc or in an affine chart of $\mathbb{R}^2$.

As we said before, we work at the chart of $\mathbb{RP}^3$ corresponding to $h \neq 0$, and we take $h = 1$. In

order to perform the analysis, we shall use pictures which are drawn on planes $m = m_0$ of $\mathbb{RP}^3$, having coordinates $[c : e : 1 : m_0]$. In these planes the coordinates are (c, e) where the horizontal line is the c–axis.

As the final bifurcation diagram is quite complex, it is useful to introduce colors which will be used to refer to the bifurcation surfaces:

(a) surface $(\mathcal{S}_2)$ is drawn in green (the origin becomes a cusp–type singularity);

(b) surface $(\mathcal{S}_3)$ is drawn in yellow (when the trace of a singular point becomes zero). We draw it as a continuous curve if the singular point is a focus or as a dashed curve if it is a saddle;

(c) surface $(\mathcal{S}_4)$ is drawn in purple (presence of at least one invariant straight line). We draw it as a continuous curve if it implies a topological change or as a dashed curve otherwise;

(d) surface $(\mathcal{S}_5)$ is drawn in red (two infinite singular points coalesce);

(e) surface $(\mathcal{S}_6)$ is drawn in black (an antisaddle is on the edge of turning from a node to a focus or vice versa);

(f) the two–point set $(\mathcal{S}_{6.2})$ is also drawn in black;

(g) surface $(\mathcal{S}_7)$ is also drawn in purple (connections of separatrices);

(h) surface $(\mathcal{S}_8)$ is drawn in cyan (the systems are degenerate); and

(i) surface $(\mathcal{S}_{10})$ is drawn in gray (presence of a double limit cycle).

We use the same color for $(\mathcal{S}_4)$ and $(\mathcal{S}_7)$ since both surfaces deal with connections of separatrices mostly.

The following lemmas of this section present the study of the geometrical behavior of all of these surfaces for $h \neq 0$ (the case $h = 0$ will be considered separately), that is, their singularities, their intersection points and their extrema (maxima and minima) with respect to the coordinate m.

Lemma 4.5. *Surface $(\mathcal{S}_2)$ has no singularities.*

Proof. Surface $(\mathcal{S}_2)$ is described by the equation $c+e = 0$, which is a plane. ■

Lemma 4.6. *For any $m \in \mathbb{R}$, surface $(\mathcal{S}_3)$ has no singularities.*

Proof. Surface $(\mathcal{S}_3)$ is given by the equation $c-e-2m = 0$, and such an equation describes a plane for each $m \in \mathbb{R}$. ■

Lemma 4.7. *For $h \neq 0$, surface $(\mathcal{S}_4)$ has five straight lines of singularities given by $[0 : 0 : 1 : m]$, $[0 : e : 1 : -1 - e/2]$, $[-2 : 0 : 1 : m]$, $[-2 : e : 1 : -e/2]$ and $[c : 0 : 1 : -1 - c/2]$.*

Proof. When $h = 1$, surface $(\mathcal{S}_4)$ is described by the equation $ce(c+2)(c+e+2m+2) = 0$. Such an equation tells us that surface $(\mathcal{S}_4)$ is the union of four planes, namely $\{c = 0\}$, $\{e = 0\}$, $\{c + 2 = 0\}$ and $\{c+e+2m+2 = 0\}$. As the planes themselves have no singularities, the singularities of such a surface consist of the intersections among these planes, which are the straight lines $[0 : 0 : 1 : m]$, $[0 : e : 1 : -1 - e/2]$, $[-2 : 0 : 1 : m]$, $[-2 : e : 1 : -e/2]$ and $[c : 0 : 1 : -1 - c/2]$. Note that as $\{c = 0\}$ and $\{c+2 = 0\}$ are parallel, they do not provide us any intersection. ■

Lemma 4.8. *For $h \neq 0$, surface $(\mathcal{S}_5)$ has no singularities.*

Proof. When $h = 1$, surface $(\mathcal{S}_5)$ is written as $c^2 - 8e + 4cm + 4m^2 = 0$. This equation describes a parabolic cylindrical surface which has no singularities. ■

Lemma 4.9. *For $h \neq 0$, the point $[-2 : 0 : 1 : 1]$ is the only singularity of surface $(\mathcal{S}_6)$.*

Proof. When $h = 1$, surface $(\mathcal{S}_6)$ is given by the quadric $Q = c^2-8e-2ce+e^2+4cm+4em+4m^2 = 0$. Computing the derivatives of Q, we obtain:

$$\frac{\partial Q}{\partial c} = 2(c - e + 2m), \quad \frac{\partial Q}{\partial e} = -2(4 + c - e - 2m),$$
$$\frac{\partial Q}{\partial m} = 4(c + e + 2m).$$

These three surfaces (together with Q) have the common point $(-2, 0, 1)$. We point out that Q is

a quadric whose reduced equation is given by

$$\left(\sqrt{3}+2\right)x_2^2+\frac{1}{2}\left(\sqrt{3}+1\right)y_2^2-z_2^2=0,$$

for some coordinate system (Σ,O), with $O=(x_2,y_2,z_2)$ obtained from (c,e,m) with the rigid movements of translation and rotation. ■

Lemma 4.10. *For $h\neq 0$, surface $(\mathcal{S}_8)$ has no singularities.*

Proof. When $h=1$, surface $(\mathcal{S}_8)$ is described by equation $e-cm=0$. This equation describes a hyperbolic paraboloid surface, known as a saddle surface, which has no singularities. ■

Lemma 4.11. *For $h\neq 0$, surfaces $(\mathcal{S}_2)$ and $(\mathcal{S}_3)$ intersect along the straight line $[c:-c:1:c]$.*

Proof. For $h=1$, solving the system of equations

$$\begin{aligned}(\mathcal{S}_2):&\ c+e=0,\\(\mathcal{S}_3):&\ c-e-2m=0,\end{aligned}$$

we obtain $e=-c$ and $m=c$. This result corresponds to the straight line $[c:-c:1:c]$. ■

Lemma 4.12. *For $h\neq 0$, surfaces $(\mathcal{S}_2)$ and $(\mathcal{S}_4)$ intersect along the straight lines $[0:0:1:m]$, $[-2:2:1:m]$ and $[c:-c:1:-1]$.*

Proof. For $h=1$, we have the system of equations

$$\begin{aligned}(\mathcal{S}_2):&\ c+e=0,\\(\mathcal{S}_4):&\ ce(c+2)(c+e+2m+2)=0.\end{aligned}$$

As the equation of surface $(\mathcal{S}_4)$ has four factors, we have to compute the intersection of each one of them with the equation of surface $(\mathcal{S}_2)$. Calculations yield:

- $c=0$ and $e=0$. This solution corresponds to the curve $[0:0:1:m]$ and it has multiplicity two;
- $c=-2$ and $e=2$. This solution corresponds to the curve $[-2:2:1:m]$;
- $e=-c$ and $m=-1$. This solution corresponds to the curve $[c:-c:1:-1]$.

■

Lemma 4.13. *For $h\neq 0$, surfaces $(\mathcal{S}_2)$ and $(\mathcal{S}_5)$ intersect along the curves $[c:-c:1:-\sqrt{-2c}-c/2]$ and $[c:-c:1:\sqrt{-2c}-c/2]$. Moreover, the curve $[c:-c:1:-\sqrt{-2c}-c/2]$ assumes its extremum (with relation to the coordinate m) for $c=-2$.*

Proof. For $h=1$, we have the system of equations

$$\begin{aligned}(\mathcal{S}_2):&\ c+e=0,\\(\mathcal{S}_5):&\ c^2-8e+4cm+4m^2=0.\end{aligned}$$

Solving this system we obtain the following solutions:

- $e=-c$ and $m=-\sqrt{-2c}-c/2$. This solution corresponds to the curve $[c:-c:1:-\sqrt{-2c}-c/2]$;
- $e=-c$ and $m=\sqrt{-2c}-c/2$. This solution corresponds to the curve $[c:-c:1:\sqrt{-2c}-c/2]$.

In order to find the extremum of the curve $[c:-c:1:-\sqrt{-2c}-c/2]$ we equalize the last coordinate to m and compute the discriminant with respect to c of the obtained function:

$$\mathrm{Discrim}_c(-8c-c^2-4cm-4m^2)=64(m+1),$$

whose solution is $m=-1$. Finally, solving the equation $-\sqrt{-2c}-c/2=m$ by substituting m by the zero of the discriminant (i.e. $m=-1$), we obtain $c=-2$, which is the extremum value of the curve with respect to m. ■

Lemma 4.14. *For $h\neq 0$, surfaces $(\mathcal{S}_2)$ and $(\mathcal{S}_6)$ intersect along the curves $[-e:e:1:-\sqrt{(2-e)e}]$ and $[-e:e:1:\sqrt{(2-e)e}]$. Moreover, these curves assume their extremum (with relation to the coordinate m) for $e=1$.*

Proof. For $h=1$, we have the system of equations

$$\begin{aligned}(\mathcal{S}_2):&\ c+e=0,\\(\mathcal{S}_6):&\ c^2-8e-2ce+e^2+4cm+4em+4m^2=0.\end{aligned}$$

Solving this system we obtain the following solutions:

- $c=-e$ and $m=-\sqrt{(2-e)e}$. This solution corresponds to the curve $[-e:e:1:-\sqrt{(2-e)e}]$;

- $c = -e$ and $m = \sqrt{(2-e)e}$. This solution corresponds to the curve $[-e : e : 1 : \sqrt{(2-e)e}]$.

In order to find the extremum of the curve $[-e : e : 1 : -\sqrt{(2-e)e}]$ we equalize the last coordinate to m and compute the discriminant with respect to e of the obtained function:

$$\text{Discrim}_e(2e - e^2 - m^2) = 4 - 4m^2,$$

whose solutions are $m = \pm 1$. Finally, solving the equation $-\sqrt{(2-e)e} = m$ by substituting m by the zeroes of the discriminant (i.e. $m = \pm 1$), we obtain $e = 1$ for $m = -1$ and we do not obtain solution for $m = 1$.
Analogously, for the curve $[-e : e : 1 : \sqrt{(2-e)e}]$ calculations yield the same discriminant as before, whose solutions are $m = \pm 1$. Solving the equation $\sqrt{(2-e)e} = m$ by substituting m by the zeroes of the discriminant (i.e. $m = \pm 1$), we obtain $e = 1$ for $m = 1$ and we do not obtain solution for $m = -1$. Therefore, $e = 1$ is the extremum value of both curves with respect to m. ■

Lemma 4.15. *For $h \neq 0$, the two–point set $(\mathcal{S}_{6.2})$ belongs to the surfaces $(\mathcal{S}_2)$ to $(\mathcal{S}_4)$, $(\mathcal{S}_6)$ and $(\mathcal{S}_8)$. Moreover, $(\mathcal{S}_5)$ intercepts the two–point set $(\mathcal{S}_{6.2})$ at $\mathcal{S}_{6.22}$=$\{(0,0,0)\}$.*

Proof. For $h = 1$, it is easy to show that $\mathcal{S}_{6.21}$=$\{(-1,1,-1)\}$ and $\mathcal{S}_{6.22}$=$\{(0,0,0)\}$ verify this result. ■

Lemma 4.16. *For $h \neq 0$, surfaces $(\mathcal{S}_2)$ and $(\mathcal{S}_8)$ intersect along the straight lines $[0 : 0 : 1 : m]$ and $[c : -c : 1 : -1]$.*

Proof. For $h = 1$, we have the system of equations

$$(\mathcal{S}_2) : c + e = 0,$$
$$(\mathcal{S}_8) : e - cm = 0.$$

Solving this system we obtain the following solutions:

- $c = 0$ and $e = 0$. Then we have the straight line $[0 : 0 : 1 : m]$;
- $e = -c$ and $m = -1$. This corresponds to the straight line $[c : -c : 1 : -1]$.

■

Lemma 4.17. *For $h \neq 0$, surfaces $(\mathcal{S}_3)$ and $(\mathcal{S}_4)$ intersect along the straight lines $[0 : e : 1 : -e/2]$, $[c : 0 : 1 : c/2]$, $[-2 : e : 1 : -1 - e/2]$ and $[-1 : e : 1 : -(1+e)/2]$.*

Proof. For $h = 1$, we have the system of equations

$$(\mathcal{S}_3) : c - e - 2m = 0,$$
$$(\mathcal{S}_4) : ce(c+2)(c+e+2m+2) = 0.$$

As the equation of surface $(\mathcal{S}_4)$ has four factors, we have to compute the intersection of each one of them with the equation of surface $(\mathcal{S}_3)$. Calculations yield the following solutions:

- $c = 0$ and $m = -e/2$. This solution corresponds to the straight line $[0 : e : 1 : -e/2]$;
- $e = 0$ and $m = c/2$. This solution corresponds to the straight line $[c : 0 : 1 : c/2]$;
- $c = -2$ and $m = -1 - e/2$. This solution corresponds to the straight line $[-2 : e : 1 : -1 - e/2]$;
- $c = -1$ and $m = -(1+e)/2$. This solution corresponds to the straight line $[-1 : e : 1 : -(1+e)/2]$.

■

Lemma 4.18. *For $h \neq 0$, surfaces $(\mathcal{S}_3)$ and $(\mathcal{S}_5)$ intersect along the curves $[c : 2(2+c+2\sqrt{c+1}) : 1 : -2(1+\sqrt{c+1})-c/2]$ and $[c : 2(2+c-2\sqrt{c+1}) : 1 : -2(1-\sqrt{c+1})-c/2]$. Moreover, this last curve assumes its extremum (with relation to the coordinate m) for $c = 3$.*

Proof. For $h = 1$, we have the system of equations

$$(\mathcal{S}_3) : c - e - 2m = 0,$$
$$(\mathcal{S}_5) : c^2 - 8e + 4cm + 4m^2 = 0.$$

Solving this system we obtain the following solutions:

- $e = 2(2 + c + 2\sqrt{c+1})$ and $m = -2(1 + \sqrt{c+1}) - c/2$. This solution corresponds to the curve $[c : 2(2 + c + 2\sqrt{c+1}) : 1 : -2(1 + \sqrt{c+1}) - c/2]$;
- $e = 2(2 + c - 2\sqrt{c+1})$ and $m = -2(1 - \sqrt{c+1}) - c/2$. This solution corresponds to the curve $[c : 2(2 + c - 2\sqrt{c+1}) : 1 : -2(1 - \sqrt{c+1}) - c/2]$.

In order to find the extremum of the curve $[c : 2(2+c-2\sqrt{c+1}) : 1 : -2(1-\sqrt{c+1})-c/2]$, we equalize the last coordinate to m and compute the discriminant with respect to c of the obtained function:

$$\text{Discrim}_c(-2c-c^2/4-4m-cm-m^2) = 4-8m,$$

whose solution is $m = 1/2$. Finally, solving the equation $-2(1-\sqrt{c+1})-c/2 = m$ by substituting $m = 1/2$, we obtain $c = 3$, which is the extremum value of the curve with respect to m. ■

Lemma 4.19. *For $h \neq 0$, surfaces $(\mathcal{S}_3)$ and $(\mathcal{S}_6)$ intersect along the curves $[(e-\sqrt{e^2+8e})/2 : e : 1 : -(\sqrt{e}+\sqrt{e+8})\sqrt{e}/4]$ and $[(e+\sqrt{e^2+8e})/2 : e : 1 : -(\sqrt{e}-\sqrt{e+8})\sqrt{e}/4]$.*

Proof. For $h = 1$, we have the system of equations

$$(\mathcal{S}_3) : c-e-2m = 0,$$
$$(\mathcal{S}_6) : c^2-8e-2ce+e^2+4cm+4em+4m^2 = 0.$$

Solving this system we obtain the following solutions:

- $c = (e-\sqrt{e^2+8e})/2$ and $m = -(\sqrt{e}+\sqrt{e+8})\sqrt{e}/4$. This solution corresponds to the curve $[(e-\sqrt{e^2+8e})/2 : e : 1 : -(\sqrt{e}+\sqrt{e+8})\sqrt{e}/4]$;
- $c = (e+\sqrt{e^2+8e})/2$ and $m = -(\sqrt{e}-\sqrt{e+8})\sqrt{e}/4$. This solution corresponds to the curve $[(e+\sqrt{e^2+8e})/2 : e : 1 : -(\sqrt{e}-\sqrt{e+8})\sqrt{e}/4]$.

■

Lemma 4.20. *For $h \neq 0$, surfaces $(\mathcal{S}_3)$ and $(\mathcal{S}_8)$ intersect along the hyperbola $[c : c^2/(c+2) : 1 : c/(c+2)]$.*

Proof. For $h = 1$, we have the system of equations

$$(\mathcal{S}_3) : c-e-2m = 0,$$
$$(\mathcal{S}_8) : e-cm = 0.$$

Solving this system we obtain $e = c^2/(c+2)$ and $m = c/(c+2)$. Then we have the hyperbola $[c : c^2/(c+2) : 1 : c/(c+2)]$. ■

Lemma 4.21. *For $h \neq 0$, surfaces $(\mathcal{S}_4)$ and $(\mathcal{S}_5)$ intersect along the curves $[0 : m^2/2 : 1 : m]$, $[-2 : (m-1)^2/2 : 1 : m]$, $[c : 0 : 1 : -c/2]$ and $[c : 2 : 1 : -2-c/2]$. Moreover, the straight lines $[c : 0 : 1 : -c/2]$ and $[c : 2 : 1 : -2-c/2]$ correspond to a contact of order two between these two surfaces.*

Proof. For $h = 1$, we have the system of equations

$$(\mathcal{S}_4) : c(c+2)e(c+e+2m+2) = 0,$$
$$(\mathcal{S}_5) : c^2-8e+4cm+4m^2 = 0.$$

As the equation of surface $(\mathcal{S}_4)$ has four factors, we have to compute the intersection of each one of them with the equation of surface $(\mathcal{S}_5)$. Calculations yield the following solutions:

- $c = 0$ and $e = m^2/2$. This solution corresponds to the parabola $[0 : m^2/2 : 1 : m]$;
- $c = -2$ and $e = (m-1)^2/2$. This solution corresponds to the parabola $[-2 : (m-1)^2/2 : 1 : m]$;
- $e = 0$ and $m = -c/2$. This solution corresponds to the straight line $[c : 0 : 1 : -c/2]$;
- $e = 2$ and $m = -2-c/2$. This solution corresponds to the straight line $[c : 2 : 1 : -2-c/2]$.

Moreover, for $h = 1$ surface $(\mathcal{S}_5)$ has a contact of order two with the plane $e = 0$ (then with the surface $(\mathcal{S}_4)$) along the straight line $\gamma_1 = [c : 0 : 1 : -c/2]$. In fact, by computing the resultant with respect to c of $e = 0$ and $(\mathcal{S}_5)$ we see that $\text{Res}_c[e, (\mathcal{S}_5)] = e^2$. In order to conclude the proof of this claim it is enough to observe that the gradient vector of the plane $e = 0$ in every point $[c : e : 1 : m]$ is $[0 : 1 : 1 : 0]$ whereas the gradient vector of $(\mathcal{S}_5)$ along the straight line γ_1 is $\nabla\mathcal{S}_5(\gamma_1) = [0 : -8 : 1 : 0]$, then the surface $(\mathcal{S}_5)$ remains only on one of the two topological subspaces delimited by the plane $e = 0$.

Analogously, for $h = 1$ surface $(\mathcal{S}_5)$ has a contact of order two with the plane $c+e+2m+2 = 0$ (then with the surface $(\mathcal{S}_4)$) along the straight line $\gamma_2 = [c : 2 : 1 : -2-c/2]$. Indeed, as before, by computing the resultant with respect to c of $c+e+2m+2 = 0$ and $(\mathcal{S}_5)$ we see that $\text{Res}_c[c+e+2m+2, (\mathcal{S}_5)] = (e-2)^2$. Moreover, we observe that the gradient vector of the plane $c+e+2m+2 = 0$ in every point $[c : e : 1 : m]$

is $[1:1:1:2]$ whereas the gradient vector of $(\mathcal{S}_5)$ along the straight line γ_2 is $\nabla\mathcal{S}_5(\gamma_2) = [-8:-8:1:-16]$, then the surface $(\mathcal{S}_5)$ remains only on one of the two topological subspaces delimited by the plane $c+e+2m+2=0$. ■

Lemma 4.22. *For $h \neq 0$, surfaces $(\mathcal{S}_4)$ and $(\mathcal{S}_6)$ intersect along the curves $[0:e:1:-\sqrt{2e}-e/2]$, $[0:e:1:\sqrt{2e}-e/2]$, $[-2:e:1:1-e/2]$, $[c:0:1:-c/2]$ and $[-2+1/e:e:1:-(e^2+1)/(2e)]$. Moreover, the curve $[0:e:1:\sqrt{2e}-e/2]$ has its extremum (with relation to the coordinate m) for $e=2$ and the curve $[-2+1/e:e:1:-(e^2+1)/(2e)]$ has its extremum for $e=\pm 1$. In addition, the straight lines $[-2:e:1:1-e/2]$ and $[c:0:1:-c/2]$ correspond to a contact of order two between these two surfaces.*

Proof. For $h=1$, we have the system of equations

$$(\mathcal{S}_4): c(c+2)e(c+e+2m+2)=0,$$
$$(\mathcal{S}_6): c^2-8e-2ce+e^2+4cm+4em+4m^2=0.$$

As the equation of surface $(\mathcal{S}_4)$ has four factors, we have to compute the intersection of each one of them with the equation of surface $(\mathcal{S}_6)$. Calculations yield the solutions:

- $c=0$ and $m=-\sqrt{2e}-e/2$. This solution corresponds to the curve $[0:e:1:-\sqrt{2e}-e/2]$;
- $c=0$ and $m=\sqrt{2e}-e/2$. This solution corresponds to the curve $[0:e:1:\sqrt{2e}-e/2]$;
- $c=-2$ and $m=1-e/2$. This solution corresponds to the straight line $[-2:e:1:1-e/2]$;
- $e=0$ and $m=-c/2$. This solution corresponds to the straight line $[c:0:1:-c/2]$;
- $c=-2+1/e$ and $m=-(e^2+1)/(2e)$. This solution corresponds to the hyperbola $[-2+1/e:e:1:-(e^2+1)/(2e)]$.

In order to find the extremum of the curve $[0:e:1:\sqrt{2e}-e/2]$ we equalize the last coordinate to m and compute the discriminant with respect to e of the obtained function:

$$\mathrm{Discrim}_e(8e-e^2-4em-4m^2) = -64(m-1),$$

whose solution is $m=1$. Now, solving the equation $\sqrt{2e}-e/2=m$ by substituting $m=1$, we obtain $e=2$, which is the extremum value of the curve with respect to m.
Analogously, in order to find the extrema of the curve $[-2+1/e:e:1:-(e^2+1)/(2e)]$ we equalize the last coordinate to m and compute the discriminant with respect to e of the obtained function:

$$\mathrm{Discrim}_e(-1-e^2-2em) = 4(m^2-1),$$

whose solutions are $m=\pm 1$. Proceeding, solving the equation $-(e^2+1)/(2e)=m$ by substituting $m=1$ we obtain $e=-1$, and by substituting $m=-1$ we obtain $e=1$. Therefore, $e=\pm 1$ are the extrema values of the curve with respect to m.
It remains to show that the straight lines $[-2:e:1:1-e/2]$ and $[c:0:1:-c/2]$ correspond to a contact of order two between surfaces $(\mathcal{S}_4)$ and $(\mathcal{S}_6)$.
In fact, for $h=1$ surface $(\mathcal{S}_6)$ has a contact of order two with the plane $e=0$ (then with the surface $(\mathcal{S}_4)$) along the straight line $\gamma_3=[c:0:1:-c/2]$. Indeed, by computing the resultant with respect to c of $e=0$ and $(\mathcal{S}_6)$ we see that $\mathrm{Res}_c[e,(\mathcal{S}_6)] = e^2$. In order to conclude the proof of this claim we observe that the gradient vector of the plane $e=0$ in every point $[c:e:1:m]$ is $[0:1:1:0]$ whereas the gradient vector of $(\mathcal{S}_6)$ along the straight line γ_3 is $\nabla\mathcal{S}_6(\gamma_3) = [0:-4(2+c):1:0]$, then, for each fixed value of the parameter c the surface $(\mathcal{S}_6)$ remains only on one of the two topological subspaces delimited by the plane $e=0$.
Analogously, for $h=1$ surface $(\mathcal{S}_6)$ has a contact of order two with the plane $c+2=0$ (then with the surface $(\mathcal{S}_4)$) along the straight line $\gamma_4=[-2:e:1:1-e/2]$. In fact, as before, by computing the resultant with respect to e of $c+2=0$ and $(\mathcal{S}_6)$ we see that $\mathrm{Res}_e[c+2,(\mathcal{S}_6)] = (c+2)^2$. Moreover, we observe that the gradient vector of the plane $c+2=0$ in every point $[c:e:1:m]$ is $[1:0:1:0]$ whereas the gradient vector of $(\mathcal{S}_6)$ along the straight line γ_4 is $\nabla\mathcal{S}_6(\gamma_4) = [-4e:0:1:0]$, then, for each fixed value of the parameter e the surface $(\mathcal{S}_6)$ remains only on one of the two topological subspaces delimited by the plane $c+2=0$. ■

Lemma 4.23. *For $h \neq 0$, surfaces $(\mathcal{S}_4)$ and $(\mathcal{S}_8)$ intersect along the straight lines $[c:0:1:0]$, $[0:0:1:m]$, $[-2:-2m:1:m]$ and $[c:-c:1:-1]$.*

Proof. For $h = 1$, we have the system of equations

$$(\mathcal{S}_4) : c(c+2)e(c+e+2m+2) = 0,$$
$$(\mathcal{S}_8) : e - cm = 0.$$

As the equation of surface $(\mathcal{S}_4)$ has four factors, we have to compute the intersection of each one of them with the equation of surface $(\mathcal{S}_8)$. Calculations yield the solutions:

- $e = 0$ and $m = 0$. This solution corresponds to the straight line $[c : 0 : 1 : 0]$;
- $c = 0$ and $e = 0$. This solution corresponds to the straight line $[0 : 0 : 1 : m]$ and it has multiplicity three;
- $c = -2$ and $e = -2m$. This solution corresponds to the straight line $[-2 : -2m : 1 : m]$ and it has multiplicity two;
- $e = -c$ and $m = -1$. This solution corresponds to the straight line $[c : -c : 1 : -1]$.

■

Lemma 4.24. *For $h \neq 0$, surfaces $(\mathcal{S}_5)$ and $(\mathcal{S}_6)$ intersect along the curves $[c : 0 : 1 : -c/2]$, $[c : 4(4+c+2\sqrt{2c+4}) : 1 : -2\sqrt{2c+4} - c/2 - 4]$, and $[c : 4(4+c-2\sqrt{2c+4}) : 1 : 2\sqrt{2c+4} - c/2 - 4]$. Moreover, this last curve takes its extremum (with relation to the coordinate m) for $c = 6$. In addition, the straight line $[c : 0 : 1 : -c/2]$ corresponds to a contact of order two between these two surfaces.*

Proof. For $h = 1$, we have the system of equations

$$(\mathcal{S}_5) : c^2 - 8e + 4cm + 4m^2 = 0,$$
$$(\mathcal{S}_6) : c^2 - 8e - 2ce + e^2 + 4cm + 4em + 4m^2 = 0.$$

Solving this system we obtain:

- $e = 0$ and $m = -c/2$. This solution corresponds to the straight line $[c : 0 : 1 : -c/2]$;
- $e = 4(4+c+2\sqrt{2c+4})$ and $m = -2\sqrt{2c+4} - c/2 - 4$. This solution corresponds to the curve $[c : 4(4+c+2\sqrt{2c+4}) : 1 : -2\sqrt{2c+4} - c/2 - 4]$;
- $e = 4(4+c-2\sqrt{2c+4})$ and $m = 2\sqrt{2c+4} - c/2 - 4$. This solution corresponds to the curve $[c : 4(4+c-2\sqrt{2c+4}) : 1 : 2\sqrt{2c+4} - c/2 - 4]$.

In order to find the extremum of the curve $[c : 4(4+c-2\sqrt{2c+4}) : 1 : 2\sqrt{2c+4} - c/2 - 4]$, we equalize the last coordinate to m and compute the discriminant with respect to c of the obtained function:

$$\mathrm{Discrim}_c(4c - c^2/4 - 8m - cm - m^2) = -16(m-1),$$

whose solution is $m = 1$. Finally, solving the equation $2\sqrt{2c+4} - c/2 - 4 = m$ by substituting m by the zero of the discriminant (i.e. $m = 1$), we obtain $c = 6$, which is the extremum value of the curve with respect to m.

To prove the contact between both surfaces along the straight line $\gamma = [c : 0 : 1 : -c/2]$, we start by computing the resultant of these two surfaces with respect to c. As a result we obtain $\mathrm{Res}_c[(\mathcal{S}_5), (\mathcal{S}_6)] = e^2(e^2 + 16e(m-2) + 64m^2)$. In order to conclude the proof of this claim we apply the affine change of coordinates given by $m = -(c+2v)/2$, $v \in \mathbb{R}$. Under this transformation, the gradient vector of $(\mathcal{S}_5)$ along the curve γ is $\nabla\mathcal{S}_5(\gamma) = [0 : -8 : 1 : 0]$, whereas the gradient vector of $(\mathcal{S}_6)$ along the curve γ is $\nabla\mathcal{S}_6(\gamma) = [0 : -8 - 4c : 1 : 0]$, whose second coordinate is positive or negative, for each fixed value of the parameter c. As $\nabla\mathcal{S}_5(\gamma)$ does not change its sign, this vector will point to the same direction (or to the contrary direction, depending on the value of the parameter c) in relation to $(\mathcal{S}_6)$ restricted to the previous change of coordinates. Then, for each fixed value of the parameter c, the surface $(\mathcal{S}_6)$ remains only on one of the two topological subspaces delimited by the plane $e = 0$, and for all values of the parameter c the surface $(\mathcal{S}_5)$ remains only on one of the two topological subspaces delimited by the plane $e = 0$. ■

Lemma 4.25. *For $h \neq 0$, surfaces $(\mathcal{S}_5)$ and $(\mathcal{S}_8)$ intersect along the parabola $[c : c^2/2 : 1 : c/2]$. In addition, this parabola corresponds to a contact of order two between these two surfaces.*

Proof. For $h = 1$, we have the system of equations

$$(\mathcal{S}_5) : c^2 - 8e + 4cm + 4m^2 = 0,$$
$$(\mathcal{S}_8) : e - cm = 0.$$

Solving this system we obtain $e = c^2/2$ and $m = c/2$. This solution corresponds to the parabola $[c : c^2/2 : 1 : c/2]$.

In order to prove the contact between both surfaces along the parabola $\gamma = [c : c^2/2 : 1 : c/2]$, we start by computing the resultant of these two surfaces with respect to m. As a result we obtain $\mathrm{Res}_m[(\mathcal{S}_5), (\mathcal{S}_8)] = (c^2 - 2e)^2$. In order to conclude the proof of this claim we apply the affine change of coordinates given by $m = (c - 2v)/2$, $v \in \mathbb{R}$. Under this transformation, the gradient vector of $(\mathcal{S}_8)$ along the curve γ is $\nabla\mathcal{S}_8(\gamma) = [-c : 1 : 1 : c]$, whereas the gradient vector of $(\mathcal{S}_5)$ along the curve γ is $\nabla\mathcal{S}_5(\gamma) = [8c : -8 : 1 : -8c]$, whose second coordinate is always negative. As for each fixed value of the parameter c we have that $\nabla\mathcal{S}_8(\gamma)$ does not change its sign, this vector will always point to the opposite direction in relation to $(\mathcal{S}_5)$ restricted to the previous change of coordinates. Then, the surface $(\mathcal{S}_8)$ remains only on one of the two topological subspaces delimited by the surface $(\mathcal{S}_5)$. ■

Lemma 4.26. *For $h \neq 0$, surfaces $(\mathcal{S}_6)$ and $(\mathcal{S}_8)$ intersect along the hyperbola $[c : c^2/(c+2) : 1 : c/(c+2)]$. Moreover, this hyperbola corresponds to a contact of order two between these two surfaces.*

Proof. For $h = 1$, we have the system of equations

$$(\mathcal{S}_6) : c^2 - 8e - 2ce + e^2 + 4cm + 4em + 4m^2 = 0,$$
$$(\mathcal{S}_8) : e - cm = 0.$$

Solving this system we obtain $e = c^2/(c+2)$ and $m = c/(c+2)$. This solution corresponds to the hyperbola $[c : c^2/(c+2) : 1 : c/(c+2)]$, for $c \neq -2$. In order to prove the contact between both surfaces along the hyperbola $\gamma = [c : c^2/(c+2) : 1 : c/(c+2)]$, we start by computing the resultant of these two surfaces with respect to m. As a result we obtain $\mathrm{Res}_m[(\mathcal{S}_6), (\mathcal{S}_8)] = (c^2 - (c+2)e)^2$. In order to conclude the proof of this claim we apply the affine change of coordinates given by $m = (c - 2v - cv)/(c+2)$, $v \in \mathbb{R}, c \neq -2$. Under this transformation, the gradient vector of $(\mathcal{S}_8)$ along the curve γ is $\nabla\mathcal{S}_8(\gamma) = [-1 + 4/(c+2)^2 : 1 : 1 : c]$, whereas the gradient vector of $(\mathcal{S}_6)$ along the curve γ is $\nabla\mathcal{S}_6(\gamma) = [(8c(c+4))/(c+2)^2 : -8 : 1 : -8c]$, whose second coordinate is always negative. As for each fixed value of the parameter c we have that $\nabla\mathcal{S}_6(\gamma)$ does not change its sign, this vector will always point to the opposite direction in relation to $(\mathcal{S}_8)$ restricted to the previous change of coordinates. Then, the surface $(\mathcal{S}_6)$ remains only on one of the two topological subspaces delimited by the surface $(\mathcal{S}_8)$. ■

The purpose now is to find the slices in which the intersection among at least three surfaces or other equivalent phenomena happen. Since there are 36 distinct curves of intersections or contacts between two any surfaces, we need to study 666 different possible intersections of these surfaces. As the relation is very long, we will reproduce only a few of them deploying the different algebraic techniques used to solve them. The full set of proves can be found in the Mathematica file available at link `http://mat.uab.es/~artes/articles/qvfsn2SN11B/sn2SN11B.nb`.

Remark 4.27. In the next five lemmas we use the following notation. A curve of singularities of a surface or a curve of intersection or contact between two surfaces will be denoted by solABxC, where $A < B$ are the numbers of the surfaces involved in the intersection or contact and C is a cardinal. We point out that on such lemmas we indicate only one value of the parameter m where the respective intersection occurs, i.e. the corresponding surfaces may have intersection in other value of m. Moreover, these five lemmas illustrate how we obtain the intersection among at least three surfaces or other equivalent phenomena.

Lemma 4.28. *Surfaces $(\mathcal{S}_2)$, $(\mathcal{S}_3)$ and $(\mathcal{S}_4)$ intersect in slice when $m = 0$.*

Proof. By Lemmas 4.11 and 4.12, we have the curves sol23x1 $= [c : -c : 1 : c]$ and sol24x1 $= [0 : 0 : 1 : m]$. Equalizing each corresponding coordinate:

$$c = 0, \quad -c = 0, \quad c = m,$$

and solving the obtained system, we have the solution $c = 0, m = 0$. Since the curves are parametrized by c and m, we must substitute the solutions of the system in the expressions of the curves and consider the value of the coordinate m. Then,

$$\text{sol23x1}|_{c=0} = [0 : 0 : 1 : 0]$$

and

$$\text{sol24x1}|_{m=0} = [0 : 0 : 1 : 0],$$

implying that the value of m where the three surfaces intersect is $m = 0$. ■

Lemma 4.29. *Surfaces $(\mathcal{S}_2)$, $(\mathcal{S}_4)$ and $(\mathcal{S}_5)$ intersect in slice when $m = 3$.*

Proof. By Lemmas 4.12 and 4.13, we have the curves sol24x2 $= [-2 : 2 : 1 : m]$ and sol25x2 $= [c : -c : 1 : \sqrt{-2c} - c/2]$. Equalizing each corresponding coordinate:

$$c = -2, \quad -c = 2, \quad m = \sqrt{-2c} - c/2,$$

and solving the obtained system, we have the solution $c = -2, m = 3$. Since the curves are parametrized by c and m, we must substitute the solutions of the system in the expressions of the curves and consider the value of the coordinate m. Then,

$$\text{sol24x2}|_{m=3} = [-2 : 2 : 1 : 3]$$

and

$$\text{sol25x2}|_{c=-2} = [-2 : 2 : 1 : 3],$$

implying that the value of m where the three surfaces intersect is $m = 3$. ■

Lemma 4.30. *Surfaces $(\mathcal{S}_2)$, $(\mathcal{S}_4)$ and $(\mathcal{S}_6)$ intersect in slice when $m = -1$.*

Proof. By Lemmas 4.12 and 4.14, we have the curves sol24x3 $= [c : -c : 1 : -1]$ and sol26x1 $= [-e : e : 1 : -\sqrt{(2-e)e}]$. Equalizing each corresponding coordinate:

$$c = -e, \quad -c = e, \quad -\sqrt{(2-e)e} = -1,$$

and solving the obtained system, we have the solution $c = -1, e = 1$. Since the curves are parametrized by c and e, we must substitute the solutions of the system in the expressions of the curves and consider the value of the coordinate m. Then,

$$\text{sol24x3}|_{c=-1} = [-1 : 1 : 1 : -1]$$

and

$$\text{sol26x1}|_{e=1} = [-1 : 1 : 1 : -1],$$

implying that the value of m where the three surfaces intersect is $m = -1$. ■

Lemma 4.31. *Surfaces $(\mathcal{S}_3)$, $(\mathcal{S}_4)$ and $(\mathcal{S}_5)$ intersect in slice when $m = -4$.*

Proof. By Lemmas 4.17 and 4.18, we have the curves sol35x1 $= [c : 2(2 + c + 2\sqrt{c+1}) : 1 : -2(\sqrt{c+1} + 1) - c/2]$ and sol45x1 $= [0 : m^2/2 : 1 : m]$. Equalizing each corresponding coordinate:

$$c = 0, \quad m^2/2 = 2(2 + c + 2\sqrt{c+1}),$$

and

$$m = -2(\sqrt{c+1} + 1) - c/2,$$

and solving the obtained system, we have the solution $c = 0, m = -4$. Since the curves are parametrized by c and m, we must substitute the solutions of the system in the expressions of the curves and consider the value of the coordinate m. Then,

$$\text{sol35x1}|_{c=0} = [0 : 8 : 1 : -4]$$

and

$$\text{sol45x1}|_{m=-4} = [0 : 8 : 1 : -4],$$

implying that the value of m where the three surfaces intersect is $m = -4$. ■

Lemma 4.32. *Surfaces $(\mathcal{S}_4)$, $(\mathcal{S}_5)$ and $(\mathcal{S}_6)$ intersect in slice when $m = 1$.*

Proof. By Lemmas 4.21 and 4.22, we have the curves sol45x3 $= [c : 0 : 1 : -c/2]$ and sol46x3 $= [-2 : e : 1 : 1 - e/2]$. Equalizing each corresponding coordinate:

$$c = -2, \quad e = 0, \quad -c/2 = 1 - e/2,$$

and solving the obtained system, we have the solution $c = -2, e = 0$. Since the curves are parametrized by c and e, we must substitute the solutions of the system in the expressions of the curves and consider the value of the coordinate m. Then,

$$\text{sol45x3}|_{c=-2} = [-2 : 0 : 1 : 1]$$

and

$$\text{sol46x3}|_{e=0} = [-2 : 0 : 1 : 1],$$

implying that the value of m where the three surfaces intersect is $m = 1$. ■

The next result presents all the algebraic values of m corresponding to singular slices in the bifurcation diagram. Its proof follows from Remark 4.2, Lemmas 4.28 to 4.32 and by computing all the remaining different possible intersections, singularities or contacts among three or more surfaces.

Lemma 4.33. *The full set of needed algebraic singular slices in the bifurcation diagram of family* $\mathbf{QsnSN_{11}(B)}$ *is formed by* 18 *elements which correspond to the values of* m *in* (9)*. These elements indicate the* 17 *finite slices plus the infinite one.*

$$
\begin{aligned}
&m_1 = +\infty,\ m_3 = 3,\ m_5 = 1,\ m_7 = \frac{1}{2},\ m_{13} = 0,\\
&m_{15} = \frac{1}{2}\left(2\sqrt{2} - 3\right),\ m_{17} = -\frac{1}{2},\ m_{21} = -\frac{8}{9},\\
&m_{23} = -\frac{24}{25},\ m_{25} = -1,\ m_{35} = -\frac{5}{4},\ m_{37} = -\frac{3}{2},\\
&m_{39} = -2,\ m_{41} = \frac{1}{2}\left(-2\sqrt{2} - 3\right),\ m_{43} = -3,\\
&m_{45} = -4,\ m_{47} = -\frac{21}{5},\ m_{53} = -8.
\end{aligned}
\tag{9}
$$

The numeration in (9) is not consecutive since we reserve numbers for other slices not algebraically determined and for generic slices.

Now we sum up the content of the previous lemmas. In (9) we list all the algebraic values of m where significant phenomena occur for the bifurcation diagram generated by singularities. We first have the two extreme values for m, i.e. $m = +\infty$ (corresponding to $h = 0$) and $m = -8$. We remark that to perform the bifurcation diagram of all singularities for $m = +\infty$ we set $h = 0$ and, in the remaining three variables (c, e, m), yielding the point $[c : e : m]$ in $\mathbb{RP}^2$, we take the chart $m \neq 0$ in which we may assume $m = 1$.

In order to determine all the parts generated by the bifurcation surfaces from $(\mathcal{S}_2)$ to $(\mathcal{S}_{10})$, we first draw the horizontal slices of the three–dimensional parameter space which correspond to the explicit values of m obtained in Lemma 4.33. However, as it will be discussed later, the presence of nonalgebraic bifurcation surfaces will be detected and the singular slices corresponding to their singular behavior as we move from slice to slice will be approximately determined. We add to each interval of singular values of m an intermediate value for which we represent the bifurcation diagram of singularities. The diagram will remain essentially unchanged in these open intervals except the parts affected by the bifurcation. All the sufficient values of m are shown in (10).

The values indexed by positive odd indices in (10) correspond to explicit values of m for which there is a bifurcation in the behavior of the systems on the slices. Those indexed by even values are just intermediate points which are necessary to the coherence of the bifurcation diagram.

$$
\begin{array}{ll}
m_1 = +\infty & m_{28} = -1 - \varepsilon_7\\
m_2 = 4 & m_{29} = -1 - \varepsilon_7^*\\
m_3 = 3 & m_{30} = -1 - \varepsilon_8\\
m_4 = 2 & m_{31} = -1 - \varepsilon_8^*\\
m_5 = 1 & m_{32} = -1 - \varepsilon_9\\
m_6 = 3/4 & m_{33} = -1 - \varepsilon_9^*\\
m_7 = 1/2 & m_{34} = -1 - \varepsilon_{10}\\
m_8 = 1/2 - \varepsilon_1 & m_{35} = -5/4\\
m_9 = 1/2 - \varepsilon_1^* & m_{36} = -13/10\\
m_{10} = 1/2 - \varepsilon_2 & m_{37} = -3/2\\
m_{11} = 1/2 - \varepsilon_2^* & m_{38} = -7/4\\
m_{12} = 1/2 - \varepsilon_3 & m_{39} = -2\\
m_{13} = 0 & m_{40} = -5/2\\
m_{14} = -5/100 & m_{41} = (-2\sqrt{2} - 3)/2\\
m_{15} = (2\sqrt{2} - 3)/2 & m_{42} = -295/100\\
m_{16} = -1/4 & m_{43} = -3\\
m_{17} = -1/2 & m_{44} = -7/2\\
m_{18} = -1/2 - \varepsilon_4 & m_{45} = -4\\
m_{19} = -1/2 - \varepsilon_4^* & m_{46} = -4 - \varepsilon_{11}\\
m_{20} = -1/2 - \varepsilon_5 & m_{47} = -21/5\\
m_{21} = -8/9 & m_{48} = -21/5 - \varepsilon_{12}\\
m_{22} = -9/10 & m_{49} = -21/5 - \varepsilon_{12}^*\\
m_{23} = -24/25 & m_{50} = -21/5 - \varepsilon_{13}\\
m_{24} = -98/100 & m_{51} = -21/5 - \varepsilon_{13}^*\\
m_{25} = -1 & m_{52} = -21/5 - \varepsilon_{14}\\
m_{26} = -1 - \varepsilon_6 & m_{53} = -8\\
m_{27} = -1 - \varepsilon_6^* & m_{54} = -10
\end{array}
\tag{10}
$$

Due to the presence of many branches of nonalgebraic bifurcation surfaces, we cannot point out exactly neither predict the concrete value of m where the changes in the parameter space happen. Thus, with the purpose to set an order for these changes in the parameter space, we introduce the following notation. If the bifurcation happens between two concrete values of m, then we add or subtract a sufficiently small positive value ε_i or ε_j^* to/from a concrete value of m; this concrete value of m (which is a reference value) can be any of the two values that define the range where the non–concrete values of m are inserted. The representation ε_i means that the m_i refers to a generic slice, whereas ε_j^* means that the m_j refers to a singular slice. Moreover, considering the values ε_i, ε_i^*, ε_{i+1} and ε_{i+1}^*, it means that $\varepsilon_i < \varepsilon_i^* < \varepsilon_{i+1} < \varepsilon_{i+1}^*$ meanwhile they belong to the same interval determined by algebraic bifurcations.

We now begin the analysis of the bifurcation diagram by studying completely one generic slice

and after by moving from slice to slice and explaining all the changes that occur. As an exact drawing of the curves produced by intersecting the surfaces with the slices gives us very small parts which are difficult to distinguish, and points of tangency are almost impossible to recognize, we have produced topologically equivalent figures where parts are enlarged and tangencies are easy to observe.

The reader may find the exact pictures of the 17 finite singular slices (containing only the algebraic surfaces) described in (9) in a PDF file available at the link `http://mat.uab.es/~artes/articles/qvfsn2SN11B/sn2SN11B.pdf`.

We now describe the labels used for each part of the bifurcation space. As we have mentioned in Remark 1.5, the subsets of dimensions 3, 2, 1 and 0, of the partition of the parameter space will be denoted respectively by V, S, L and P for Volume, Surface, Line and Point, respectively. The surfaces are named using a number which corresponds to each bifurcation surface which is placed on the left side of the letter S. To describe the portion of the surface we place an index. The curves that are intersection of surfaces are named by using their corresponding numbers on the left side of the letter L, separated by a point. To describe the segment of the curve we place an index. Volumes and Points are simply indexed (since three or more surfaces may be involved in such an intersection).

We consider an example: surface $(\mathcal{S}_2)$ splits into 20 different two–dimensional parts labeled from $2S_1$ to $2S_{20}$, plus some one–dimensional arcs labeled as $2.iL_j$ (where i denotes the other surface intersected by $(\mathcal{S}_2)$ and j is a number), and some zero–dimensional parts. In order to simplify the labels in all figures we see **V1** which stands for the TEX notation V_1. Analogously, **2S1** (respectively, **2.3L1**) stands for $2S_1$ (respectively, $2.3L_1$), see Fig. 16, for example.

In Fig. 14 we represent the generic slice of the parameter space when $m = m_2 = 4$, showing only the algebraic surfaces. We note that there are some dashed branches of surface $(\mathcal{S}_3)$ (in yellow) and $(\mathcal{S}_4)$ (in purple). This means the existence of a weak saddle, in the case of surface $(\mathcal{S}_3)$, and the existence of an invariant straight line without separatrix connection, in the case of surface $(\mathcal{S}_4)$; they do not mean a topological change in the phase portraits but a C^∞ change. In the next figures we will use the same representation for these characteristics of these two surfaces.

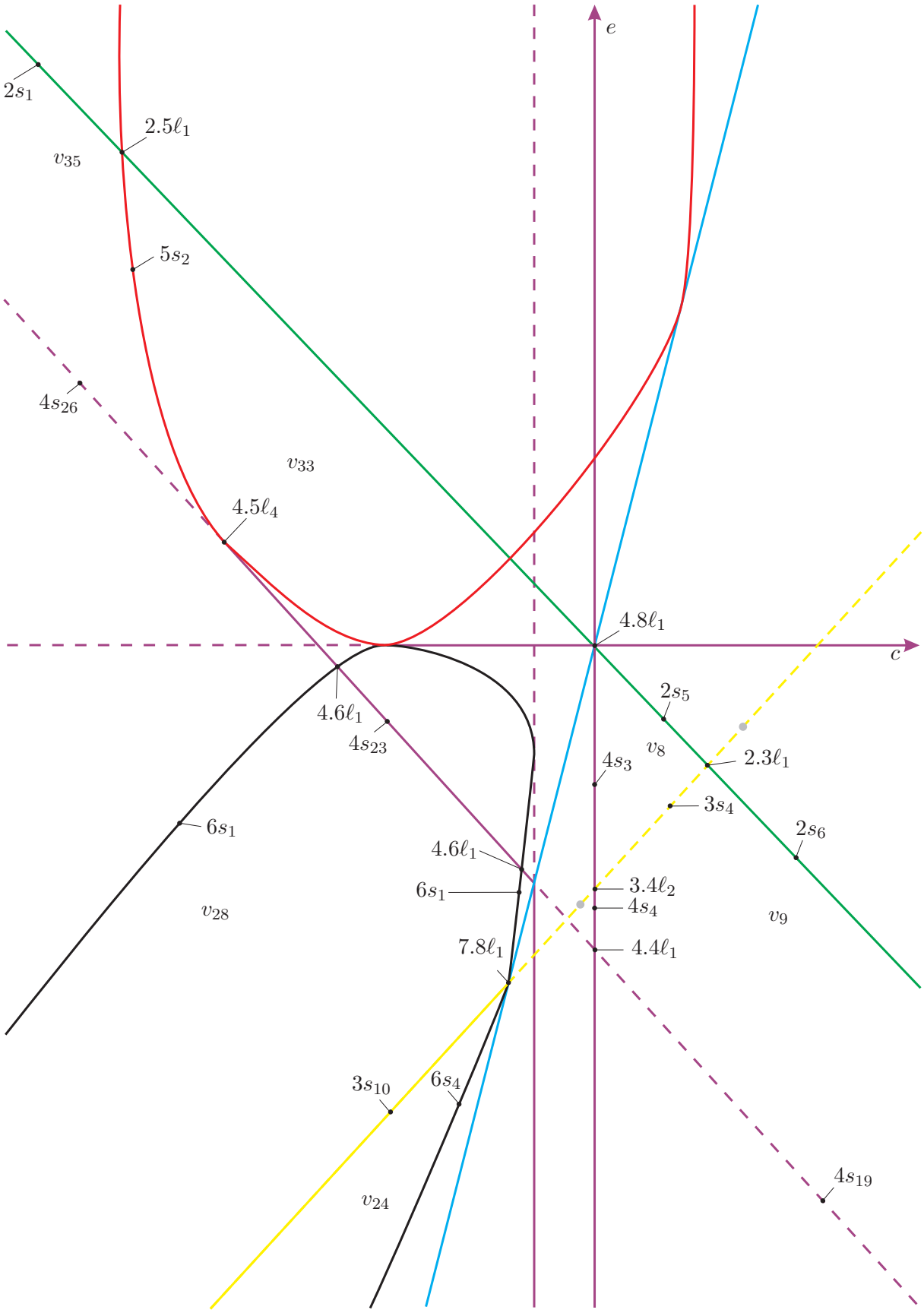

Fig. 14. Slice of parameter space when $m = 4$ (only algebraic surfaces)

We also point out that the gray dots that appear in surface $(\mathcal{S}_3)$ indicate weak singularities of order two or higher, according to Remarks 4.2 and 4.3.

With the purpose to explain all the changes in the bifurcation diagram, we would have to present two versions of the picture of each slice: one of them without labels and the other with labels in each new part (as it was done, for instance, in [Artés *et al.*, 2013b] and [Artés *et al.*, 2014]).

However, as the number of slices is considerably large (see equation (10) – 54 slices to be more precise) we would have to present 108 pictures, which would occupy a large number of pages. Then, we will present only the labeled drawings (just the "important part" in each slice) containing the algebraic and nonalgebraic bifurcation surfaces. In the next section, we prove the existence of such nonalgebraic surfaces and their necessity for the coherence of the bifurcation diagram.

Remark 4.34. Wherever two parts of equal dimension d are separated only by a part of dimension $d-1$ of the black bifurcation surface $(\mathcal{S}_6)$, their respective phase portraits are topologically equivalent since the only difference between them is that a finite antisaddle has turned into a focus without change of stability and without appearance of limit cycles. We denote such parts with different labels, but we do not give specific phase portraits in pictures attached to Theorem 1.1 for the parts with the focus. We only give portraits for the parts with nodes, except in the case of existence of a limit cycle or a graphic where the singular point inside them is portrayed as a focus. Neither do we give specific invariant description in Sec. 6 distinguishing between these nodes and foci.

4.2. Bifurcation surfaces due to connections (nonalgebraic) in the affine part of $\mathbb{RP}^3$

We start this section explaining the generic slice when $m=4$ presented in Fig. 14. In this slice we will make a complete study of all its parts, whereas in the next slices we will only describe the changes. Some singular slices will produce only few changes which are easy to describe, but others can produce simultaneously many changes, even a complete change of all parts and these will need a more detailed description.

As said in last section, in Fig. 14 we present the slice when $m=4$ with only the algebraic surfaces. We now place for each set of the partition on this slice the local behavior of the flow around the singular points. For a specific value of the parameters of each one of the sets in this partition we compute the global phase portrait with the numerical program P4 [Artés *et al.*, 2005, Dumortier *et al.*, 2006].

In this slice we have a partition in two–dimensional parts bordered by curved polygons, some of them bounded, others bordered by infinity. From now on, we use lower–case letters provisionally to describe the sets found algebraically in order to do not interfere with the final partition described with capital letters.

For each two–dimensional part we obtain a phase portrait which is coherent with those of all their borders. Except four parts, which are shown in Fig. 14 and named as follows:

- v_8: the triangle bordered by green, purple and yellow curves;
- v_9: the pentagon bordered by green, yellow and purple curves and infinity;
- v_{28}: the curved pentagon bordered by black, purple and yellow curves and infinity;
- v_{35}: curved quadrilateral bordered by green, red and purple curves and infinity.

The study of these parts is quite important for the coherence of the bifurcation diagram. That is why we have decided to present only these parts in Fig. 14.

We begin with the analysis of the parts v_8 and v_9. First we consider part v_8. If we are sufficiently close to part $2s_5$, the respective phase portrait is topologically equivalent to the one in V_8, because in $2s_5$ we have the phase portrait topologically equivalent to $2S_5$, see Fig. 2. However, on $4s_3$, the separatrix of the infinite saddle–node connects with a separatrix of the finite saddle–node producing an invariant straight line linking the pair of infinite saddle–nodes. When perturbing this straight line by entering part v_8, this connection is broken and the separatrix of the infinite saddle–node connects to the infinite stable node and the separatrix of the finite saddle–node connects with the infinite unstable node, leading to a phase portrait topologically

different from V_8. This proves that the region v_8 must be split into at least two connected regions. On the other hand, on $2s_5$ the phase portrait possesses a cusp point and all the canonical regions in its corresponding phase portrait are topologically the same as in phase portrait V_8, except for the *infinite basin* involving the finite saddle–node which became the cusp point. By a *basin* we understand a region bordered by two separatrices of one same singularity which have the same limit–object, most commonly, they end at an infinite singularity and we call it an *infinite basin* or they end at a finite singularity and we call it a *finite basin*.

As we have concluded that we have at least two different phase portraits inside region v_8, there must exist at least one element $7S_1$ of surface $(\mathcal{S}_7)$ dividing part v_8 into two "new" parts, V_8 and V_{10}, which represents a bifurcation due to the connection between a separatrix of a finite saddle–node with a separatrix of a finite saddle. It is worth mentioning that the segment $3s_4$ refers to the presence of weak saddle which shows that the movement from v_8 to v_9 does not imply a topological change. Then, part v_9 must also be divided into V_9 and V_{11} by an element $7S_2$ of surface $(\mathcal{S}_7)$ with the same bifurcation as $7S_1$. In fact, $7S_2$ is clearly a "continuation" of $7S_1$. Coupled with this idea, we have parametrized the yellow surface, "walked" on it and found that there is a topological change in the obtained phase portraits.

Then, $7S_1$ has one of its endpoints on $3s_4$ (dividing it into $3S_4$ and $3S_5$) and Lemma 4.35 assures that the other endpoint is $4.8\ell_1$.

We show the sequence of phase portraits along these subsets in Fig. 15. We also draw the complete bifurcation diagram for these two parts in Fig. 16.

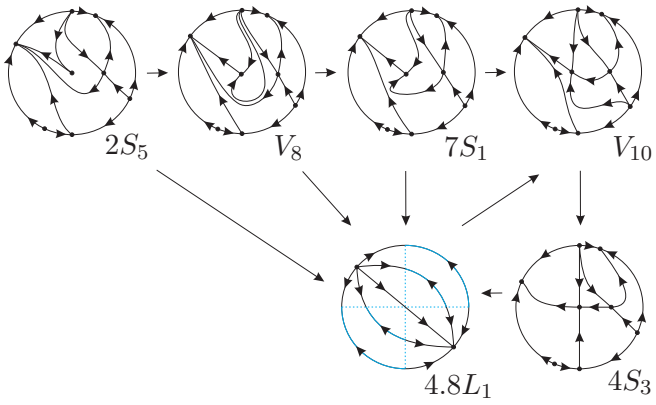

Fig. 15. Sequence of phase portraits in parts v_8 and v_9 of slice $m = 4$ (the labels are according to Fig. 16). We start from v_8. We recall that the phase portrait $3S_4$ (respectively, $3.7L_1$ and $3S_5$) is equivalent to the phase portrait V_8 (respectively, $7S_1$ and V_{10}) up to a weak saddle. If we start on $2s_5$ we can reach V_{10} by the path $2S_5 \to 4.8L_1 \to V_{10}$. When crossing $2s_5$, we shall obtain the phase portrait V_8 in a subset of v_8. From this point we may choose three different ways to reach the subset V_{10} by crossing the purple surface: (1) from the phase portrait $3.7L_1$ to the V_{10}; (2) from the phase portrait $7S_1$ to the V_{10}; and (3) from the degenerate phase portrait $4.8L_1$ to the V_{10}. Now, from v_9, when crossing $2s_6$ (topologically equivalent to $2s_5$), we shall obtain the phase portrait V_9 (topologically equivalent to V_8) in a subset of v_9. From this point we may choose two different ways to reach the subset V_{11} (topologically equivalent to V_{10}) by crossing the purple surface: (1) from the phase portrait $3.7L_1$ to the V_{11} or (2) from the phase portrait $7S_2$ (topologically equivalent to $7S_1$) to the V_{11}

Lemma 4.35. *The endpoint of* $7S_1$ *(rather than the one which is on* $3s_4$*) is* $4.8\ell_1$*. Moreover,* $7S_2$ *is not bounded.*

Proof. Numerical tools show that the endpoint of $7S_1$, rather than the one which is on $3s_4$, is $4.8\ell_1$. In what follows, we prove that this endpoint cannot be on segments $4s_3$ and $2s_5$. Moreover, $7S_2$ is not bounded.

If this endpoint was located on $4s_3$, as we said before, there must exist a connection between a separatrix of a finite saddle–node with a separatrix of a finite saddle. Then, in this case, the invariant line would be broken in order to make this bifurcation to happen.

We point out that the endpoint of $7S_1$ also cannot be located on $2s_5$, since $7S_1$ describes a connection between a separatrix of a finite saddle with a separatrix of a finite saddle–node and this separatrix (of the saddle–node) disappears when on $2s_5$ the finite saddle–node becomes a cusp–type singularity.

Therefore, as the endpoint of $7S_1$ is neither on $4s_3$ nor on $2s_5$, this confirms the evidence pointed out by the numerical calculations that $7S_1$ ends at $4.8\ell_1$.

Moreover, as we know that on $4s_{19}$ there is no invariant straight line that produces a topological change, it is not relevant whether $7S_2$ crosses $4s_{19}$ or not. ■

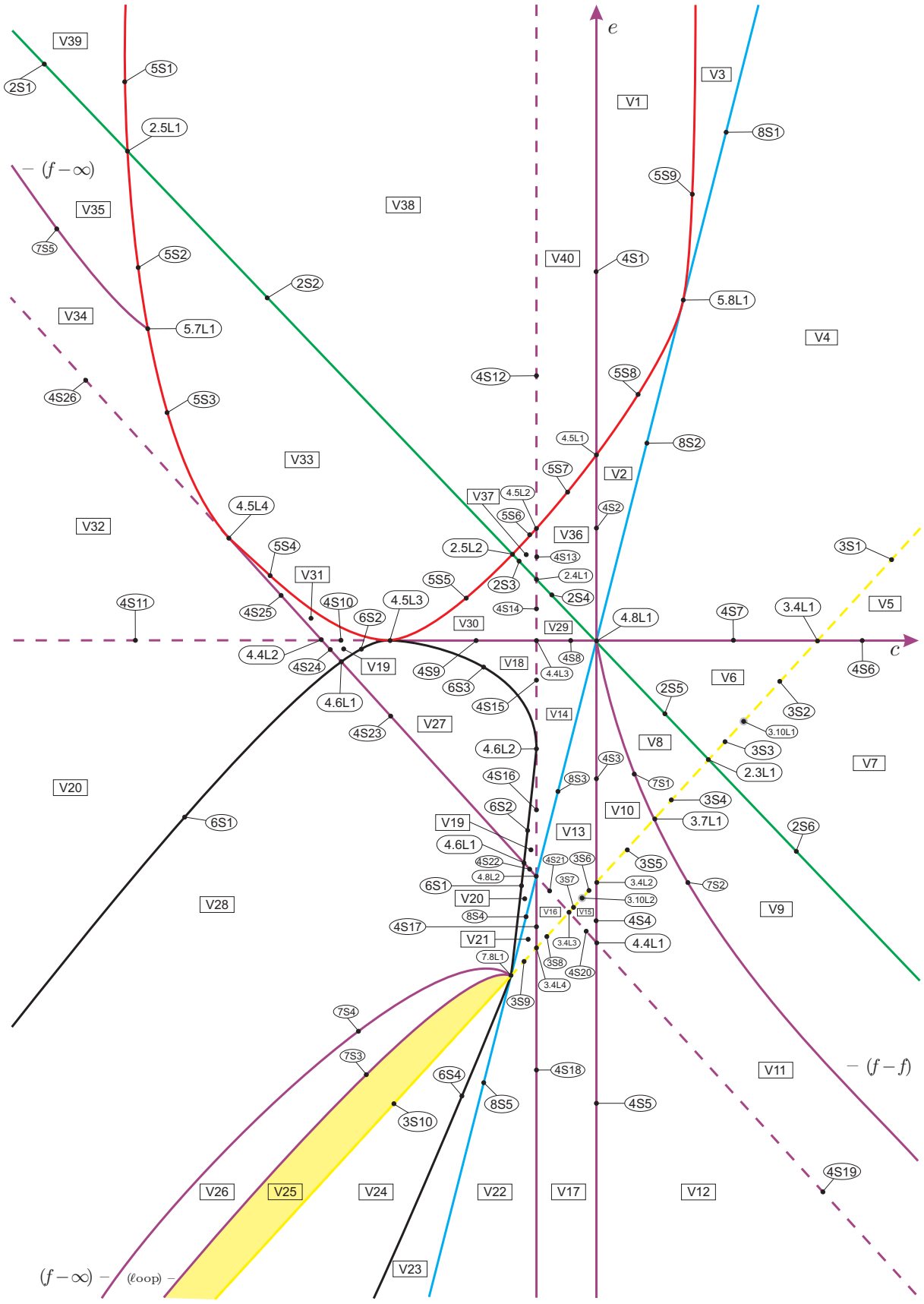

Fig. 16. Complete bifurcation diagram for slice $m = 4$

We have added in the bifurcation diagram a label associated to each part of the bifurcation $(\mathcal{S}_7)$ indicating the type of connection produced by this bifurcation. The possibilities are "(ℓoop)", "(f–f)" (for a connection between different finite singularities), "(f–∞)" (for a connection between a finite singularity and an infinite one), and "(∞–∞)" (for a connection between different infinite singularities). These labels are indicated only in the first time that the corresponding nonalgebraic bifurcation is detected.

We now perform the study of part v_{28}. We consider the segment $3s_{10}$ in Fig. 14, which is one of the borders of part v_{28}. Analogously, on this segment, the corresponding phase portrait possesses a weak focus (of order one) and, consequently, this branch of surface $(\mathcal{S}_3)$ corresponds to a Hopf bifurcation. This means that either in v_{24} or in v_{28} we must have a limit cycle; in fact it is in v_{28}.

However, when we get close to $6s_1$ and $4s_{23}$, the limit cycle has been lost, which implies the existence of at least one more element of surface $(\mathcal{S}_7)$ (see $7S_3$ in Fig. 16) in a neighborhood of $3s_{10}$; furthermore, the phase portrait in a small neighborhood of $6s_1$ (respectively, $4s_{23}$) is not coherent to that obtained just after making disappear the limit cycle. If we fix a value of the parameter c in order to be in this part and we make the parameter e increase from $3s_{10}$ towards $4s_{23}$, then we obtain generically three topologically distinct phase portraits inside part v_{28}, which implies the existence of not only one but at least two elements of surface $(\mathcal{S}_7)$, namely, $7S_3$ and $7S_4$ in Fig. 16. Such new phase portraits are V_{25}, with limit cycle, V_{26} and V_{28}, without limit cycles (see Fig. 17 for a sequence of phase portraits in these parts). Even though parts V_{26} and V_{28} have no limit cycles, they provide topologically distinct phase portraits since the connection of separatrices on $7S_4$ is due to the saddle–node $\binom{1}{1} SN$ and the finite saddle–node, i.e. connection of separatrices from different points, whereas the connection on $7S_3$ is due to a saddle–node to itself (i.e. a loop–type connection). In Lemma 4.36 we show that $7S_3$ and $7S_4$ have one of its ends at the curve $7.8\ell_1$ and, in addition, they are not bounded. We plot the complete bifurcation diagram for these two parts in Fig. 16.

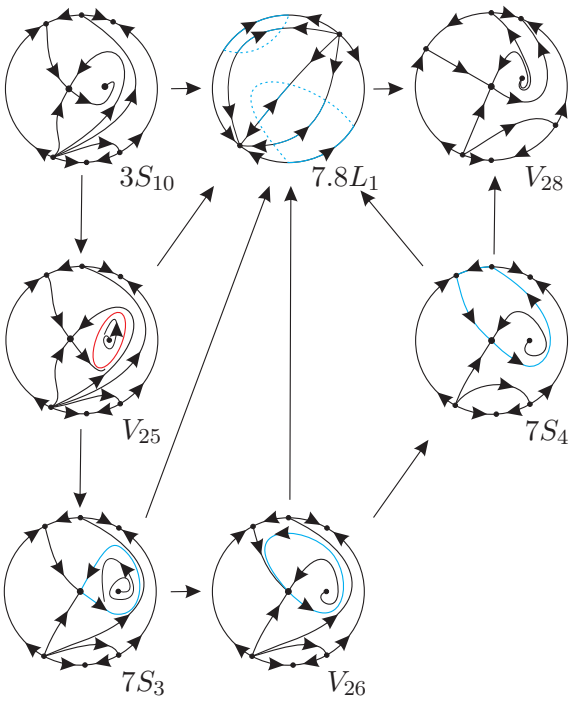

Fig. 17. Sequence of phase portraits in part v_{28} of slice $m = 4$ (the labels are according to Fig. 16). By starting on $3s_{10}$ we can reach V_{28} by the path $3S_{10} \to 7.8L_1 \to V_{28}$. Now, when crossing $3s_{10}$, we shall obtain phase portrait V_{25} (with limit cycle) in a subset of v_{28}. From this point we may choose at least five different ways to reach the phase portrait of the region V_{28}: (1) $V_{25} \to 7.8L_1 \to V_{28}$; (2) $V_{25} \to 7S_3 \to 7.8L_1 \to V_{28}$; (3) $V_{25} \to 7S_3 \to V_{26} \to 7.8L_1 \to V_{28}$; (4) $V_{25} \to 7S_3 \to V_{26} \to 7S_4 \to 7.8L_1 \to V_{28}$; and (5) $V_{25} \to 7S_3 \to V_{26} \to 7S_4 \to V_{28}$

Lemma 4.36. *One of the endpoints of $7S_3$ and $7S_4$ is $7.8\ell_1$. Moreover, $7S_3$ and $7S_4$ are not bounded.*

Proof. Numerical analysis suggest that surfaces $7S_3$ and $7S_4$, which corresponds to a loop–type bifurcation and finite–infinite separatrix connection, respectively, have one of its ends on the curve $7.8\ell_1$. Indeed, if the starting point of any of these surfaces is any point of $3s_{10}$, then a portion of this subset must not refer to a Hopf bifurcation, which contradicts the fact that on $3s_{10}$ we have a weak focus of order one. On the other hand, we observe that it is not possible that the starting point of these surfaces is on $6s_1$, since on black surfaces we have only a C^∞ node–focus bifurcation. In fact, this can happen only if surface $(\mathcal{S}_6)$ intersects other surfaces like $(\mathcal{S}_3)$ and $(\mathcal{S}_8)$. Moreover, the endpoint of $7S_3$

and $7S_4$ cannot be on $4s_{23}$ because, in order to have this, in any case, first we need to break the invariant straight line. Then, the only possible endpoint of surfaces $7S_3$ and $7S_4$ is $7.8\ell_1$. Using the same arguments we can conclude that such surfaces are not bounded. ■

Now, we carry out the analysis of part v_{35}. The phase portrait in v_{35} near $2s_1$ possesses a finite basin passing through the finite saddle–node, i.e. two separatrices of the finite saddle–node start at the same finite antisaddle, whereas the phase portrait in v_{35} near $4s_{26}$ does not possess the finite basin. Then, there must exist at least one element $7S_5$ of surface $(\mathcal{S}_7)$ dividing part v_{35} into two "new" parts, V_{34} and V_{35}, which represents a bifurcation due to the connection between a separatrix of a finite saddle–node with a separatrix of an infinite saddle (see Fig. 18 for a sequence of phase portraits in these parts). As the segment $5s_2$ corresponds to changes in the infinite singular points, the finite part of the phase portraits remains unchanged and this element of surface $(\mathcal{S}_7)$ must intersect $5s_2$ having this intersection point as one of its endpoints, since in v_{33} we have only one infinite singularity, namely, the infinite saddle–node. With these arguments we have parametrized the red surface, "walked" on it and found that there is a topological change in the phase portraits obtained. In Lemma 4.37 we prove that $7S_5$ is unbounded and it has $5.7\ell_1$ as endpoint. We plot the complete bifurcation diagram for these two parts in Fig. 16.

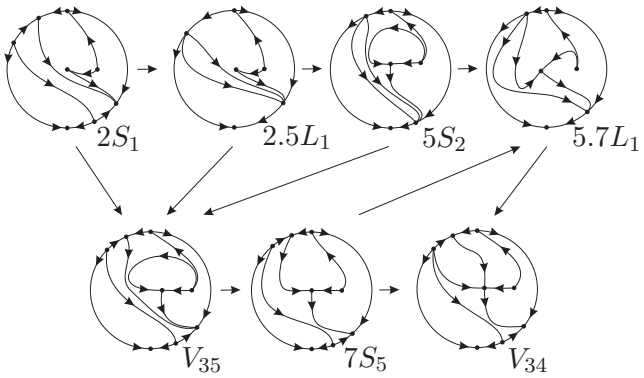

Fig. 18. Sequence of phase portraits in part v_{35} of slice $m = 4$ (the labels are according to Fig. 16). By starting on $2s_1$ we can reach V_{34} by one of the following paths: (1) $2S_1 \to 2.5L_1 \to 5S_2 \to 5.7L_1 \to V_{34}$; (2) $2S_1 \to 2.5L_1 \to 5S_2 \to V_{35} \to 7S_5 \to V_{34}$; (3) $2S_1 \to 2.5L_1 \to 5S_2 \to V_{35} \to 7S_5 \to 5.7L_1 \to V_{34}$; (4) $2S_1 \to 2.5L_1 \to V_{35} \to 7S_5 \to V_{34}$; and (5) $2S_1 \to V_{35} \to 7S_5 \to V_{34}$

Lemma 4.37. *The element $7S_5$ of surface $(\mathcal{S}_7)$ is unbounded and it has $5.7\ell_1$ as endpoint.*

Proof. Numerical tools indicate that one of the endpoints of $7S_5$ is $5.7\ell_1$. In what follows, we prove that it cannot be on $4s_{26}$ and $2s_1$.
In fact, as $4s_{26}$ represents the existence of an invariant line which does not indicate a topological change, it cannot contain an endpoint of $7S_5$, unless there is a degenerate portion of $4s_{26}$ where this endpoint is located. Moreover, as on $2s_1$ the finite saddle–node already has become a cusp–type singularity, we do not have a finite saddle–node in order to perform the topological changes given by $7S_5$. Then, $7S_5$ must intersect the red surface. In fact, its endpoint is $5.7\ell_1$ because in v_{33} we do not have the necessary number of infinite singularities in such a way that the bifurcations given by $7S_5$ could happen.
Therefore, we confirm the evidence pointed out by the numerical calculations that $7S_5$ has $5.7\ell_1$ as an endpoint. By the same arguments we conclude that such a surface is unbounded. ■

Having analyzed all the parts pointed out on page 33 and explained the existence of all possible nonalgebraic surfaces in there (modulo islands), we have finished the study of the generic slice $m = 4$. However, we cannot be sure that these are all the additional bifurcation surfaces in this slice. There could exist others which are closed surfaces small enough to escape our numerical research. For all other two–dimensional parts of the partition of this slice, whenever we join two points which are close to different borders of the part, the two phase portraits are topologically equivalent. So, we do not encounter more situations than the ones mentioned above. In short, it is expected that the complete bifurcation diagram for $m = 4$ is the one shown in Fig. 16. In this and the next figures, we have colored in light yellow the open regions with one limit cycle, in black the labels referring to new parts which are created in a slice and in red the labels corresponding to parts which has already appeared in previous slices.

We already know that there are no more geometrical singular slices for $m > 3$. We have to

prove also that there are no other significant non-algebraic slices for $m \geq 4$. In order to do this we must describe the slice at infinity, which correspond to the case $h = 0$ and $m = 1$. By studying and describing all the phase portraits in these slices and finding coherence in continuity between the phase portraits on the infinite slice and the slice $m = 4$, we will have proved that we do not need more singular slices. In the limit to infinity, the bifurcation diagram (of the algebraic surfaces) tends to be the one shown in Fig. 19.

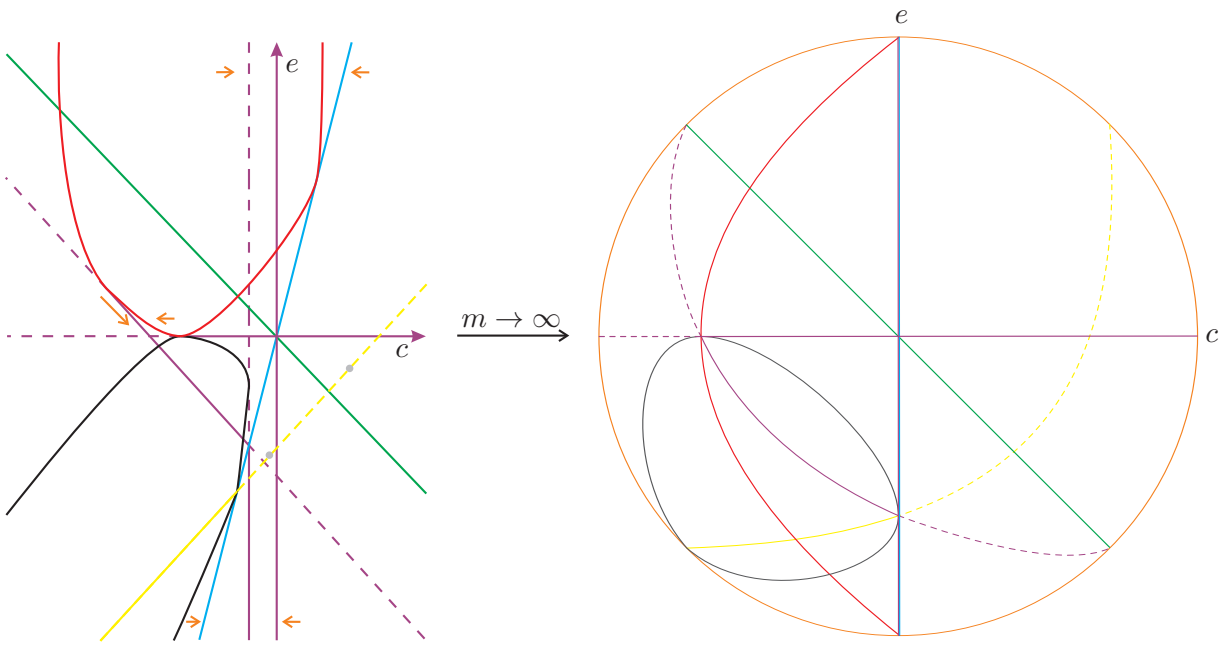

Fig. 19. The transition from $m > 4$ to infinity. The orange arrows show the movement that the surfaces must do as $m \to \infty$

4.3. Bifurcation surfaces at the infinite part of $\mathbb{RP}^3$

In order to make this transition (or convergence) clearer, we need to describe the algebraic curves which appear in the slice $m = +\infty$. In fact, as we said before, the slice $m = +\infty$ is obtained by considering $h = 0$ and $m = 1$ in the normal form (5), which becomes

$$\begin{aligned} \dot{x} &= cx + cy - cx^2, \\ \dot{y} &= ex + ey - ex^2 + 2xy. \end{aligned} \tag{11}$$

In this way, according to the definition of surfaces $(\mathcal{S}_2)$ to $(\mathcal{S}_{10})$ we observe that, under these conditions of the parameters h and m, we have:

- surface $(\mathcal{S}_2)$ remains the same;
- surface $(\mathcal{S}_3)$ needs to be redefined since now we have $\mathcal{T}_i = 0, i = 1, \ldots, 4$;
- surface $(\mathcal{S}_4)$ reduces to $ce(c + e + 2) = 0$;
- surfaces $(\mathcal{S}_5)$ and $(\mathcal{S}_6)$ must also be redefined since now we have $\eta = W_4 = 0$, respectively;
- two–point set $(\mathcal{S}_{6.2})$ does not make sense here, since $G_9 = 0$; and
- surface $(\mathcal{S}_8)$ reduces to $c = 0$.

Then, we must define surfaces $(\mathcal{S}_3)$, $(\mathcal{S}_5)$ and $(\mathcal{S}_6)$ in terms of others nonzero invariants (or comitants) which represent the same geometrical meaning as those ones that were vanished.

The curve at slice $m = +\infty$ of C^∞ bifurcation due to a strong saddle or a strong focus changing the sign of their traces (weak saddle or weak focus)

$(\mathcal{S}_3')$ This is the bifurcation surface due to finite weak singularities, which occurs when the trace of a finite singular point is zero. Calculations yield

$$\mathcal{T}_4 = \mathcal{T}_3 = \mathcal{T}_2 = \mathcal{T}_1 = 0, \quad \sigma = c + e + 2x(1 - c) \neq 0.$$

According to [Vulpe, 2011], Main Theorem, item (e), under the above conditions, systems (5) could possess one and only one weak singularity. Moreover these systems have one weak singularity, which is of the type indicated below if and only if one of the following conditions holds:

- $s^{(1)} \Leftrightarrow \mathcal{F}_1 \neq 0, \mathcal{H} = \mathcal{B}_1 = 0, \mathcal{B}_2 > 0$;
- $f^{(1)} \Leftrightarrow \mathcal{F}_1 \neq 0, \mathcal{H} = \mathcal{B}_1 = 0, \mathcal{B}_2 < 0$.

Therefore, for $h = 0$ and $m = 1$ systems (5) do not have weak singularities of order two or higher. Moreover, under these conditions we have:

$$\begin{aligned} &\mathcal{F}_1 = -2c^2(c + 3e + 2), \quad \mathcal{H} = 0, \\ &\mathcal{B}_1 = 2c^2(c + e)^2(c - e - 2), \\ &\mathcal{B}_2 = -2c^3(c + e)(c - 3e - 4)(c - 1)^2. \end{aligned}$$

According to the Main Theorem just mentioned, if the conditions $\mathcal{F}_1 \neq 0$ and $\mathcal{B}_1 = 0$ imply $\mathcal{B}_2 \neq 0$, then we have a weak focus or a weak saddle. In fact, the condition $\mathcal{B}_1 = 0$ implies $c = e + 2$ and the condition $\mathcal{F}_1 \neq 0$ implies $c \neq 0$ and $c + 3e + 2 \neq 0$ (i.e. $e + 1 \neq 0$). So, from the expression of $\mathcal{B}_2$ we have

$$c - 3e - 4 = -2(e + 1) \neq 0.$$

Therefore, in the slice $m = +\infty$ we define surface $(\mathcal{S}_3')$ by the equation of the straight line

$$(\mathcal{S}_3') \colon c - e - 2 = 0.$$

The bifurcation curve in slice $m = +\infty$ due to multiplicities of infinite singularities

$(\mathcal{S}_5')$ This is the bifurcation surface due to multiplicity of infinite singularities. As we said before, under the conditions $h = 0$ and $m = 1$ we have that $\eta = 0$. Then, we already have that two infinite singularities have coalesced. In order to detect when we have a triple infinite singularity, we calculate

$$\widetilde{M} = -8(c + 2)^2x^2, \quad C_2 = x^2(ex - y(2 + c)).$$

According to Lemma 5.5 from [Artés *et al.*, 2021], a triple infinite singularity occurs if and only if $\widetilde{M} = 0$ and $C_2 \neq 0$. Therefore, in the slice $m = +\infty$ we have a coalescence of infinite singularities on the straight line

$$(\mathcal{S}_5') \colon c + 2 = 0.$$

In fact, this argument shows the reason why we have drawn a red straight line instead of a parabola in Fig. 19.
On the other hand, according to the mentioned Lemma, if $(c, e) = (-2, 0)$, then the line at infinity is filled up with singularities, since $C_2 = 0$.

The curve in slice $m = +\infty$ of C^∞ bifurcation due to a node becoming a focus

$(\mathcal{S}_6')$ This surface will contain the points of the parameter space where a finite node of the systems turns into a focus. This surface is a C^∞ but not a topological bifurcation surface. In fact, when we only cross surface $(\mathcal{S}_6')$ in the bifurcation diagram, the topological phase portraits do not change. However, as in the affine part of $\mathbb{RP}^3$, this surface is relevant for isolating the regions where a limit cycle surrounding an antisaddle cannot exist. Using the results of [Artés *et al.*, 2008, Artés *et al.*, 2021], as we have (under the conditions $h = 0$ and $m = 1$) $G_9 = W_4 = 0$, we must consider the invariant $W_7 = 0$, which defines

$$(\mathcal{S}_6')\colon c^2 - 2c(e-2) + (e+2)^2 = 0,$$

that is, a parabola.

Since these curves have the same geometrical meaning as those previous ones that became zero, we keep the respective colors for these curves as we have described before.

Another bifurcation algebraic curve which play an important role in this slice is the following one.

Bifurcation algebraic curve in the slice $m = +\infty$ due to the presence of an infinite nilpotent singularity of type $\widehat{\binom{1}{2}}E - H$

$(\mathcal{L}_0)$ For $h = 0$ and $m = 1$, the corresponding phase portraits on the line $c + 1 = 0$ in the bifurcation diagram possess an infinite singularity of the type $\widehat{\binom{1}{2}}E - H$, which is the transition between the singularities $\widehat{\binom{1}{2}}\,PEP - H$ and $\widehat{\binom{1}{2}}\,E - PHP$. Such a straight line is needed for the coherence of the bifurcation diagram. In fact, according to [Artés *et al.*, 2021] we know that the comitant $\widetilde{N}$ is related to a triple infinite singularity and such a comitant only makes sense in the slices where such a kind of singularity appears, i.e. in the slices where we do not have a triple infinite singularity this comitant does not influence at all. Moreover, $\widetilde{N}$ "works like" $\mathcal{T}_4$, in the sense that the curve $\widetilde{N} = 0$ splits the parameter space into two distinct canonical regions and the phase portrait over $\widetilde{N} = 0$ is topologically equivalent to the phase portrait in one of its sides and topologically distinct to the one in the other side. In such a way we need to determine the points on the parameter space that verifies the equation $\widetilde{N} = 0$. Calculations yield

$$\widetilde{N} = -4(c+1)x^2.$$

It is clear that the straight line $c + 1 = 0$ verifies this equation. Therefore we define the curve $(\mathcal{L}_0)$ by the equation

$$(\mathcal{L}_0)\colon c + 1 = 0,$$

and we draw such a straight line with the brown color.

In order to determine the endpoints of each one of these curves, we take the respective projective equation with homogeneous coordinates C, E and M, we put $M = 0$ and then we calculate the roots of the resulting polynomial.

As in slice $m = +\infty$ we are in a surface, in fact the upper half–sphere $\mathbb{S}^2$, we point out that all the "generic" parts in this slice are labeled as $9S_j$, the lines are labeled as $9.iL_j$ and the points as points. We use the orange color for the equator of $\mathbb{S}^2$, i.e. $h = m = 0$.

We now have finished describing the algebraic curves that appear at slice $m = +\infty$. In Fig. 20 we present this slice completely and properly labeled. We draw special attention to the fact that the nonalgebraic curves (numerically detected and which existence was proved before) still remain in this slice and they maintain the same relative positions with respect to the algebraic curves in the transition from slice $m = 4$ to slice $m = +\infty$, numerical tools support this claim.

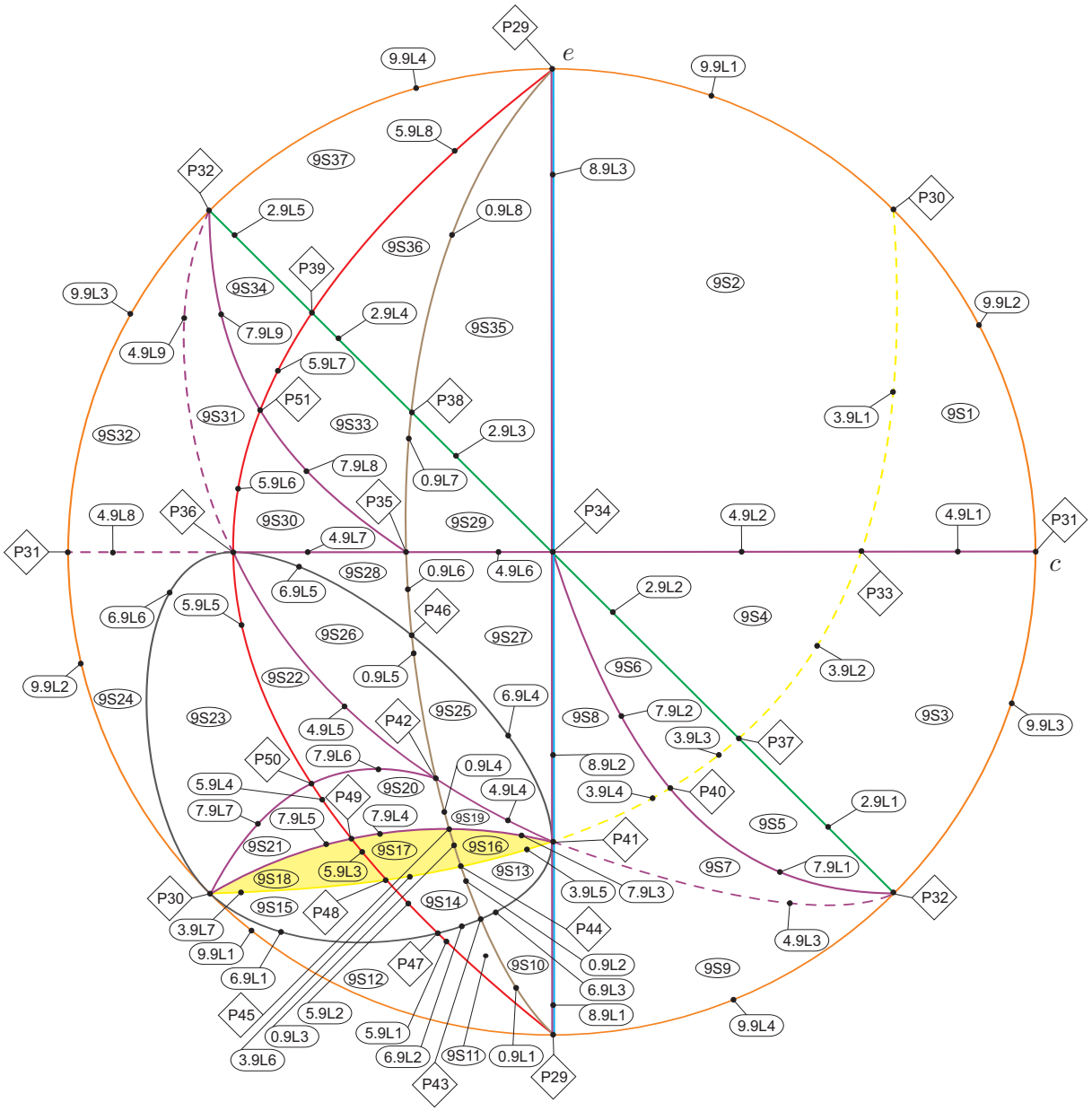

Fig. 20. Slice of parameter space when $m = +\infty$

There are some relevant facts on the bifurcation diagram that are worth to be remarked. On one side we already have the curve ($\mathcal{L}_0$) which has topological relevance only on $h = 0$, as we already have described. Moreover, we also have that surface ($\mathcal{S}_5$) which is a parabola in the affine slices degenerates as a double line when $h = 0$. This degeneration apart from collapsing some parts of the bifurcation diagram, introduces a new bifurcation in some other parts where before it did not exist. Such bifurcations also will be relevant for large negative values of m. Even more, we also have surface ($\mathcal{S}_7$) which in slice $m = 4$, its part $7S_5$ splits V_{34} from V_{35}, but it does not affect part V_{33} neither V_{30}. However, at infinity, after the collapse of the parabola ($\mathcal{S}_5$) the border of region V_{30} on $h = 0$ is also splited into two because of $7.9L_8$. The difference between the topological behavior in $9S_{30}$ and $9S_{33}$ deals with the existence of separatrices of an elliptic–saddle at infinity. This allows the possibility of a separatrix connection between one of this separatrices and a separatrix of the finite saddle–node. Since the elliptic–saddle does not exist for $h = 1$ this bifurcation loses all the sense in the affine space. Since we have detected the two possible bifurcations from the separatrix connection implied by $7.9L_8$, we then prove its existence. See all the respective phase portraits in Figs. 1 to 7. These are the reasons why some three–dimensional parts of the affine space which have their border on $h = 0$ split in several two–dimensional regions (plus the corresponding one–dimensional borders).

In Table 3 we indicate the "death" of all volumetric parts from slice $m = 4$ to $m = +\infty$. Then we have established the correspondence between the phase portraits of the slices $m = 4$ and $m = +\infty$. Therefore, the convergence presented in Fig. 19 is coherent.

Table 3. Transition from slice $m = 4$ to $m = +\infty$. Here we present the correspondence between the volumetric regions from slice $m = 4$ and the respective parts from slice $m = +\infty$

Parts in slice $m = 4$	Parts in slice $m = +\infty$	Parts in slice $m = 4$	Parts in slice $m = +\infty$
V_1	$8.9L_3$	V_{21}	P_{41}
V_2	$8.9L_3$	V_{22}	$8.9L_1$
V_3	$8.9L_3$	V_{23}	$9S_{10}$, $9S_{11}$, $9S_{12}$
V_4	$9S_2$	V_{24}	$9S_{13}$, $9S_{14}$, $9S_{15}$
V_5	$9S_1$	V_{25}	$9S_{16}$, $9S_{17}$, $9S_{18}$
V_6	$9S_4$	V_{26}	$9S_{19}$, $9S_{20}$, $9S_{21}$
V_7	$9S_3$	V_{27}	$9S_{25}$, $9S_{26}$
V_8	$9S_6$	V_{28}	$9S_{22}$, $9S_{23}$
V_9	$9S_5$	V_{29}	P_{34}
V_{10}	$9S_8$	V_{30}	$9S_{29}$, $9S_{30}$, $9S_{33}$
V_{11}	$9S_7$	V_{31}	P_{36}
V_{12}	$9S_9$	V_{32}	$9S_{32}$
V_{13}	$8.9L_2$	V_{33}	$5.9L_6$, $5.9L_7$, P_{51}
V_{14}	$8.9L_2$	V_{34}	$9S_{31}$
V_{15}	P_{41}	V_{35}	$9S_{34}$
V_{16}	P_{41}	V_{36}	$8.9L_3$
V_{17}	$8.9L_1$	V_{37}	$9S_{35}$, $9S_{36}$
V_{18}	$9S_{27}$, $9S_{28}$	V_{38}	$5.9L_8$
V_{19}	P_{36}, P_{41}	V_{39}	$9S_{37}$
V_{20}	$9S_{24}$, P_{41}	V_{40}	$8.9L_3$

4.4. Transition from slice to slice in the affine part of $\mathbb{RP}^3$

Since there is coherence (modulo islands, as discussed in Sec. 5) between the slices $m = +\infty$ and $m = 4$, no more slices $m > 4$ are needed.

Having finished the complete study of slice $m = 4$ and having presented the transition from $m = 4$ to $m = +\infty$, the next step is to decrease the values of m, according to equation (10), and make an analogous study for each one of the slices that we need to consider and also search for changes when going from one slice to the next one.

We now start decreasing the values of the parameter m in order to explain as much as we can the bifurcations in the parameter space.

We consider the curved triangle V_{37} in the second quadrant of slice $m = 4$ (see Fig. 16), having $2.4L_1$ as a vertex. As we move down from $m = 4$ to $m = 3$ (a singular slice), this triangle collapses to a single point, which we denote by P_1 in Fig. 21.

When we go to the next generic slice, $m = 2$, we observe that from this P_1 a new curved triangle V_{41} was born, "pushing to the right" the old curved triangle V_{36}, as we can see in Fig. 22.

Now, studying the singular slice $m = 1$ we observe the following phenomena (compare Figs. 16 and 23):

- the curve $4.5L_3$ of the red parabola coalesces with $4.4L_3$ (see Fig. 16) and also with $4.5L_5$ (see Fig. 22), forming the point P_2 presented in Fig. 23. This movement makes region V_{30} vanishes;

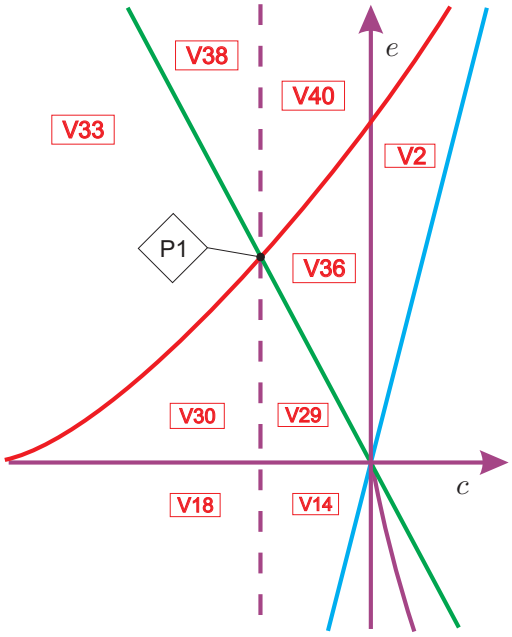

Fig. 21. Slice of parameter space when $m = 3$ (see Fig. 16)

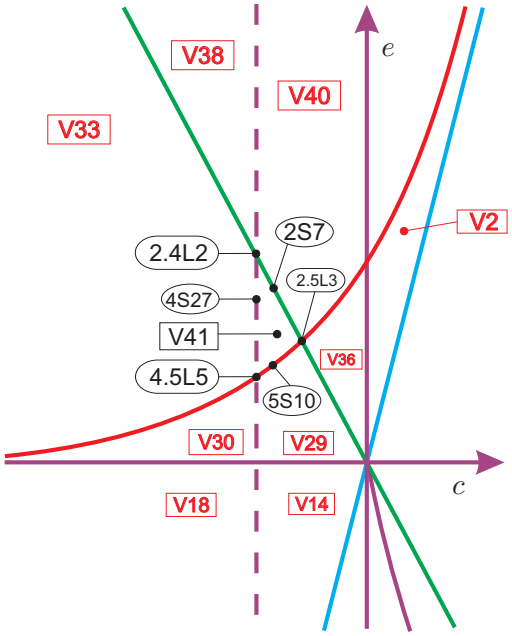

Fig. 22. Slice of parameter space when $m = 2$ (see Fig. 21)

- the black parabola degenerates and becomes a double straight line, which is now parallel to the yellow straight line and it still intersects the red parabola at P_2 (this fact was expected by the shape of the black surface shown in Fig. 13);
- the cyan straight line is parallel to the black and yellow surfaces.

Having in mind all these movements together, we observe from Fig. 16 that it is clear that the regions $V_{30}, V_{18}, V_{27}, V_{28}, V_{24}, V_{25}$ and V_{26} must vanish. As we now have that the black, cyan and yellow surfaces intersect at infinity (because they are parallel), in particular the nonalgebraic surfaces $7S_3$ and $7S_4$ "have gone" to infinity of the third quadrant of the bifurcation diagram. In fact, later we will detect that they will "return" at the first quadrant of the next generic slice, $m = 3/4$. Moreover, the appearance of the black surface as a double straight line splits each one of the regions V_1, V_3, V_{40} and V_{41} into two regions each, which are separated in this slice but which are continuous in the three–dimensional space. So they received the same label. About the respective borders, we will indicate (in black color) only those containing the black straight line, since the others already have been defined previously and they were not "modified" by the presence of the black straight line. In addition, we observe that the nonalgebraic surfaces $7S_1$, $7S_2$ and $7S_5$ still remain in this slice. As in this slice we detect significant changes in the bifurcation diagram, in Fig. 23 we present one picture that gives a global idea of the bifurcation diagram when $m = 1$.

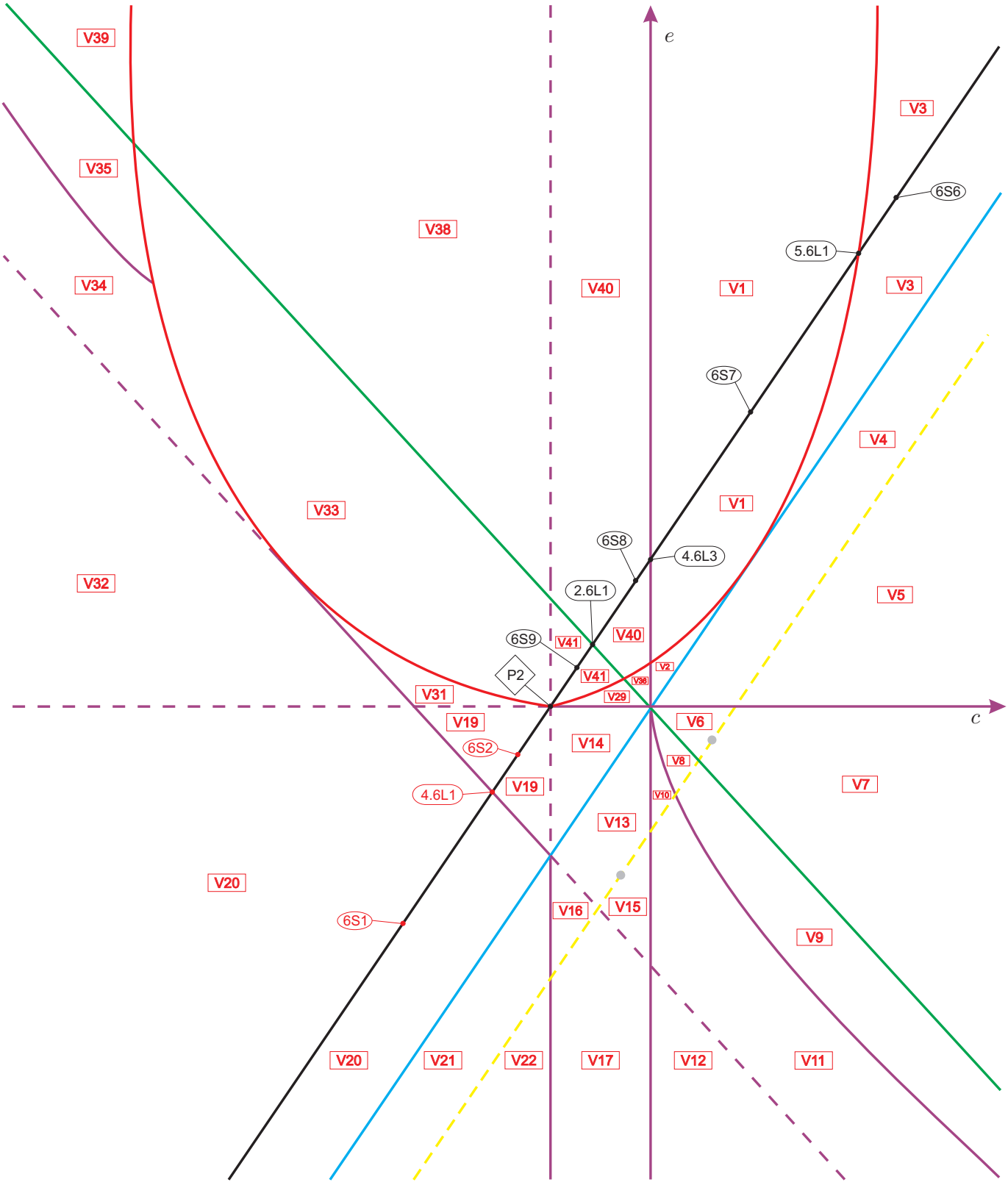

Fig. 23. Slice of parameter space when $m = 1$ (see Fig. 22)

Going on with the study of the slices, we pass to the study of the generic slice $m = 3/4$, see Fig. 26. This is a very interesting slice. Here we observe that the black straight line again has become a parabola, now in the semi–positive plane (in fact, this was expected by Fig. 13). Such a parabola generates six new volume regions, namely, v_{44} to v_{48} plus v_{51} (see Fig. 25). This is implied by the fact that as in the slice $m = 4$, one of its branches intersects the cyan and the yellow straight line in a point, namely, $7.8L_1$. Because of this triple intersection there must exist the new volume regions v_{48} and v_{51}, see Fig. 25. We have denoted them in lower case and we have produced a gap in the numeration because we detect that some new nonalgebraic surface will be needed, producing new volume regions.

Performing an analysis of this slice we note that the nonalgebraic surfaces $7S_1$, $7S_2$ and $7S_5$ remain. In addition, for each two–dimensional part we obtain a phase portrait which is coherent with those of all their borders. Except for the part v_{48} (the curved triangle bordered by the black, yellow and infinite line in Fig. 25), which corresponds to part V_{48} in Fig. 26, which as we will see, will be split into several regions. Consider the segment $3s_{11}$ in Fig. 25, which is one of the borders of part v_{48}. On this segment the corresponding phase portrait possesses a weak focus (of order one) and, consequently, this branch of surface $(\mathcal{S}_3)$ corresponds to a Hopf bifurcation. This means that either in v_{47} or in v_{48} we must have a limit cycle; in fact it is in v_{48}. However, approaching $6s_5$, the limit cycle has been lost, which implies the existence of at least one more element of surface $(\mathcal{S}_7)$ (surface $7S_6$ in Fig. 26) in a neighborhood of surface $3S_{11}$; furthermore, the phase portrait in a small neighborhood of $6s_5$ is not coherent to that one obtained just after making disappear the limit cycle. If we fix a value of the parameter c in order to be in this part and we make the parameter e decrease from $3s_{11}$ towards $6s_5$, then we obtain three topologically distinct phase portraits inside part v_{48}, which implies the existence of not only one but at least two elements of surface $(\mathcal{S}_7)$, the surfaces $7S_6$ and $7S_7$ in Fig. 26; such new phase portraits are V_{48}, with limit cycle, V_{49} and V_{50}, without limit cycles (see Fig. 24 for a sequence of phase portraits in these parts). Even though parts V_{49} and V_{50} have no limit cycles, they provide topologically distinct phase portraits since the connection on $7S_6$ is due to a saddle–node to itself (i.e. a loop–type connection), whereas the connection of separatrices on $7S_7$ is due to the finite saddle–node and the infinite saddle, i.e. connection of separatrices from different points. In Lemma 4.38 we show that $7S_6$ and $7S_7$ have one of its ends at the point $7.8\ell_2$ and, in addition, they are not bounded. We plot the complete bifurcation diagram for these two parts in Fig. 26.

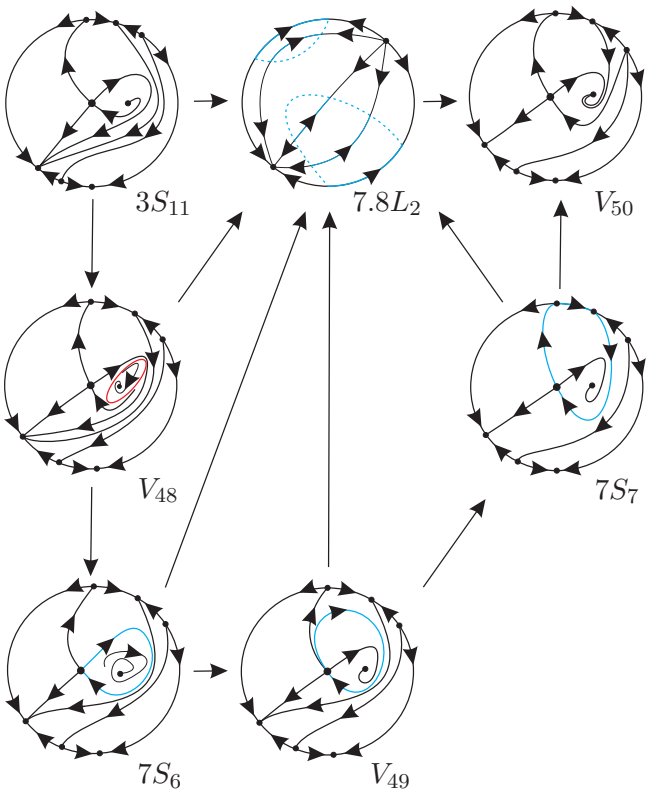

Fig. 24. Sequence of phase portraits in part v_{48} of slice $m = 3/4$ (the labels are according to Fig. 26). By starting on $3s_{11}$ we can reach region V_{50} by the path $3S_{11} \to 7.8L_2 \to V_{50}$. Now, when crossing $3s_{11}$, we shall obtain the phase portrait V_{48} (containing a limit cycle) in a subset of v_{48}. From this point we may choose five different ways to reach the subset V_{50}: (1) $V_{48} \to 7.8L_2 \to V_{50}$; (2) $V_{48} \to 7S_6 \to 7.8L_2 \to V_{50}$; (3) $V_{48} \to 7S_6 \to V_{49} \to 7.8L_2 \to V_{50}$; (4) $V_{48} \to 7S_6 \to V_{49} \to 7S_7 \to 7.8L_2 \to V_{50}$; and (5) $V_{48} \to 7S_6 \to V_{49} \to 7S_7 \to V_{50}$

Lemma 4.38. *One of the endpoints of $7S_6$ and $7S_7$ is $7.8\ell_2$. Moreover, $7S_6$ and $7S_7$ are not bounded.*

Proof. We proceed exactly as in the proof of Lemma

4.36. In fact, numerical analysis suggests that $7S_6$ and $7S_7$, which corresponds to a loop–type bifurcation and a finite–infinite separatrix connection, respectively, have one of its ends in the curve $7.8\ell_2$. Indeed, if the starting point of any of these surfaces were any point of segment $3s_{11}$, then a portion of this subset must not refer to a Hopf bifurcation, which contradicts the fact that on $3s_{11}$ we have a weak focus of order one. On the other hand, we observe that it is not possible that the starting point of these surfaces be on $6s_5$, since on black surfaces we only have a C^∞ node–focus bifurcation. In fact, this could happen unless we have a degenerate portion of black surface in which these surfaces would start. Then, the only possible endpoint of surfaces $7S_6$ and $7S_7$ is $7.8\ell_2$. Using the same arguments we can conclude that such surfaces are not bounded. ■

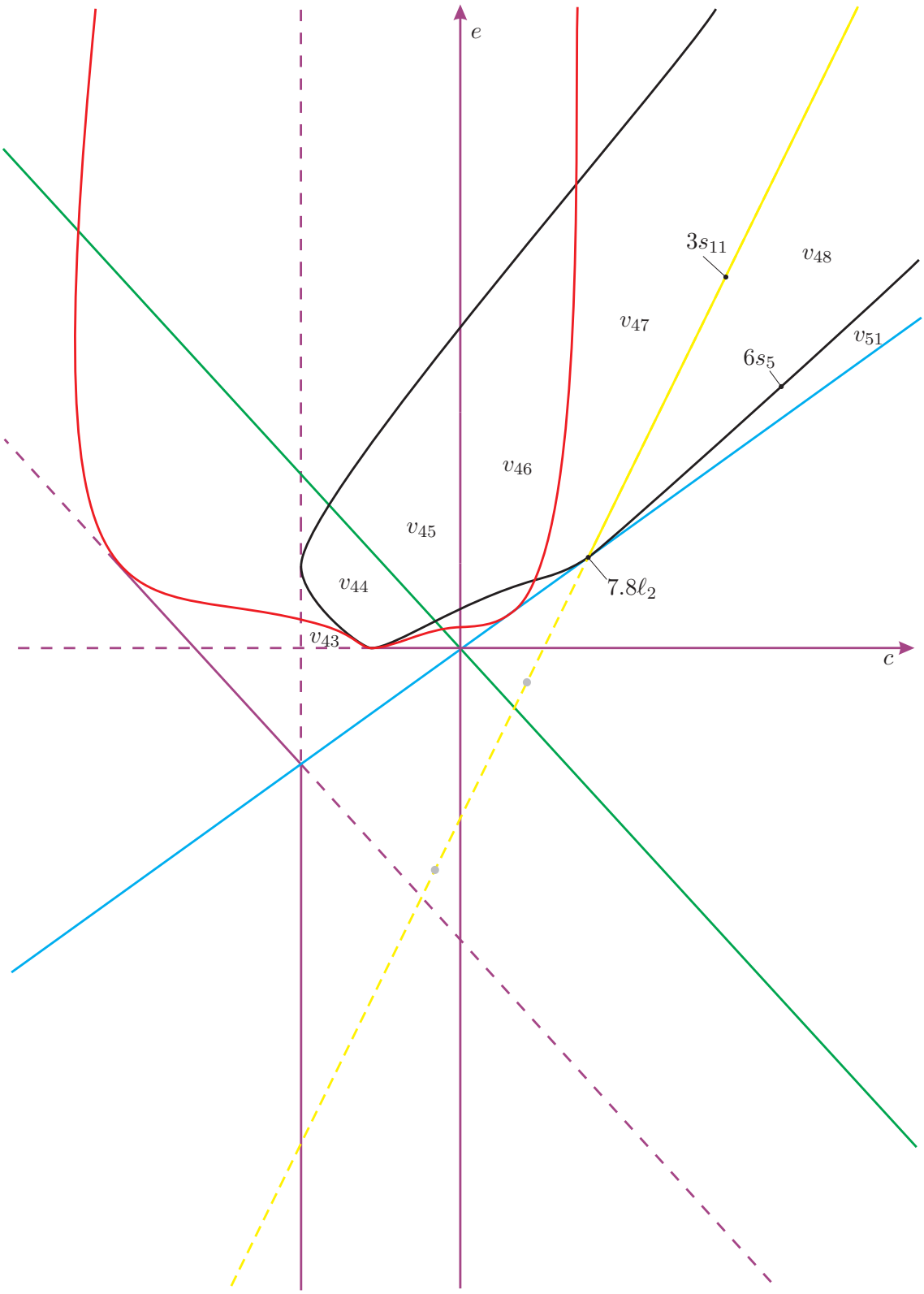

Fig. 25. Slice of parameter space when $m = 3/4$ (only algebraic surfaces)

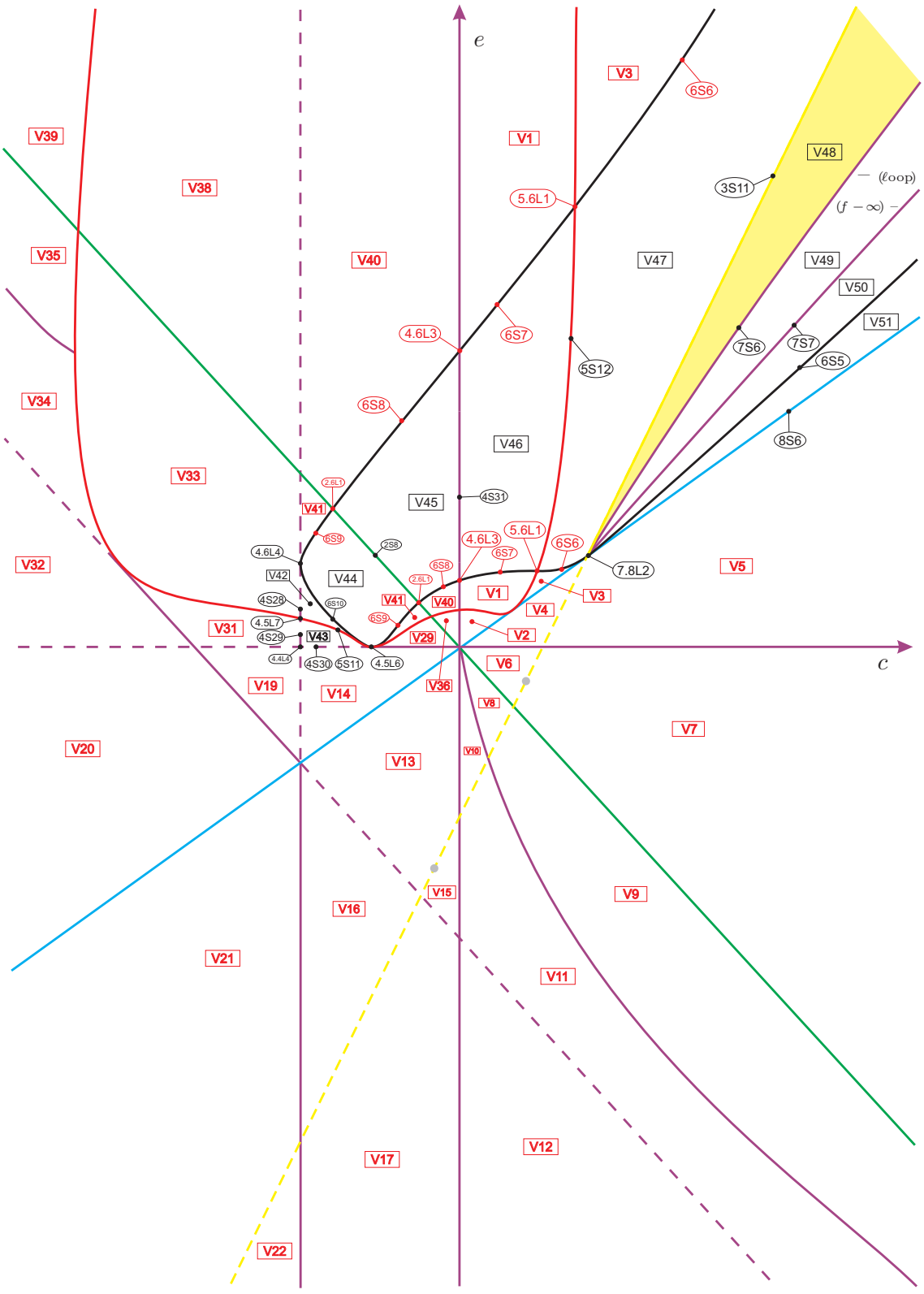

Fig. 26. Slice of parameter space when $m = 3/4$ (see Fig. 23)

The regions V_{44} to V_{47} do not bring any new topologically distinct phase portrait since all of them border already known phase portraits by a node–focus bifurcation. Also the borders $2S_8$, $4S_{31}$ and $5S_{12}$ are already known phase portraits. In fact, the only new phase portraits discovered in this slice are those ones in Fig. 24.

We will follow the list of slices presented in (10) and now we study the singular slice $m = 1/2$. Here we observe the existence of a contact point between the red parabola and the yellow straight line. We denote this contact by $3.5L_1$, see Fig. 27. In fact, for $m = 1/2$ this is the only significant change in the bifurcation diagram.

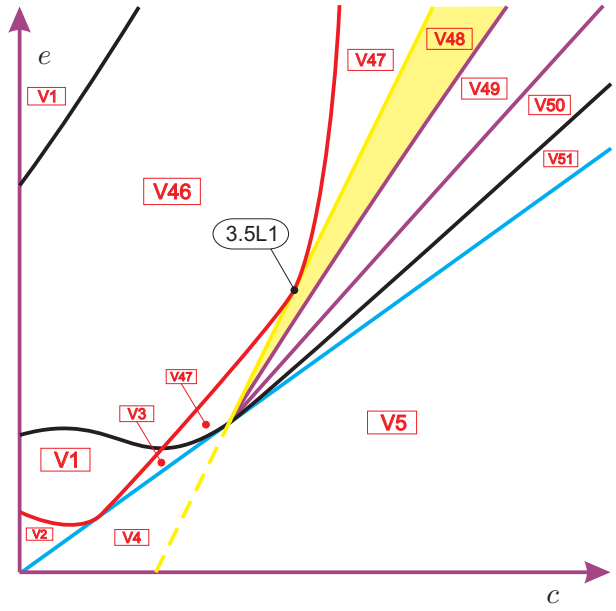

Fig. 27. Slice of parameter space when $m = 1/2$ (see Fig. 26)

Now, when we move down from $m = 1/2$ we observe that, from values of m less than but very close to $1/2$ the red parabola "keeps moving" and making $3.5L_1$ to generate a new volume region. Such a region has a semi–circumference shape and we denote it by V_{52}, see Fig. 28. As we have already proved, there are two elements of surface $(\mathcal{S}_7)$ in region V_{48} (which now contains V_{52}) and after numerical analysis for values of m less than $1/2$, but very close to it, we still verify the same changes in the phase portraits as shown in the sequence in Fig. 24. We also verify that it does not occur any topological change in the phase portrait described by $5S_{13}$. These arguments allow us to conclude that the red parabola has "crossed" the yellow straight line, but it did not touch the purple surface $7S_6$.

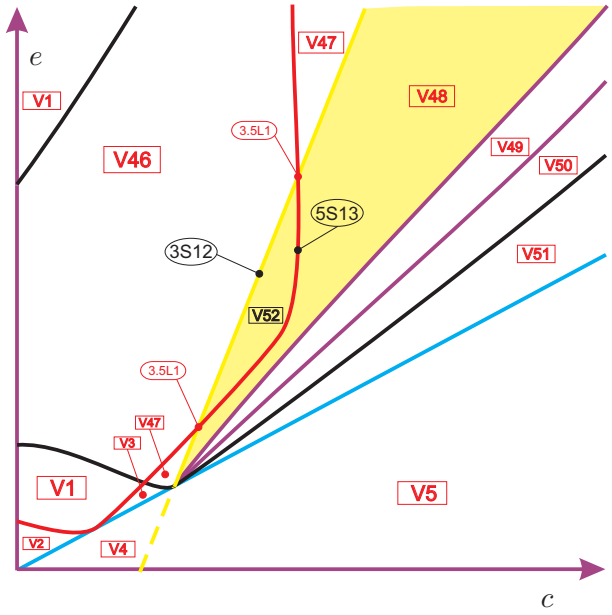

Fig. 28. Slice of parameter space when $m = 1/2 - \varepsilon_1$ (see Fig. 27)

In order to obtain a coherence of the bifurcation diagram, having in mind the presence of two nonalgebraic surfaces in region V_{48}, we did a careful study of this region. After having obtained the last generic slice, numerical analysis suggest that the red parabola, for a smaller and close value of m, must touch surface $7S_6$ in a curve, namely, $5.7L_2$, as in Fig. 29.

Going further with our numerical analysis, we observe that after decreasing a little bit the values of m, a new volume region V_{53} appears, limited by the two surfaces which are $5S_{14}$ and $7S_8$ and the curve $5.7L_2$ (as always the representation that we see in figures are one–dimensional less). Surface $5S_{14}$ splits region V_{49} from V_{53} and surface $7S_8$ splits the region V_{52} from V_{53}, see Fig. 30.

We point out that our numerical analysis is a valid argument, since we have the coherence of the obtained phase portraits.

For a better comprehension of the graphics producing limit cycles in perturbations, in Fig. 31 we present an amplification of the neighborhood in the parameter space of the curve $5.7L_2$ (see Fig. 30) with the corresponding phase portraits.

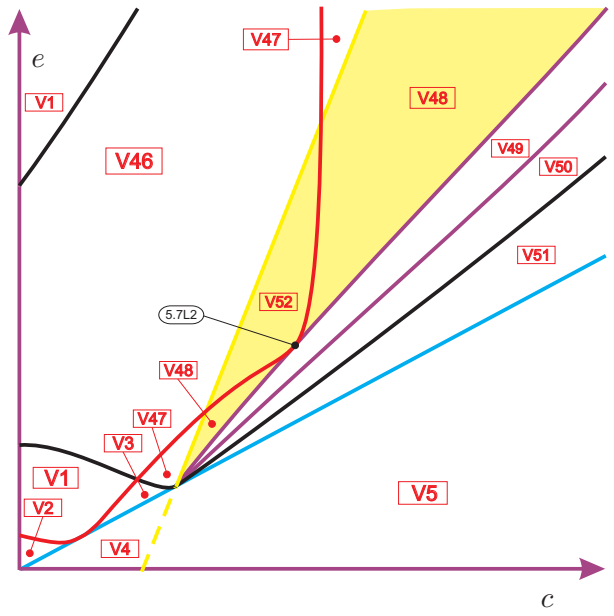

Fig. 29. Slice of parameter space when $m = 1/2 - \varepsilon_1^*$ (see Fig. 28)

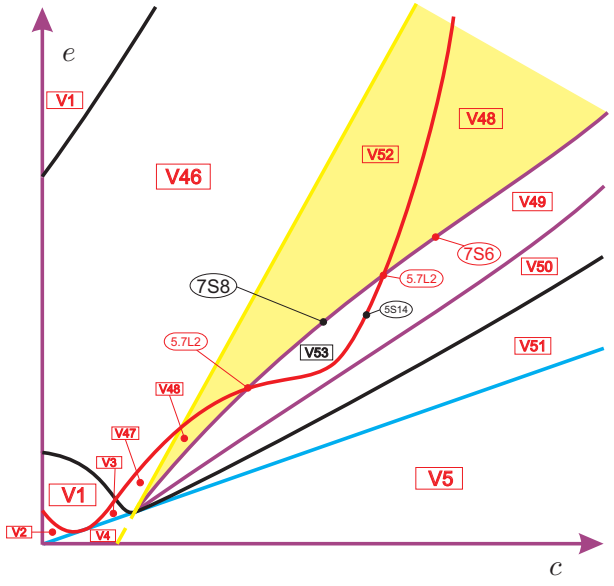

Fig. 30. Slice of parameter space when $m = 1/2 - \varepsilon_2$ (see Fig. 29)

Now, for the next singular slice, numerical analysis suggest that surface $5S_{14}$ must touch surface $7S_7$ again in a curve, namely, $5.7L_3$, splitting the part $7S_7$ as in Fig. 32.

We detect that for an even smaller value of m, surface $(\mathcal{S}_5)$ crosses surface $(\mathcal{S}_7)$ but this does not generates a new volume region, because the bifur-

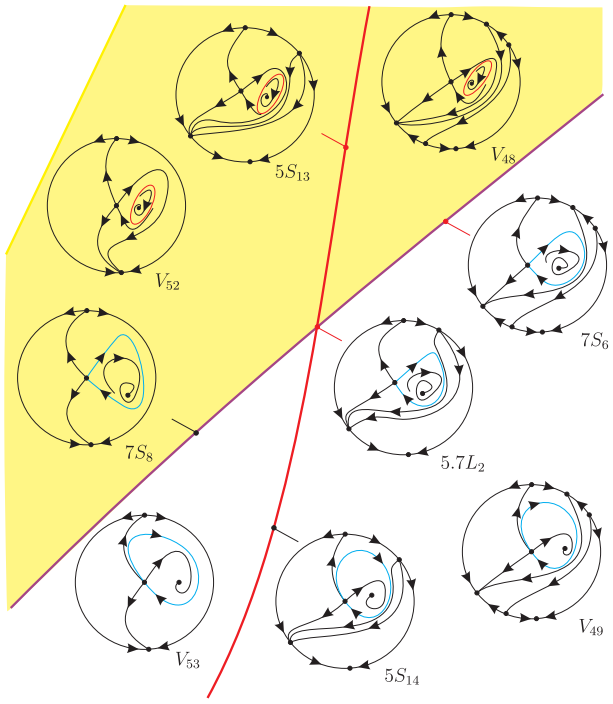

Fig. 31. Graphics producing limit cycles: neighborhood of $5.7L_2$ (see Fig. 30)

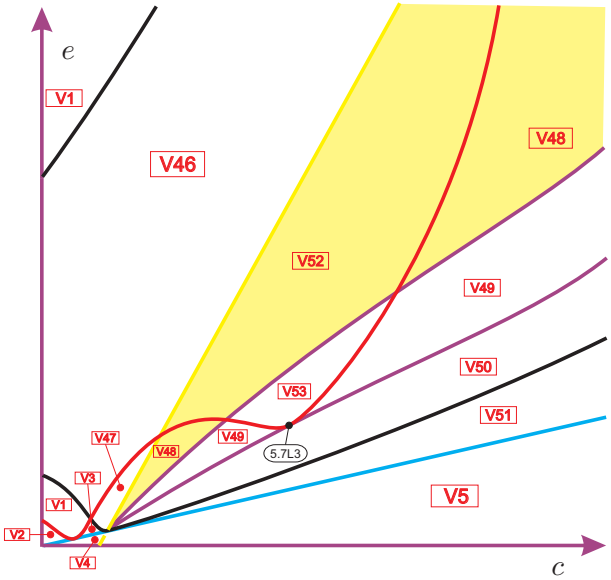

Fig. 32. Slice of parameter space when $m = 1/2 - \varepsilon_2^*$ (see Fig. 30)

cation given by the part $7S_7$ deals with a separatrix of an infinite singularity which does not exist in region V_{53}. However, it does generate a new bifurcation surface, namely, $5S_{15}$, which is the bor-

der between V_{50} and V_{53}. All the respective phase portraits are coherent with their neighbors and this generic slice is presented in Fig. 33. In such a figure we intend to give an idea of the global bifurcation diagram, specially to show how "close" to the origin some surfaces are. This notion is very important in order to better understand the next singular slice, namely, $m = 0$.

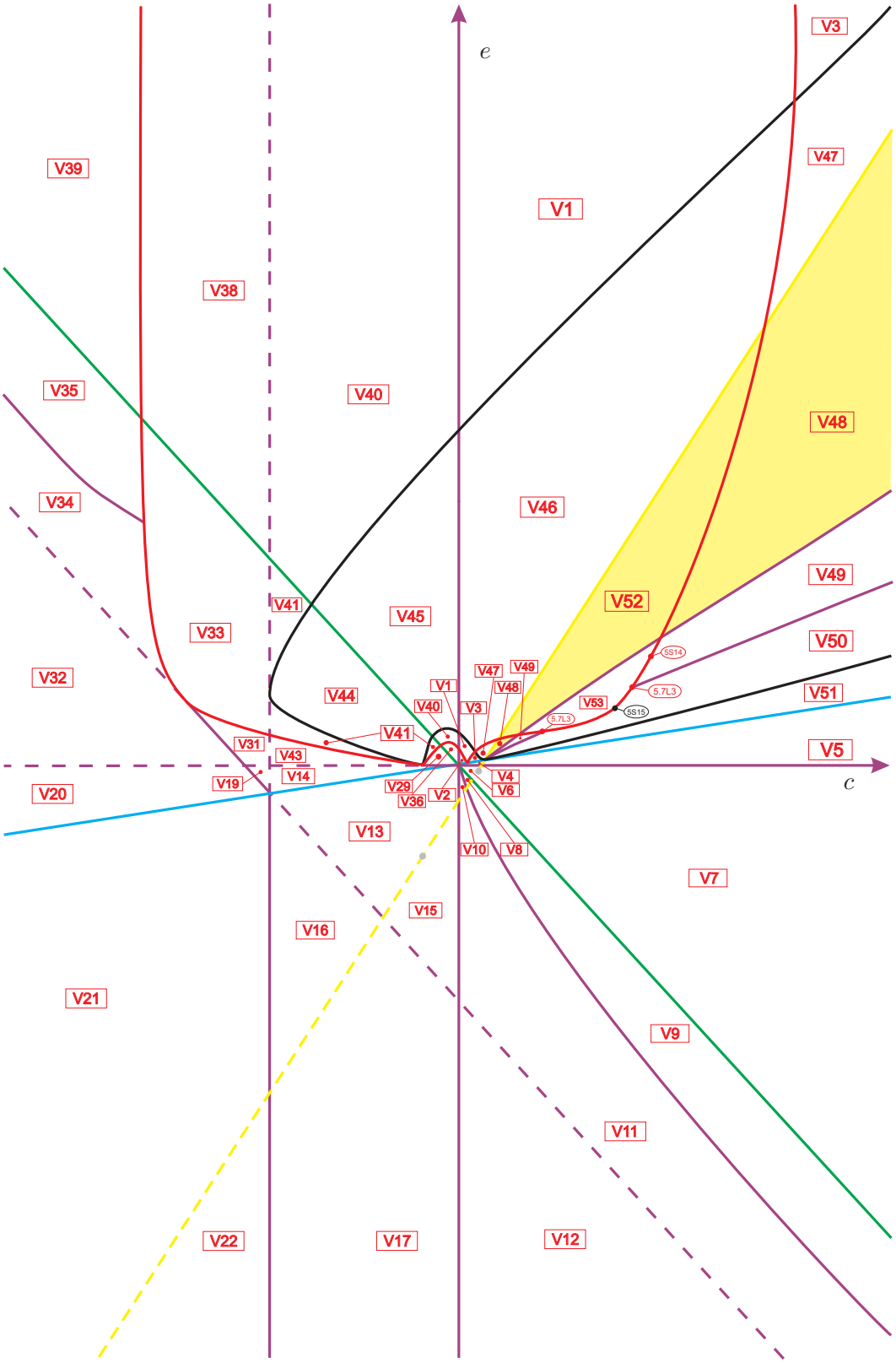

Fig. 33. Slice of parameter space when $m = 1/2 - \varepsilon_3$ (see Fig. 32)

The next slice to be analyzed is the singular slice $m = 0$. As we mentioned before and we saw in Fig. 33, several surfaces were "very close" to the origin. When $m = 0$, several things happened simultaneously:

- the cyan straight line coalesced with the c–axis. This movement makes to vanish regions V_4, V_5, V_{14}, V_{19} and V_{20}. We denote by $4.8L_3$ to $4.8L_5$ the three new one–dimensional parts of c–axis, by P_3 the origin and by P_5 the point $(c, e) = (-2, 0)$;

- the red parabola now is tangent to the c–axis at the origin. This makes regions V_2, V_{29} and V_{36} to vanish;

- the black parabola is also tangent to the c–axis at the origin and this makes regions V_1 (curved quadrilateral bordered by black, red and purple surfaces), V_3 (curved triangle bordered by black, cyan and red surfaces), and V_{40} (curved quadrilateral bordered by black, green, red and purple surfaces) to vanish. Moreover, the black parabola is also tangent to the straight line $c = -2$ at the point P_4 making the region V_{41} to vanish;

- the yellow straight line now passes through the origin, making V_6, V_8 and V_{10} to vanish, and it coalesces $3.10L_1$ to P_3;

- the curve $5.7L_3$ has gone to the origin, making V_{47} (curved triangle bordered by black, red and yellow surfaces), V_{48} (curved triangle bordered by purple, red and yellow surfaces) and V_{49} (curved triangle bordered by red and purple surfaces) to vanish;

- the purple straight line, which is parallel to the green one, passes through P_5.

The critical slice $m = 0$ is shown in Fig. 34, where, as usual, we indicate in red colors the old labels and in black color the new ones.

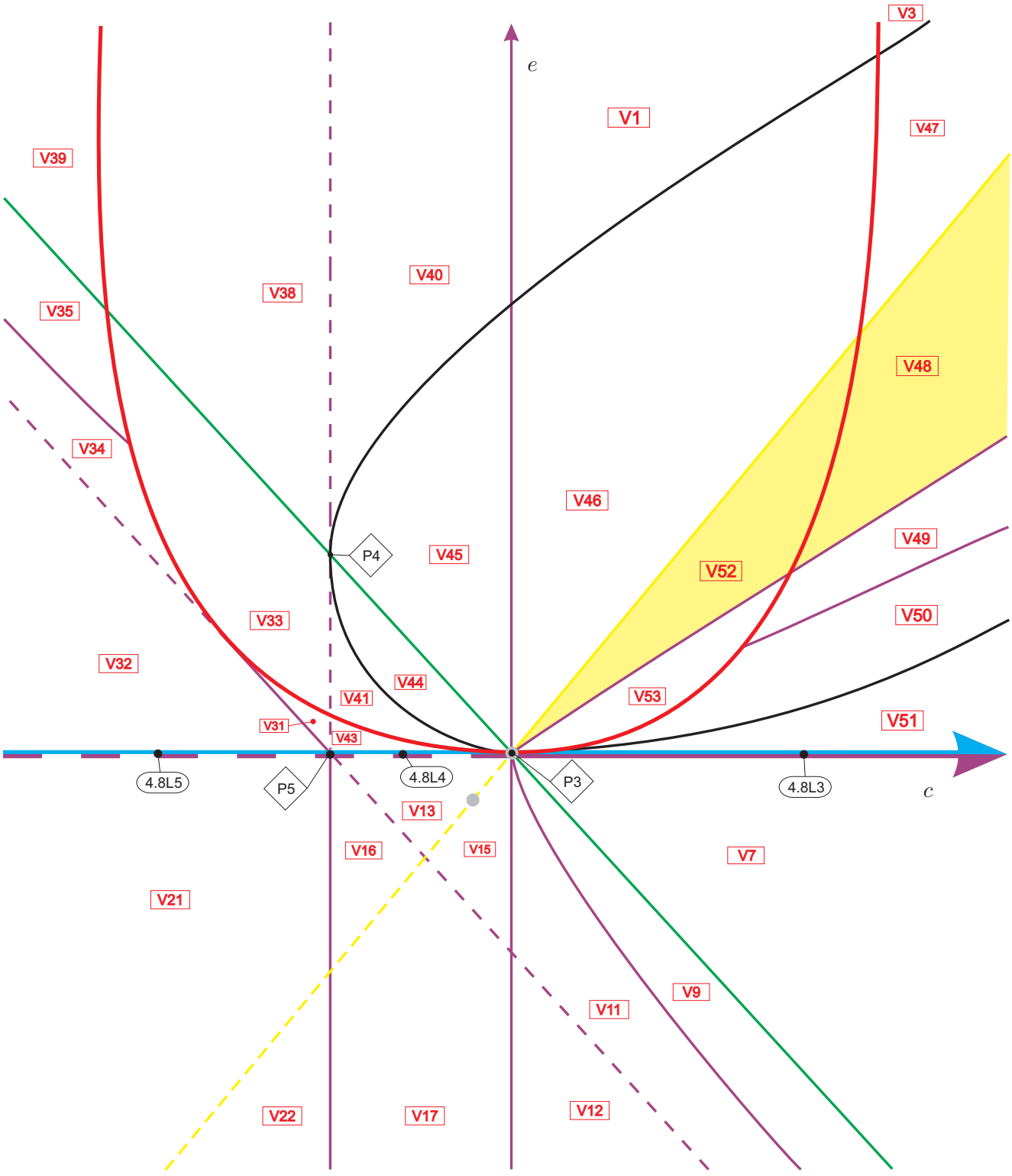

Fig. 34. Slice of parameter space when $m = 0$ (see Fig. 33)

Now we begin the study of slices corresponding to negative values of m, see (10). The first slice to be considered is $m = -5/100$. As we saw in the slice $m = 0$, the displacement of the black, cyan, yellow and red surfaces caused the "death" of several regions. As we move down, such surfaces keep moving themselves and it is natural to expect that several regions "born" when we go from $m = 0$ to $m = -5/100$. In fact, in this new slice we observe that such surfaces (and also the purple one that crossed the c–axis at P_5 when $m = 0$) moved and gave "birth" to the following 20 volume regions v_{54} to v_{73}, and all its borders, as in Fig. 37. Moreover, the curve $3.10L_1$ (from slice $m = 1/2 - \varepsilon_3$) that was carried to the origin when $m = 0$ now becomes $3.10L_2$, which already appeared in previous slices. The reason why it belongs to the same curve is that in the next slice we will find a single point which here is split into two. This also makes that the segment in surface $(\mathcal{S}_3)$ that we see in this slice between $3.4L_6$ and $3.10L_2$ which appears from the bifurcation, is linked in a lower slice with part $3S_7$ and so it receives the same name. On the other hand, due to the presence of the cyan straight line (in which systems (5) are degenerate) and due to its movement between two slices, we can found new nonalgebraic surfaces splitting some volume regions. This phenomena happens here. Indeed, almost all the phase portraits obtained from each "new" two–dimensional part are coherent with those of all their borders. We have only four exceptions, which are shown in Fig. 36 and named as follows:

- v_{58}: the curved quadrilateral bordered by black, green, purple and red surfaces;
- v_{59}: the curved triangle bordered by black, green and purple surfaces;
- v_{61}: the curved quadrilateral bordered by black, green, yellow and red surfaces;
- v_{67}: the right triangle bordered by purple surfaces.

We start analyzing parts v_{58} and v_{59}. First we consider part v_{59}. The respective phase portrait is topologically equivalent to the one in V_{59}. On $4s_{40}$, the separatrix of the infinite saddle–node connects with a separatrix of the finite saddle–node producing an invariant straight line linking the pair of infinite saddle–nodes. When entering part v_{59}, this connection is broken and the separatrix of the infinite saddle–node connects to the infinite unstable node and the separatrix of the finite saddle–node connects with the infinite stable node. However, when we approach $2s_9$, the phase portrait in a neighborhood of this segment is topologically different from the one we described just after entering part v_{59}. Indeed, the phase portrait in v_{59} near $2s_9$ possesses an infinite basin passing through the finite saddle–node, i.e. two separatrices of the finite saddle–node end at the same infinite singular point (in this case, the infinite saddle–node), whereas the phase portrait in v_{59} near $4s_{40}$ does not possess the infinite basin and each one of the same two separatrices of the saddle–node ends in different infinite singular points. Then, there must exist at least one element $7S_{10}$ of surface $(\mathcal{S}_7)$ dividing part v_{59} in two "new" parts, V_{59} and V_{71}, which represents a bifurcation due to the connection between a separatrix of a finite saddle–node with a separatrix of an infinite saddle. It is worth mentioning that the segment $6s_{13}$ refers to the C^∞ surface of node–focus bifurcation, which implies that whatever we find in part v_{58} there must exist in part v_{59} and viceversa. Then, part v_{58} must also be divided in V_{58} and V_{70} by an element $7S_9$ of surface $(\mathcal{S}_7)$ with the same bifurcation as $7S_{10}$. Clearly we have that $7S_9$ is a "continuation" of $7S_{10}$. Coupled with this idea, we have parametrized the black surface, "walked" on it and found that there is a topological change in the phase portraits obtained.

Then, we know that $7S_{10}$ has one of its endpoints on $6s_{13}$ (dividing it in $6S_{13}$ and $6S_{12}$) and Lemma 4.39 assures that the other endpoint is $4.8\ell_6$. We show the sequence of phase portraits along these subsets in Fig. 35.

Moreover, as the segment $5s_{18}$ corresponds to changes in the infinite singular points, the finite part of the phase portraits remains unchanged and then segment $7s_9$ must intersect $5s_{18}$ having this intersection point as one of its endpoints, since in v_{57} we have only one infinite singularity, namely, the infinite saddle–node. With these arguments we also have parametrized the red surface, "walked" on it and found that there is a topological change in the phase portraits obtained. In fact, in Lemma

4.40 we prove that surface $7S_9$ has $5.7\ell_4$ as endpoint. As V_{58} is topologically equivalent to V_{59} and V_{70} is topologically equivalent to V_{71}, the sequence of phase portraits along these subsets then is given by the path $V_{71} \to V_{59}$ presented in Fig. 35.

We plot the complete bifurcation diagram for these two parts in Fig. 37.

Lemma 4.39. *The endpoint of $7S_{10}$ (rather than the one which is on $6s_{13}$) is $4.8\ell_6$.*

Proof. Numerical tools evidence that the endpoint of $7S_{10}$, rather than the one which is on $6s_{13}$, is $4.8\ell_6$. In what follows, we prove that this endpoint cannot be on segments $4s_{40}$ and $2s_9$. In fact, if this endpoint was located on $4s_{40}$, then there should exists a portion of this segment in which the separatrix of the infinite saddle–node connects to the infinite unstable node, causing the break of the invariant straight line. As we are considering projective coordinates, this fact contradicts Lemma 2.2. On the other hand the endpoint of $7S_{10}$ cannot be located on $2s_9$, since $7S_{10}$ describes a connection between a separatrix of a finite saddle–node with a separatrix of an infinite saddle and on $2s_9$ the finite saddle–node already has become a cusp–type singularity. Therefore, as the endpoint of $7S_{10}$ is not on $4s_{40}$ nor in $2s_9$, this confirms the evidence pointed out by the numerical calculations that $7S_{10}$ ends at $4.8\ell_6$. ■

Lemma 4.40. *The endpoint of $7S_9$ (rather than the one which is on $6s_{13}$) is $5.7\ell_4$.*

Proof. Numerical tools evidence that the endpoint of $7S_9$ is $5.7\ell_4$. As V_{58} is topologically equivalent to V_{59} and V_{70} is topologically equivalent to V_{71}, repeating the same arguments used in the proof of Lemma 4.39 we conclude that $7S_9$ must intersect the red surface. In fact, its endpoint is $5.7\ell_4$ because on v_{57} we do not have the necessary number of infinite singularities in such a way that the bifurcation given by $7S_9$ could happen. ■

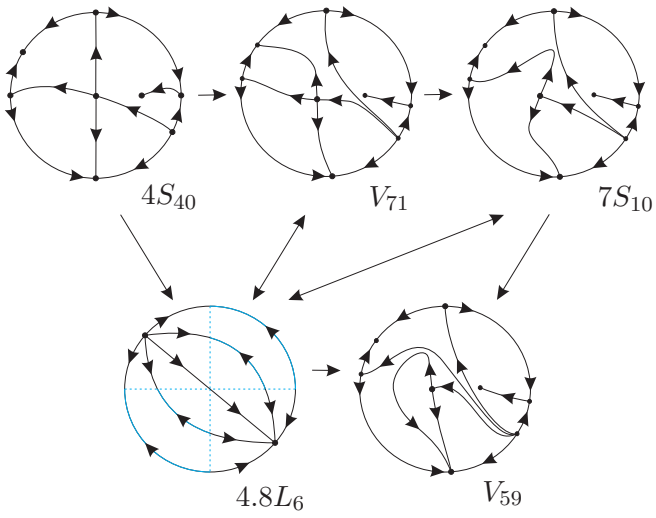

Fig. 35. Sequence of phase portraits in parts v_{59} and v_{58} of slice $m = -5/100$ (the labels are according to Fig. 37). We start by analyzing v_{59}. First we recall that the phase portrait $4S_{40}$ (respectively, V_{71}, $7S_{10}$ and V_{59}) is topologically equivalent to the phase portrait $4S_{39}$ (respectively, V_{70}, $7S_9$ and V_{58}) due to a node–focus bifurcation. If we start on $4s_{40}$ we can reach V_{59} by one of the six following paths: (1) $4S_{40} \to 4.8L_6 \to V_{59}$; (2) $4S_{40} \to 4.8L_6 \to 7S_{10} \to V_{59}$; (3) $4S_{40} \to 4.8L_6 \to V_{71} \to 7S_{10} \to V_{59}$; (4) $4S_{40} \to V_{71} \to 4.8L_6 \to 7S_{10} \to V_{59}$; (5) $4S_{40} \to V_{71} \to 7S_{10} \to 4.8L_6 \to V_{59}$; and (6) $4S_{40} \to V_{71} \to 7S_{10} \to V_{59}$

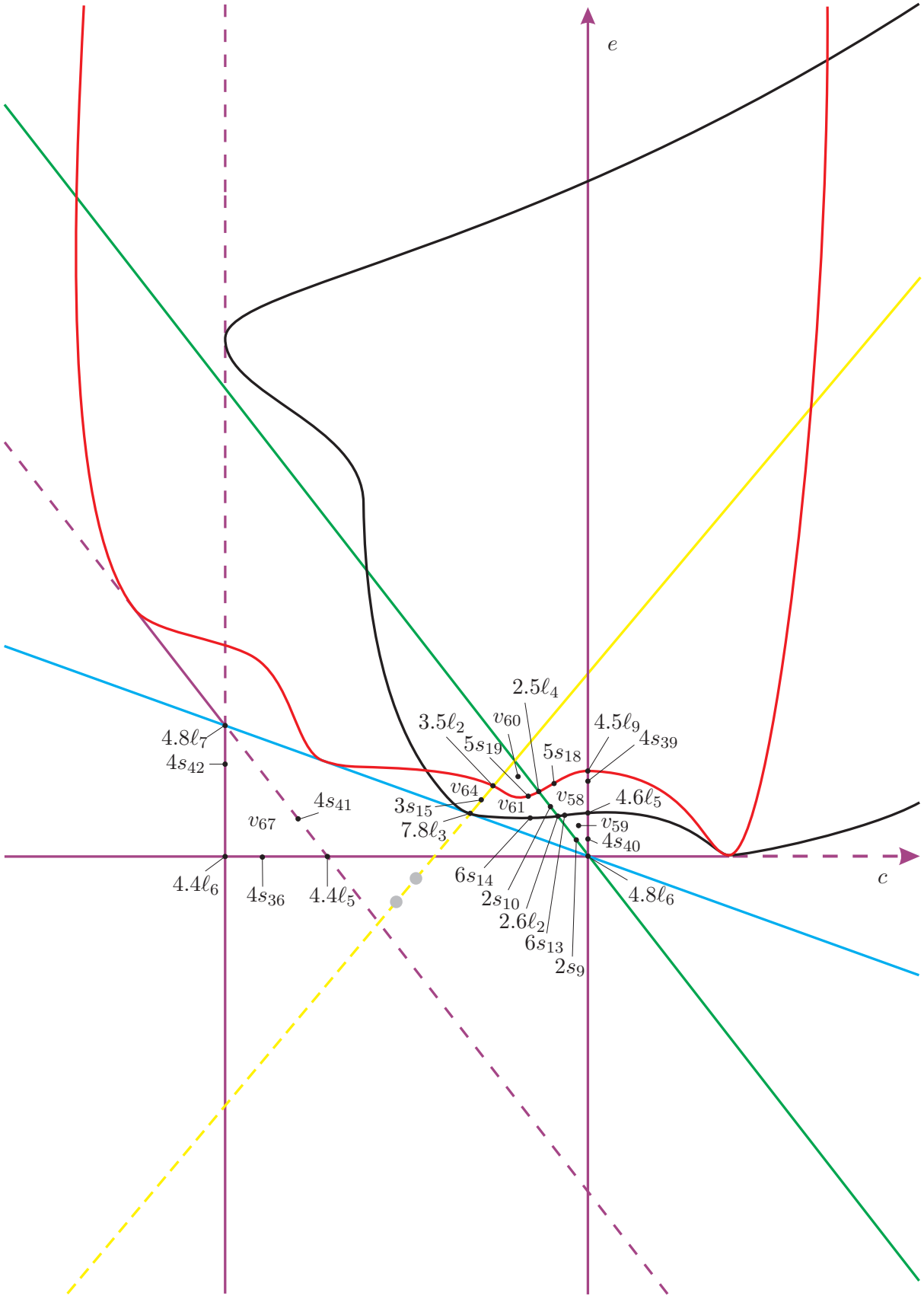

Fig. 36. Slice of parameter space when $m = -5/100$ (only algebraic surfaces)

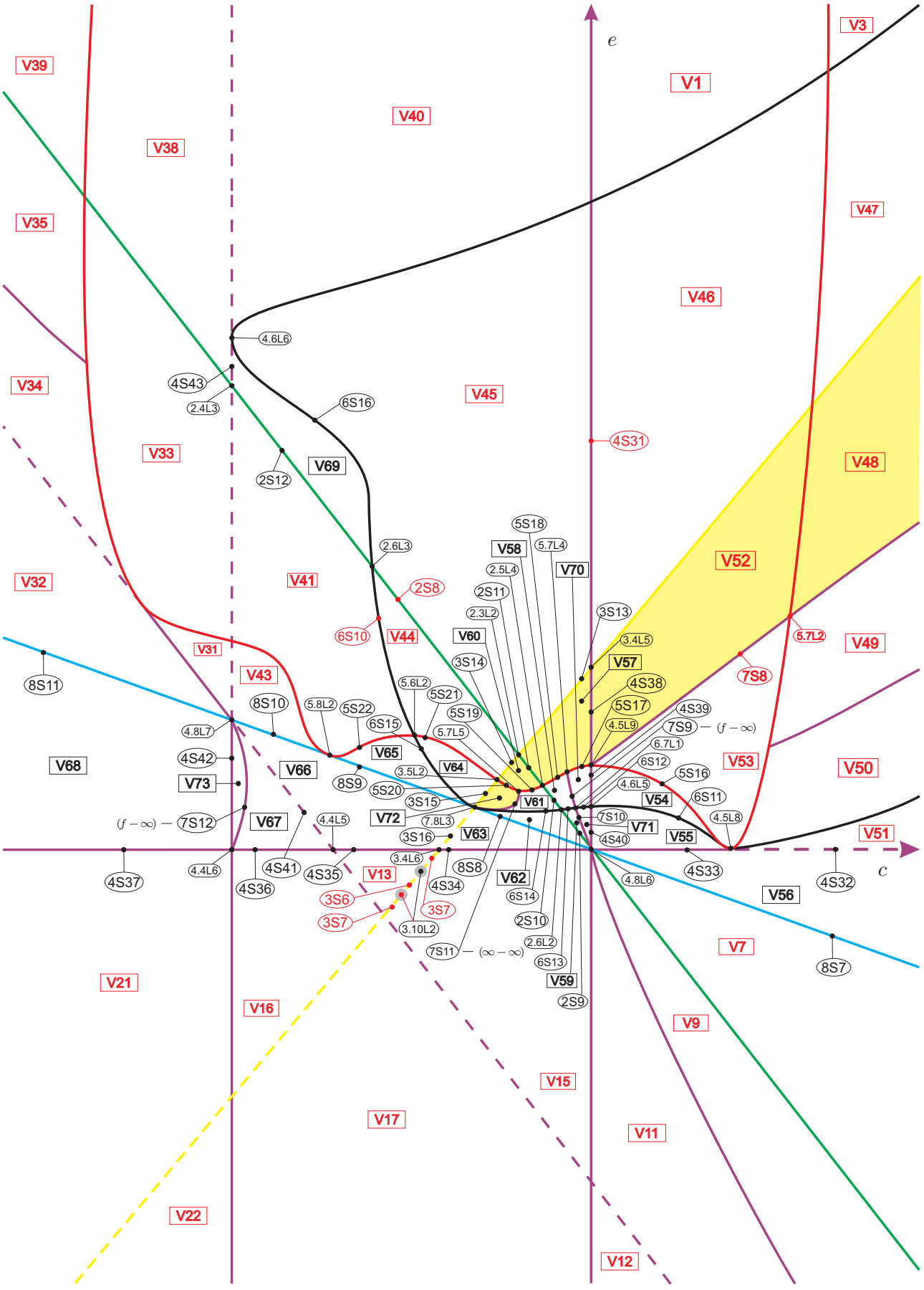

Fig. 37. Complete bifurcation diagram for slice $m = -5/100$ (see Fig. 34)

We now present the study of part v_{61}. Let us consider the segment $2s_{10}$ in Fig. 36, which is one of the borders of part v_{61}. The respective phase portrait in this border is topologically equivalent to the one in $2S_{10}$, with the origin being a cusp–type singularity. When entering part v_{61} near $2s_{10}$ the infinite saddle–node has a separatrix starting at the infinite unstable node. On the other hand, in the phase portrait in v_{61} near $3s_{15}$ such a separatrix has a limit cycle as its α–limit. Then, there must exist at least one element $7S_{11}$ of surface $(\mathcal{S}_7)$ dividing part v_{61} in two "new" parts, V_{61} and V_{72}, which represents a bifurcation due to the connection between a separatrix of an infinite saddle–node with a separatrix of an infinite saddle. Moreover, as the segment $5s_{19}$ corresponds to changes in the infinite singular points, the finite part of the phase portraits remain unchanged and then $7S_{11}$ must intersect $5s_{19}$ having this intersection point as one of its endpoints, since in v_{60} we have only one infinite singularity, namely, the infinite saddle–node. With these arguments we have parametrized the red surface, "walked" on it and found that there is a topological change in the phase portraits obtained. In fact, in Lemma 4.41 we prove that surface $7S_{11}$ has $7.8\ell_3$ as endpoint. We show the sequence of phase portraits along these subsets in Fig. 38 and the complete bifurcation diagram for this part is presented in Fig. 37.

Lemma 4.41. *The endpoint of* $7S_{11}$ *(rather than the one which is on* $5s_{19}$*) is* $7.8\ell_3$.

Proof. Numerical tools evidence that the endpoint of $7S_{11}$, rather than the one which is on $5s_{19}$, is $7.8\ell_3$. In fact, as we described before, $7S_{11}$ represents a bifurcation due to the connection between a separatrix of an infinite saddle–node with a separatrix of an infinite saddle. We point out that it is not possible that the endpoint of this surface be on $6s_{14}$, since on black surfaces we have only a C^∞ node–focus bifurcation. Indeed, this could happen unless we have a degenerate portion of black surface in which $7S_{11}$ would start. On the other hand, if the endpoint was on $3s_{15}$ then should exists a degenerate portion of $3s_{15}$ in which $7S_{11}$ ends, since that otherwise a portion of this subset must not refer to a Hopf bifurcation, which contradicts the fact that on $3s_{15}$ we have a weak focus of order one. ■

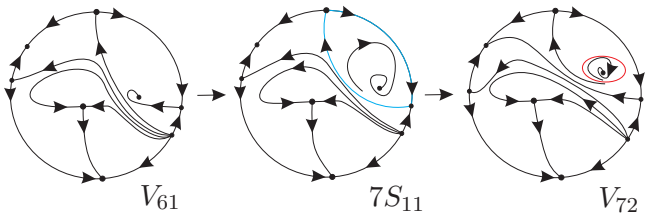

Fig. 38. Sequence of phase portraits in part v_{61} of slice $m = -5/100$ (the labels are according to Fig. 37). When crossing $2s_{10}$, we shall obtain the phase portrait V_{61} in a subset of v_{61}. From this point we can reach the subset V_{72} by crossing the purple surface $7S_{11}$. We observe that the separatrix of the infinite saddle–node coalesces with the separatrix of the infinite saddle, forming a closed graph, which breaks, given birth to a limit cycle

The last case to be considered is part v_{67}. The respective phase portrait on surface $4S_{41}$ is topologically equivalent to V_{66} because on this point, surface $(\mathcal{S}_4)$ produces a straight line not formed by separatrices. On the other hand, on $4s_{42}$ there is a connection between the separatrix of the infinite saddle–node with the separatrix of the finite saddle, forming an invariant straight line. Moreover, the phase portrait possesses an infinite basin passing through the infinite unstable node, i.e. two separatrix of the finite saddle–node start at the infinite unstable node. When entering part v_{67} the separatrix connection is broken and the separatrix of the finite saddle starts at the unstable infinite node and the separatrix of the infinite saddle–node ends at the infinite stable node. In addition, the infinite basin remains on this phase portrait. But this is not the same when we are close to $4s_{36}$ and $4s_{41}$, since when we approach them, we detect that the infinite basin is lost and the separatrix of the infinite saddle–node now ends at the finite saddle–node. This topological change suggests that there must exist at least one element $7S_{12}$ of surface $(\mathcal{S}_7)$ dividing part v_{67} in two "new" parts, V_{67} and V_{73}, which represents a bifurcation due to the connection between a separatrix of a finite saddle–node with a separatrix of an infinite saddle–node (see Fig. 39 for a sequence of phase portraits in these parts). In Lemma 4.42 we prove that $7S_{12}$ has $4.4\ell_6$ and $4.8\ell_7$ as start/endpoints. The complete bifurcation diagram for these two parts is shown in Fig. 37.

Lemma 4.42. *The nonalgebraic surface* $7S_{12}$ *has*

$4.4\ell_6$ and $4.8\ell_7$ as start/endpoints.

Proof. Numerical tools evidence that this result is valid. Indeed, as we mentioned before, $7S_{12}$ represents a bifurcation due to the connection between a separatrix of an infinite saddle–node with a separatrix of a finite saddle–node. We start by observing that if $7S_{12}$ has one of its start/endpoints at any point of the segment $4s_{42}$ (without the extreme points) then there would exists a portion of such a segment in which the invariant line has been broken, contradicting the fact that on $4S_{42}$ we have an invariant straight line. Analogously we conclude that $7S_{12}$ cannot have one of its start/endpoints at any point of segment $4s_{36}$ (without the extreme points). Finally, the endpoint cannot be on $4s_{41}$ (or even in the point $4.4\ell_5$) since $4s_{41}$ represents only an invariant straight line without separatrices connection (otherwise would exists a degenerate portion of $4s_{41}$ in which $7S_{12}$ would have its start/endpoint). Therefore, the nonalgebraic surface $7S_{12}$ has $4.4\ell_6$ and $4.8\ell_7$ as start/endpoints. ■

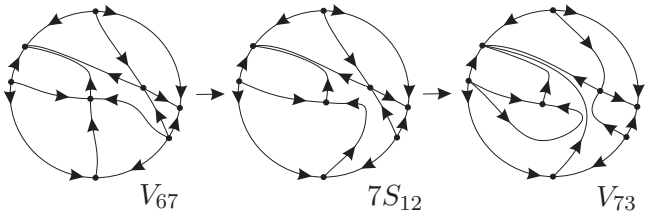

Fig. 39. Sequence of phase portraits in part v_{67} of slice $m = -5/100$ (the labels are according to Fig. 37). When crossing $4s_{41}$, we shall obtain the phase portrait V_{67} in a subset of v_{67}. From this point we can reach the subset V_{73} by crossing the purple surface $7S_{12}$. We observe that the separatrix of the infinite saddle–node coalesces with the separatrix of the finite saddle–node, and then such a connection is broken, forming an infinite basin passing through the infinite unstable node

Before we go to the next slice, in order to finish describing the role slice $m = -5/100$, we point out that in this slice we have limit cycles at the following new regions: V_{57}, V_{60} and V_{72}. In addition, numerical analysis confirm that the nonalgebraic surfaces $7S_2$ and $7S_5$ to $7S_8$ are still present at this slice. In particular, surfaces $7S_6$ and $7S_8$ still intersect along the curve $5.7L_2$. The only thing that remains to be proved is that, according to Fig. 37, the nonalgebraic surface $7S_8$ has $4.5\ell_9$ as an endpoint, see Lemma 4.43.

Lemma 4.43. *For $m = -5/100$, the endpoint of $7S_8$ (rather than $5.7\ell_2$) is $4.5\ell_9$.*

Proof. Numerical analysis suggests that surface $7S_8$, which corresponds to a loop–type bifurcation, have one of its ends at the point $4.5\ell_9$. Indeed, using the same argument as in the proof of Lemma 4.38 we conclude that the endpoint of this surface is not on $3s_{12}$. Now, if the endpoint is on $4s_{38}$ then should exists a portion of this segment in which the respective invariant straight line would be broken. Finally, if the endpoint is on $5s_{16}$, then should exists a portion of red parabola which is a "path" between V_{52} and V_{54}. We know that crossing the red parabola means that two infinite singularities coalesce. Then, if in V_{54} we make the infinite saddle and the infinite node to coalesce, then we would have a saddle–node of type $\binom{\overline{0}}{2}SN$. Even if this infinite singularity disappear, we would be crossing the red parabola, going to V_{52} and arriving there without limit cycle (since this transition does not change the finite part, for instance, the separatrix of the finite saddle–node which has the finite antisaddle as a ω–limit does not disappear), a contradiction, since we already know that on V_{52} the respective phase portrait has a limit cycle. Then, we conclude the proof of this result. ■

Remark 4.44. In the next figures we present a local behavior with red and black labels (indicating the "old" regions and the "new" ones, respectively), but we also present some regions without labels, just for the reader follows the movement of the surfaces. Of course, the respective red labels can be found looking for previous figures. For instance, in Fig. 40 the curved quadrilateral region bordered by black, green, red and yellow surfaces corresponds to the region V_{44} in Fig. 37.

In Remark 4.2 we have concluded that the equation $\mathcal{T}_4 = \mathcal{F}_1 = 0$ has one double root if $\Delta = 0$, i.e. $m = \left(\pm 2\sqrt{2} - 3\right)/2$. In this way, the slice $m = \left(2\sqrt{2} - 3\right)/2$ is singular because the curve $3.10L_2$ which cut twice the slices $m = const.$ with $m \in \left(\left(2\sqrt{2} - 3\right)/2, 0\right)$, at this slice it cuts in a single point. Moreover, the part $3S_6$ vanishes. The result can be seen in Fig. 40.

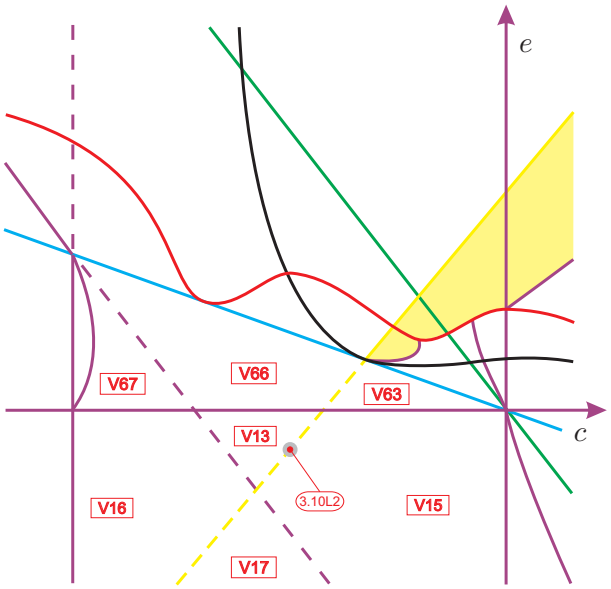

Fig. 40. Slice of parameter space when $m = \left(2\sqrt{2}-3\right)/2$ (see Fig. 37)

Analogously, again according to Remark 4.2 we proved that the equation described by $\mathcal{T}_4 = \mathcal{F}_1 = 0$ has no real roots for $\Delta < 0$, i.e. for $m \in \left(\left(-2\sqrt{2}-3\right)/2, \left(2\sqrt{2}-3\right)/2\right)$. Therefore, on the next generic slice, namely, $m = -1/4$, the only important thing that we observe is that the curve $3.10L_2$ does not cuts these slices, see Fig. 41.

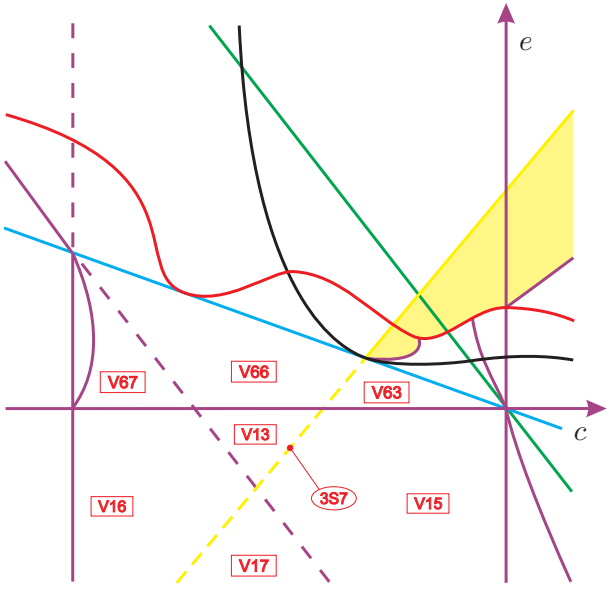

Fig. 41. Slice of parameter space when $m = -1/4$ (see Fig. 40)

Proceeding with the study of the next singular slice, $m = -1/2$, we observe that triangle V_{13} (see Fig. 41) collapses into a point, namely, P_6. This is caused by the displacement of yellow and purple algebraic surfaces. The rest of the bifurcation diagram remains topologically equivalent to the previous one. We present this result in Fig. 42.

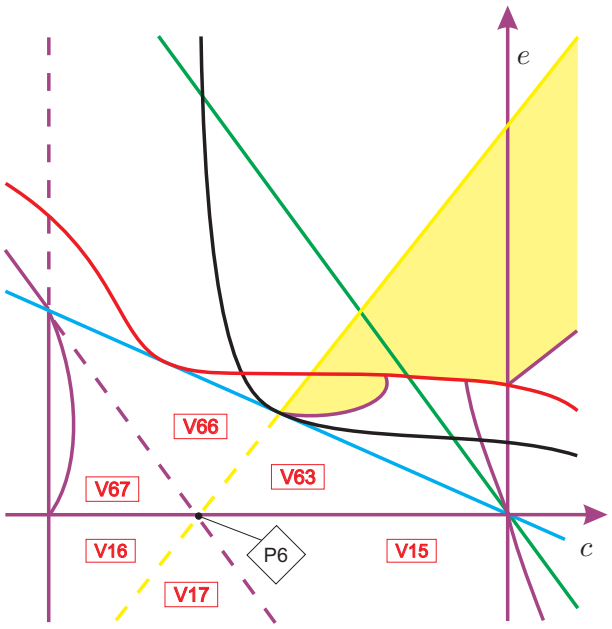

Fig. 42. Slice of parameter space when $m = -1/2$ (see Fig. 41)

When we move down with values of the parameter m very close to $m = -1/2$, we verify that the yellow and purple surfaces mentioned before keep their movement and from the point P_6 arises a new volume region which we denote by V_{74}. We denote this generic slice by $m = -1/2 - \varepsilon_4$ and we present it in Fig. 43. The phase portrait will be equivalent to the one in V_{63} since the bifurcation that splits them is just due to a straight line that does not represent a separatrix connection.

Following the study of values of m less than but closer to $m = -1/2$ numerical analysis indicate that there must exist a point (see P_7 in Fig. 44) in which $5.7L_5$ coalesces with $2.5L_4$ (see Fig. 37). This situation gives a singular slice $m = -1/2 - \varepsilon_4^*$ which we describe in Fig. 44.

We detect that from point P_7, due to the displacement of the surfaces, yet for values less than but closer to $m = -1/2$, we now have a new volume region with a curved triangle shape which we denote

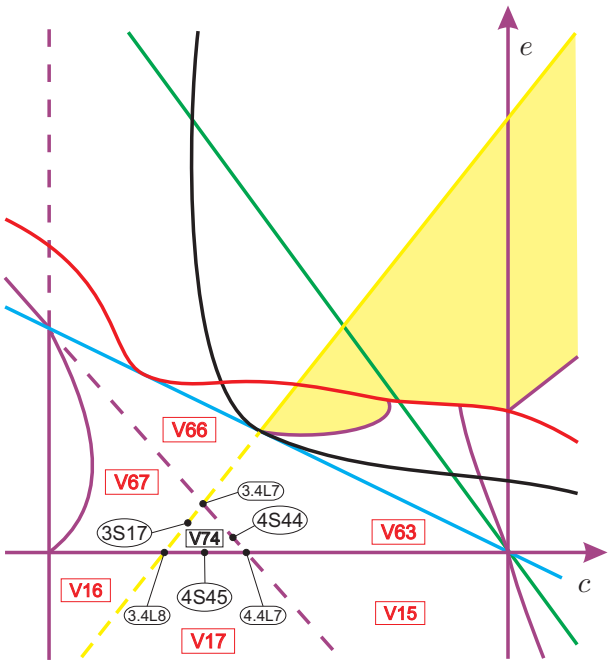

Fig. 43. Slice of parameter space when $m = -1/2 - \varepsilon_4$ (see Fig. 42)

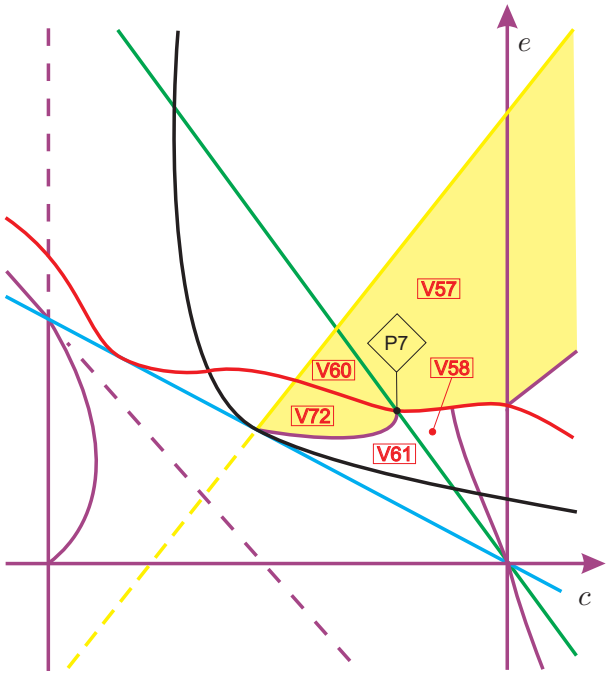

Fig. 44. Slice of parameter space when $m = -1/2 - \varepsilon_4^*$ (see Fig. 43)

by V_{75}. Such a region is detected by taking a small neighborhood of $2S_{10}$ (by above) and of $5S_{18}$ (by below) and then by decreasing the value of the parameter c up to the intersection point between these two surfaces (see Fig. 37). Moreover, this region contains a limit cycle and one of its edges (namely, $7S_{13}$) must be a continuation of the nonalgebraic surface $7S_{11}$. In fact, both pieces of nonalgebraic surface indicate a connection between a separatrix of the infinite saddle–node of type $\binom{\overline{1}}{1}SN$ and a separatrix of the infinite saddle. This nonalgebraic bifurcation given by $7S_{13}$ is exactly what we need in order to have a coherent transition between V_{58} and V_{75}. In addition, as in V_{57} we only have the infinite saddle–node of type $\binom{\overline{1}}{1}SN$, as it was expected by Fig. 43, the nonalgebraic surface $7S_{13}$ must have one of its ends now on $5.7L_6$, which splits the already known part $5S_{18}$ from the new part $5S_{23}$. In Fig. 45 we present this generic slice and we denote it by $m = -1/2 - \varepsilon_5$.

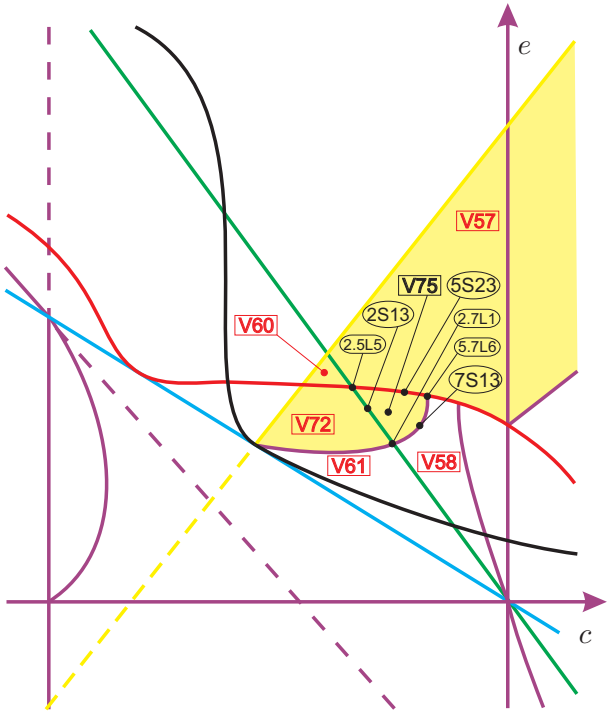

Fig. 45. Slice of parameter space when $m = -1/2 - \varepsilon_5$ (see Fig. 44)

Now we observe that for $m = -8/9$, the volume region V_{60} died. Indeed, it was reduced to the point P_8, as in Fig. 46.

Proceeding with the study of the next generic slice, $m = -9/10$, from the point P_8 arises a new volume region, which we denote by V_{76}, see Fig. 47.

When $m = -24/25$, the volume region V_{44} died.

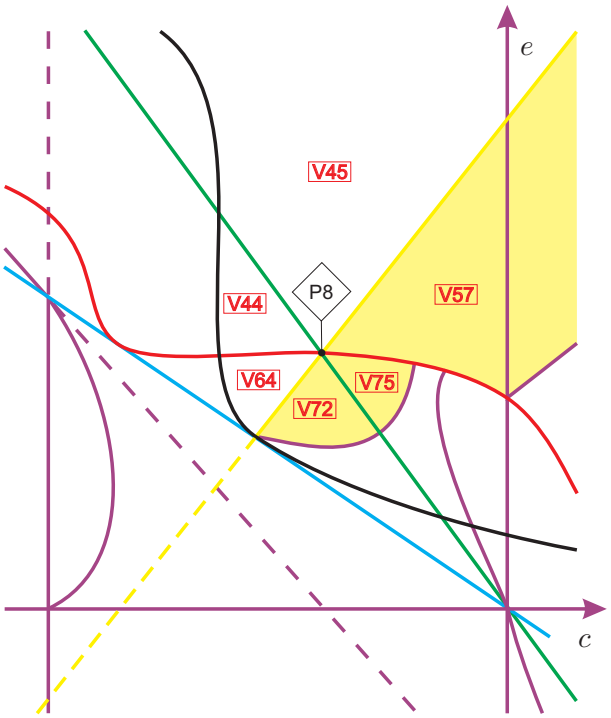

Fig. 46. Slice of parameter space when $m = -8/9$ (see Fig. 45)

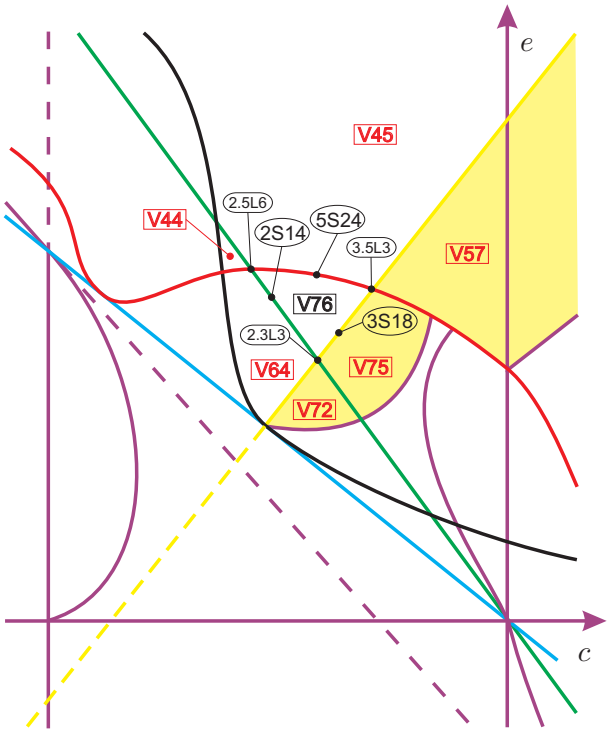

Fig. 47. Slice of parameter space when $m = -9/10$ (see Fig. 46)

In fact, it was reduced to the point P_9, as in Fig. 48.

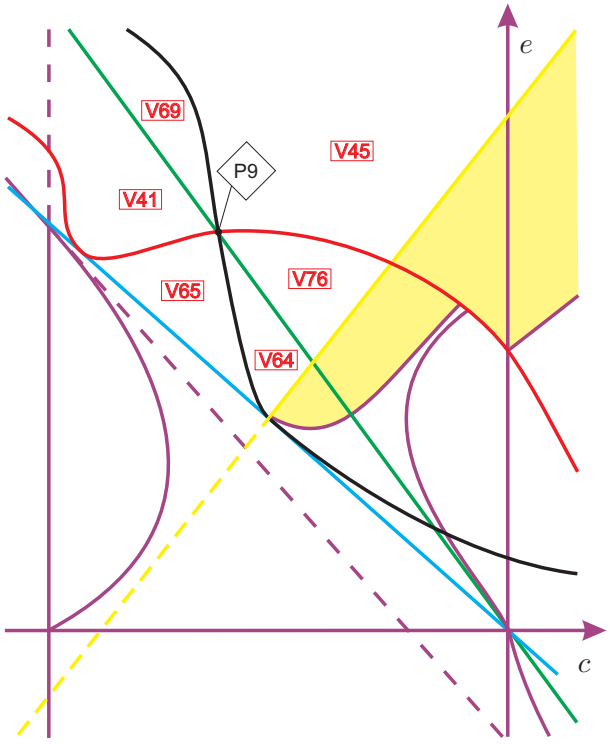

Fig. 48. Slice of parameter space when $m = -24/25$ (see Fig. 47)

In the next generic slice, $m = -98/100$, from the point P_9 arises a new volume region, which we denote by V_{77}, see Fig. 49.

In the next singular slice, $m = -1$, we have a coalescence of the cyan, green and purple surfaces and this displacement kills the following 18 volume regions: V_7, V_9, V_{11}, V_{15}, V_{31}, V_{32}, V_{33}, V_{34}, V_{35}, V_{41}, V_{43}, V_{61}, V_{62}, V_{63}, V_{64}, V_{65}, V_{66} and V_{72} (see these regions in Fig. 49). Moreover, when $m = -1$ we also have that the yellow surface passes trough P_{13}, making the volume region V_{16} disappear. In addition, by using numerical tools, we detect the death of the volume regions V_{58} and V_{59}. In fact, this phenomena is caused by the coalescence of the two pieces $7S_9$ and $7S_{13}$ of the nonalgebraic surface $(\mathcal{S}_7)$. This is why we have drawn these two surfaces very close to each other up to Fig. 49. We denote by $7.7L_1$ the nonalgebraic surface that corresponds to this coalescence and in Fig. 50 we indicate it with ticker line. It is clear that such a surface has one of its ends on the red surface (more precisely, at the point P_{14}, which represents the coalescence of $5.7L_4$ and $5.7L_6$, respectively) and due to the na-

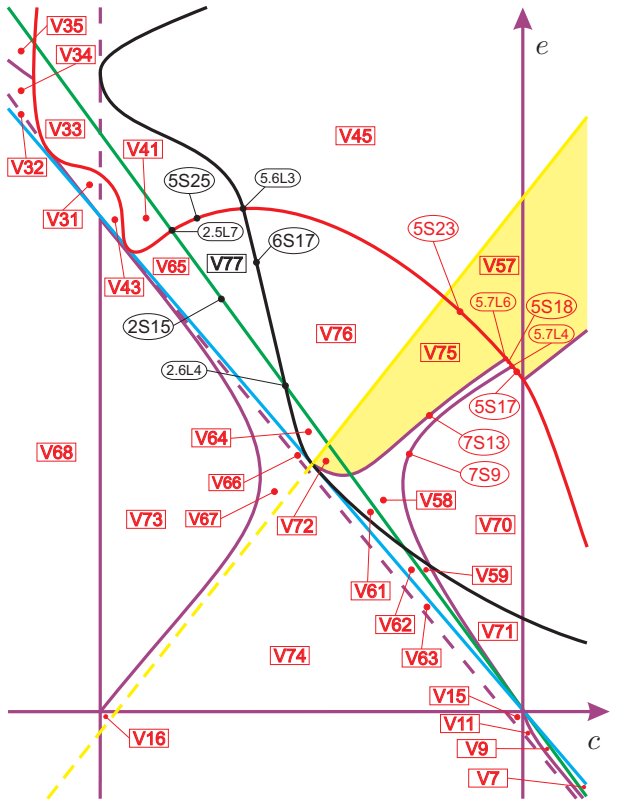

Fig. 49. Slice of parameter space when $m = -98/100$ (see Fig. 48)

ture of the bifurcation described by $7S_9$, the other endpoint of $7.7L_1$ is P_{11}. On the other hand, again by using numerical tools, we detect that the non-algebraic surface $7S_{12}$ now has one of its endpoints also at P_{11} (the other endpoint remains at P_{13}). In Fig. 50 we present this slice properly labeled. Moreover, by using carefully the numerical program P4 [Artés *et al.*, 2005, Dumortier *et al.*, 2006] we take a small neighborhood below the yellow surface, i.e. $e = c - 2m - \varepsilon$ and $m = -1$, we detect that for

$$c = \delta - 1, \quad \varepsilon = \delta + \delta^2, \quad \delta \in \mathbb{R},$$

we have that

$$(c, e) = (\delta - 1, 1 - \delta^2), \quad \delta \in \mathbb{R},$$

and then, surface $7S_{12}$ together with $7.7L_1$ could be approximated by the equation

$$e = -c^2 - 2c,$$

which is a parabola (an algebraic equation) on the ce–plane. Then we can also have an approximation for the point P_{14} (the tangent point of such a parabola with the red surface). On the other hand, we detect that, under the previous conditions over the parameters c, e, m (and from the beginning, $h = 1$) we have the algebraic invariant curve

$$g(x, y) = (1+\delta)(-1+\delta+x)x+(-1+\delta+2x)y, \quad \delta \in \mathbb{R},$$

with cofactor $2y$. These facts are particularly amazing, since therefore $7.7L_1$ is algebraic and represents an algebraic connection given by the coalescence of the two pieces $7S_9$ and $7S_{13}$ of the nonalgebraic surface $(\mathcal{S}_7)$. The resulting parabola has one piece which represents a single connection of separatrices (namely, $7S_{12}$), one piece which represents simultaneously two distinct connections of separatrices (namely, $7.7L_1$) and the remaining part of this parabola does not indicate any additional topological change for the bifurcation diagram. But in order to indicate the existence of such a parabola, in Fig. 50 we have drawn $7S_{12}$ together with $7.7L_1$ resembling a parabola and the respective piece that does not represents any topological change is drawn as a dashed curve.

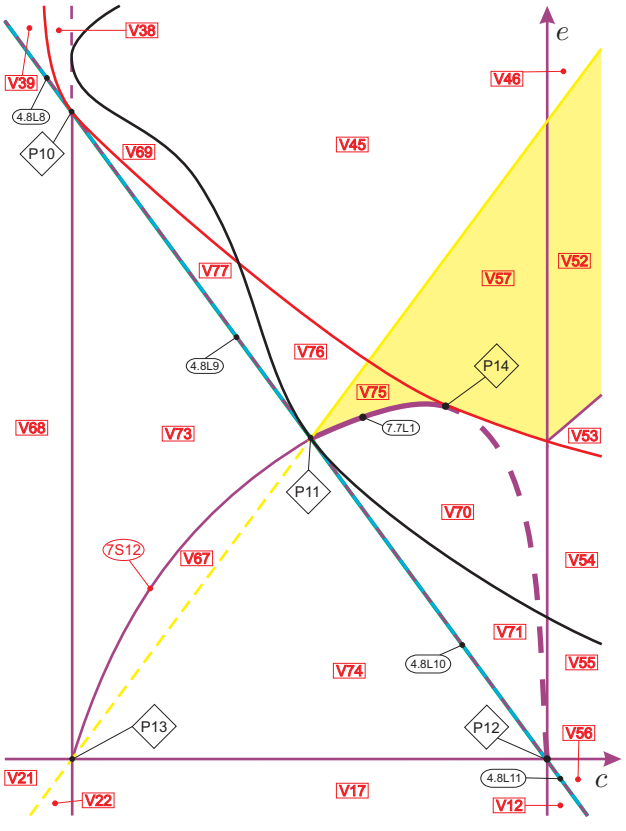

Fig. 50. Slice of parameter space when $m = -1$ (see Fig. 49)

By finishing analyzing this singular slice, when we keep going down with the values of the parameter m, due to the continuous displacement of such surfaces it is natural to expect the birth of several new volume regions. In fact, when we consider a generic slice $m = -1 - \varepsilon_6$, very close to $m = -1$, we get the following 21 new volume regions: V_{78} to V_{98}. Such regions and their respective borders are drawn in Fig. 51. In what follows we explain a little bit about the existence of the pieces of nonalgebraic surfaces $7S_{14}$ to $7S_{21}$ presented in such a figure.

Numerical analysis indicate that surface $7.7L_1$ (from Fig. 50) splits itself into two new pieces of nonalgebraic surface $(\mathcal{S}_7)$, as in Fig. 51. Moreover, we also have the birth of the following three volume regions: V_{78}, V_{79}, and V_{80}. In what follows we justify the existence of such nonalgebraic surfaces and, consequently, of these new volume regions.

We begin by recalling that before the slice $m = -1$, we had that the nonalgebraic surface $7S_{13}$ had a continuation $7S_{11}$ (which was "squeezed" in the slice $m = -1$ by the triple surface). Numerical analysis suggest that, after the splitting of the triple surface, the nonalgebraic surface $7S_{14}$ has a continuation, which we denote by $7S_{20}$. In fact, by taking a small neighborhood of $4S_{55}$ and start decreasing the value of the parameter c, we detect that, in some moment, (by above) the region V_{70} becomes V_{78} and (by below) V_{86} becomes V_{87}. As V_{70} is topologically equivalent to V_{86} and V_{78} is topologically equivalent to V_{87} then we have the existence of some element of surface $(\mathcal{S}_7)$, namely $7S_{20}$, being a continuation of $7S_{14}$. Both nonalgebraic surfaces describe a connection between a separatrix of the infinite saddle–node and a separatrix of the infinite saddle. So, $7S_{20}$ has one endpoint on $4.7L_1$. We observe that the nonalgebraic surface $7S_{20}$ cannot have its other endpoint neither on surface $6S_{18}$ (which represents only a $\mathcal{C}^\infty$ node–focus bifurcation, unless there is a degenerate portion of such a surface being an endpoint of $7S_{20}$) nor on $3S_{20}$ (since otherwise a portion of this subset must not refer to a Hopf bifurcation, which contradicts the fact that on $3S_{20}$ we have a weak focus of order one). Then, the other endpoint of $7S_{20}$ is $7.8L_4$.

We now pass to analyze V_{78}. As before, when we approach $5S_{23}$ by below, we obtain a phase portrait that is topologically equivalent to V_{75}. However, by taking a small neighborhood of $5S_{17}$ (and, respectively, $5S_{23}$) and by decreasing (respectively, increasing) the value of the parameter c, we obtain a phase portrait that does not belong neither to V_{70} nor to V_{75}. In fact, this phase portrait contains a limit cycle (as in V_{75}) but it does not contain the infinite basin (presented in V_{75}) as in V_{70}. This facts suggest that must exist a new volume region (which we denote by V_{78} in Fig. 51) "between" V_{70} and V_{75}. Consequently, there must exist two pieces of nonalgebraic surface $(\mathcal{S}_7)$ bordering this new region. We denote such surfaces by $7S_{14}$ (which describes a connection between a separatrix of the infinite saddle–node and a separatrix of the infinite saddle) and $7S_{15}$ (which indicates a connection between a separatrix of the finite saddle–node and a separatrix of the infinite saddle). Since in V_{57} we do not have a sufficient number of infinite singularities in order to make the bifurcation given by these two nonalgebraic surfaces to happen, we conclude that these surfaces must have one of their endpoints on the red surface, indeed, on the curves $5.7L_7$ and $5.7L_8$, respectively. Then we also have a new piece $5S_{26}$ of surface $(\mathcal{S}_5)$ bordering this new region. By the previous paragraph we already have two other borders of V_{78} (and also of V_{87}). On the other hand, when we approach $3S_{18}$ by below, we obtain a phase portrait that is topologically equivalent to V_{75} and, by taking a small neighborhood below $3S_{18}$, when we decrease the value of parameter e we get a phase portrait that is topologically equivalent to V_{78}. So, the nonalgebraic surface $7S_{15}$ must intersect the yellow surface, splitting $3S_{18}$ into two, namely, $3S_{18}$ and $3S_{19}$. This is confirmed if we parametrize and "walk above" the yellow surface between its intersection with the red surface and the purple one. Therefore, we have obtained all the borders of regions V_{78} (and V_{87}).

We now pass to describe the existence of the volume region V_{79} and also the nonalgebraic surface $7S_{16}$. In fact, when we approach $5S_{24}$ by below, we obtain a phase portrait that is topologically equivalent to V_{76}, but when we approach $4S_{57}$ by above, we obtain a phase portrait that is different from the previous one (which we denote by V_{79}). In fact, if in region V_{76} we fix a value of the parameter c and start decreasing the parameter e, we observe that, in some moment, the infinite basin from V_{76} is lost. This phenomena happens due to a connection between a separatrix of the finite saddle–node and a

separatrix of the infinite saddle. Then it must exist a nonalgebraic surface $7S_{16}$ splitting the volume region V_{76} into two, namely, V_{76} and V_{79}. Moreover, if we take a small neighborhood above the yellow surface, we detect that surface $7S_{16}$ has one of its endpoints on the yellow surface. Indeed, surface $7S_{16}$ is clearly a continuation of surface $7S_{15}$, because both surfaces represent the same nonalgebraic bifurcation and they have endpoint on the yellow surface, in fact, at the curve $3.7L_2$. We also observe that surface $7S_{16}$ has its another endpoint on the black surface, indeed, at the curve $6.7L_2$. On the other hand, as the black surface only represents a $\mathcal{C}^\infty$ node–focus bifurcation, we conclude that surface $7S_{16}$ must cross the black surface and, indeed, a careful numerical analysis indicate that exists a piece of nonalgebraic surface $7S_{17}$ being a continuation of $7S_{16}$ and splitting V_{77} into V_{77} and V_{80}. Moreover, if we parametrize surface $5S_{25}$ we detect that, for some negative value of the parameter c, the same bifurcation described by $7S_{17}$ happens at $5.7L_9$, which splits $5S_{25}$ into $5S_{25}$ and $5S_{27}$. Since as in V_{69} we do not have the sufficient number of separatrices in order to happen the bifurcation described by $7S_{17}$ we conclude that $5.7L_9$ is, in fact, the other endpoint of $7S_{17}$. As in Fig. 51, this nonalgebraic surface is a border of V_{80} which is topologically equivalent to V_{89} (since surface $4S_{58}$ represents an invariant straight line which does not indicate a separatrix connection).

We have seen that up to slice $m = -98/100$, we had the existence of the nonalgebraic surface $7S_2$ being a common border of the regions V_9 and V_{11}. Such a surface was "squeezed" in the slice $m = -1$ by the triple surface (formed by cyan, green and purple surfaces) and, it is natural to expect that after the splitting of this triple surface, arises a new piece of nonalgebraic surface in the neighborhood of the region where $7S_2$ was located. In fact, it happens here. If we approach $4S_{52}$ by below, we obtain a phase portrait that is topologically equivalent to V_{83} and, when we approach $2S_{19}$ by above we obtain a phase portrait which is topologically equivalent to V_{82}. This suggests that there is some element of surface $(\mathcal{S}_7)$ between $4S_{52}$ and $2S_{19}$, which represents a nonalgebraic bifurcation due to the connection between a separatrix of the finite saddle–node with a separatrix of the infinite saddle–node. We denote such a nonalgebraic surface by $7S_{18}$. We observe that as in $2S_{19}$ the finite saddle–node has become a cusp–type singularity, then $7S_{18}$ cannot have an endpoint on $2S_{19}$. Moreover, as the dashed surface $4S_{52}$ only represents a $\mathcal{C}^\infty$ bifurcation, then $7S_{18}$ also cannot have an endpoint on it. On the other hand, if $7S_{18}$ has an endpoint on $4S_{47}$, then in order to make the respective bifurcation to happen, the corresponding invariant straight line would be broken. Therefore, $7S_{18}$ has $4.8L_{12}$ as an endpoint and by using the same arguments we conclude that such a surface is unbounded.

On the other hand in slice $m = -1$ (and before it), we had the existence of the nonalgebraic surface $7S_{12}$ being a common border of the regions V_{67} and V_{73} and describing a connection between a separatrix of the finite saddle–node with a separatrix of the infinite saddle–node. We observe that even after the splitting of the triple surface, this nonalgebraic surface remains in this region, but now numerical analysis indicate that it intersects the yellow surface at two curves, which are denoted by $3.7L_3$. Indeed, when we are "close" to the curve $4.4L_9$ (see Fig. 51), due to the displacement of the yellow surface, numerical analysis suggest that it "cuts" the nonalgebraic surface $7S_{12}$. In fact, when we take a small neighborhood above $3S_{17}$ and start decreasing the value of the parameter c, we observe that, in some moment, the region V_{67} becomes V_{73} and, if we take the same neighborhood below $3S_{17}$ and start decreasing the value of the parameter c, we observe that, in some moment, the region V_{74} becomes V_{97}. As V_{73} is topologically equivalent to V_{97} and V_{67} is topologically equivalent to V_{74} then we have the existence of some element of surface $(\mathcal{S}_7)$, namely $7S_{19}$, being a continuation of $7S_{12}$. So, $7S_{19}$ has one endpoint on $3.7L_3$. We note that $7S_{19}$ cannot have its other endpoint neither on $4S_{49}$ nor on $4S_{45}$, since otherwise the respective invariant lines would be broken in order to make the respective nonalgebraic bifurcation to happen (as we already proved before for surface $7S_{12}$). Then, the other endpoint of $7S_{19}$ is $4.4L_9$. Now, if we are "close" to the curve $2.3L_4$ (see Fig. 51) and we take a small neighborhood above the yellow surface and start decreasing the value of the parameter c, we observe that, in some moment, the region V_{73} becomes V_{67} and if we take a small neighborhood below the yellow surface we obtain the same sequence of phase portraits. These facts suggest that the nonalgebraic

surface $7S_{12}$ has another piece of nonalgebraic surface (which we also denote by $7S_{19}$) being its continuation and which due to the bifurcation that it represents, it cannot intersect surfaces $2S_{18}$ and $4S_{45}$, then it must have its other endpoint on $4.8L_{12}$.

Moreover, up to slice $m = -98/100$, we had the existence of the nonalgebraic surface $7S_5$ being a common border of the regions V_{34} and V_{35}. Such a surface was "squeezed" in the slice $m = -1$ by the triple surface and, it is natural to expect that after the splitting of this triple surface, arises a new piece of nonalgebraic surface in the neighborhood of the region where $7S_5$ was located. In fact, it happens here. If we approach $4S_{60}$ by below, we obtain a phase portrait that is topologically equivalent to V_{96} and, when we approach $2S_{16}$ by above we obtain a phase portrait which is topologically equivalent to V_{95}. This suggests that there is some element of surface $(\mathcal{S}_7)$ between $4S_{60}$ and $2S_{16}$, which represents a nonalgebraic bifurcation due to the connection between a separatrix of the finite saddle–node with a separatrix of the finite saddle. We denote such a nonalgebraic surface by $7S_{21}$. We observe that as in $2S_{16}$ the finite saddle–node has become a cusp–type singularity, then $7S_{21}$ cannot have an endpoint on $2S_{16}$. In addition, as the dashed surface $4S_{60}$ only represents a $\mathcal{C}^\infty$ bifurcation, then $7S_{16}$ also cannot have an endpoint on it. On the other hand, if $7S_{18}$ has an endpoint on $4S_{50}$, then in order to make the respective bifurcation to happen, the invariant straight line would be broken. Therefore, $7S_{21}$ has $4.8L_{13}$ as an endpoint and such a surface is unbounded.

In Fig. 51 we sum up all the information given on the previous paragraphs.

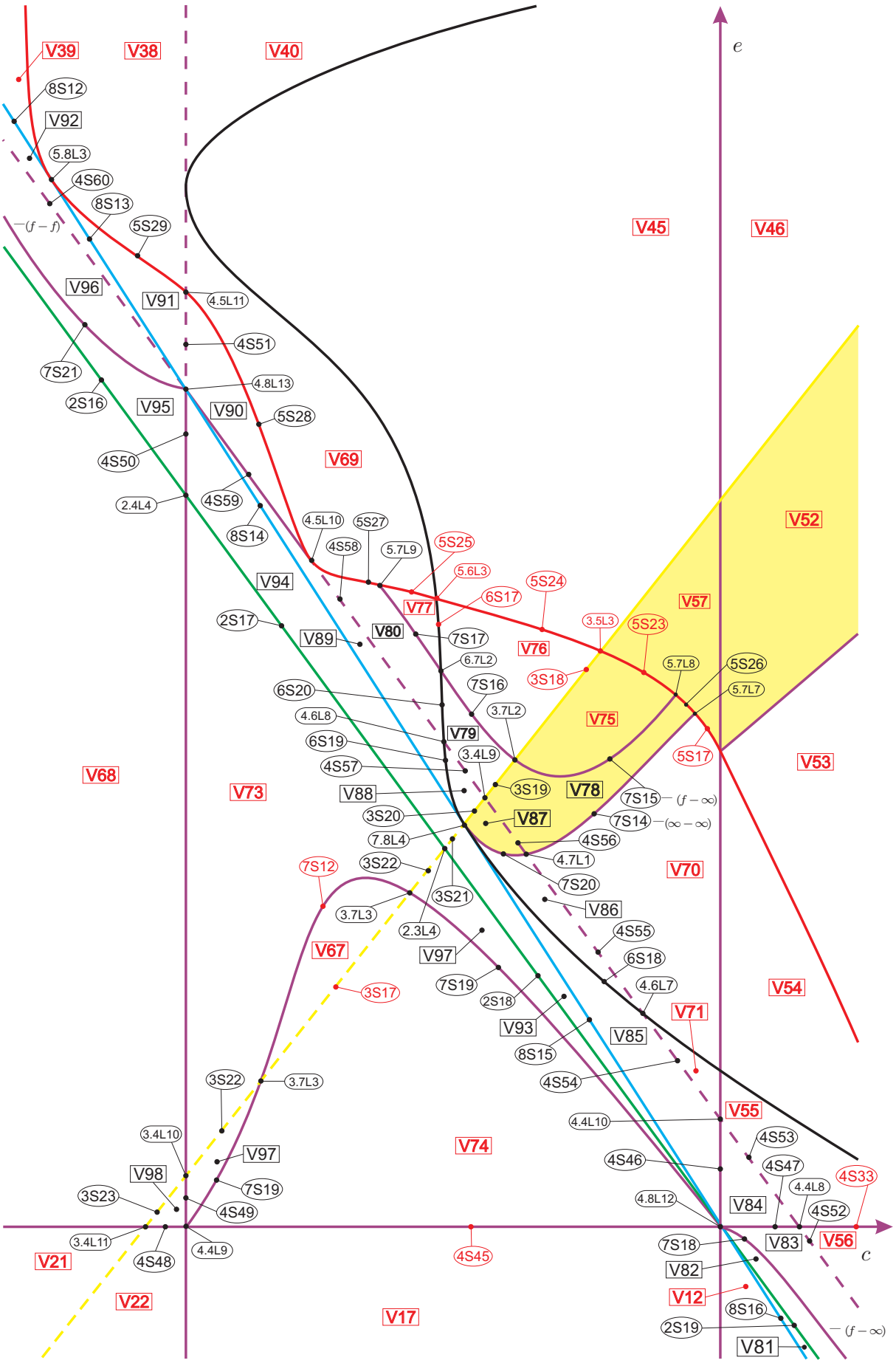

Fig. 51. Slice of parameter space when $m = -1 - \varepsilon_6$ (see Fig. 50)

After numerical analysis for values of m less than $m = -1 - \varepsilon_6$, but very close to it, we observe that must exist a singular value of the parameter m in which the curves $3.5L_3$ and $5.7L_8$ coalesce and this makes the volume region V_{75} disappear. In fact, such a region is reduced to the point P_{15} from slice $m = -1 - \varepsilon_6^*$, as in Fig. 52.

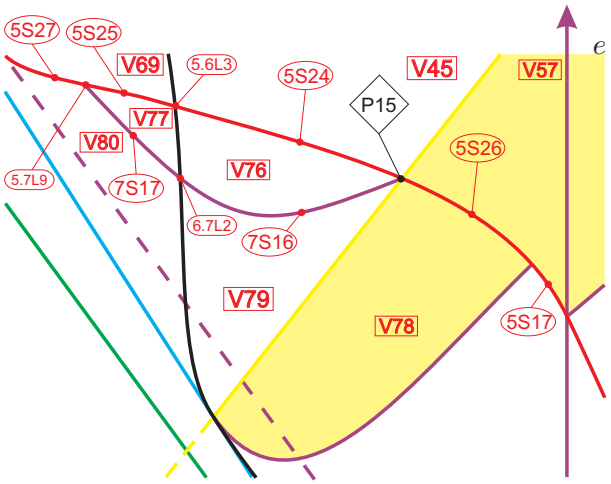

Fig. 52. Slice of parameter space when $m = -1 - \varepsilon_6^*$ (see Fig. 51)

Numerical analysis suggest that for a little bit smaller value of the parameter m, namely $m = -1 - \varepsilon_7$, corresponding to the point P_{15} we now have two curves and a piece of the red surface (namely, $3.5L_4$, $5.7L_{10}$, and $5S_{30}$, respectively) as in Fig. 53.

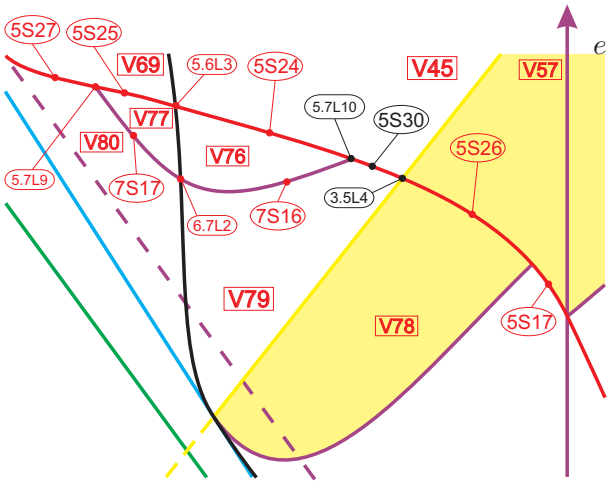

Fig. 53. Slice of parameter space when $m = -1 - \varepsilon_7$ (see Fig. 52)

Again by using numerical tools we detect that there must exist a singular value $m = -1 - \varepsilon_7^*$ in which the curves $5.6L_3$ and $5.7L_9$ coalesce, making the volume region V_{77} to disappear. Indeed, such a region is reduced to the point P_{16}, as in Fig. 54.

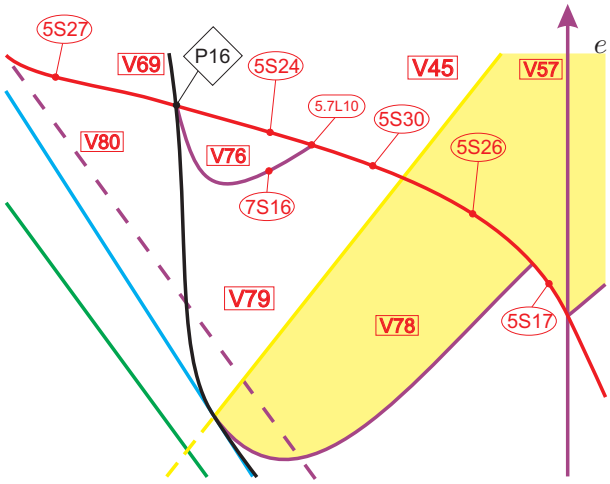

Fig. 54. Slice of parameter space when $m = -1 - \varepsilon_7^*$ (see Fig. 53)

Moving on with our numerical analysis, we observe that in generic slice $m = -1 - \varepsilon_8$, from the point P_{16} we now have two curves and a piece of the red surface (namely, $5.6L_4$, $5.7L_{10}$, and $5S_{30}$, respectively) as in Fig. 55.

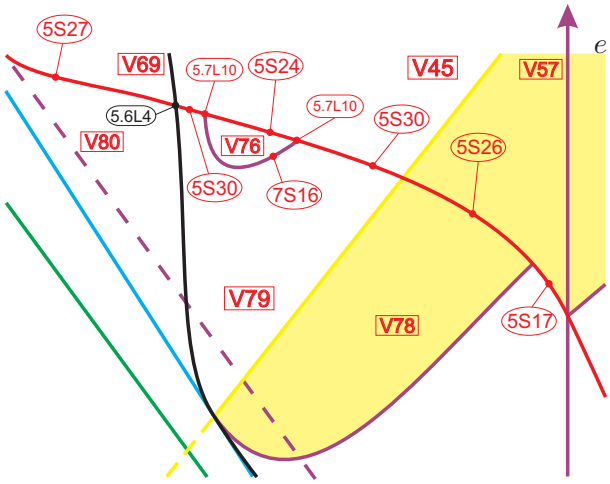

Fig. 55. Slice of parameter space when $m = -1 - \varepsilon_8$ (see Fig. 54)

Now, we detect that must exist a singular value $m = -1 - \varepsilon_8^*$ in which the curves $5.7L_{10}$ coalesce, making the volume region V_{76} to disappear, see Fig. 56.

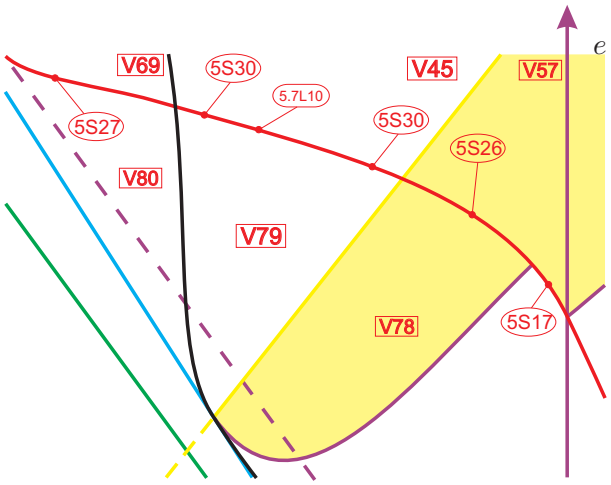

Fig. 56. Slice of parameter space when $m = -1 - \varepsilon_8^*$ (see Fig. 55)

The next nonalgebraic generic slice, $m = -1 - \varepsilon_9$, is again obtained by numerical tools and it represents the absence of the curve $5.7L_{10}$ and the displacement of the nonalgebraic surface $7S_{12}$ towards $3S_{17}$, making the volume region V_{67} to be "smaller". See the representation in Fig. 57.

On the other hand, as it was expected, due to the movement of these surfaces, there must exist a singular value $m = -1 - \varepsilon_9^*$ in which V_{67} vanishes. In fact, it is reduced to the curve $3.7L_3$ as in Fig. 58.

When we keep going down with the parameter m, we detect that for $m = -1-\varepsilon_{10}$ the nonalgebraic surface $7S_{19}$ no longer intersects $3S_{22}$. In fact, we describe this situation in Fig. 59.

We draw special attention for the fact that, up to here, the volume regions V_{71} and V_{80} have become even more smaller (see Fig. 59). Indeed, when we have the algebraic singular slice $m = -5/4$, such regions are reduced to the points P_{18} and P_{17}, respectively, as in Fig. 60.

In the generic slice $m = -13/10$, we observe that from the points P_{18} and P_{17} arise the volume regions V_{99} and V_{100}, respectively. Such regions, and their respective borders are presented in Fig. 61 in which we intend to show all the volume regions (modulo islands) in this slice.

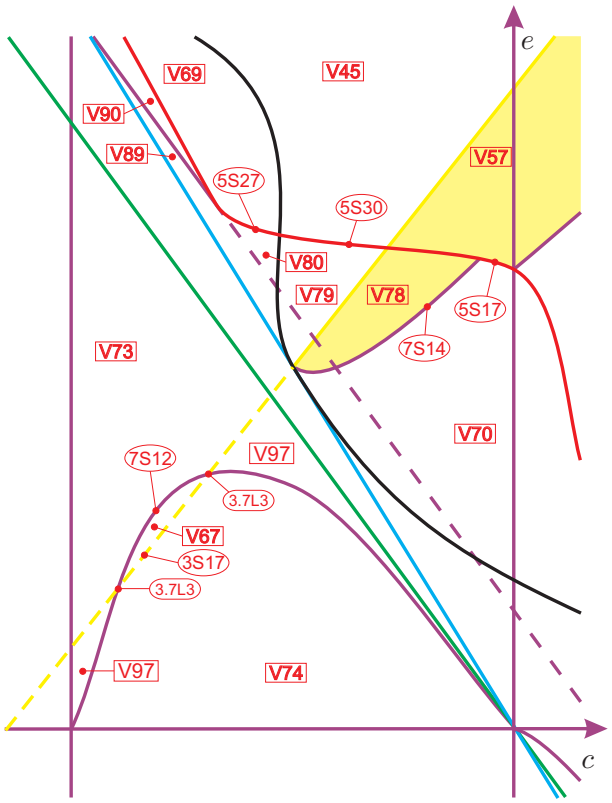

Fig. 57. Slice of parameter space when $m = -1 - \varepsilon_9$ (see Fig. 56)

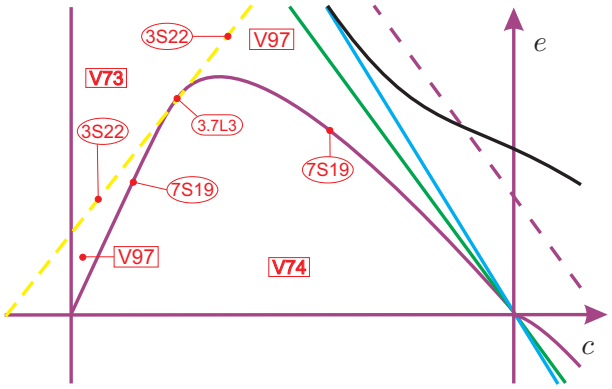

Fig. 58. Slice of parameter space when $m = -1 - \varepsilon_9^*$ (see Fig. 57)

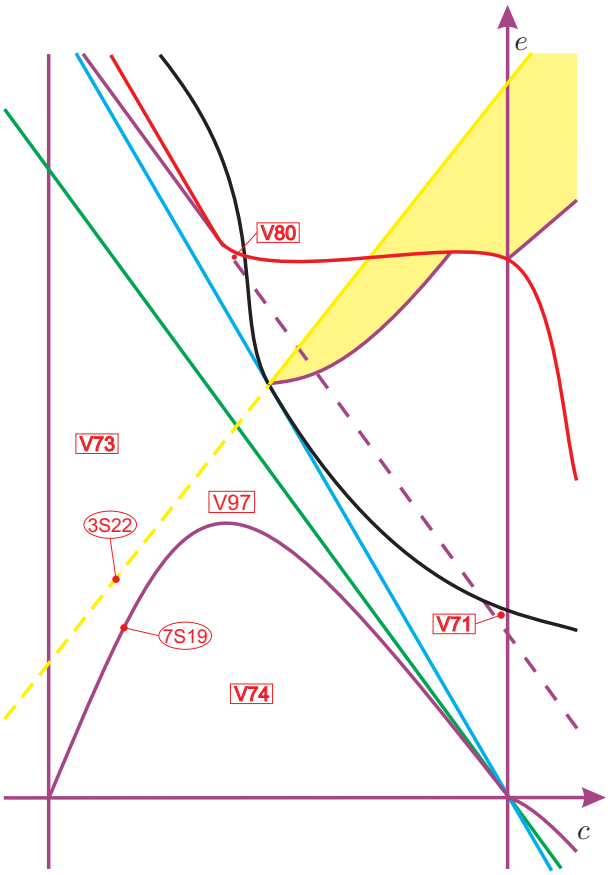

Fig. 59. Slice of parameter space when $m = -1 - \varepsilon_{10}$ (see Fig. 58)

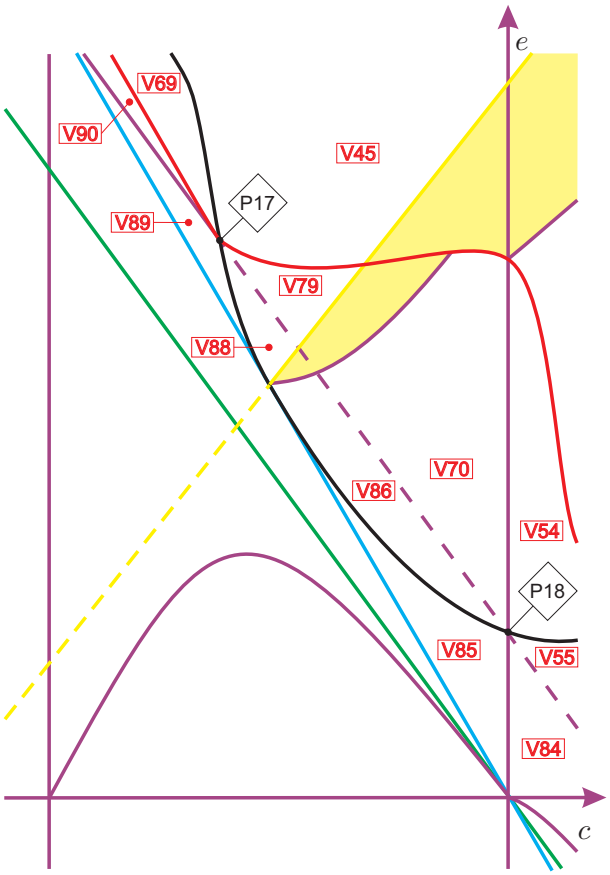

Fig. 60. Slice of parameter space when $m = -5/4$ (see Fig. 59)

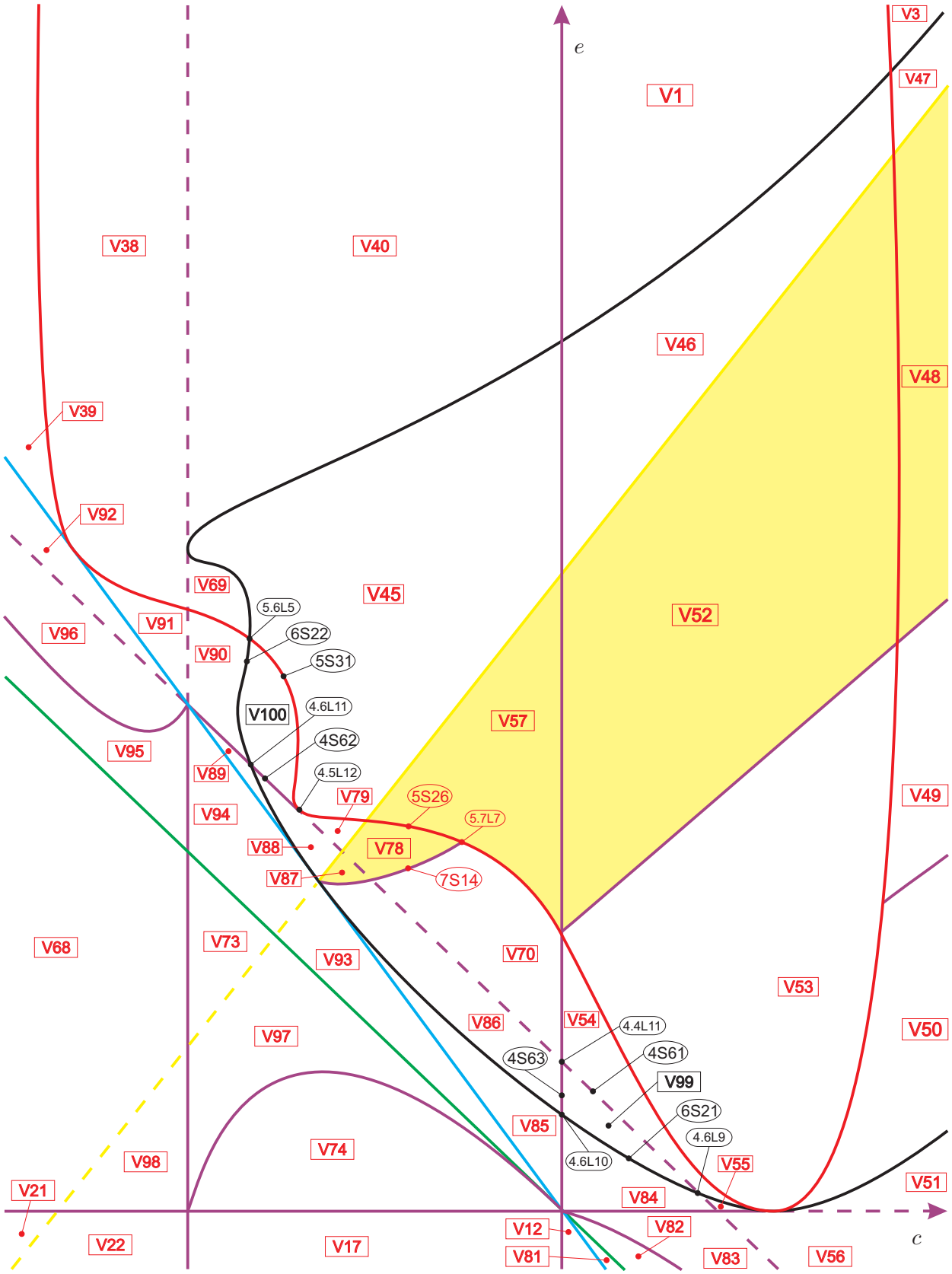

Fig. 61. Slice of parameter space when $m = -13/10$ (see Fig. 60)

By performing the study of the next singular slice, namely, $m = -3/2$, we only have one significant change in the bifurcation diagram. In fact, for this value of the parameter m the volume region V_{79} reduces to the point P_{19}, as in Fig. 62.

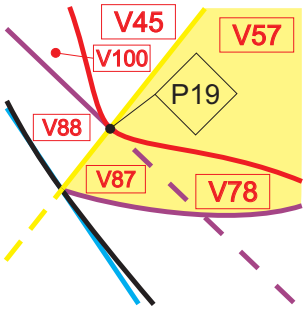

Fig. 62. Slice of parameter space when $m = -3/2$ (see Fig. 61)

Due to the displacement of all the surfaces, as it was expected, from the point P_{19} arises a new volume region, which we denote by V_{101}. In Fig. 63 we present a piece of the bifurcation diagram containing V_{101} when we consider the generic value $m = -7/4$.

Now when we go to the singular slice $m = -2$, we detect that the volume regions V_{70} (together with V_{78}) and V_{73} are reduced to the points P_{20} and P_{21}, respectively. The remaining bifurcation diagram does not present any other significant change, see Fig. 64.

By studying the next generic slice, $m = -5/2$, we observe that due to the displacement of the yellow surface, from the point P_{21} arises a new volume region which we denote by V_{103}. Moreover, due to the displacement of the purple surface (which is parallel to the green one) and the red surface, we detect the birth of two new volume regions, namely, V_{102} and V_{104}. In what follows, we explain a little bit about the existence of this two volume regions, in particular, we explain why there is the respective nonalgebraic surface $7S_{22}$. In fact, when we approach $4S_{67}$ to the right hand side we obtain a phase portrait that is topologically equivalent to V_{104}. On the other hand, when we approach $4S_{65}$ by above we obtain a phase portrait that is topologically equivalent to V_{102}. Then, there must exist a piece of surface $(\mathcal{S}_7)$ being a common border of these two regions. We denote this piece of nonalgebraic surface by $7S_{22}$, which corresponds to a

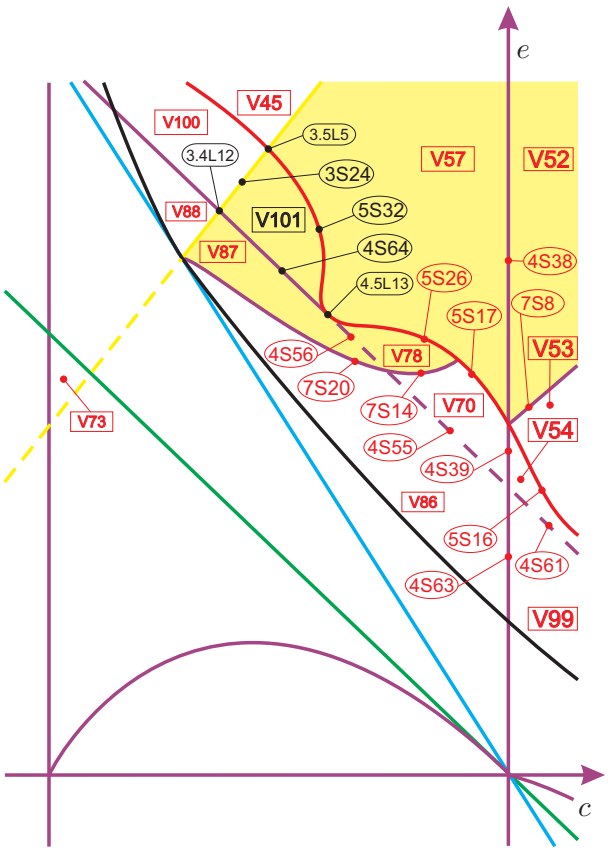

Fig. 63. Slice of parameter space when $m = -7/4$ (see Fig. 62)

loop–type bifurcation (of the finite saddle–node to itself). When we parametrize and make a study of the red surface, we obtain $5S_{33}$ being a border of V_{102} and $5S_{34}$ being a border of V_{104}, respectively. Then the nonalgebraic surface $7S_{22}$ has one of its endpoints on the red surface, more precisely, at $5.7L_{11}$. In fact, since $5S_{33}$ is a border of V_{53} and $5S_{34}$ is a border of V_{52}, we conclude that $7S_{22}$ is a continuation of the nonalgebraic surface $7S_8$. We claim that the other endpoint of $7S_{22}$ is $4.4L_{12}$. Indeed, if the other endpoint of $7S_{22}$ is in $4S_{67}$, then the invariant straight line should be broken in order to make the respective loop–type bifurcation to happen. For the same reason the endpoint of $7S_{22}$ cannot be in $4S_{65}$. In Fig. 65 we present this slice.

For a better comprehension of the graphics producing limit cycles in perturbations, in Fig. 66 we present an amplification of the neighborhood in the parameter space of the curve $4.4L_{12}$ (see Fig. 65) with the corresponding phase portraits.

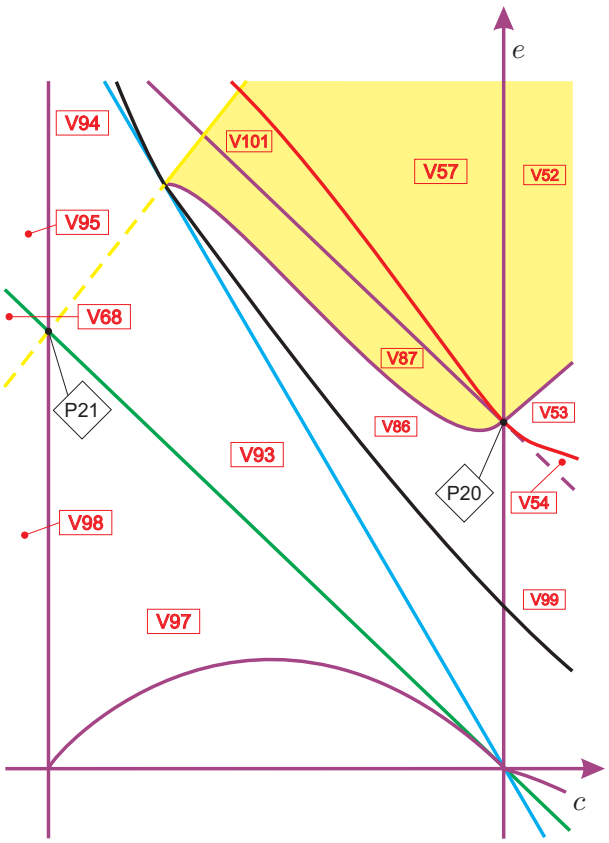

Fig. 64. Slice of parameter space when $m = -2$ (see Fig. 62)

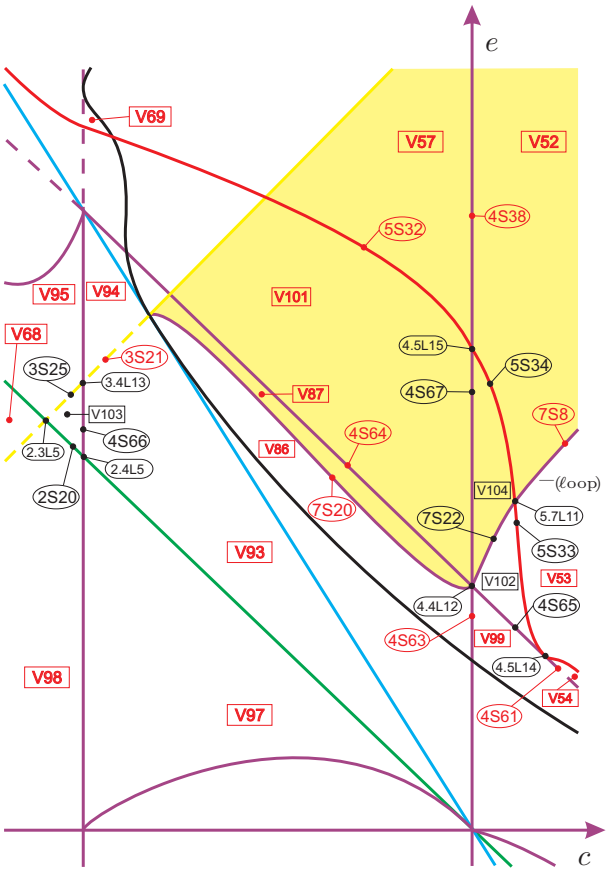

Fig. 65. Slice of parameter space when $m = -5/2$ (see Fig. 64)

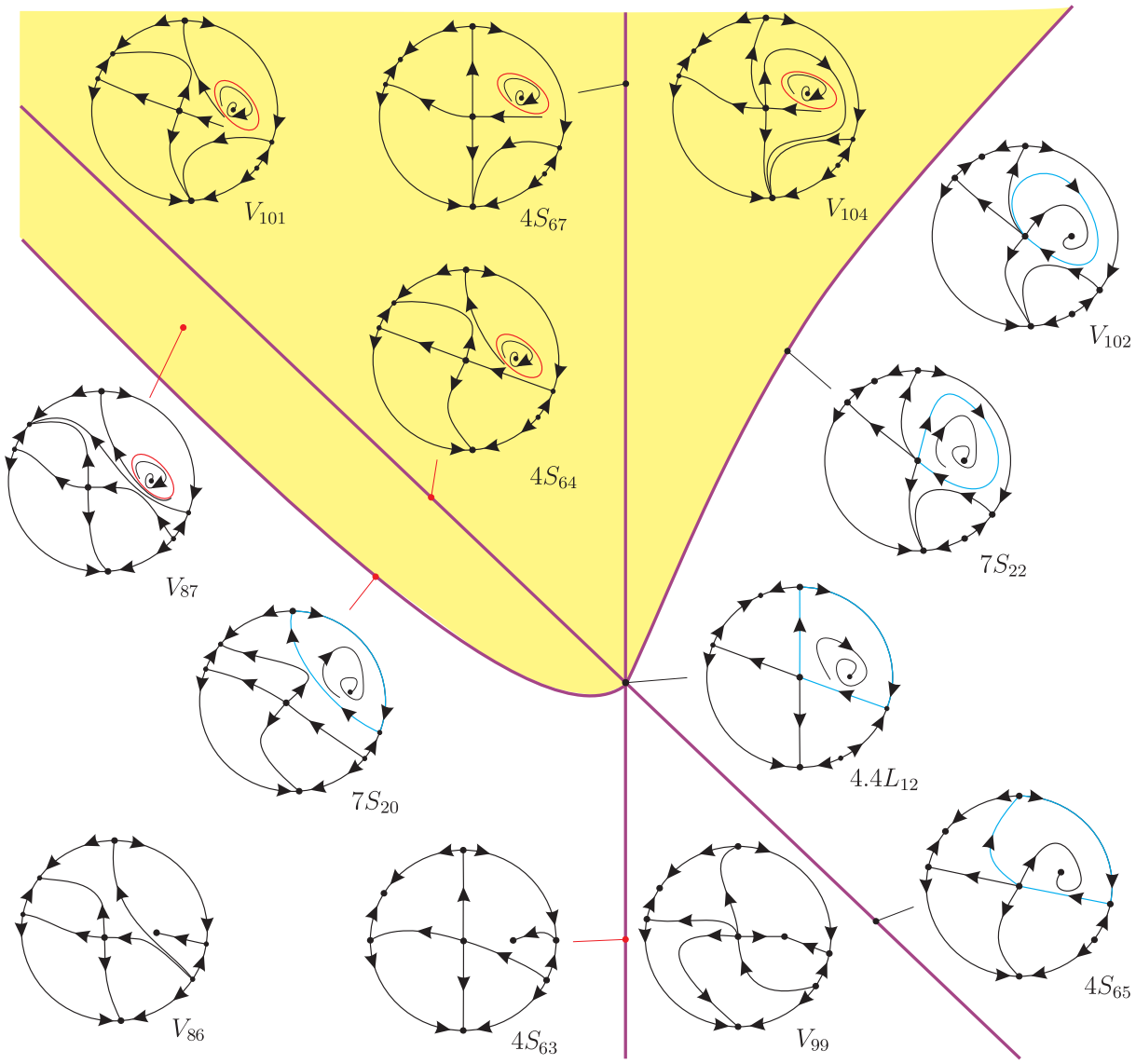

Fig. 66. Graphics producing limit cycles: neighborhood of $4.4L_{12}$ (see Fig. 65)

In Remark 4.2 we have concluded that the equation $\mathcal{T}_4 = \mathcal{F}_1 = 0$ has one double root if $\Delta = 0$, i.e. $m = \left(\pm 2\sqrt{2} - 3\right)/2$. In this way, the slice $m = \left(-2\sqrt{2} - 3\right)/2$ is singular. In fact, at this value of the parameter m we have a double curve $3.10L_3$, which in this case indicates a weak saddle of order two. This point splits surface $3S_{21}$ into two. Since these two pieces of surface $(\mathcal{S}_3)$ clearly produce topologically equivalent phase portraits, we denote both pieces by $3S_{21}$. The result can be seen in Fig. 67.

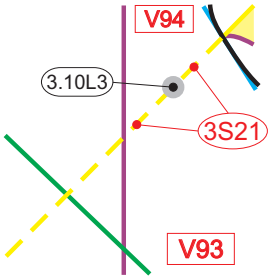

Fig. 67. Slice of parameter space when $m = \left(-2\sqrt{2} - 3\right)/2$ (see Fig. 65)

On the other hand, again according to Remark 4.2 we have proved that the equation $\mathcal{T}_4 = \mathcal{F}_1 = 0$ has two real roots for $\Delta > 0$, i.e. for $m \notin \left(\left(-2\sqrt{2} - 3\right)/2, \left(2\sqrt{2} - 3\right)/2\right)$. Therefore, on the next generic slice, namely, $m = -295/100$, the curve $3.10L_3$ became two, creating surface $3S_{26}$, as in Fig. 68.

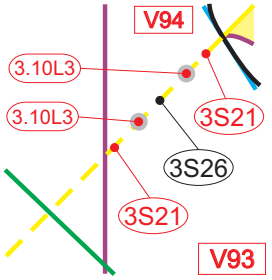

Fig. 68. Slice of parameter space when $m = -295/100$ (see Fig. 67)

Proceeding the study of the next singular slice, $m = -3$, we observe that the curved triangle V_{69} (see Fig. 65) coalesces in a point, namely P_{22}. This is caused by the displacement of the black and red surfaces. Moreover, we also note that the two curves $3.10L_3$ moved themselves, causing the death of both pieces of surface $3S_{21}$. Then we have the corresponding points P_{23} and P_{24}. The remaining of the bifurcation diagram is topologically equivalent to the previous one. We present this result in Fig. 69.

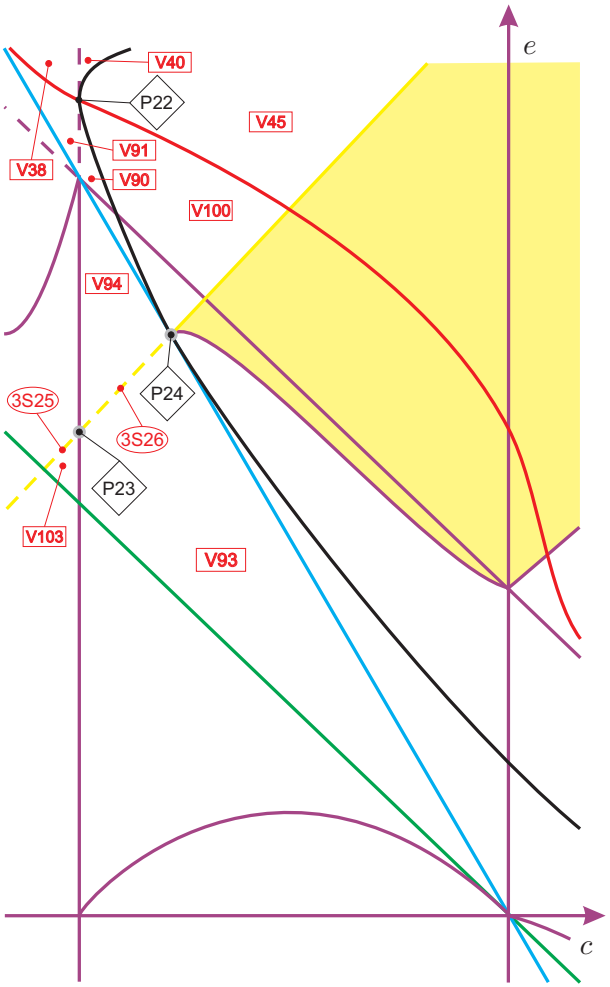

Fig. 69. Slice of parameter space when $m = -3$ (see Fig. 68)

When we make a study of values of the parameter m less than $m = -3$, but very close to it, up to $m = -7/2$ we detect three important things: First, from the point P_{22} arises a new volume region, which we denote by V_{105}. Second, from P_{23} a piece of surface $(\mathcal{S}_3)$ is born, namely, $3S_{29}$. The third thing (which is the more interesting one) is that from P_{24} two pieces of surface $(\mathcal{S}_3)$ are born, namely, $3S_{28}$ (without limit cycle) and $3S_{27}$ (with limit cycle). In order to have coherence on the bifurcation diagram, we observe that both pieces of sur-

face must have an endpoint of surface $7S_{20}$ (which refers to a connection between a separatrix of the infinite saddle–node and a separatrix of the infinite saddle) being a common edge. In fact, numerical analysis support this claim. We observe that there must exist a continuation of the nonalgebraic surface $7S_{20}$ and this fact can be checked by using numerical tools. Indeed, we start by approaching $3S_{28}$ by above and then we obtain a phase portrait V_{106}, which contains a limit cycle. However, when we approach $4S_{62}$ and also $6S_{19}$ we obtain (in both cases) a phase portrait that is topologically equivalent to V_{88} (without limit cycles). Then we must have an element of surface $(\mathcal{S}_7)$ which corresponds to a bifurcation due to a connection between a separatrix of the infinite saddle–node and a separatrix of the infinite saddle. Therefore, such a piece of nonalgebraic surface (which we call $7S_{23}$) is indeed a continuation of $7S_{20}$. Due to our numerical analysis described above and due to the fact that on black surfaces we can only have a $\mathcal{C}^\infty$ node–focus bifurcation, we conclude that the other endpoint of $7S_{23}$ is $7.8L_5$. Then, this piece of nonalgebraic surface is a border of the new volume region V_{106}.

On the other hand, surface $3S_{27}$ has $3.10L_5$ (the gray surface) being a common edge with $3S_{20}$, in fact, such a surface represents a weak focus of order two. As surface $3S_{27}$ contains a limit cycle and we know that on surface $(\mathcal{S}_3)$ one can have Hopf bifurcations, we can expect that in some neighborhood of this surface we have a region containing two limit cycles. Indeed, when we approach such a surface by below we obtain a phase portrait that is topologically equivalent to V_{87} (i.e. containing only one limit cycle) and, on the other hand, when we approach $3S_{27}$ by above we obtain a phase portrait V_{107}, which contains 2 limit cycles surrounding the same focus. However, when we approach $4S_{62}$ and also $6S_{19}$ we obtain (in both cases) a phase portrait that is topologically equivalent to V_{88} (without limit cycles). Then there must have an element $10S_1$ of surface $(\mathcal{S}_{10})$ which corresponds to a bifurcation of double limit cycle in order to keep the coherence in the bifurcation diagram. Lemma 4.45 assures the existence of such a surface and there we indicate its endpoints.

Lemma 4.45. *Surface* $10S_1$ *corresponds to a bifurcation of a double limit cycle and its endpoints are on* $7.8L_5$ *and* $3.10L_5$.

Proof. We consider Fig. 70. Part V_{87} first appeared in slice when $m = -1 - \varepsilon_6$ and its corresponding phase portrait possesses a limit cycle. We note that on surfaces $3S_{20}$, $3S_{27}$, $3S_{28}$ and on their linking points the phase portraits possess a weak focus of order at least one and, consequently, they refer to a Hopf bifurcation. If we are in part V_{87} and cross surface $3S_{20}$, we enter part V_{88} and the limit cycle is lost. Following this idea, the same should happens if we cross surface $3S_{27}$, but that is not what happens. After crossing this surface, the limit cycle persist when entering part V_{107}. In fact the Hopf bifurcation creates a second limit cycle. We note that these two limit cycles are around the same focus, because there is only one focus in this portion of the parameter space. Then, as in part V_{88} we do not have limit cycles and in V_{107} we have two of them (around the same focus), there must exist at least one element $10S_1$ of surface $(\mathcal{S}_{10})$ dividing these two parts and corresponding to the presence of a double limit cycle.
Now, it remains to prove where $10S_1$ starts from. We know that curve $3.10L_5$ corresponds to the presence of a weak focus of order two. With this in mind, it is more comprehensible that leaving part V_{87} and crossing the yellow surface, we enter in two topologically distinct parts, one with limit cycles and the other without them. The linking curve $3.10L_5$ of surfaces $3S_{20}$ and $3S_{27}$ is responsible for this, i.e. if we "walk" along surface $3S_{20}$, which does not possess limit cycle, and cross $3.10L_5$, the focus becomes weaker and a Hopf bifurcation happens, implying the birth of a limit cycle in the representatives of $3S_{27}$. Then, by this argument and by numerical evidences, surface $10S_1$ starts from $3.10L_5$. Moreover, since surface $3S_{27}$ has a limit cycle and this limit cycle is lost when we pass by the curve $3.7L_4$, and (on the bifurcation diagram) if we take several parallel straight lines sufficiently close to $3S_{28}$ and $3S_{27}$ by above, we detect numerically that, in fact, the other endpoint of surface $10S_1$ is $7.8L_5$. ■

We present the slice $m = -7/2$ in Fig. 70 and we show in Fig. 71 an amplification of the neighborhood in the parameter space of the curve $3.7L_4$ with the corresponding phase portraits. In these and in the next figures we have colored in light green the

regions whose the respective phase portraits possess two limit cycles.

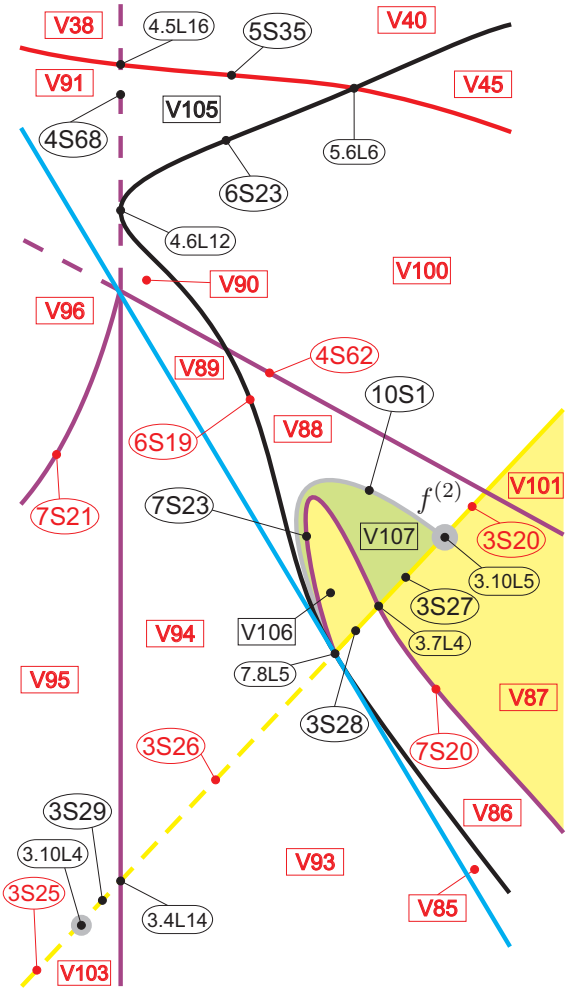

Fig. 70. Slice of parameter space when $m = -7/2$ (see Fig. 69)

Regarding the previous lemma, we have to explain a little bit about three situations that cannot hapen here:

1. surfaces $10S_1$ and $7S_{23}$ cannot intersect each other, since otherwise we would necessarily have a region containing 3 limit cycles (1 from V_{106} plus 2 generated by a piece of surface $10S_1$) being neighbor of V_{88}, which does not contain limit cycles, a contradiction. In Fig. 72 we present this hypothetic situation indicating only the respective number of limit cycles in each region. In this and in the next figures we have colored in light purple the regions whose the respective phase portraits possess three limit cycles.

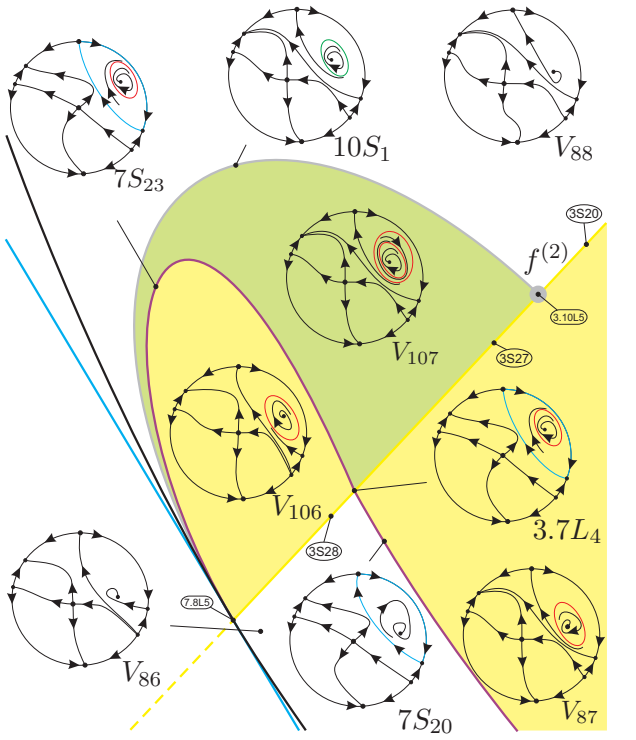

Fig. 71. Neighborhood in the parameter space of the curve $3.7L_4$ with the corresponding phase portraits: the existence of double limit cycle from a $f^{(2)}$

2. surface $10S_1$ cannot have an endpoint on $7S_{23}$, since otherwise we would have a piece of $7S_{23}$ with one (simple) limit cycle and other piece without limit cycles. Then the linking point would be a bifurcation due to a double limit cycle. In Fig. 73 we present this hypothetical situation and as before, we indicate only the respective number of limit cycles in each region.

3. the endpoint of $10S_1$ cannot be on $3.7L_4$, due to the different stability of the antisaddles on the neighbors of $3.7L_4$. In fact, this situation could happen unless we have a singularity of type center. But, according to [Vulpe, 2011; Main Theorem, item (b_4)], for the normal form (5) we do not have such a singularity, since on Remark 4.2 we saw that $\mathcal{F}_3\mathcal{F}_4 \neq 0$. In Fig. 74 we present this hypothetic situation and again we only indicate the respective number of limit cycles in each region.

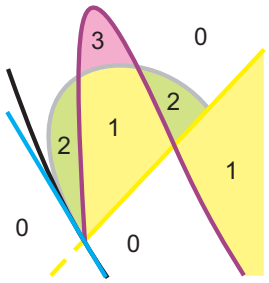

Fig. 72. Hypothetic situation of intersection between $7S_{23}$ and $10S_1$. We indicate the respective number of limit cycles that each region possesses (see Fig. 71)

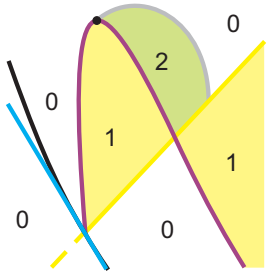

Fig. 73. Hypothetic situation in which surface $10S_1$ has an endpoint on $7S_{23}$. We indicate the respective number of limit cycles that each region possesses (see Fig. 71)

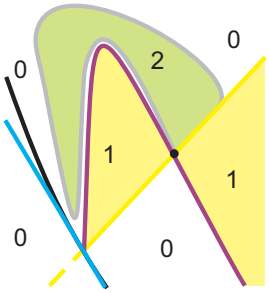

Fig. 74. Hypothetic situation in which surface $10S_1$ has an endpoint on $3.7L_4$. We indicate the respective number of limit cycles that each region possesses (see Fig. 71)

The next important value of the parameter m to be considered is $m = -4$. At this level, the volume region V_{57} (see Fig. 65) reduces to the point P_{25} as in Fig. 75.

By studying values of the parameter m less than but closer to $m = -4$, namely $m = -4 - \varepsilon_{11}$, we observe that from the point P_{25} arises a new volume region, which we denote by V_{108} as in Fig. 76.

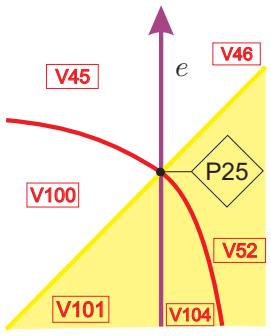

Fig. 75. Slice of parameter space when $m = -4$ (see Fig. 70)

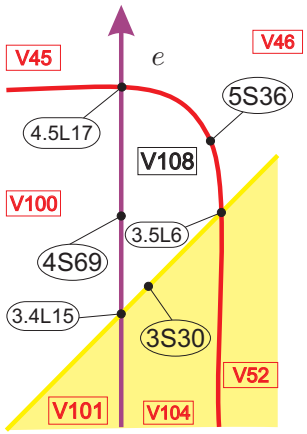

Fig. 76. Slice of parameter space when $m = -4 - \varepsilon_{11}$ (see Fig. 75)

Regarding Remark 4.2, we know that for $m = -21/5$ we have a third order weak singularity. In fact, as we saw in such a remark, this singularity comes from equation

$$\mathcal{T}_4 = \mathcal{F}_1 = \mathcal{F}_2 = 0,$$

then if we move down from $m = -7/2$ (see Fig. 70) towards $m = -21/5$, we observe that the curve $3.10L_5$ (which was indicating a weak focus of second order) for $m = -7/2$ represents a weak focus of third order. As we saw in Remark 4.2, this situation happens for only one value of the parameter m, i.e. we have a point that represents this weak focus of third order. We denote such a point by P_{26}, see Fig. 77.

Now, for smaller values of m, close to $m = -21/5$, the weak singularity is again of order two. Moreover, if we parametrize the yellow surface and

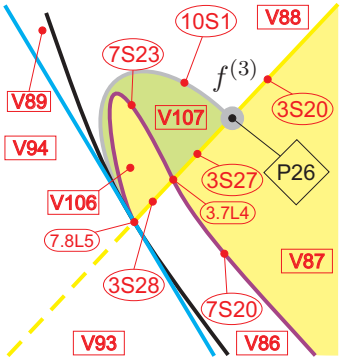

Fig. 77. Slice of parameter space when $m = -21/5$ (see Fig. 76)

"walk" on it, by starting on the piece that represents $3S_{20}$ and move down with the parameter c, in a certain moment we pass by a bifurcation that allows us to detect the existence of two limit cycles on a portion of the yellow surface. After that we pass by another bifurcation that gives us a phase portrait that is topologically equivalent to $3S_{27}$. We denote the portion containing two limit cycles by $3S_{31}$. As this surface contains two limit cycles and we know that on surface $(\mathcal{S}_3)$ one can have Hopf bifurcations, we can expect that in some neighborhood of this surface we have a region containing three limit cycles. Indeed, we already know that by above this surface we have a phase portrait corresponding to V_{107}, i.e. containing two limit cycles. When we approach such a surface by below we obtain a phase portrait V_{109}, which contains 3 limit cycles surrounding the same focus. However, when we approach $3S_{20}$, $3S_{27}$ (by below) and also in a neighborhood above of the nonalgebraic border $7S_{20}$ we obtain (in all the cases) a phase portrait that is topologically equivalent to V_{87} (with only one limit cycle). Then there must exist an element $10S_2$ of surface $(\mathcal{S}_{10})$ which corresponds to a bifurcation of double limit cycle in order to keep the coherence in the bifurcation diagram. In fact, we detect that $10S_2$ is a continuation of $10S_1$. Lemma 4.46 assures the existence of such a surface and there we indicate its endpoints.

Lemma 4.46. *Surface $10S_2$ corresponds to a bifurcation of a double limit cycle and its endpoints are on $3.10L_6$ and $3.10L_7$.*

Proof. We consider Fig. 78. Part V_{107} first appeared in slice when $m = -7/2$ and its corresponding phase portrait possesses two limit cycles. If we are in this part and cross surface $3S_{27}$, we enter part V_{87} and one of the limit cycles is lost. Following this idea, the same should happens if we cross surface $3S_{31}$, but that is not what happens. After crossing this surface, due to the presence of two limit cycles on this surface, the Hopf bifurcation creates a third limit cycle. We note that these three limit cycles are around the same focus, because there is only one focus in this portion of the parameter space. Then, as in part V_{87} we have one limit cycle and in V_{109} we have three of them (around the same focus), there must exist at least one element $10S_2$ of surface $(\mathcal{S}_{10})$ dividing these two parts and corresponding to the presence of a double limit cycle.
Now, it remains to prove where $10S_2$ starts from. We know that curve $3.10L_7$ corresponds to the presence of a weak focus of order two. With this in mind, it is more comprehensible that leaving part V_{107} and crossing the yellow surface, we enter in two topologically distinct parts, one with one limit cycle and the other with three of them. The linking curve $3.10L_7$ of surfaces $3S_{27}$ and $3S_{31}$ is responsible for this, i.e. if we "walk" along surface $3S_{27}$, which possess one limit cycle, and cross $3.10L_7$, the focus becomes weaker and a Hopf bifurcation happens, implying the birth of second limit cycle in the representatives of $3S_{31}$. Then, by this argument and by numerical evidences, surface $10S_2$ starts from $3.10L_7$. Moreover, since surface $3S_{31}$ has two limit cycles and one of them is lost when we pass by the curve $3.10L_7$, and (on the bifurcation diagram) if we take several parallel straight lines sufficiently close to $3S_{31}$ and $3S_{20}$ by above and by below, we detect numerically that, in fact, the other endpoint of surface $10S_2$ is $3.10L_6$ and therefore such a surface is a continuation of surface $10S_1$. ■

We present the generic slice $m = -21/5 - \varepsilon_{12}$ in Fig. 78 as an amplification of the neighborhood in the parameter space of the curve $3.10L_7$ with the corresponding phase portraits. Not that, in this figure and also in the two next ones, it is possible to verify the corresponding bifurcations due to the presence of graphics.

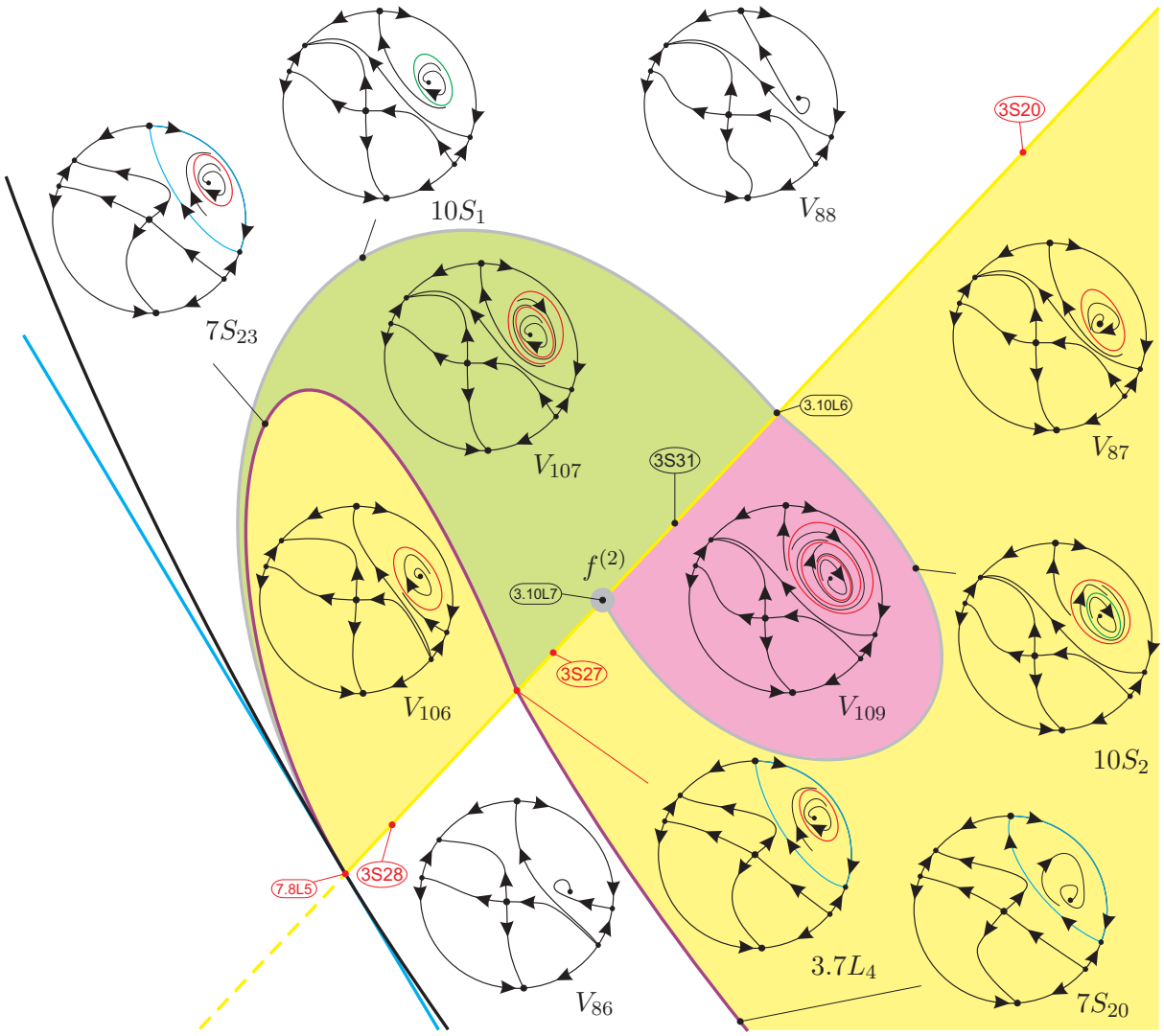

Fig. 78. Slice of parameter space when $m = -21/5 - \varepsilon_{12}$ (see Fig. 77)

When we keep going down, by performing the study of values of the parameter m yet less than $m = -21/5$, but very close to it, numerical analysis suggest that for some singular nonalgebraic value $m = -21/5 - \varepsilon_{12}^{*}$, the curves $3.10L_7$ and $3.7L_4$ coalesce, creating the point P_{27}, which represents a weak focus of order two, see Fig. 79.

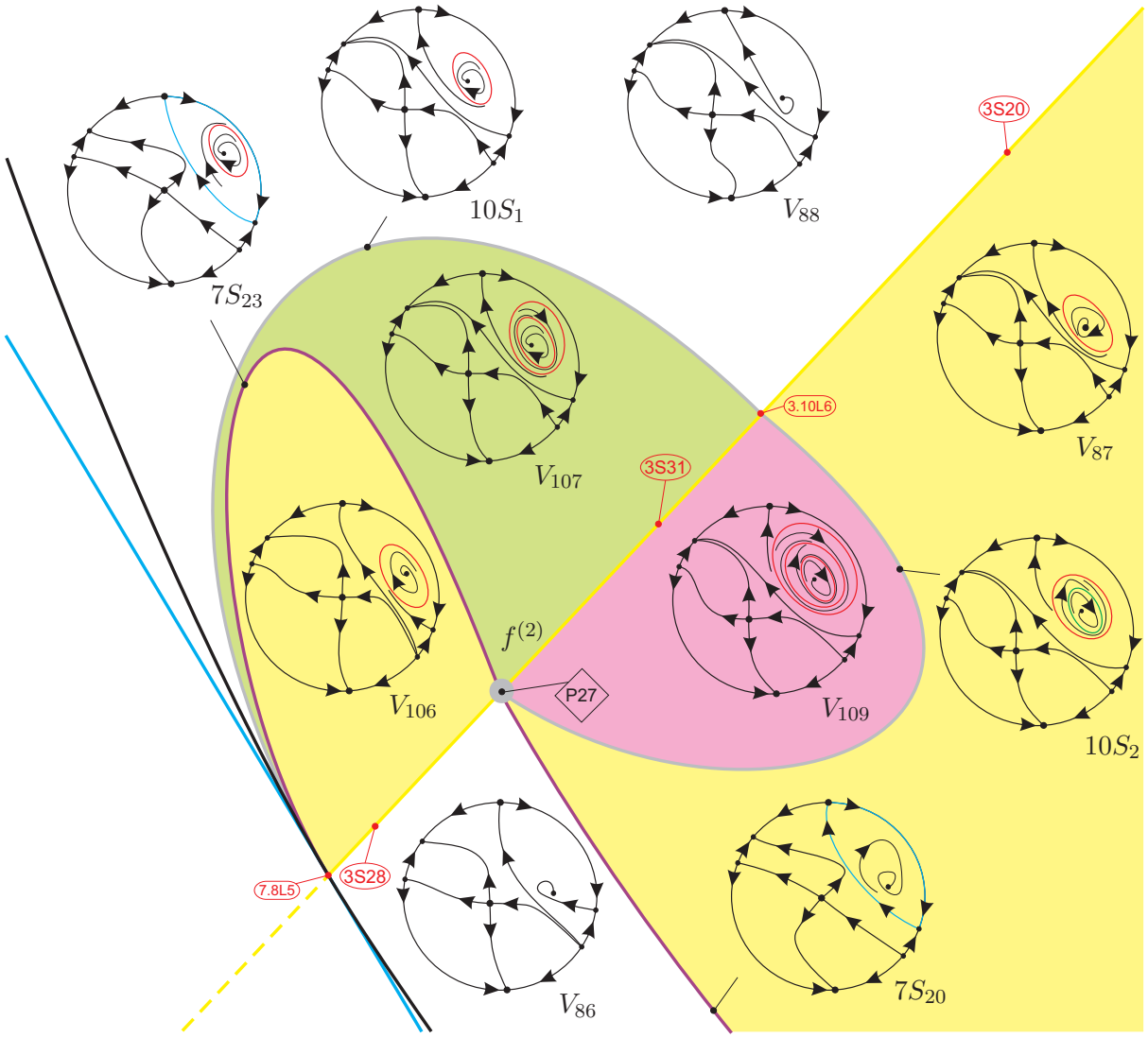

Fig. 79. Slice of parameter space when $m = -21/5 - \varepsilon_{12}^{*}$ (see Fig. 78)

Having analyzed the next generic slice (modulo islands) $m = -21/5 - \varepsilon_{13}$ we note that from the point P_{27} arises a new piece of surface $(\mathcal{S}_3)$, namely, $3S_{32}$, which contains a limit cycle. Such a piece of surface has an endpoint on $3.7L_5$ (the connection between $3S_{31}$ and $3S_{32}$, which refer to a connection between a separatrix of the infinite saddle–node and a separatrix of the infinite saddle) and its another endpoint is the gray curve $3.10L_8$, which is a weak focus of order two. As surface $3S_{32}$ contains a limit cycle and we know that on surface $(\mathcal{S}_3)$ we can have Hopf bifurcations, we can expect that in some neighborhood of this surface we have a region containing two limit cycles. Indeed, when we approach such a surface by above we obtain a phase portrait that is topologically equivalent to V_{106} (i.e. containing only one limit cycle). On the other hand, when we approach $3S_{32}$ by below we obtain a phase portrait V_{110}, which contains 2 limit cycles surrounding the same focus. However, when we approach $3S_{28}$ by below and $6S_{18}$ by above we get (in both cases) a phase portrait that is topologically equivalent to V_{86} (without limit cycles). Then we must have an element $10S_3$ of surface $(\mathcal{S}_{10})$ which corresponds to a bifurcation of double limit cycle in order to keep the coherence in the bifurcation diagram. We observe that surface $10S_3$ is a continuation of surface $10S_2$. Lemma 4.47 assures the existence of surface $10S_3$ and there we prove where are located its endpoints. As we do not have other significant change in the bifurcation diagram, here we only present in Fig. 80 an amplification of the neighborhood in the parameter space of the curve $3.7L_5$ with the corresponding phase portraits.

Lemma 4.47. *Surface $10S_3$ corresponds to a bifurcation of a double limit cycle and its endpoints are on $7.10L_1$ and $3.10L_8$.*

Proof. We consider Fig. 80. Part V_{106} first appeared in slice when $m = -7/2$ and its corresponding phase portrait possesses one limit cycle. We note that on surfaces $3S_{28}$, $3S_{32}$ and at their linking curve $3.10L_8$, the respective phase portraits possess a weak focus of order at least one and, consequently, they refer to a Hopf bifurcation. If we are in part V_{106} and cross the surface $3S_{28}$, we enter part V_{86} and the limit cycle is lost. Following this idea, the same should happens if we cross the surface $3S_{32}$, but that is not what happens. After crossing this surface, the limit cycle persist when entering part V_{110}. In fact the Hopf bifurcation creates a second limit cycle. We note that these two limit cycles are around the same focus, because there is only one focus in this portion of the parameter space. Then, as in part V_{86} we do not have limit cycles and in V_{110} we have two of them (around the same focus), there must exist at least one element $10S_3$ of surface $(\mathcal{S}_{10})$ dividing these two parts and corresponding to the presence of a double limit cycle.

Now, it remains to prove where $10S_3$ starts from. We know that the curve $3.10L_8$ corresponds to the presence of a weak focus of order two. With this in mind, it is more comprehensible that leaving part V_{106} and crossing the yellow surface, we enter into two topologically distinct parts, one with limit cycles and the other without them. The linking curve $3.10L_8$ of the surfaces $3S_{28}$ and $3S_{32}$ is responsible for this, i.e. if we "walk" along the surface $3S_{28}$, which does not possess limit cycle, and cross $3.10L_8$, the focus becomes weaker and a Hopf bifurcation happens, implying the birth of a limit cycle in the representatives of $3S_{32}$. Then, by this argument and by numerical evidences, surface $10S_3$ starts from $3.10L_8$. Moreover, since surface $3S_{32}$ has one limit cycle and when we pass by the curve $3.7L_5$ we have two of them, and (on the bifurcation diagram) if we take several parallel straight lines sufficiently close to $3S_{32}$ and $3S_{31}$ by below, we detect that there is no element of V_{86} neither V_{87} between V_{110} and V_{109}. Therefore the other endpoint of surface $10S_3$ is $7.10L_1$ and such a surface is a continuation of surface $10S_2$. ■

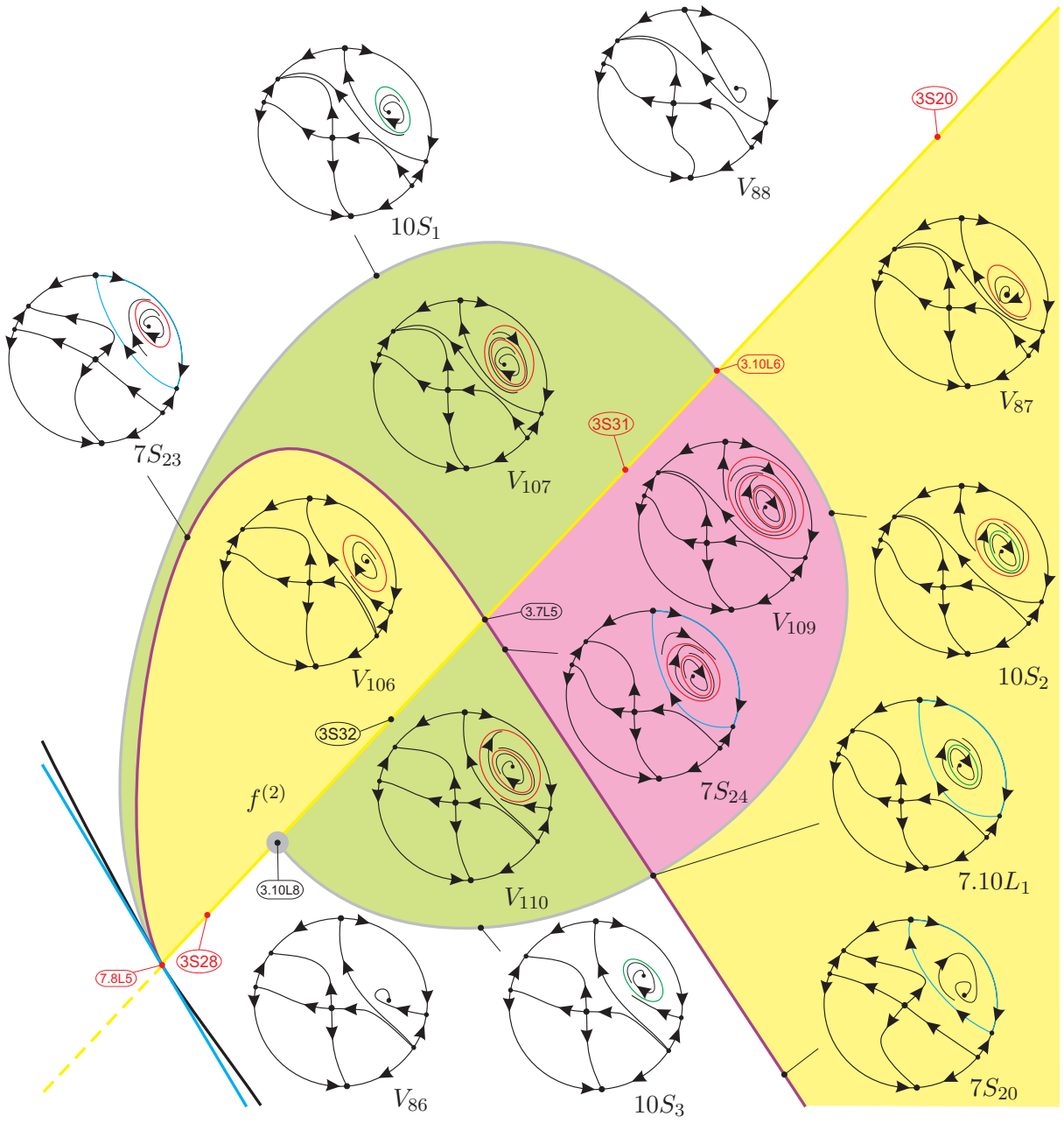

Fig. 80. Neighborhood in the parameter space of the curve $3.7L_5$ with the corresponding phase portraits: the existence of double limit cycle from $f^{(2)}$ and for $m = -21/5 - \varepsilon_{13}$

When we perform the study of the values of the parameter m small but very close to $m = -21/5 - \varepsilon_{13}$, we observe that must exist a nonalgebraic singular value $m = -21/5 - \varepsilon^*_{13}$ in which the nonalgebraic surface $7S_{21}$ is tangent to the piece of surface $3S_{29}$ (see Fig. 70) at $3.7L_6$. We present this fact in Fig. 81.

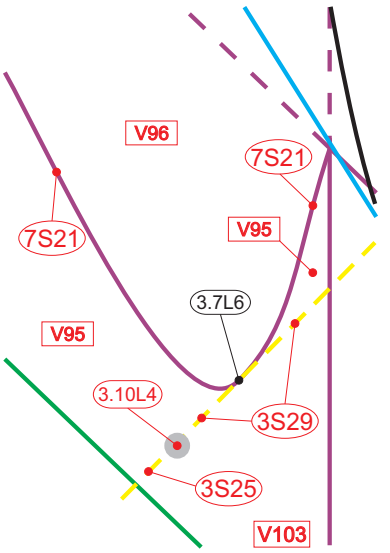

Fig. 81. Slice of parameter space when $m = -21/5 - \varepsilon^*_{13}$ (see Fig. 80)

Now, for some generic nonalgebraic value $m = -21/5 - \varepsilon_{14}$, as it was expected, from $3.7L_6$ arises a new volume region, which we denote by V_{111}, see Fig. 82.

The last singular slice ($m = -8$) describes the death of the volumetric region V_{45} (see for instance Fig. 61). Indeed, it reduces to the point P_{28} as in Fig. 83.

We finally arrive at the last generic slice, namely, $m = -10$. Here, the only important thing is that from the point P_{28} we have the birth of the volumetric region V_{112}. The remaining bifurcation diagram does not present any other significant change. We show this new volumetric region (and its borders) in Fig. 84. In such a figure we intend to give an idea of the entire bifurcation diagram from $m = -10$.

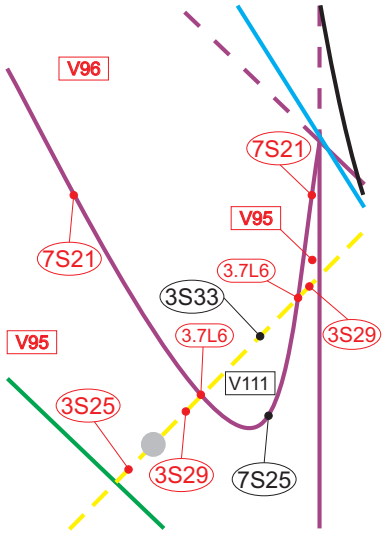

Fig. 82. Slice of parameter space when $m = -21/5 - \varepsilon_{14}$ (see Fig. 81)

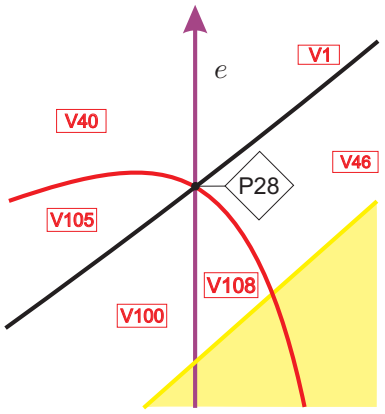

Fig. 83. Slice of parameter space when $m = -8$ (see Fig. 82)

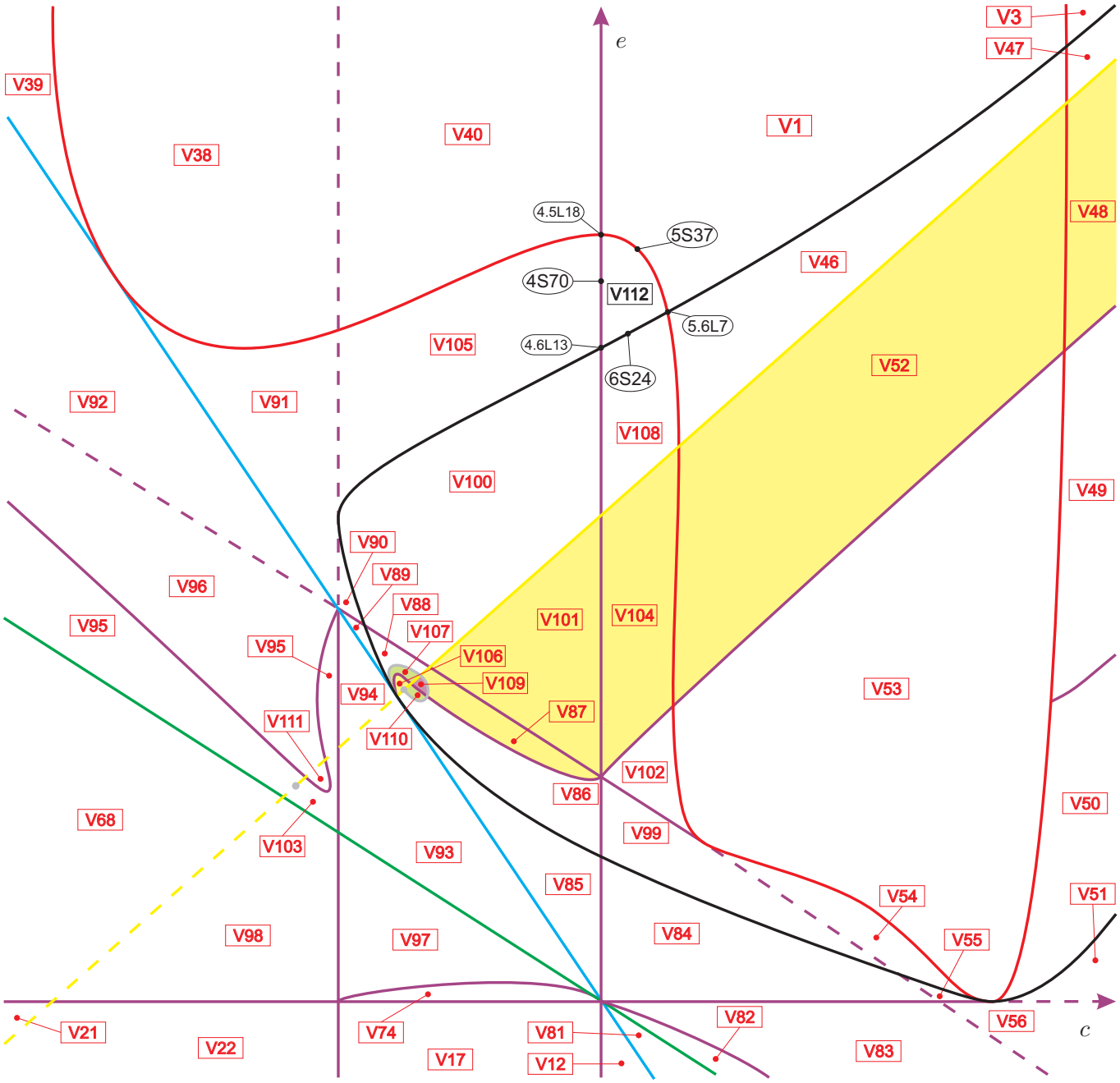

Fig. 84. Slice of parameter space when $m = -10$ (see Fig. 83)

After having finished the study of all values of the parameter m presented in (10), when we compare the two finite extreme values of such a parameter, i.e. $m = 4$ and $m = -10$, we observe that the regions $V_1, V_3, V_{12}, V_{17}, V_{21}, V_{22}, V_{38}, V_{39}$, and V_{40} appear in all slices.

We point out that the slice $m = -\infty$ is easily obtained from the slice $m = +\infty$. In fact, due to the symmetry in h (see page 16), the slices $m = +\infty$ and $m = -\infty$ are symmetrical. These slices correspond to $h = 0$ and $m = \pm 1$, respectively. Setting $h = 0$ and $m = -1$, systems (5) become

$$\begin{aligned} \dot{x} &= cx + cy - cx^2, \\ \dot{y} &= ex + ey - ex^2 - 2xy, \end{aligned} \tag{12}$$

which differs from (11) only by the sign of the parameter m (i.e. by the sign of the $2xy$–term).

Due to the symmetry in discussion, in Fig. 85 we present the slice when $m = -\infty$ properly labeled. As we mentioned before for the slice $m = +\infty$, here we draw special attention for the fact that the nonalgebraic surfaces (numeric detected and which existence was proved before) still remain at this slice and they "follow the movements" of the algebraic surfaces during the transition between the slices $m = -10$ and $m = -\infty$. Moreover, in Table 4 we indicate the death of all volumetric parts from slice $m = -10$ to $m = -\infty$. Then we have established the correspondence between the phase portraits of the slices $m = -10$ and $m = -\infty$.

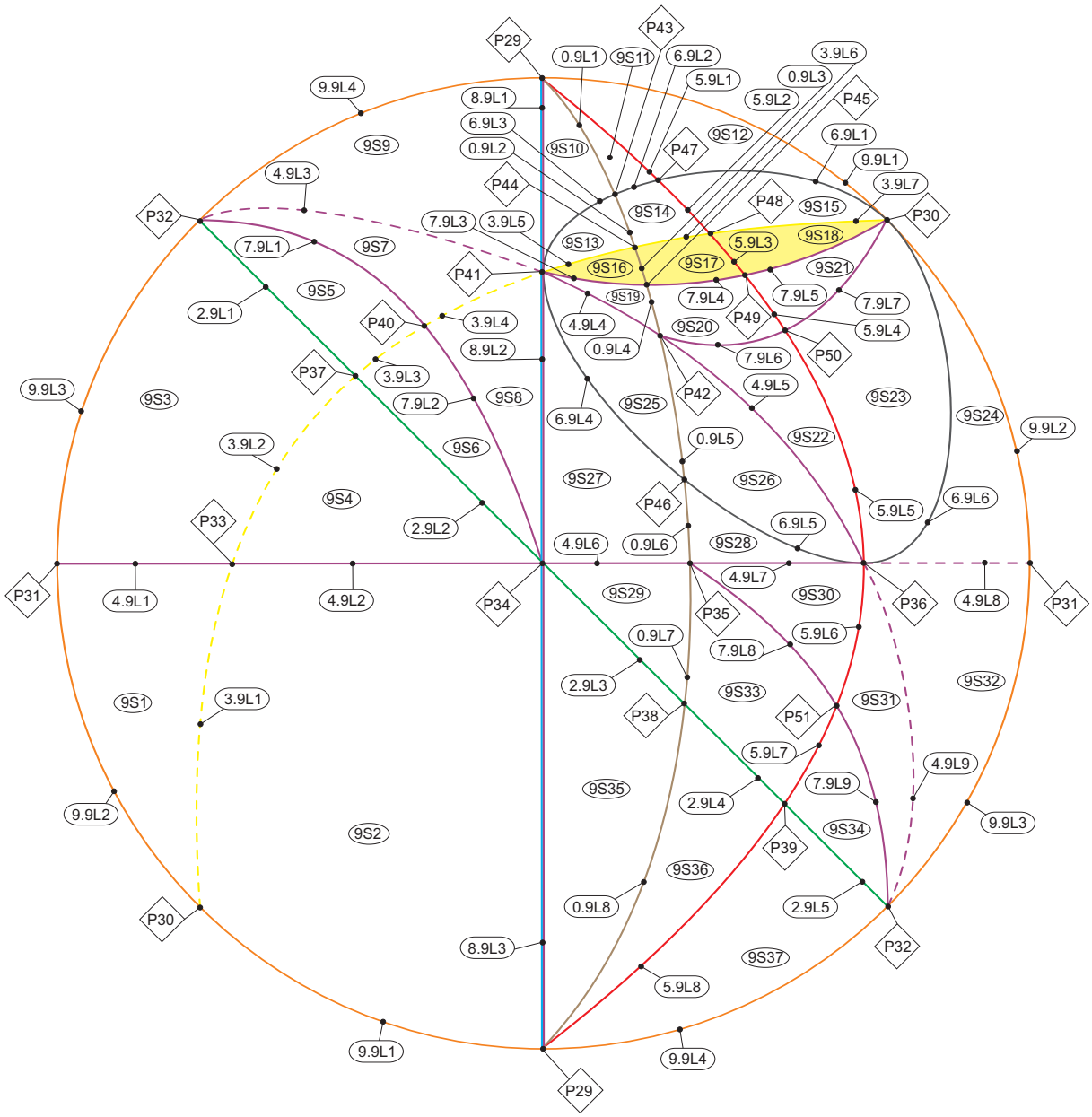

Fig. 85. Slice of parameter space when $m = -\infty$

Table 4. Transition from slice $m = -10$ to $m = -\infty$. Here we present the correspondence between the volumetric regions from slice $m = -10$ and the respective parts from slice $m = -\infty$

Parts in slice $m = -10$	Parts in slice $m = -\infty$	Parts in slice $m = -10$	Parts in slice $m = -\infty$
V_1	$5.9L_1$	V_{86}	P_{41}
V_3	$9S_{12}$	V_{87}	P_{41}
V_{12}	$8.9L_3$	V_{88}	P_{41}
V_{17}	$8.9L_3$	V_{89}	P_{41}
V_{21}	$9S_1$	V_{90}	P_{41}
V_{22}	$9S_2$	V_{91}	$8.9L_1$
V_{38}	$5.9L_1$	V_{92}	$9S_9$
V_{39}	$8.9L_1$	V_{93}	P_{34}
V_{40}	$5.9L_1$	V_{94}	P_{41}
V_{46}	$5.9L_2$	V_{95}	$9S_5$
V_{47}	$9S_{15}$	V_{96}	$9S_7$
V_{48}	$9S_{18}$	V_{97}	P_{34}
V_{49}	$9S_{21}$	V_{98}	$9S_4$
V_{50}	$9S_{23}$	V_{99}	$9S_{25}$, $9S_{26}$
V_{51}	$9S_{24}$	V_{100}	P_{41}
V_{52}	$5.9L_3$	V_{101}	P_{41}
V_{53}	$5.9L_4$, P_{50}, $5.9L_5$	V_{102}	$9S_{19}$, $9S_{20}$, $9S_{22}$
V_{54}	P_{36}	V_{103}	$9S_6$
V_{55}	P_{36}	V_{104}	$9S_{16}$, $9S_{17}$
V_{56}	$9S_{32}$	V_{105}	$8.9L_1$
V_{68}	$9S_3$	V_{106}	P_{41}
V_{74}	P_{34}	V_{107}	P_{41}
V_{81}	$9S_{35}$, $9S_{36}$, $9S_{37}$	V_{108}	$9S_{13}$, $9S_{14}$
V_{82}	$9S_{29}$, $9S_{33}$, $9S_{34}$	V_{109}	P_{41}
V_{83}	$9S_{30}$, $9S_{31}$	V_{110}	P_{41}
V_{84}	$9S_{27}$, $9S_{28}$	V_{111}	$9S_8$
V_{85}	$8.9L_2$, P_{34}, P_{41}	V_{112}	$9S_{10}$, $9S_{11}$

Since there is coherence among the generic slices bordering the most singular slices $m = 1$, $m = 0$ and $m = -1$, with their respective generic side slices, no more slices are needed for the complete coherence of the bifurcation diagram. So, all the values of m in (10) are sufficient for the coherence of the bifurcation diagram. Thus, we can affirm that we have described a complete bifurcation diagram for class $\overline{\mathbf{QsnSN_{11}(B)}}$ modulo islands, as we discuss in Sec. 5.

5. Other relevant facts about the bifurcation diagrams

The bifurcation diagram we have obtained for the class $\overline{\mathbf{QsnSN_{11}(B)}}$ is completely coherent, i.e. in this family, by taking any two points in the parameter space and joining them by a continuous curve, along this curve the changes in phase portraits that occur when crossing the different bifurcation surfaces we mention can be completely explained.

Nevertheless, we cannot be sure that this bifurcation diagram is the complete bifurcation diagram for $\overline{\mathbf{QsnSN_{11}(B)}}$ due to the possibility of the existence of "islands" inside the parts bordered by unmentioned bifurcation surfaces. In case they exist, these "islands" would not mean any modification of the nature of the singular points. So, on the border of these "islands" we could only have bifurcations due to saddle connections or multiple limit cycles.

In case there were more bifurcation surfaces, we should still be able to join two representatives of any two parts of the 631 parts of $\overline{\mathbf{QsnSN_{11}(B)}}$ found until now with a continuous curve either without crossing such a bifurcation surface or, in case the curve crosses it, it must do it an even number of times without tangencies, otherwise one must take into account the multiplicity of the tangency, so the total number must be even. This is why we call these potential bifurcation surfaces "*islands*".

However, we have not found a different phase portrait which could fit in such an island. A potential "island" would be the set of parameters for which the phase portraits possess a double limit cycle and this "island" would be inside the parts where $W_4 < 0$ since we have the presence of a focus (recall item (iii) of Sec. 3).

6. Completion of the proof of the main theorem

In the bifurcation diagram we may have topologically equivalent phase portraits belonging to distinct parts of the parameter space. As here we have 631 distinct parts of the parameter space, to help us to identify or to distinguish phase portraits, we need to introduce some invariants and we actually choose integer valued, character and symbol invariants. Some of them were already used in [Artés *et al.*, 2013b], [Artés *et al.*, 2014], [Artés *et al.*, 2015], and [Artés *et al.*, 2020b], but we recall them and introduce some needed ones. These invariants yield a classification which is easier to grasp.

Definition 6.1. We denote by $I_1(S)$ a symbol from the set $\{\emptyset, [\times], [\cup], [)(]\}$ which indicate the following configuration of curves filled up with singularities, respectively: none (nondegenerate systems – in this case all systems does not contain a curve

filled up with singularities), two real straight lines intersecting at a finite point, a parabola and an hyperbola. This invariant only makes sense to distinguish the degenerate phase portrait obtained.

Definition 6.2. We denote by $I_2(S)$ the sum of the indices of the isolated real finite singular points.

Definition 6.3. We denote by $I_3(S)$ the number of the real infinite singular points. We note that this number can also be infinity, which is represented by ∞.

Definition 6.4. For a given infinite singularity s of a system S, let ℓ_s be the number of global or local separatrices beginning or ending at s and which do not lie on the line at infinity. We have $0 \leq \ell_s \leq 4$. We denote by $I_4(S)$ the sequence of all such ℓ_s when s moves in the set of infinite singular points of the system S. We start the sequence at the infinite singular point which receives (or sends) the greatest number of separatrices and take the direction which yields the greatest absolute value, e.g. the values 2110 and 2011 for this invariant are symmetrical (and, therefore, they are the same), so we consider 2110.

Definition 6.5. We denote by $I_5(S)$ the total number of local or global separatrices of the finite multiple singularity which link it with the infinite multiple singular points.

Definition 6.6. We denote by $I_6(S)$ a character from the set $\{\overline{sn}_{(2)}, \widehat{cp}_{(2)}\}$ which describes the type of the multiple singularity located at the origin.

Definition 6.7. We denote by $I_7(S)$ the number of local or global separatrices starting or ending at the nodal sector of the finite saddle–node.

Definition 6.8. We denote by $I_8(S)$ a character from the set $\{n, y\}$ which indicate if the separatrix of the infinite saddle–node $\overline{\binom{1}{1}}SN$ has the same limit of a separatrix of the finite saddle–node $\overline{sn}_{(2)}$.

Definition 6.9. We denote by $I_9(S)$ a character from the set $\{n, y\}$ describing the nonexistence ("n") or the existence ("y") of basins (see page 34).

Definition 6.10. We denote by $I_{10}(S)$ a character from the set $\{n, y\}$ describing the nonexistence ("n") or the existence ("y") of graphics.

Definition 6.11. We denote by $I_{11}(S)$ the number of local or global separatrices starting or ending at the finite antisaddle.

Definition 6.12. We denote by $I_{12}(S)$ the total number of local or global separatrices linking the finite simple singularity to the infinite saddle–node $\overline{\binom{1}{1}}SN$.

Definition 6.13. We denote by $I_{13}(S)$ the number of limit cycles around a foci.

Definition 6.14. In case there is an infinite singularity which does not belong to the hyperbola filled up with singularities, we denote by $I_{14}(S)$ a character from the set $\{n, y\}$ (for **n**o or **y**es, respectively) describing if the infinite singularity is located between two other infinite singularities which belong to the same branch of the hyperbola filled up with singularities.

As we have noted previously in Remark 4.34, we do not distinguish between phase portraits whose only difference is that in one we have a finite node and in the other a focus. Both phase portraits are topologically equivalent and they can only be distinguished within the C^1 class. In case we may want to distinguish between them, a new invariant may easily be introduced.

Theorem 6.15. *Consider the class* $\overline{\mathbf{QsnSN_{11}(B)}}$ *and all the phase portraits that we have obtained for this family. The values of the affine invariant* $\mathcal{I} = (I_1, I_2, I_3, I_4, I_5, I_6, I_7, I_8, I_9, I_{10}, I_{11}, I_{12}, I_{13}, I_{14})$ *given in the diagram from Tables 7 to 12 yield a partition of these phase portraits of the class* $\overline{\mathbf{QsnSN_{11}(B)}}$.

Furthermore, for each value of $\mathcal{I}$ *in this diagram there corresponds a single phase portrait; i.e.* S *and* S' *are such that* $\mathcal{I}(S) = \mathcal{I}(S')$*, if and only if* S *and* S' *are topologically equivalent.*

The bifurcation diagram for $\overline{\mathbf{QsnSN_{11}(B)}}$ has 631 parts which produce 226 topologically different phase portraits as described in Tables 7 to 26. The remaining 405 parts do not produce any new phase portrait which was not included in the 226 previous

ones. The difference is basically the presence of a strong focus instead of a node and vice versa and weak points.

The phase portraits having neither limit cycle nor graphic have been denoted surrounded by parenthesis, for example (V_{77}); the phase portraits having one, two or three limit cycles have been denoted surrounded by brackets, for example $[V_{57}]$ possessing one limit cycle, $[[V_{107}]]$ possessing two limit cycles, and $[[[V_{109}]]]$ possessing three limit cycles; the phase portraits having one graphic have been denoted surrounded by $\{*\}$ and those ones having two or more graphics have been denoted surrounded by $\{\{*\}\}$, for example $\{5S_{17}\}$ and $\{\{9S_{10}\}\}$, respectively. Moreover, the phase portraits having one limit cycle and one (respectively, more than one) graphic have been denoted surrounded by $[\{*\}]$ (respectively, $[\{\{*\}\}]$), for example $[\{7S_{23}\}]$ (respectively, $[\{\{9S_{17}\}\}]$). In addition, the phase portraits possessing a double limit cycle have been denoted surrounded by $[*]^2$ and those ones which possesses a double limit cycle and also a simple one have been denoted surrounded by $[[*]^2]$, for instance $[10S_1]^2$ and $[[10S_2]^2]$, respectively.

Proof of Theorem 6.15. The above result follows from the results in the previous sections and a careful analysis of the bifurcation diagrams given in Sec. 4, in Figs. 14 to 85, the definition of the invariants I_j and their explicit values for the corresponding phase portraits. ■

We recall some observations regarding the equivalence relations used in this study: the affine and time rescaling, C^1 and topological equivalences.

The coarsest one among these three is the topological equivalence and the finest is the affine equivalence. We can have two systems which are topologically equivalent but not C^1-equivalent. For example, we could have a system with a finite antisaddle which is a structurally stable node and in another system with a focus, the two systems being topologically equivalent but belonging to distinct C^1-equivalence classes, separated by the surface $(\mathcal{S}_6)$ on which the node turns into a focus.

In Tables 13 to 26 we list in the first column 226 parts with all the distinct phase portraits of Figs. 1 to 7. Corresponding to each part listed in column one we have in each row all parts whose phase portraits are topologically equivalent to the phase portrait appearing in column 1 of the same row.

In the second column we set all the parts whose systems yield topologically equivalent phase portraits to those in the first column, but which may have some algebro–geometric features related to the position of the orbits. In the third column we present all the parts which are topologically equivalent to the ones from the first column having a focus instead of a node.

In the fourth (respectively, fifth; and sixth) column we list all parts whose phase portraits have a node which is at a bifurcation point producing foci close to the node in perturbations, a node–focus to shorten (respectively, a finite weak singular point; and possess an invariant curve not yielding a connection of separatrices).

The last column refers to other reasons associated to different geometrical aspects and they are described as follows:

(1) the degenerate phase portrait possesses either a weak finite singular point, or a node–focus, or a cusp–type singularity, or an invariant line, or even a combination of these elements;

(2) the phase portrait possesses a singularity of type $\binom{\widehat{1}}{2}E-H$ at infinity;

(3) the phase portraits correspond to symmetric parts of the bifurcation diagram.

Whenever phase portraits appear in a row in a specific column, the listing is done according to the decreasing dimension of the parts where they appear, always placing the lower dimensions on lower lines.

6.1. Proof of the main theorem

The bifurcation diagram described in Sec. 4, plus Tables 7 to 12 of the geometrical invariants distinguishing the 226 phase portraits, plus Tables 13 to 26 giving the equivalences with the remaining phase portraits lead to the proof of the main statement of Theorem 1.1.

As it was expected, in the class $\overline{\mathbf{QsnSN_{11}(B)}}$, all the unfoldings of the phase portraits corresponding to parts of volumetric regions yield a phase portrait of codimension one from groups (A) and (C) (i.e. with a finite saddle–node $\overline{sn}_{(2)}$ and with a infinite saddle–node of type $\binom{\overline{1}}{1}SN$, respectively, see

page 1 for the description of these groups and also [Artés *et al.*, 2021] for more details). In tables 5 and 6 we present the correspondence between the phase portraits of the volume regions with their respective unfoldings of codimension one. In such tables, on the first column we present all the topologically distinct phase portraits of the volumetric regions from the class $\overline{\mathbf{QsnSN_{11}(B)}}$. On the second (respectively, third, fourth and fifth) column we present the phase portrait obtained after we perform a perturbation of the respective phase portrait from the first column in order to split the finite saddle–node $\overline{sn}_{(2)}$ into a saddle plus a node (respectively, to make the finite saddle–node $\overline{sn}_{(2)}$ disappear, to make the infinite saddle–node $\overline{\binom{1}{1}}SN$ loose a saddle (respectively, a node) for the finite part). In all of these columns, when the phase portrait possesses a limit cycle, we indicate the corresponding phase portrait which does not possesses limit cycle (for instance, $V_{25} \equiv V_{23}(L.C.)$ means that the phase portrait V_{25} is topologically equivalent to V_{23} with limit cycle). Moreover, we indicate [Artés *et al.*, 2018] for the notation and respective phase portraits of codimension one that appear as unfoldings on these tables.

Table 5. The respective unfoldings of codimension one of the phase portraits corresponding to parts of volume

	Unfoldings of codimension one			
Phase portrait from	Splitting	Disappearing	Splitting	Splitting
$\overline{\mathbf{QsnSN_{11}(B)}}$	$\overline{sn}_{(2)}$	$\overline{sn}_{(2)}$	$\overline{\binom{1}{1}}SN\ (\downarrow s)$	$\overline{\binom{1}{1}}SN\ (\downarrow n)$
V_1	$\mathbb{U}^1_{C,2}$	$\mathbb{U}^1_{C,1}$	$\mathbb{U}^1_{A,3}$	$\mathbb{U}^1_{A,12}$
V_2	$\mathbb{U}^1_{C,23}$	$\mathbb{U}^1_{C,17}$	$\mathbb{U}^1_{A,32}$	$\mathbb{U}^1_{A,61}$
V_3	$\mathbb{U}^1_{C,26}$	$\mathbb{U}^1_{C,16}$	$\mathbb{U}^1_{A,23}$	$\mathbb{U}^1_{A,66}$
V_4	$\mathbb{U}^1_{C,7}$	$\mathbb{U}^1_{C,4}$	$\mathbb{U}^1_{A,15}$	$\mathbb{U}^1_{A,32}$
V_6	$\mathbb{U}^1_{C,6}$	$\mathbb{U}^1_{C,4}$	$\mathbb{U}^1_{A,18}$	$\mathbb{U}^1_{A,27}$
V_8	$\mathbb{U}^1_{C,10}$	$\mathbb{U}^1_{C,4}$	$\mathbb{U}^1_{A,17}$	$\mathbb{U}^1_{A,42}$
V_{10}	$\mathbb{U}^1_{C,12}$	$\mathbb{U}^1_{C,4}$	$\mathbb{U}^1_{A,16}$	$\mathbb{U}^1_{A,52}$
V_{13}	$\mathbb{U}^1_{C,14}$	$\mathbb{U}^1_{C,4}$	$\mathbb{U}^1_{A,14}$	$\mathbb{U}^1_{A,55}$
V_{14}	$\mathbb{U}^1_{C,22}$	$\mathbb{U}^1_{C,17}$	$\mathbb{U}^1_{A,55}$	$\mathbb{U}^1_{A,61}$
V_{20}	$\mathbb{U}^1_{C,30}$	$\mathbb{U}^1_{C,16}$	$\mathbb{U}^1_{A,51}$	$\mathbb{U}^1_{A,67}$
V_{21}	$\mathbb{U}^1_{C,12}$	$\mathbb{U}^1_{C,4}$	$\mathbb{U}^1_{A,15}$	$\mathbb{U}^1_{A,53}$
V_{23}	$\mathbb{U}^1_{C,18}$	$\mathbb{U}^1_{C,15}$	$\mathbb{U}^1_{A,28}$	$\mathbb{U}^1_{A,57}$
$V_{25} \equiv V_{23}(L.C.)$	$\mathbb{U}^1_{C,18}(L.C.)$	$\mathbb{U}^1_{C,15}(L.C.)$	$\mathbb{U}^1_{A,28}(L.C.)$	$\mathbb{U}^1_{A,57}(L.C.)$
V_{26}	$\mathbb{U}^1_{C,24}$	$\mathbb{U}^1_{C,15}(L.C.)$	$\mathbb{U}^1_{A,43}$	$\mathbb{U}^1_{A,64}$
V_{29}	$\mathbb{U}^1_{C,20}$	$\mathbb{U}^1_{C,17}$	$\mathbb{U}^1_{A,42}$	$\mathbb{U}^1_{A,60}$
V_{33}	$\mathbb{U}^1_{C,3}$	$\mathbb{U}^1_{C,1}$	$\mathbb{U}^1_{A,9}$	$\mathbb{U}^1_{A,11}$
V_{35}	$\mathbb{U}^1_{C,31}$	$\mathbb{U}^1_{C,16}$	$\mathbb{U}^1_{A,36}$	$\mathbb{U}^1_{A,69}$
V_{36}	$\mathbb{U}^1_{C,21}$	$\mathbb{U}^1_{C,17}$	$\mathbb{U}^1_{A,27}$	$\mathbb{U}^1_{A,60}$
V_{38}	$\mathbb{U}^1_{C,2}$	$\mathbb{U}^1_{C,1}$	$\mathbb{U}^1_{A,2}$	$\mathbb{U}^1_{A,11}$
V_{39}	$\mathbb{U}^1_{C,26}$	$\mathbb{U}^1_{C,16}$	$\mathbb{U}^1_{A,22}$	$\mathbb{U}^1_{A,65}$
$V_{48} \equiv V_3(L.C.)$	$\mathbb{U}^1_{C,26}(L.C.)$	$\mathbb{U}^1_{C,16}(L.C.)$	$\mathbb{U}^1_{A,23}(L.C.)$	$\mathbb{U}^1_{A,66}(L.C.)$
V_{49}	$\mathbb{U}^1_{C,31}$	$\mathbb{U}^1_{C,16}(L.C.)$	$\mathbb{U}^1_{A,37}$	$\mathbb{U}^1_{A,70}$
V_{51}	$\mathbb{U}^1_{C,30}$	$\mathbb{U}^1_{C,15}$	$\mathbb{U}^1_{A,52}$	$\mathbb{U}^1_{A,68}$
$V_{52} \equiv V_1(L.C.)$	$\mathbb{U}^1_{C,2}(L.C.)$	$\mathbb{U}^1_{C,1}(L.C.)$	$\mathbb{U}^1_{A,3}(L.C.)$	$\mathbb{U}^1_{A,12}(L.C.)$
V_{53}	$\mathbb{U}^1_{C,3}$	$\mathbb{U}^1_{C,1}(L.C.)$	$\mathbb{U}^1_{A,10}$	$\mathbb{U}^1_{A,13}$
V_{55}	$\mathbb{U}^1_{C,22}$	$\mathbb{U}^1_{C,15}$	$\mathbb{U}^1_{A,55}$	$\mathbb{U}^1_{A,62}$
$V_{57} \equiv V_{38}(L.C.)$	$\mathbb{U}^1_{C,2}(L.C.)$	$\mathbb{U}^1_{C,1}(L.C.)$	$\mathbb{U}^1_{A,2}(L.C.)$	$\mathbb{U}^1_{A,11}(L.C.)$
V_{59}	$\mathbb{U}^1_{C,25}$	$\mathbb{U}^1_{C,15}$	$\mathbb{U}^1_{A,41}$	$\mathbb{U}^1_{A,63}$
$V_{60} \equiv V_{33}(L.C.)$	$\mathbb{U}^1_{C,3}(L.C.)$	$\mathbb{U}^1_{C,1}(L.C.)$	$\mathbb{U}^1_{A,9}(L.C.)$	$\mathbb{U}^1_{A,11}(L.C.)$
V_{62}	$\mathbb{U}^1_{C,19}$	$\mathbb{U}^1_{C,15}$	$\mathbb{U}^1_{A,25}$	$\mathbb{U}^1_{A,56}$
V_{63}	$\mathbb{U}^1_{C,13}$	$\mathbb{U}^1_{C,4}$	$\mathbb{U}^1_{A,16}$	$\mathbb{U}^1_{A,54}$
V_{65}	$\mathbb{U}^1_{C,27}$	$\mathbb{U}^1_{C,16}$	$\mathbb{U}^1_{A,39}$	$\mathbb{U}^1_{A,65}$
V_{68}	$\mathbb{U}^1_{C,11}$	$\mathbb{U}^1_{C,4}$	$\mathbb{U}^1_{A,18}$	$\mathbb{U}^1_{A,45}$
V_{71}	$\mathbb{U}^1_{C,28}$	$\mathbb{U}^1_{C,15}$	$\mathbb{U}^1_{A,54}$	$\mathbb{U}^1_{A,68}$

Table 6. The respective unfoldings of codimension one of the phase portraits corresponding to parts of volume

	Unfoldings of codimension one			
Phase portrait from $\overline{\mathbf{QsnSN_{11}(B)}}$	Splitting $\overline{sn}_{(2)}$	Disappearing $\overline{sn}_{(2)}$	Splitting $\overline{\binom{1}{1}}SN\ (\downarrow s)$	Splitting $\overline{\binom{1}{1}}SN\ (\downarrow n)$
$V_{72} \equiv V_{65}(L.C.)$	$\mathbb{U}^1_{C,27}(L.C.)$	$\mathbb{U}^1_{C,16}(L.C.)$	$\mathbb{U}^1_{A,39}(L.C.)$	$\mathbb{U}^1_{A,65}(L.C.)$
V_{73}	$\mathbb{U}^1_{C,9}$	$\mathbb{U}^1_{C,4}$	$\mathbb{U}^1_{A,17}$	$\mathbb{U}^1_{A,41}$
$V_{75} \equiv V_{77}(L.C.)$	$\mathbb{U}^1_{C,32}(L.C.)$	$\mathbb{U}^1_{C,16}(L.C.)$	$\mathbb{U}^1_{A,30}(L.C.)$	$\mathbb{U}^1_{A,69}(L.C.)$
V_{77}	$\mathbb{U}^1_{C,32}$	$\mathbb{U}^1_{C,16}$	$\mathbb{U}^1_{A,30}$	$\mathbb{U}^1_{A,69}$
$V_{78} \equiv V_{80}(L.C.)$	$\mathbb{U}^1_{C,29}(L.C.)$	$\mathbb{U}^1_{C,16}(L.C.)$	$\mathbb{U}^1_{A,26}(L.C.)$	$\mathbb{U}^1_{A,67}(L.C.)$
V_{80}	$\mathbb{U}^1_{C,29}$	$\mathbb{U}^1_{C,16}$	$\mathbb{U}^1_{A,26}$	$\mathbb{U}^1_{A,67}$
V_{81}	$\mathbb{U}^1_{C,18}$	$\mathbb{U}^1_{C,15}$	$\mathbb{U}^1_{A,27}$	$\mathbb{U}^1_{A,56}$
V_{82}	$\mathbb{U}^1_{C,24}$	$\mathbb{U}^1_{C,15}$	$\mathbb{U}^1_{A,42}$	$\mathbb{U}^1_{A,63}$
V_{90}	$\mathbb{U}^1_{C,23}$	$\mathbb{U}^1_{C,17}$	$\mathbb{U}^1_{A,31}$	$\mathbb{U}^1_{A,61}$
V_{92}	$\mathbb{U}^1_{C,7}$	$\mathbb{U}^1_{C,4}$	$\mathbb{U}^1_{A,16}$	$\mathbb{U}^1_{A,33}$
V_{93}	$\mathbb{U}^1_{C,5}$	$\mathbb{U}^1_{C,4}$	$\mathbb{U}^1_{A,18}$	$\mathbb{U}^1_{A,25}$
V_{95}	$\mathbb{U}^1_{C,8}$	$\mathbb{U}^1_{C,4}$	$\mathbb{U}^1_{A,17}$	$\mathbb{U}^1_{A,35}$
$V_{101} \equiv V_{90}(L.C.)$	$\mathbb{U}^1_{C,23}(L.C.)$	$\mathbb{U}^1_{C,17}(L.C.)$	$\mathbb{U}^1_{A,31}(L.C.)$	$\mathbb{U}^1_{A,61}(L.C.)$
V_{102}	$\mathbb{U}^1_{C,20}$	$\mathbb{U}^1_{C,17}(L.C.)$	$\mathbb{U}^1_{A,43}$	$\mathbb{U}^1_{A,59}$
$V_{104} \equiv V_{112}(L.C.)$	$\mathbb{U}^1_{C,21}(L.C.)$	$\mathbb{U}^1_{C,17}(L.C.)$	$\mathbb{U}^1_{A,28}(L.C.)$	$\mathbb{U}^1_{A,58}(L.C.)$
$V_{106} \equiv V_{71}(L.C.)$	$\mathbb{U}^1_{C,28}(L.C.)$	$\mathbb{U}^1_{C,15}(L.C.)$	$\mathbb{U}^1_{A,54}(L.C.)$	$\mathbb{U}^1_{A,68}(L.C.)$
$V_{107} \equiv V_{80}(2\ L.C.)$	$\mathbb{U}^1_{C,29}(2\ L.C.)$	$\mathbb{U}^1_{C,16}(2\ L.C.)$	$\mathbb{U}^1_{A,26}(2\ L.C.)$	$\mathbb{U}^1_{A,67}(2\ L.C.)$
$V_{109} \equiv V_{80}(3\ L.C.)$	$\mathbb{U}^1_{C,29}(3\ L.C.)$	$\mathbb{U}^1_{C,16}(3\ L.C.)$	$\mathbb{U}^1_{A,26}(3\ L.C.)$	$\mathbb{U}^1_{A,67}(3\ L.C.)$
$V_{110} \equiv V_{71}(2\ L.C.)$	$\mathbb{U}^1_{C,28}(2\ L.C.)$	$\mathbb{U}^1_{C,15}(2\ L.C.)$	$\mathbb{U}^1_{A,54}(2\ L.C.)$	$\mathbb{U}^1_{A,68}(2\ L.C.)$
V_{112}	$\mathbb{U}^1_{C,21}$	$\mathbb{U}^1_{C,17}$	$\mathbb{U}^1_{A,28}$	$\mathbb{U}^1_{A,58}$

Table 7. Geometric classification for the family $\mathbf{QsnSN_{11}(B)}$

$$
I_1=\left\{\begin{array}{l}
\emptyset\ \&\ I_2=\left\{\begin{array}{l}
-1\ \&\ I_3=\left\{\begin{array}{l}
2\ \&\ I_4=\left\{\begin{array}{l}
2210\ \{\{4.9L_1\}\},\\
3101\ \{\{7.9L_1\}\},\\
3201\ \&\ I_5=\left\{\begin{array}{l}
1\ \&\ I_6=\left\{\begin{array}{l}
\overline{sn}_{(2)}\ \{\{9S_7\}\},\\
\widehat{cp}_{(2)}\ \{\{2.9L_1\}\},
\end{array}\right.\\
2\ \{\{9S_1\}\},
\end{array}\right.\\
3310\ \{\{9S_3\}\},\\
4201\ \{\{9S_5\}\},
\end{array}\right.\\
3\ \&\ I_4=\left\{\begin{array}{l}
111110\ (4.4L_6),\\
111111\ (4S_{34}),\\
211011\ (2.4L_4),\\
211101\ \&\ I_5=\left\{\begin{array}{l}
1\ (4S_{17}),\\
2\ (4S_3),
\end{array}\right.\\
211111\ \&\ I_7=\left\{\begin{array}{l}
0\ (7S_{12}),\\
2\ (V_{13}),
\end{array}\right.\\
211210\ (4S_{37}),\\
211211\ (V_{63}),\\
212110\ (7S_{21}),\\
221101\ (4S_{42}),\\
221110\ (7S_1),\\
221201\ (2S_{16}),\\
221210\ \&\ I_8=\left\{\begin{array}{l}
n\ (V_{21}),\\
y\ (V_{10}),
\end{array}\right.\\
311011\ (4S_{50}),\\
311110\ (4S_6),\\
311111\ (2S_{17}),\\
312110\ \&\ I_5=\left\{\begin{array}{l}
0\ (V_{92}),\\
1\ (V_4),
\end{array}\right.\\
321021\ (V_{95}),\\
321110\ (2S_5),\\
311111\ (V_{73}),\\
321201\ (V_{68}),\\
331110\ (V_8),\\
411111\ (V_{93}),\\
421110\ (V_6),
\end{array}\right.
\end{array}\right.\\
1\ \&\ I_3=\mathcal{A}_1\ \textit{(next page)},
\end{array}\right.\\
[\times]\ \&\ I_3=\left\{\begin{array}{l}
2\ \{\{P_3\}\},\\
3\ \{\{4.8L_1\}\},
\end{array}\right.\\
[\cup]\ \&\ I_3=\left\{\begin{array}{l}
1\ \{\{P_{29}\}\},\\
2\ \{\{9.9L_1\}\},
\end{array}\right.\\
[)(]\ \&\ I_3=\left\{\begin{array}{l}
2\ \{\{5.8L_1\}\},\\
3\ \&\ I_{14}=\left\{\begin{array}{l}
n\ \{\{8S_1\}\},\\
y\ (8S_2),
\end{array}\right.
\end{array}\right.
\end{array}\right.
$$

Table 8. Geometric classification for the family $\mathbf{QsnSN_{11}(B)}$ *(cont.)*

$$
I_1=\left\{\begin{array}{l}
\begin{array}{c}\mathcal{A}_1\\ \left[\begin{array}{l}I_1=\emptyset,\\ I_2=1\end{array}\right]\end{array}\ \&\ I_3=\left\{\begin{array}{l}
1\ \&\ I_4=\left\{\begin{array}{l}
11\ \&\ I_5=\left\{\begin{array}{l}
1\ \&\ I_6=\left\{\begin{array}{l}
\overline{sn}_{(2)}\ \&\ I_7=\left\{\begin{array}{l}0\ \&\ I_{13}=\left\{\begin{array}{l}(0)\ (V_{33}),\\ (1)\ [V_{60}],\end{array}\right.\\ 1\ \{7S_8\},\\ 2\ \{V_{53}\},\end{array}\right.\\
\widehat{cp}_{(2)}\ \&\ I_{13}=\left\{\begin{array}{l}(0)\ (2S_2),\\ (1)\ [2S_{11}],\end{array}\right.
\end{array}\right.\\
2\ \&\ I_{13}=\left\{\begin{array}{l}(0)\ (4S_1),\\ (1)\ [4S_{38}],\end{array}\right.
\end{array}\right.\\
21\ \&\ I_7=\left\{\begin{array}{l}
0\ \&\ I_{13}=\left\{\begin{array}{l}(0)\ \&\ I_9=\left\{\begin{array}{l}n\ (P_{51}),\\ y\ (V_{38}),\end{array}\right.\\ (1)\ [V_{57}],\end{array}\right.\\
1\ \&\ I_{13}=\left\{\begin{array}{l}(0)\ \&\ I_{10}=\left\{\begin{array}{l}n\ (V_1),\\ y\ \{P_{50}\},\end{array}\right.\\ (1)\ [V_{52}],\end{array}\right.
\end{array}\right.\\
22\ \&\ I_6=\left\{\begin{array}{l}
\overline{sn}_{(2)}\ \&\ I_7=\left\{\begin{array}{l}0\ (5.9L_7),\\ 1\ \{P_{49}\},\\ 2\ \{5.9L_4\},\end{array}\right.\\
\widehat{cp}_{(2)}\ (P_{39}),
\end{array}\right.\\
31\ \&\ I_{10}=\left\{\begin{array}{l}n\ (5.9L_6),\\ y\ \{5.9L_5\},\end{array}\right.\\
32\ \&\ I_7=\left\{\begin{array}{l}0\ (5.9L_8),\\ 1\ \&\ I_{13}=\left\{\begin{array}{l}(0)\ (5.9L_1),\\ (1)\ [5.9L_3],\end{array}\right.\end{array}\right.
\end{array}\right.\\
2\ \&\ I_4=\left\{\begin{array}{l}
1110\ \&\ I_7=\left\{\begin{array}{l}0\ \{\{4.9L_6\}\},\\ 1\ \{\{4.9L_4\}\},\end{array}\right.\\
1111\ \&\ I_5=\left\{\begin{array}{l}2\ \&\ I_7=\left\{\begin{array}{l}0\ (4.5L_3),\\ 2\ \{4.5L_{14}\},\end{array}\right.\\ 3\ \{P_{20}\},\end{array}\right.\\
2100\ \&\ I_7=\left\{\begin{array}{l}0\ (7.9L_9),\\ 1\ \{7.9L_7\},\end{array}\right.\\
2101\ \&\ I_5=\left\{\begin{array}{l}0\ (9S_{24}),\\ 1\ \&\ I_6=\left\{\begin{array}{l}\overline{sn}_{(2)}\ \&\ I_7=\left\{\begin{array}{l}0\ \{\{9S_{29}\}\},\\ 1\ \{\{7.9L_3\}\},\\ 2\ \{\{9S_{19}\}\},\end{array}\right.\\ \widehat{cp}_{(2)}\ \{\{2.9L_3\}\},\end{array}\right.\\ 2\ \{\{9S_{27}\}\},\end{array}\right.\\
2110\ \&\ I_{12}=\left\{\begin{array}{l}0\ (4.5L_8),\\ 1\ (4.5L_4),\end{array}\right.\\
\mathcal{A}_2\ \textit{(next page)},
\end{array}\right.\\
3\ \&\ I_4=\mathcal{A}_3\ \textit{(next page)},\\
\infty\ \{\{P_{36}\}\},
\end{array}\right.
\end{array}\right.
$$

Table 9. Geometric classification for the family $\mathbf{QsnSN_{11}(B)}$ *(cont.)*

$$
I_1=\left\{\begin{array}{l}
\mathcal{A}_2\ \begin{bmatrix} I_1=\emptyset, \\ I_2=1, \\ I_3=2 \end{bmatrix}\ \&\ I_4=\left\{\begin{array}{l}
2111\ \&\ I_5=\left\{\begin{array}{l}
1\ \&\ I_6=\left\{\begin{array}{l}
\overline{sn}_{(2)}\ \&\ I_7=\left\{\begin{array}{l} 0\ (5S_5), \\ 1\ \{\{4.9L_7\}\}, \\ 2\ \&\ I_{11}=\left\{\begin{array}{l} 0\ \{5.7L_{11}\}, \\ 2\ \{\{4.9L_5\}\}, \end{array}\right. \\ 3\ \{5S_{33}\}, \end{array}\right. \\
\widehat{cp}_{(2)}\ (2.5L_2),
\end{array}\right. \\
2\ \&\ I_7=\left\{\begin{array}{l} 0\ (4.5L_1), \\ 1\ \&\ I_{13}=\left\{\begin{array}{l} (0)\ \&\ I_{11}=\left\{\begin{array}{l} 1\ (4.5L_{18}), \\ 3\ (5S_4), \end{array}\right. \\ (1)\ [4.5L_{15}], \end{array}\right. \\ 2\ \{5S_{16}\}, \end{array}\right. \\
3\ \&\ I_7=\left\{\begin{array}{l} 0\ \{P_{14}\}, \\ 1\ \&\ I_{13}=\left\{\begin{array}{l} (0)\ \&\ I_{10}=\left\{\begin{array}{l} n\ (4.5L_{10}), \\ y\ \{4.5L_9\}, \end{array}\right. \\ (1)\ [4.5L_{13}], \end{array}\right. \end{array}\right.
\end{array}\right. \\
2120\ \&\ I_7=\left\{\begin{array}{l} 0\ (5.7L_1), \\ 1\ \{5.7L_3\}, \end{array}\right. \\
2121\ \&\ I_{11}=\left\{\begin{array}{l}
0\ \&\ I_{13}=\left\{\begin{array}{l} (0)\ \{5.7L_7\}, \\ (1)\ [5.7L_8], \end{array}\right. \\
1\ \&\ I_5=\left\{\begin{array}{l} 2\ \{\{7.9L_6\}\}, \\ 3\ (5.7L_9), \end{array}\right. \\
3\ \&\ I_5=\left\{\begin{array}{l} 2\ \{\{9S_{28}\}\}, \\ 3\ \{\{7.9L_8\}\}, \end{array}\right.
\end{array}\right. \\
2200\ \&\ I_{11}=\left\{\begin{array}{l} 0\ \{7.9L_5\}, \\ 1\ \{9S_{21}\}, \\ 2\ (2.9L_5), \\ 3\ (9S_{34}), \end{array}\right. \\
2211\ \&\ I_{13}=\left\{\begin{array}{l} (0)\ \&\ I_{12}=\left\{\begin{array}{l} 0\ (5S_8), \\ 1\ (5S_{28}), \end{array}\right. \\ (1)\ [5S_{32}], \end{array}\right. \\
3101\ \&\ I_7=\left\{\begin{array}{l} 0\ \{\{9S_{35}\}\}, \\ 1\ \&\ I_{13}=\left\{\begin{array}{l} (0)\ \{\{9S_{10}\}\}, \\ (1)\ [\{\{9S_{16}\}\}], \end{array}\right. \end{array}\right. \\
3111\ \&\ I_5=\left\{\begin{array}{l}
2\ \&\ I_6=\left\{\begin{array}{l}
\overline{sn}_{(2)}\ \&\ I_7=\left\{\begin{array}{l} 0\ (5S_6), \\ 2\ \&\ I_{13}=\left\{\begin{array}{l} (0)\ (5S_{37}), \\ (1)\ [5S_{34}], \end{array}\right. \end{array}\right. \\
\widehat{cp}_{(2)}\ \{P_7\},
\end{array}\right. \\
3\ \{5.7L_4\},
\end{array}\right. \\
3120\ \&\ I_5=\left\{\begin{array}{l}
1\ \&\ I_6=\left\{\begin{array}{l}
\overline{sn}_{(2)}\ \&\ I_7=\left\{\begin{array}{l} 0\ (5S_2), \\ 2\ \{5S_{14}\}, \end{array}\right. \\
\widehat{cp}_{(2)}\ (2.5L_1),
\end{array}\right. \\
2\ \&\ I_{10}=\left\{\begin{array}{l} n\ (5S_3), \\ y\ \&\ I_{11}=\left\{\begin{array}{l} 0\ \{5.7L_2\}, \\ 2\ \{5S_{15}\}, \end{array}\right. \end{array}\right.
\end{array}\right. \\
\mathcal{A}_4\ \textit{(next page)},
\end{array}\right.
\end{array}\right.
$$

Table 10. Geometric classification for the family $\mathbf{QsnSN_{11}(B)}$ *(cont.)*

$$
I_1 = \left\{ \begin{array}{l}
\mathcal{A}_4 \\ \begin{bmatrix} I_1 = \emptyset, \\ I_2 = 1, \\ I_3 = 2 \end{bmatrix} \ \& \ I_4 = \left\{ \begin{array}{l}
3121 \ \& \ I_5 = \left\{ \begin{array}{l}
1 \ \& \ I_6 = \left\{ \begin{array}{l} \overline{sn}_{(2)} \ \& \ I_7 = \left\{ \begin{array}{l} 1 \ \{\{9S_{33}\}\}, \\ 3 \ \{\{9S_{20}\}\}, \end{array} \right. \\ \widehat{cp}_{(2)} \ \{\{2.9L_4\}\}, \end{array} \right. \\
2 \ \& \ I_{13} = \left\{ \begin{array}{l} (0) \ \& \ I_{11} = \left\{ \begin{array}{l} 0 \ \{\{7.9L_4\}\}, \\ 1 \ (2.5L_7), \\ 2 \ \{\{9S_{22}\}\}, \\ 3 \ \{\{9S_{30}\}\}, \end{array} \right. \\ (1) \ [2.5L_5], \end{array} \right. \\
3 \ \& \ I_{13} = \left\{ \begin{array}{l} (0) \ \& \ I_{10} = \left\{ \begin{array}{l} n \ (5S_{27}), \\ y \ \{5S_{17}\}, \end{array} \right. \\ (1) \ [5S_{26}], \end{array} \right.
\end{array} \right. \\
3200 \ \& \ I_{13} = \left\{ \begin{array}{l} (0) \ \& \ I_{11} = \left\{ \begin{array}{l} 1 \ (9S_{12}), \\ 2 \ (9S_{37}), \end{array} \right. \\ (1) \ [9S_{18}], \end{array} \right. \\
3211 \ \{5.7L_6\}, \\
3221 \ \& \ I_{13} = \left\{ \begin{array}{l} (0) \ (5S_{25}), \\ (1) \ [5S_{23}], \end{array} \right. \\
4111 \ \& \ I_5 = \left\{ \begin{array}{l} 2 \ \{2.5L_4\}, \\ 3 \ \{5.7L_5\}, \end{array} \right. \\
4120 \ \& \ I_7 = \left\{ \begin{array}{l} 0 \ (5S_1), \\ 1 \ \& \ I_{13} = \left\{ \begin{array}{l} (0) \ (5S_9), \\ (1) \ [5S_{13}], \end{array} \right. \end{array} \right. \\
4121 \ \& \ I_5 = \left\{ \begin{array}{l}
2 \ \& \ I_7 = \left\{ \begin{array}{l} 0 \ \{\{9S_{36}\}\}, \\ 2 \ \& \ I_{13} = \left\{ \begin{array}{l} (0) \ \{\{9S_{11}\}\}, \\ (1) \ [\{\{9S_{17}\}\}], \end{array} \right. \end{array} \right. \\
3 \ \& \ I_{13} = \left\{ \begin{array}{l} (0) \ (5S_{22}), \\ (1) \ [5S_{20}], \end{array} \right.
\end{array} \right. \\
4211 \ \{5S_{18}\}, \\
5111 \ \{5S_{19}\},
\end{array} \right. \\
\mathcal{A}_3 \\ \begin{bmatrix} I_1 = \emptyset, \\ I_2 = 1, \\ I_3 = 3 \end{bmatrix} \ \& \ I_4 = \left\{ \begin{array}{l}
110110 \ \& \ I_5 = \left\{ \begin{array}{l} 1 \ \& \ I_7 = \left\{ \begin{array}{l} 0 \ (4S_8), \\ 2 \ \{4S_{65}\}, \end{array} \right. \\ 2 \ \{4.4L_{12}\}, \end{array} \right. \\
111010 \ \& \ I_5 = \left\{ \begin{array}{l} 0 \ (4S_{22}), \\ 1 \ (4S_{33}), \end{array} \right. \\
\mathcal{A}_5 \ \textit{(next page)},
\end{array} \right.
\end{array} \right.
$$

Table 11. Geometric classification for the family $\mathbf{QsnSN_{11}(B)}$ *(cont.)*

$$
I_1 = \left\{ \begin{array}{l}
\mathcal{A}_5 \\
\begin{bmatrix} I_1 = \emptyset, \\ I_2 = 1, \\ I_3 = 3 \end{bmatrix}
\end{array} \right. \;\&\; I_4 = \left\{ \begin{array}{ll}
111110 \;\&\; I_5 = \left\{ \begin{array}{ll}
0 \;\&\; I_7 = \left\{ \begin{array}{l} 0\ (7S_5), \\ 1\ \{7S_7\}, \end{array} \right. \\
1 \;\&\; I_7 = \left\{ \begin{array}{ll}
0\ \{7.7L_1\}, \\
1 \;\&\; I_{13} = \left\{ \begin{array}{ll}
(0) \;\&\; I_{11} = \left\{ \begin{array}{l} 1\ (4S_{59}), \\ 3\ (V_{14}), \end{array} \right. \\
(1)\ [4S_{64}], \end{array} \right. \\
2\ (V_{55}), \end{array} \right. \\
2\ (4S_{40}), \end{array} \right. \\
111111 \;\&\; I_7 = \left\{ \begin{array}{ll}
0 \;\&\; I_{13} = \left\{ \begin{array}{l} (0)\ (7S_{17}), \\ (1)\ [7S_{15}], \end{array} \right. \\
1 \;\&\; I_{13} = \left\{ \begin{array}{l}
(0)\ \{7S_{14}\} \\
(1)\ [\{7S_{23}\}], \\
(2)\ [[\{7S_{24}\}]] \\
(1)^2\ [\{7.10L_1\}]^2, \end{array} \right. \end{array} \right. \\
210110 \;\&\; I_5 = \left\{ \begin{array}{ll}
1 \;\&\; I_6 = \left\{ \begin{array}{ll}
\overline{sn}_{(2)} \;\&\; I_{11} = \left\{ \begin{array}{l} 0\ \{7S_{22}\}, \\ 1\ \{V_{102}\}, \\ 3\ (V_{29}), \end{array} \right. \\
\widehat{cp}_{(2)}\ (2S_3), \end{array} \right. \\
2 \;\&\; I_{13} = \left\{ \begin{array}{ll}
(0) \;\&\; I_{11} = \left\{ \begin{array}{l} 1\ (4S_{70}), \\ 2\ (4S_2), \end{array} \right. \\
(1)\ [4S_{67}], \end{array} \right. \end{array} \right. \\
211010 \;\&\; I_7 = \left\{ \begin{array}{l} 0\ (7S_{18}), \\ 1\ \{7S_4\}, \end{array} \right. \\
211011 \;\&\; I_6 = \left\{ \begin{array}{l} \overline{sn}_{(2)}\ (7S_9), \\ \widehat{cp}_{(2)}\ \{2.7L_1\}, \end{array} \right. \\
211101 \;\&\; I_6 = \left\{ \begin{array}{ll}
\overline{sn}_{(2)} \;\&\; I_7 = \left\{ \begin{array}{l} 0\ (V_{35}), \\ 1\ \{7S_6\}, \\ 2\ \{V_{49}\}, \end{array} \right. \\
\widehat{cp}_{(2)}\ (2S_1), \end{array} \right. \\
211110 \;\&\; I_5 = \left\{ \begin{array}{ll}
0 \;\&\; I_{12} = \left\{ \begin{array}{l} 0\ (V_{51}), \\ 1\ (V_{20}), \end{array} \right. \\
1 \;\&\; I_{13} = \left\{ \begin{array}{l} (0)\ (V_{90}), \\ (1)\ [V_{101}], \end{array} \right. \\
2\ (V_2), \end{array} \right. \\
\mathcal{A}_6\ \textit{(next page)}, \end{array} \right.
$$

Table 12. Geometric classification for the family $\mathbf{QsnSN_{11}(B)}$ *(cont.)*

$$
I_1 = \left\{ \begin{array}{c} \mathcal{A}_6 \\ \left[\begin{array}{l} I_1 = \emptyset, \\ I_2 = 1, \\ I_3 = 3 \end{array}\right] \end{array} \ \& \ I_4 = \left\{ \begin{array}{l}
211111 \ \& \ I_6 = \left\{ \begin{array}{l}
\overline{sn}_{(2)} \ \& \ I_{13} = \left\{ \begin{array}{l}
(0) \ \& \ I_{12} = \left\{ \begin{array}{l} 0 \ (V_{71}), \\ 1 \ (V_{80}), \end{array}\right. \\
(1) \ \& \ I_7 = \left\{ \begin{array}{l} n \ [V_{78}], \\ y \ [V_{106}], \end{array}\right. \\
(1)^2 \ \& \ I_7 = \left\{ \begin{array}{l} n \ [10S_1]^2, \\ y \ [10S_3]^2, \end{array}\right. \\
(2) \ \& \ I_7 = \left\{ \begin{array}{l} n \ [[V_{107}]], \\ y \ [[V_{110}]], \end{array}\right. \\
(1), (1)^2 \ \left[[10S_2]^2\right], \\
(3) \ [[[V_{109}]]],
\end{array}\right. \\
\widehat{cp}_{(2)} \ \& \ I_{13} = \left\{ \begin{array}{l} (0) \ (2S_{15}), \\ (1) \ [2S_{13}], \end{array}\right.
\end{array}\right. \\
221101 \ \{7S_{13}\}, \\
221111 \ \& \ I_{13} = \left\{ \begin{array}{l} (0) \ (V_{77}), \\ (1) \ [V_{75}], \end{array}\right. \\
310110 \ \& \ I_7 = \left\{ \begin{array}{l}
0 \ (V_{36}), \\
2 \ \& \ I_{13} = \left\{ \begin{array}{l} (0) \ (V_{112}), \\ (1) \ [V_{104}], \end{array}\right.
\end{array}\right. \\
311010 \ \& \ I_6 = \left\{ \begin{array}{l}
\overline{sn}_{(2)} \ \& \ I_7 = \left\{ \begin{array}{l} 0 \ (V_{82}), \\ 1 \ \{7S_3\}, \\ 2 \ \{V_{26}\}, \end{array}\right. \\
\widehat{cp}_{(2)} \ (2S_{19}),
\end{array}\right. \\
311011 \ \& \ I_6 = \left\{ \begin{array}{l} \overline{sn}_{(2)} \ \{7S_{11}\}, \\ \widehat{cp}_{(2)} \ (2S_9), \end{array}\right. \\
311101 \ \& \ I_{11} = \left\{ \begin{array}{l} 0 \ [V_{48}], \\ 1 \ (V_3), \\ 2 \ (V_{39}), \end{array}\right. \\
311111 \ \& \ I_{13} = \left\{ \begin{array}{l} (0) \ (V_{65}), \\ (1) \ [V_{72}], \end{array}\right. \\
321011 \ (V_{59}), \\
411010 \ \& \ I_7 = \left\{ \begin{array}{l}
0 \ (V_{81}), \\
1 \ \& \ I_{13} = \left\{ \begin{array}{l} (0) \ (V_{23}), \\ (1) \ [V_{25}], \end{array}\right.
\end{array}\right. \\
411011 \ (V_{62}).
\end{array}\right.
$$

Table 13. Topological equivalences for the family $\mathbf{QsnSN_{11}(B)}$

Presented phase portrait	Identical under perturbations	Finite antisaddle focus	Finite antisaddle node–focus	Finite weak point	Possessing invariant curve (no separatrix)	Other reasons
V_1		V_{46}	$6S_7$	$3S_{12}$		
V_2						
V_3		V_{47}	$6S_6$	$3S_{11}$		
V_4	V_5			$3S_1$		
V_6	V_7			$3S_2$, $3S_3$ $3.10L_1$		
V_8	V_9			$3S_4$		
V_{10}	V_{11}, V_{12}			$3S_5$	$4S_{19}$	
V_{13}	V_{15}, V_{16}, V_{17}			$3S_6$, $3S_7$, $3S_8$ $3.4L_3$, $3.10L_2$	$4S_{20}$, $4S_{21}$	
V_{14}	V_{18}, V_{19}, V_{31}, V_{43}	V_{27}	$6S_2$, $6S_3$ $4.6L_2$		$4S_{10}$, $4S_{15}$, $4S_{16}$, $4S_{29}$, $4S_{30}$ $4.4L_4$	
V_{20}	V_{32}, V_{34}	V_{28}	$6S_1$		$4S_{11}$, $4S_{26}$	

Table 14. Topological equivalences for the family $\mathbf{QsnSN_{11}(B)}$ *(cont.)*

Presented phase portrait	Identical under perturbations	Finite antisaddle focus	Finite antisaddle node–focus	Finite weak point	Possessing invariant curve (no separatrix)	Other reasons
V_{21}	V_{22}			$3S_9$		
V_{23}		V_{24}	$6S_4$	$3S_{10}$		
V_{25}						
V_{26}						
V_{29}	V_{30}				$4S_{14}$	
V_{33}	V_{41}, V_{42}	V_{44}	$6S_9$, $6S_{10}$ $4.6L_4$	$3S_{14}$	$4S_{27}$, $4S_{28}$	
V_{35}						
V_{36}	V_{37}				$4S_{13}$	
V_{38}	V_{40}, V_{69}	V_{45}	$6S_8$, $6S_{16}$ $4.6L_6$	$3S_{13}$	$4S_{12}$, $4S_{43}$	
V_{39}						
V_{48}						
V_{49}						
V_{51}	V_{56}, V_{83}	V_{50}	$6S_5$		$4S_{32}$, $4S_{52}$	
V_{52}						
V_{53}						

Table 15. Topological equivalences for the family **QsnSN$_{11}$(B)** *(cont.)*

Presented phase portrait	Identical under perturbations	Finite antisaddle focus	Finite antisaddle node–focus	Finite weak point	Possessing invariant curve (no separatrix)	Other reasons
V_{55}	V_{84}	V_{54}, V_{99}	$6S_{11}$, $6S_{21}$ $4.6L_9$		$4S_{53}$, $4S_{61}$	
V_{57}						
V_{59}		V_{58}	$6S_{13}$			
V_{60}						
V_{62}		V_{61}	$6S_{14}$			
V_{63}	V_{66}, V_{67}, V_{74}			$3S_{16}$, $3S_{17}$ $3.4L_7$	$4S_{41}$, $4S_{44}$	
V_{65}		V_{64}	$6S_{15}$	$3S_{15}$		
V_{68}	V_{98}			$3S_{23}$		
V_{71}	V_{85}	V_{70}, V_{86}	$6S_{12}$, $6S_{18}$ $4.6L_7$	$3S_{28}$ $3.10L_8$	$4S_{54}$, $4S_{55}$	
V_{72}						
V_{73}	V_{97}			$3S_{22}$		
V_{75}						
V_{77}		V_{76}	$6S_{17}$	$3S_{18}$		
V_{78}	V_{87}			$3S_{27}$ $3.10L_7$	$4S_{56}$	

Table 16. Topological equivalences for the family **QsnSN$_{11}$(B)** *(cont.)*

Presented phase portrait	Identical under perturbations	Finite antisaddle focus	Finite antisaddle node–focus	Finite weak point	Possessing invariant curve (no separatrix)	Other reasons
V_{80}	V_{89}	V_{79}, V_{88}	$6S_{19}$, $6S_{20}$ $4.6L_8$	$3S_{19}$, $3S_{20}$ $3.4L_9$, $3.10L_5$ P_{26}	$4S_{57}$, $4S_{58}$	
V_{81}						
V_{82}						
V_{90}	V_{91}, V_{105}	V_{100}	$6S_{22}$, $6S_{23}$ $4.6L_{12}$	$3S_{24}$	$4S_{51}$, $4S_{68}$	
V_{92}	V_{96}, V_{111}			$3S_{33}$	$4S_{60}$	
V_{93}	V_{94}			$3S_{21}$, $3S_{26}$ $3.10L_3$		
V_{95}	V_{103}			$3S_{25}$, $3S_{29}$ $3.10L_4$		
V_{101}						
V_{102}						
V_{104}						
V_{106}				$3S_{32}$		
V_{107}				$3S_{31}$		
V_{109}						
V_{110}						
V_{112}		V_{108}	$6S_{24}$	$3S_{30}$		

Table 17. Topological equivalences for the family **QsnSN$_{11}$(B)** *(cont.)*

Presented phase portrait	Identical under perturbations	Finite antisaddle focus	Finite antisaddle node–focus	Finite weak point	Possessing invariant curve (no separatrix)	Other reasons
$2S_1$						
$2S_2$	$2S_7$, $2S_{12}$	$2S_8$	$2.6L_1$, $2.6L_3$ P_4	$2.3L_2$	$2.4L_2$, $2.4L_3$	
$2S_3$	$2S_4$				$2.4L_1$	
$2S_5$	$2S_6$			$2.3L_1$		
$2S_9$		$2S_{10}$	$2.6L_2$			
$2S_{11}$						
$2S_{13}$						
$2S_{15}$		$2S_{14}$	$2.6L_4$	$2.3L_3$		
$2S_{16}$	$2S_{20}$			$2.3L_5$		
$2S_{17}$	$2S_{18}$			$2.3L_4$		
$2S_{19}$						
$4S_1$		$4S_{31}$	$4.6L_3$	$3.4L_5$		
$4S_2$						
$4S_3$	$4S_4$, $4S_5$			$3.4L_2$	$4.4L_1$	
$4S_6$	$4S_7$			$3.4L_1$		
$4S_8$	$4S_9$				$4.4L_3$	

Table 18. Topological equivalences for the family $\mathbf{QsnSN_{11}(B)}$ *(cont.)*

Presented phase portrait	Identical under perturbations	Finite antisaddle focus	Finite antisaddle node–focus	Finite weak point	Possessing invariant curve (no separatrix)	Other reasons
$4S_{17}$	$4S_{18}$			$3.4L_4$		
$4S_{22}$	$4S_{24}$, $4S_{25}$	$4S_{23}$	$4.6L_1$		$4.4L_2$	
$4S_{33}$	$4S_{47}$				$4.4L_8$	
$4S_{34}$	$4S_{35}$, $4S_{36}$, $4S_{45}$			$3.4L_6$, $3.4L_8$	$4.4L_5$, $4.4L_7$ P_6	
$4S_{37}$	$4S_{48}$			$3.4L_{11}$		
$4S_{38}$						
$4S_{40}$	$4S_{46}$	$4S_{39}$, $4S_{63}$	$4.6L_5$, $4.6L_{10}$ P_{18}		$4.4L_{10}$, $4.4L_{11}$	
$4S_{42}$	$4S_{49}$			$3.4L_{10}$		
$4S_{50}$	$4S_{66}$			$3.4L_{13}$, $3.4L_{14}$ P_{23}		
$4S_{59}$		$4S_{62}$	$4.6L_{11}$	$3.4L_{12}$		
$4S_{64}$						
$4S_{65}$						
$4S_{67}$						
$4S_{70}$		$4S_{69}$	$4.6L_{13}$	$3.4L_{15}$		

Table 19. Topological equivalences for the family $\mathbf{QsnSN_{11}(B)}$ *(cont.)*

Presented phase portrait	Identical under perturbations	Finite antisaddle focus	Finite antisaddle node–focus	Finite weak point	Possessing invariant curve (no separatrix)	Other reasons
$5S_1$						
$5S_2$						
$5S_3$						
$5S_4$	$5S_{11}$				$4.5L_7$	
$5S_5$	$5S_{10}$				$4.5L_5$	
$5S_6$	$5S_7$				$4.5L_2$	
$5S_8$						
$5S_9$	$5S_{12}$		$5.6L_1$	$3.5L_1$		
$5S_{13}$						
$5S_{14}$						
$5S_{15}$						
$5S_{16}$						
$5S_{17}$						
$5S_{18}$						
$5S_{19}$						
$5S_{20}$						
$5S_{22}$		$5S_{21}$	$5.6L_2$	$3.5L_2$		
$5S_{23}$						
$5S_{25}$		$5S_{24}$	$5.6L_3$	$3.5L_3$		

Table 20. Topological equivalences for the family **QsnSN$_{11}$(B)** *(cont.)*

Presented phase portrait	Identical under perturbations	Finite antisaddle focus	Finite antisaddle node–focus	Finite weak point	Possessing invariant curve (no separatrix)	Other reasons
$5S_{26}$						
$5S_{27}$		$5S_{30}$				
			$5.6L_4$	$3.5L_4$		
$5S_{28}$	$5S_{29}$, $5S_{35}$	$5S_{31}$				
			$5.6L_5$, $5.6L_6$ P_{22}	$3.5L_5$	$4.5L_{11}$, $4.5L_{16}$	
$5S_{32}$						
$5S_{33}$						
$5S_{34}$						
$5S_{37}$		$5S_{36}$				
			$5.6L_7$	$3.5L_6$		
$7S_1$	$7S_2$					
				$3.7L_1$		
$7S_3$						
$7S_4$						
$7S_5$						
$7S_6$						
$7S_7$						
$7S_8$						
$7S_9$	$7S_{10}$					
			$6.7L_1$			
$7S_{11}$						
$7S_{12}$	$7S_{19}$					
				$3.7L_3$		
$7S_{13}$						

Table 21. Topological equivalences for the family **QsnSN$_{11}$(B)** *(cont.)*

Presented phase portrait	Identical under perturbations	Finite antisaddle focus	Finite antisaddle node–focus	Finite weak point	Possessing invariant curve (no separatrix)	Other reasons
$7S_{14}$	$7S_{20}$				$4.7L_1$	
				P_{27}		
$7S_{15}$						
$7S_{17}$		$7S_{16}$				
			$6.7L_2$	$3.7L_2$		
$7S_{18}$						
$7S_{21}$	$7S_{25}$					
				$3.7L_6$		
$7S_{22}$						
$7S_{23}$						
				$3.7L_4$, $3.7L_5$		
$7S_{24}$						
$8S_1$						$8S_4{}^{(1)}$, $8S_5{}^{(1)}$, $8S_6{}^{(1)}$, $8S_7{}^{(1)}$ $8S_8{}^{(1)}$, $8S_9{}^{(1)}$, $8S_{11}{}^{(1)}$, $8S_{12}{}^{(1)}$ $8S_{14}{}^{(1)}$, $8S_{15}{}^{(1)}$, $8S_{16}{}^{(1)}$ $4.8L_3{}^{(1)}$, $4.8L_5{}^{(1)}$, $4.8L_8{}^{(1)}$ $4.8L_9{}^{(1)}$, $4.8L_{10}{}^{(1)}$, $4.8L_{11}{}^{(1)}$ $7.8L_1{}^{(1)}$, $7.8L_2{}^{(1)}$, $7.8L_3{}^{(1)}$ $7.8L_4{}^{(1)}$, $7.8L_5{}^{(1)}$ $P_{11}{}^{(1)}$, $P_{24}{}^{(1)}$
$8S_2$						$8S_3{}^{(1)}$, $8S_{10}{}^{(1)}$, $8S_{13}{}^{(1)}$ $4.8L_4$
$9S_1$	$9S_2$					
				$3.9L_1$		
$9S_3$	$9S_4$					
				$3.9L_2$		

Table 22. Topological equivalences for the family **QsnSN$_{11}$(B)** *(cont.)*

Presented phase portrait	Identical under perturbations	Finite antisaddle focus	Finite antisaddle node–focus	Finite weak point	Possessing invariant curve (no separatrix)	Other reasons
$9S_5$	$9S_6$			$3.9L_3$		
$9S_7$	$9S_8$, $9S_9$			$3.9L_4$	$4.9L_3$	
$9S_{10}$		$9S_{13}$	$6.9L_3$	$3.9L_5$		$0.9{L_1}^{(2)}$, $0.9{L_2}^{(2)}$ ${P_{43}}^{(2)}$, ${P_{44}}^{(2)}$
$9S_{11}$		$9S_{14}$	$6.9L_2$	$3.9L_6$		
$9S_{12}$		$9S_{15}$	$6.9L_1$	$3.9L_7$		
$9S_{16}$						${0.9L_3}^{(2)}$
$9S_{17}$						
$9S_{18}$						
$9S_{19}$						${0.9L_4}^{(2)}$
$9S_{20}$						
$9S_{21}$						
$9S_{22}$						
$9S_{24}$	$9S_{31}$, $9S_{32}$	$9S_{23}$	$6.9L_6$		$4.9L_8$, $4.9L_9$	
$9S_{27}$		$9S_{25}$	$6.9L_4$			$0.9{L_5}^{(2)}$, $0.9{L_6}^{(2)}$ ${P_{46}}^{(2)}$
$9S_{28}$		$9S_{26}$	$6.9L_5$			
$9S_{29}$						${0.9L_7}^{(2)}$

Table 23. Topological equivalences for the family **QsnSN$_{11}$(B)** *(cont.)*

Presented phase portrait	Identical under perturbations	Finite antisaddle focus	Finite antisaddle node–focus	Finite weak point	Possessing invariant curve (no separatrix)	Other reasons
$9S_{30}$						
$9S_{33}$						
$9S_{34}$						
$9S_{35}$						$0.9L_8{}^{(2)}$
$9S_{36}$						
$9S_{37}$						
$10S_1$				$3.10L_6$		
$10S_2$						
$10S_3$						
$2.4L_4$	$2.4L_5$			P_{21}		
$2.5L_1$						
$2.5L_2$	$2.5L_3$				P_1	
$2.5L_4$						
$2.5L_5$						
$2.5L_7$		$2.5L_6$	P_9	P_8		
$2.7L_1$						
$2.9L_1$	$2.9L_2$			P_{37}		
$2.9L_3$						$P_{38}{}^{(2)}$
$2.9L_4$						
$2.9L_5$						
$4.4L_6$	$4.4L_9$			P_{13}		

Table 24. Topological equivalences for the family **QsnSN$_{11}$(B)** *(cont.)*

Presented phase portrait	Identical under perturbations	Finite antisaddle focus	Finite antisaddle node–focus	Finite weak point	Possessing invariant curve (no separatrix)	Other reasons
$4.4L_{12}$						
$4.5L_1$						
$4.5L_3$			$4.5L_6$ P_2			
$4.5L_4$						
$4.5L_8$						
$4.5L_9$						
$4.5L_{10}$		$4.5L_{12}$				
			P_{17}	P_{19}		
$4.5L_{13}$						
$4.5L_{14}$						
$4.5L_{15}$						
$4.5L_{18}$		$4.5L_{17}$				
			P_{28}	P_{25}		
$4.8L_1$						$4.8{L_2}^{(1)}$, $4.8{L_6}^{(1)}$, $4.8{L_7}^{(1)}$ $4.8{L_{12}}^{(1)}$, $4.8{L_{13}}^{(1)}$ ${P_5}^{(1)}$, ${P_{12}}^{(1)}$
$4.9L_1$	$4.9L_2$					
				P_{33}		
$4.9L_4$						
						${P_{42}}^{(2)}$
$4.9L_5$						
$4.9L_6$						
						${P_{35}}^{(2)}$
$4.9L_7$						

Table 25. Topological equivalences for the family **QsnSN$_{11}$(B)** *(cont.)*

Presented phase portrait	Identical under perturbations	Finite antisaddle focus	Finite antisaddle node–focus	Finite weak point	Possessing invariant curve (no separatrix)	Other reasons
$5.7L_1$						
$5.7L_2$						
$5.7L_3$						
$5.7L_4$						
$5.7L_5$						
$5.7L_6$						
$5.7L_7$						
$5.7L_8$						
$5.7L_9$		$5.7L_{10}$	P_{16}	P_{15}		
$5.7L_{11}$						
$5.8L_1$						$5.8{L_2}^{(1)}$, $5.8{L_3}^{(1)}$ $8.9{L_1}^{(1)}$, $8.9{L_2}^{(1)}$, $8.9{L_3}^{(1)}$
$5.9L_1$		$5.9L_2$	P_{47}, P_{48}			
$5.9L_3$						
$5.9L_4$						
$5.9L_5$						
$5.9L_6$						
$5.9L_7$						
$5.9L_8$						
$7.7L_1$						
$7.9L_1$	$7.9L_2$			P_{40}		
$7.9L_3$						${P_{45}}^{(2)}$
$7.9L_4$						
$7.9L_5$						
$7.9L_6$						

Table 26. Topological equivalences for the family **QsnSN$_{11}$(B)** *(cont.)*

Presented phase portrait	Identical under perturbations	Finite antisaddle focus	Finite antisaddle node–focus	Finite weak point	Possessing invariant curve (no separatrix)	Other reasons
$7.9L_7$						
$7.9L_8$						
$7.9L_9$						
$7.10L_1$						
$9.9L_1$						$9.9L_2{}^{(3)}$, $9.9L_3{}^{(3)}$, $9.9L_4{}^{(3)}$ $P_{30}{}^{(3)}$, $P_{31}{}^{(3)}$, $P_{32}{}^{(3)}$
P_3						$P_{10}{}^{(1)}$, $P_{34}{}^{(1)}$, $P_{41}{}^{(1)}$
P_7						
P_{14}						
P_{20}						
P_{29}						
P_{36}						
P_{39}						
P_{49}						
P_{50}						
P_{51}						

Acknowledgements. We thank the reviewers of this paper for the valuable suggestions for our paper and for having indicated the manuscript for publication. The first author is partially supported by a MEC/FEDER grant number MTM 2016–77278–P and by a CICYT grant number 2017 SGR 1617. This study was financed in part by the Coordenação de Aperfeiçoamento de Pessoal de Nivel Superior - Brazil (CAPES) - Finance Code 001 (the second author is partially supported by this grant). The third author is partially supported by CAPES, by FAPESP Processo no. 2018/21320-7, and by FAPESP Processo no. 2019/21181-0.

A. Some incompatibilities in previous classifications

It is quite common that by performing the study of a bifurcation diagram that produces some specific types of phase portraits, the authors lose one or several phase portraits. This may happen either because they do not interpret correctly some of the bifurcation parts or they miss the existence of some nonalgebraic bifurcations.

In [Artés *et al.*, 2020b] we have decided to start comparing our classification of phase portraits with already existing classifications. As we have mentioned in that occasion, we plan to do this section in every future work related to classification of phase portraits using normal forms. The aim of this study is to detect some incompatibilities in previous papers and also to help us look carefully our bifurcation diagram in order to do not lose any phase portrait. Such incompatibilities are obtained after we compare all of the phase portraits obtained in our bifurcation diagram with phase portraits from some previous papers which possess the same *topological configuration of singularities*, according to Def. 1 in [Artés *et al.*, 2020a].

This study also allows the corresponding authors to detect possible mistakes on their works. There are some previous papers which are not based on normal forms, but which seek all topological realizable phase portraits of a certain codimension (see [Artés *et al.*, 1998, Artés *et al.*, 2018, Artés *et al.*, 2020c]). We have also crossed results from all the consulted papers with them and no discrepancy has been found. Additionally, with this study we are creating a data basis containing all the obtained phase portraits, specially containing those phase portraits obtained in our topological studies, in order to create an "encyclopedia" of phase portraits from quadratic differential systems.

In this present paper we are dealing with phase portraits possessing generically a finite saddle–node $\overline{sn}_{(2)}$, a simple finite elemental singularity and an infinite saddle–node of type $\binom{\overline{1}}{1}SN$. Regarding the already existing classifications related to this paper, we know that in [Artés *et al.*, 2015] one can find a classification of phase portraits of quadratic vector fields possessing a finite saddle–node $\overline{sn}_{(2)}$ and an infinite singularity $\binom{\overline{0}}{2}SN$. Moreover, in [Jager, 1990] the author presents a classification of phase portraits possessing a nilpotent cusp singularity of multiplicity two ($\widehat{cp}_{(2)}$). Then we have to verify if all of our nondegenerate phase portraits which possess the corresponding topological configuration of singularities appear in one (or in both) papers. We also compare our phase portraits possessing weak antisaddles with those ones appearing in [Artés *et al.*, 2006].

By doing this comparison, we have detected some interesting phenomena and also some incompatibilities in the mentioned works.

We start by discussing an interesting relation among phase portraits from [Artés *et al.*, 2006], [Artés *et al.*, 2015] and [Artés *et al.*, 2018]. Phase portrait $2S_{59}$ from [Artés *et al.*, 2015] has no limit cycle and it has $2S_{61}$ as a corresponding phase portrait with a limit cycle. We observe that phase portrait $2S_{59}$ belongs to class $\mathbb{U}^1_{B,31}$ from [Artés *et al.*, 2018]. Moreover, modulo limit cycles, phase portraits $5S_8$ and $5S_9$ from [Artés *et al.*, 2006] also belong to the mentioned class. But $5S_8$ has two limit cycles (each one located in a distinct canonical region of phase portrait) whereas $5S_9$ has only one limit cycle, and there does not exist a corresponding phase portrait without limit cycles. Indeed, such a phase portrait without limit cycles should appear only if the respective focus is not of second order.

By studying the possibility of existence of third order weak singularities, we have detected that in [Artés *et al.*, 2006], the topological classification of the point P_2 given in Table 3 (page 3193) is wrong. After having analyzing the bifurcation diagram, we conclude that the correct result is to say that the phase portrait at P_2 is topologically equivalent to

the phase portrait at the curve $1.2L_5$.

We have found a little misprint in [Jager, 1990]. In fact, phase portrait number 30 from its Fig. 20 should be drawn exactly as our P_{39}.

We have also detected a few minor misprints and also some missing phase portraits in [Artés *et al.*, 2015]. In what follows, up to the end of this section we present the incompatibilities found in [Artés *et al.*, 2015] and, for each incompatibility we indicate a respective comment about it. Our whole discussion is based on the sequence of phase portraits presented in Figs. 1 to 11 and also in the complete bifurcation diagram from that paper.

In Fig. 86 we present a list of (improved or new) phase portraits from [Artés *et al.*, 2015]. The label of each phase portrait is according to the bifurcation diagram from the mentioned paper and the phase portraits are drawn exactly as in that paper.

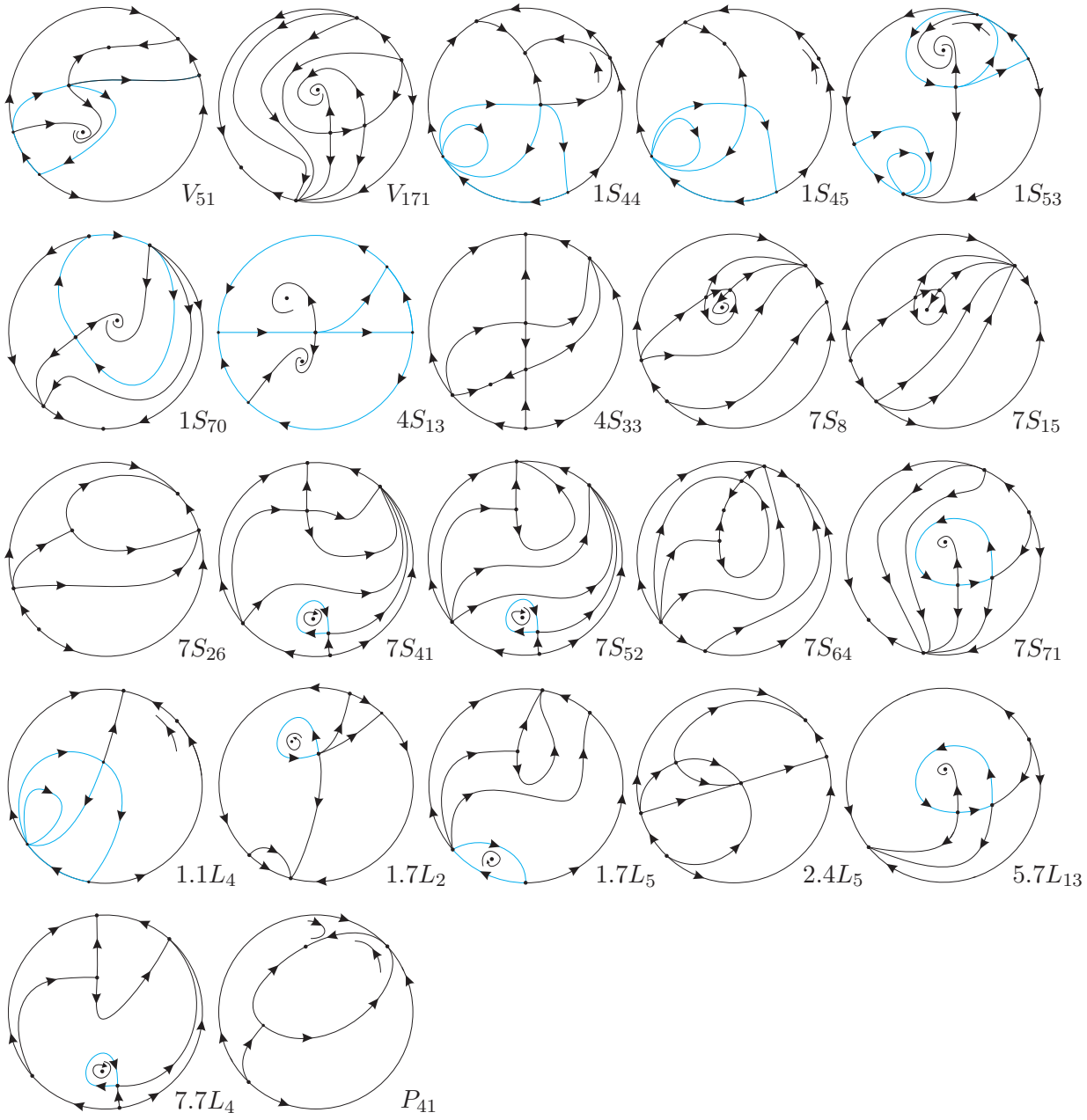

Fig. 86. Improved or new phase portraits for quadratic vector fields with a finite saddle–node $\overline{sn}_{(2)}$ and an infinite saddle–node of type $\binom{\overline{0}}{2}SN$ in the bisector of first and third quadrants – family $\overline{\mathbf{QsnSN(C)}}$ (see [Artés *et al.*, 2015])

We would like to emphasize that each incompatibility from [Artés *et al.*, 2015] is presented in this section in a different paragraph and all labels that appear from now on in this section refer to some elements (phase portraits, tables and figures) of the mentioned paper. When we refer to a figure from this current paper we use the word "our" to mean this, i.e. when we say "our Fig. 1", for instance, we refer to Fig. 1 of the present paper on page 7.

We indicate all labels which correspond to a specific phase portrait by using TEX notation, even if in a specific sentence some of these labels are referring to a region of the bifurcation diagram from [Artés *et al.*, 2015].

Phase portrait V_{51} possesses one graphic (see the correct phase portrait in our Fig. 86) and in Table 58 it should be presented as $\{V_{51}\}$.

In Fig. 23 we must add label V_{58} in the topological triangle delimited by segments $5S_{11}$, $6S_{16}$ and $6S_{17}$.

Phase portrait V_{54} is topologically equivalent to V_{94} via a symmetry. We will consider V_{94} as a representative of this class, since it possesses a node, whereas V_{54} possesses a focus. Then, in Table 58 we must consider only V_{94} and we should erase V_{54} from Table 61 and add it to the row corresponding to V_{94} in Table 63.

Phase portrait V_{102} possesses one graphic. In Table 56 it should be presented as $\{V_{102}\}$.

Phase portrait V_{107} possesses one graphic. In Table 58 it should be presented as $\{V_{107}\}$.

Phase portrait V_{124} is missing in Table 63. In fact, it is topologically equivalent to V_{104}, see Fig. 83. Additionally, in the mentioned figure segment $4S_{37}$ should be drawn as a dashed line, not a continuous one.

Phase portrait V_{126} appears twice in Table 63. In fact, it should appear once and it is topologically equivalent to V_{110}, see Fig. 85.

Phase portrait V_{144} from Fig. 109 appears twice in Table 64. In fact, it should appear once (in its own class) since it is not topologically equivalent to V_{145} from Fig. 111.

Phase portrait V_{146} is missing in Table 64. In fact, it is topologically equivalent to V_{145}, see Fig. 111.

Phase portrait V_{171} is missing. In fact, it is not topologically equivalent to V_{170} as presented in Table 65 (see the correct phase portrait in our Fig. 86). Phase portrait V_{171} was assigned the geometric invariant $I_4 = 3311$, but in fact it must be $I_4 = 4220$. Then, up to the order of this invariant, V_{171} must be in the same topological class of either V_{42} or V_{142}. Calculating the value of the invariant I_{11} for these phase portraits, we obtain $I_{11}(V_{42}) = N$, $I_{11}(V_{142}) = SN$ and $I_{11}(V_{171}) = N$. Moreover, we consider in V_{42} and in V_{171} the infinite singular point which receives four separatrices. Analyzing the two inner separatices arriving at this singular point, in V_{42} we see that one of them comes from the infinite saddle–node and the other comes from the finite saddle, whereas in V_{171}, they come from the infinite saddle–node and the finite saddle–node, which highlight the geometrical difference between them.

Phase portrait $1S_6$ possesses one graphic. In Table 53 it should be presented as $\{1S_6\}$.

The phase portraits in the first column of our Table 27 possess more than one graphic and in the respective table in [Artés *et al.*, 2015] they should have been presented with double curly brackets. We present in the same row the phase portrait, the corresponding table in [Artés *et al.*, 2015] that it appears, and the way it should have been presented.

Table 27. Correct presentation in table of geometric invariants in [Artés *et al.*, 2015]

Phase portrait	Table in [Artés *et al.*, 2015]	Correct presentation
$1S_{25}$	Table 54	$\{\{1S_{25}\}\}$
$1S_{26}$	Table 54	$\{\{1S_{26}\}\}$
$1S_{28}$	Table 50	$\{\{1S_{28}\}\}$
$1S_{30}$	Table 50	$\{\{1S_{30}\}\}$
$1S_{33}$	Table 50	$\{\{1S_{33}\}\}$
$1S_{36}$	Table 54	$\{\{1S_{36}\}\}$
$1S_{37}$	Table 53	$\{\{1S_{37}\}\}$
$1S_{40}$	Table 50	$\{\{1S_{40}\}\}$
$1S_{43}$	Table 54	$\{\{1S_{43}\}\}$
$1S_{44}$	Table 53	$\{\{1S_{44}\}\}$
$1S_{45}$	Table 53	$\{\{1S_{45}\}\}$
$1S_{59}$	Table 54	$[\{\{1S_{59}\}\}]$
$1S_{60}$	Table 54	$[\{\{1S_{60}\}\}]$
$1S_{65}$	Table 54	$\{\{1S_{65}\}\}$
$1S_{66}$	Table 54	$\{\{1S_{66}\}\}$

In addition, phase portraits $1S_{44}$, $1S_{45}$ and $1S_{53}$ possess more than one graphic. In our Fig. 86 we have colored in blue all their graphics.

Phase portrait $1S_{70}$ is missing. In fact, it is not topologically equivalent to $1S_{19}$ (see Table 66). After studying the bifurcation diagram from Fig. 112 (transition from V_{165} to V_{166}), we conclude that $1S_{70}$ is topologically equivalent to phase portrait $5S_{15}$ from the current classification, whereas $1S_{19}$ is topologically equivalent to $5S_3$ from the current classification. Phase portrait $1S_{70}$ in [Artés *et al.*, 2015] is shown in our Fig. 1. In order to distinguish $1S_{19}$ and $1S_{70}$, we calculate the geometric invariant I_{18}, obtaining $I_{18}(1S_{19}) = n$ (it has no graphics) and $I_{18}(1S_{70}) = y$ (it has a graphic). So, considering the 7–tuple $(I_1, I_2, I_3, I_4, I_6, I_7, I_{18})$ of geometric invariants for each one of these phase portraits, we must have $(2, 1, 2, 3120, (0), (1, 2), n)$ for $1S_{19}$ and $(2, 1, 2, 3120, (0), (1, 2), y)$ for $1S_{70}$, that must be corrected in Table 54 (row 12). Moreover, in Table 66 we must erase $1S_{70}$ from the row of $1S_{19}$ and include a new row with $1S_{70}$ in Table 68 between the rows of $1S_{69}$ and $1S_{71}$.

Phase portrait $3S_{56}$ appears in Table 63 and also in Table 64. In fact, it should appear once and only in Table 63, since it is topologically equivalent to V_{110}, see Fig. 85.

Phase portrait $3S_{65}$ is missing in Table 64. In fact, it is topologically equivalent to V_{147}, see Fig. 111.

Phase portrait $3S_{76}$ appears in Table 65 and also in Table 66. In fact, it should appear once and only in Table 65, since it is topologically equivalent to V_{189}, see Fig. 112.

Phase portrait $4S_9$ is topologically equivalent to V_{44}, see Fig. 23. Then $4S_9$ is an "extra" phase portrait. In this case we should remove it from Table 56. Moreover, we also should remove it from Table 70 and add it to the class of V_{44} in Table 61. Moreover, as $4S_{22}$ and $3.4L_6$ are topologically equivalent to $4S_9$, then they also must be added to the row of V_{44} in Table 61.

Phase portrait $4S_{13}$ from Figs. 6 and 21 is wrong. By analyzing the corresponding bifurcation diagram in Fig. 23 we conclude that such a phase portrait possesses the infinite saddle–node $\binom{\overline{0}}{2}SN$ on the bisector of the first and third quadrants (see the correct phase portrait in our Fig. 86). We observe that here we have a phase portrait that possesses more than one graphic, then in Table 58 it should be indicated as $\{\{4S_{13}\}\}$.

Phase portrait $4S_{15}$ appears in Table 60 and also in Table 70. In fact, it should appear once and only in Table 70, since it is topologically equivalent to $4S_{14}$, see Fig. 23. Moreover, phase portrait $4S_{15}$ from Table 60 should be $4S_5$.

In Fig. 72 we observe that $4S_{31}$ should be $7S_{31}$. Compare this figure with Fig. 70.

In Fig. 83 we observe that the segments from $4S_{32}$ to $4S_{36}$ should be drawn as a continuous line, not a dashed one. After we verify that all the corresponding neighbors are topologically distinct, we conclude that these modifications should be done in Fig. 83. Moreover, as we already have mentioned before, in such a figure segment $4S_{37}$ should be drawn as a dashed line, not a continuous one.

In addition to the last paragraph, we observe that phase portrait $4S_{33}$ is missing an arrow (see the correct phase portrait in our Fig. 86) and phase portrait $4S_{36}$ possesses one graphic (in Table 58 it should be presented as $\{4S_{36}\}$).

Phase portrait $4S_{51}$ possesses more than one graphic. In Table 58 it should be presented as $\{\{4S_{51}\}\}$.

Phase portrait $6S_{59}$ appears in Table 65 and also in Table 66. In fact, it should appear once and only in Table 65, since it is topologically equivalent to V_{189}, see Fig. 112.

Phase portrait $6S_{58}$ is missing in Table 66. In fact, it is topologically equivalent to V_{194}, see Fig. 112.

Phase portrait $7S_8$ from Figs. 7 and 15, and phase portrait $7S_{15}$ are wrongly drawn (see the correct phase portraits in our Fig. 86). For phase portrait $7S_8$ the geometric invariants are correct and it is located in the right place in Table 56 (row 17). For phase portrait $7S_{15}$ we recompute the geometric invariant $I_4 = 4120$ (instead of $I_4 = 6120$). The values of the geometric invariants up to I_4 for phase portrait $7S_{15}$ coincide with the respective values for $7S_{62}$, which is topologically distinct from $7S_{15}$. Calculating $I_7(7S_{15}) = (1, 1)$ and $I_7(7S_{62}) = (0, 2)$, we highlight the difference between both of them. In Table 57 they must be located in the second and fourth rows.

Phase portraits $7S_{26}$ and $7S_{64}$ are wrongly drawn. Since $7S_{26}$ is a bifurcation between V_{84} and V_{85} in Fig. 50 and $7S_{64}$ is a bifurcation between V_{143}

and V_{144} in Fig. 109, we conclude that such phase portraits possess the infinite saddle–node $\binom{\overline{0}}{2}SN$ on the bisector of the first and third quadrants (see the correct phase portraits in our Fig. 86). These corrections in phase portraits $7S_{26}$ and $7S_{64}$ do not imply any change in their geometric classification.

Phase portrait $7S_{33}$ possesses one graphic. In Table 55 it should be presented as $\{7S_{33}\}$.

We have detected that a few labels in some pictures of the bifurcation diagram should be changed. In each row of the first column of our Table 28 we specify the label that must be changed, in the second column we indicate the respective figure (or figures, in some cases) in [Artés *et al.*, 2015] in which such a label should be changed and in the third column we present the correct label.

Table 28. Correct labels in some figures in [Artés *et al.*, 2015]

Label	Figure in [Artés *et al.*, 2015]	Correct label
$7S_{38}$	Fig. 83	$7S_{37}$
$7S_{39}$	Fig. 83	$7S_{38}$
$7S_{40}$	Fig. 83	$7S_{39}$
$7S_{41}$	Figs. 83, 94, 95, 97	$7S_{40}$
$7S_{42}$	Figs. 83, 96, 97	$7S_{41}$
$7S_{43}$	Figs. 83, 91, 98, 99	$7S_{42}$

And we should do these modifications also in the corresponding texts regarding these figures. We point out that all of the corresponding new labels are on the right place in the classification table.

Phase portraits $7S_{41}$ and $7S_{52}$ are wrongly drawn. In fact, in the loop there are two arrows and one of them must be reversed (see the correct phase portrait in our Fig. 86).

The phase portraits in the first column of our Table 29 possess one graphic and in the respective table in [Artés *et al.*, 2015] they should have been presented with curly brackets. We present in the same row the phase portrait, the corresponding table in [Artés *et al.*, 2015] that it appears, and the way it should have been presented.

Moreover, after the study of the bifurcation diagram from Fig. 112, we conclude that phase portrait $7S_{71}$ is wrong (see the correct phase portrait in our Fig. 86). For phase portrait $7S_{71}$ we recompute the geometric invariant $I_4 = 4120$ (instead of $I_4 = 3211$). The values of the geometric invariants up to I_4 for phase portrait $7S_{71}$ coincide with the respective values for $7S_{15}$ and $7S_{62}$, according to the new classification done some paragraphs before. As we calculated, we have $I_7(7S_{15}) = (1, 1)$, $I_7(7S_{62}) = (0, 2)$, and we also have $I_7(7S_{71}) = (1, 1)$. To distinguish $7S_{15}$ and $7S_{71}$, we compute $I_{18}(7S_{15}) = n$ (it has no graphics) and $I_{18}(7S_{71}) = y$ (it has a graphic). Then we conclude that phase portraits $7S_{62}$, $7S_{71}$, and $7S_{15}$ are topologically distinct and they occupy the rows two, three and four of Table 57, respectively.

Table 29. Correct presentation in table of geometric invariants in [Artés *et al.*, 2015]

Phase portrait	Table in [Artés *et al.*, 2015]	Correct presentation
$7S_{70}$	Table 56	$\{7S_{70}\}$
$7S_{71}$	Table 56	$\{7S_{71}\}$
$7S_{72}$	Table 58	$\{7S_{72}\}$

The phase portraits in the first column of our Table 30 possess more than one graphic and in the respective table in [Artés *et al.*, 2015] they should have been presented with double curly brackets. We present in the same row the phase portrait, the corresponding table in [Artés *et al.*, 2015] that it appears, and the way it should have been presented.

Table 30. Correct presentation in table of geometric invariants in [Artés *et al.*, 2015]

Phase portrait	Table in [Artés *et al.*, 2015]	Correct presentation
$1.1L_2$	Table 50	$\{\{1.1L_2\}\}$
$1.1L_3$	Table 50	$\{\{1.1L_3\}\}$
$1.1L_4$	Table 50	$\{\{1.1L_4\}\}$
$1.2L_8$	Table 59	$\{\{1.2L_8\}\}$
$1.3L_2$	Table 53	$\{\{1.3L_2\}\}$

Moreover, in our Fig. 86 we have presented $1.1L_4$ and colored in blue all their graphics.

Phase portrait $1.4L_4$ (respectively, $1.4L_5$) possesses a graphic (respectively, more than one graphic). Then, in Table 53 (respectively, Table 50) it should be presented as $\{1.4L_4\}$ (respectively,

$\{\{1.4L_5\}\}$).

Phase portraits $1.4L_6$ and P_{42} are missing in Table 76. In fact, they are topologically equivalent to $1.4L_5$ (which possesses more than one graphic), see the corresponding bifurcation on Fig. 110.

Phase portraits $1.4L_7$, $1.4L_8$, $1.4L_{12}$ and $1.4L_{13}$ possess more than one graphic. Then, in Table 53 they should be presented as $\{\{1.4L_7\}\}$, $\{\{1.4L_8\}\}$, $\{\{1.4L_{12}\}\}$ and $\{\{1.4L_{13}\}\}$, respectively.

In Fig. 50 we observe that $1.6L_4$ should be $1.6L_3$. The correct $1.6L_4$ is the one which appears in Fig. 83.

The stability of the focus in phase portraits $1.7L_2$ and $1.7L_5$ should be changed (see the correct phase portraits in our Fig. 86). This is easily verified by looking the corresponding bifurcation diagram in Figs. 80 and 99, respectively.

In other to have a coherence in the bifurcation diagram, we observe that in Fig. 99 one must perform the following modifications: we should change $1.7L_5$ to $1.7L_4$, $1.7L_6$ to $1.7L_5$, and $1.7L_7$ to $1.7L_6$.

In Fig. 110 there is an extra $1.7L_{10}$ in the region $1S_{42}$, we should remove it from there.

Phase portraits $1.7L_{18}$ and $1.7L_{21}$ possess more than one graphic. Then, in Tables 50 and 53, respectively, they should be presented as $\{\{1.7L_{18}\}\}$ and $\{\{1.7L_{21}\}\}$, respectively.

Phase portrait $1.7L_{32}$ possesses one graphic. Then, in Table 53 it should be presented as $\{1.7L_{32}\}$.

Phase portrait $2.3L_{12}$ appears in Table 69 and also in Table 70. In fact, it should appear once and only in Table 70, since it is topologically equivalent to $2S_{59}$, see Fig. 116.

Phase portrait $2.4L_5$ is missing an arrow (see the correct phase portrait in our Fig. 86).

Phase portraits $2.8L_1$ and $2.8L_2$ possess more than one graphic. Then, in Table 50 they should be presented as $\{\{2.8L_1\}\}$ and $\{\{2.8L_2\}\}$, respectively.

We have detected the following misprints in some figures of the bifurcation diagram: in Fig. 46, $5.6L_4$ should be $3.4L_4$; in Fig. 50, $3.4L_4$ should be $3.6L_4$; in Fig. 68, $3.6L_7$ is a little bit out of its place; and in Fig. 91, $3.6L_4$ should be $3.6L_9$. These facts are easily verified by comparing the mentioned figures with the previous ones.

Phase portrait $3.7L_{12}$ appears twice in Table 73. In fact, it should appear once and it is topologically equivalent to $7S_{28}$, see Fig. 66.

Phase portrait $4.4L_1$ is topologically equivalent to $4S_8$ (see the corresponding bifurcation from Fig. 23). Indeed, in $4.4L_1$ the authors have drawn an extra separatrix. More precisely, there should not exist a separatrix connecting the finite antisaddle with the infinite antisaddle. We will consider $4S_8$ as a representative of this class, since it corresponds to a higher dimension region in the bifurcation diagram. Then, in Table 55 we must consider only $4S_8$ and we should erase all the elements from the class $4.4L_1$ from Table 78 and add all of them in the row corresponding to $4S_8$ in Table 70.

The element $5.6L_6$ in the bifurcation diagram appears in two distinct regions, according to Figs. 36 and 111. In fact, it should appear only in Fig. 36. In Fig. 111 we observe that $5.6L_6$ should be $5.6L_7$. Moreover, we should erase $5.6L_6$ from Table 72 and in Table 71 it must be set in the row of $5S_9$.

The elements $5.6L_6$, $5.6L_7$ and $5.6L_8$ in Figs. 111 and 112 should be replaced by $5.6L_7$, $5.6L_8$ and $5.6L_9$, respectively. In Table 72, $5.6L_7$ and $5.6L_8$ must be in the row of $5S_{28}$ and $5.6L_9$ in the row of $5S_{36}$.

Phase portrait $5.7L_1$ should appear in Table 78. In fact, it consists a new class, as indicated in Table 55.

Phase portrait $5.7L_4$ appears in Table 71 and also in Table 78. In fact, it should appear once and only in Table 78 (since it arises from P_2, see Fig. 27) because it is topologically equivalent to $5.7L_2$.

In Fig. 30 we observe that $5.7L_{13}$ should be $5.7L_5$ (and $5.7L_5$ is in the right place in Table 78).

Phase portrait $5.7L_{13}$ appears in Table 78 and also in Table 79, but none of them is in their correct place. In fact, phase portrait $5.7L_{13}$ is missing. By analyzing the bifurcation diagram, we have verified that it is not topologically equivalent either to $5.7L_2$ or to $7.7L_1$ as presented in Tables 78 and 79, respectively (see the correct phase portrait in our Fig. 86). In Table 79 we add a row with the class of $5.7L_{13}$ between the rows of $5.7L_{11}$ and $5.7L_{14}$. For the phase portrait $5.7L_{13}$ we compute the geometric invariant $I_4 = 21$. The values of the geometric invariants up to I_4 for phase portrait $5.7L_{13}$ coincide with the respective values for $5.7L_2$ and $5.7L_{11}$. We calculate $I_7(5.7L_2) = (1, 1)$, $I_7(5.7L_{11}) = (0, 2)$ and $I_7(5.7L_{13}) = (1, 1)$. Then, $5.7L_{11}$ represents a topological class apart from the

other two phase portraits. Computing $I_{18}(5.7L_2) = n$ and $I_{18}(5.7L_{13}) = y$, we distinguish all of these three classes of phase portraits. In Table 55, phase portraits $5.7L_2$ and $5.7L_{13}$ must be set in rows eight and nine; phase portrait $5.7L_{11}$ is well placed in the seventh row of Table 55.

We have detected that a few labels in some places of the paper under discussion should be changed. In each row of the first column of our Table 31 we specify the label that must be changed, in the second column we indicate the respective location (figure or table) in [Artés *et al.*, 2015] in which such a label should be changed and in the third column we present the correct label. We point out that the labels of the phase portraits that we do not mention in our Table 5 are correct and well placed in their respective tables of equivalent phase portraits. For instance, $5.7L_6$ is in the right place in Table 71.

Table 31. Correct labels in some locations in [Artés *et al.*, 2015]

Label	Location in [Artés *et al.*, 2015]	Correct label
$5.7L_{14}$	Fig. 34	$5.7L_6$
$5.7L_{15}$	Fig. 36	$5.7L_7$
$5.7L_4$	Fig. 50, Table 71	$5.7L_8$
$5.7L_5$	Figs. 69, 70	$5.7L_9$
$6.6L_4$	Fig. 23	$6.6L_1$
$6.6L_1$	Fig. 112	$6.6L_2$
$6.6L_2$	Figs. 114, 115, Table 46	$6.6L_3$

Phase portrait $6.7L_6$ is missing in Table 73. In fact, it is topologically equivalent to $7S_{31}$, see Figs. 78 and 70.

Phase portrait $7.7L_4$ is wrongly drawn. In fact, in the loop there are two arrows and one of them must be reversed (see the correct phase portrait in our Fig. 86).

Phase portrait P_{23} possesses more than one graphic. Then, in Table 50 it should be presented as $\{\{P_{23}\}\}$.

Phase portrait P_{31} possesses one graphic. Then, in Table 53 it should be presented as $\{P_{31}\}$.

Phase portrait P_{34} is missing in Table 73. Analyzing the bifurcation diagram of Figs. 103 to 105, we conclude that the topological triangle V_{121} shrinks together with its borders, which generates the region P_{34}. Topologically what happens is that one of the finite saddle–nodes coalesces with the infinite node generating a triple node of type $\binom{2}{1}N$ and this phase portrait is topologically equivalent to $7S_{26}$. We must add phase portrait P_{34} in Table 73 in the row of $7S_{26}$.

Phase portrait P_{41} is wrong. We present the correct picture in our Fig. 1.

The phase portraits in the first column of our Table 32 possess more than one graphic and in the respective table in [Artés *et al.*, 2015] they should have been presented with double curly brackets. We present in the same row the phase portrait, the corresponding table in [Artés *et al.*, 2015] that it appears, and the way it should have been presented.

Table 32. Correct presentation in table of geometric invariants in [Artés *et al.*, 2015]

Phase portrait	Table in [Artés *et al.*, 2015]	Correct presentation
P_{43}	Table 50	$\{\{P_{43}\}\}$
P_{57}	Table 59	$\{\{P_{57}\}\}$
P_{58}	Table 59	$\{\{P_{58}\}\}$
P_{64}	Table 59	$\{\{P_{64}\}\}$
P_6	Table 59	$\{\{P_{65}\}\}$

We have also detected that Table 1 in [Artés *et al.*, 2015] is incomplete. In fact, we have verified that phase portrait $5S_9$ from $\overline{\mathbf{QsnSN(C)}}$ is topologically equivalent to $5S_2$ from $\overline{\mathbf{QsnSN(A)}}$ (and also to $5S_3$ from $\overline{\mathbf{QsnSN(B)}}$). Moreover, our Table 33 presents three new rows to be added in that Table 1.

Table 33. Three new rows to be added to Table 1 in [Artés *et al.*, 2015]

$\overline{\mathbf{QsnSN(A)}}$	$\overline{\mathbf{QsnSN(B)}}$	$\overline{\mathbf{QsnSN(C)}}$
$5S_1$		$5S_2$
$3.5L_1$		$2.5L_4$
	$5.9L_2$	$2.5L_{11}$

Therefore, in Corollary 1.2 the number of topologically distinct phase portraits which appear simultaneously in at least two of the three fami-

lies $\overline{\mathbf{QsnSN}(\mathbf{A})}$, $\overline{\mathbf{QsnSN}(\mathbf{B})}$ and $\overline{\mathbf{QsnSN}(\mathbf{C})}$ pass from 14 to 17.

Finally, in [Artés *et al.*, 2015] the authors have obtained 371 topologically distinct phase portraits. We have seen that:

- phase portraits V_{171}, $1S_{70}$ and $5.7L_{13}$ are missing in the paper;
- phase portrait V_{54} is topologically equivalent to V_{94};
- phase portrait $4S_9$ is topologically equivalent to V_{44};
- phase portrait $4.4L_1$ is topologically equivalent to $4S_8$.

Then, the number of topologically distinct phase portraits in $\overline{\mathbf{QsnSN}(\mathbf{C})}$ remains the same.

The reader may find the new version of Tables 50 to 79 from [Artés *et al.*, 2015] in a PDF file available at the link `http://mat.uab.es/~artes/articles/qvfsn2SN11B/sn2SN02.pdf`.

References

Artés, J.C., Dumortier, F., Herssens, C., Llibre, J. & de Maesschalck, P. [2005] "Computer program P4 to study phase portraits of planar polynomial differential equations," Available at: `http://mat.uab.es/~artes/p4/p4.htm`.

Artés, J.C., Kooij, R. & Llibre, J. [1998] "Structurally stable quadratic vector fields," *Memoires Amer. Math. Soc.* **134 (639)**, 108pp.

Artés, J.C., Llibre, J. & Rezende, A.C. [2018] "Structurally unstable quadratic vector fields of codimension one." 1. ed. *Birkhäuser*. v.1. 267pp.

Artés, J.C., Llibre, J. & Schlomiuk, D. [2006] "The geometry of quadratic differential systems with a weak focus of second order," *Internat. J. Bifur. Chaos Appl. Sci. Engrg.* **16**, 3127–3194.

Artés, J.C., Llibre, J., Schlomiuk, D. & Vulpe, N. [2013a] "Geometric configurations of singularities for quadratic differential systems with total finite multiplicity lower than 2," *Bul. Acad. Ştiinţe Repub. Mold. Mat.* **71**, 72–124.

Artés, J.C., Llibre, J., Schlomiuk, D. & Vulpe, N. [2021] "Geometric configurations of singularities of planar polynomial differential systems – A global classification in the quadratic case". 1. ed. *Birkhäuser Basel*. v.1. 701 pp.

Artés, J.C., Llibre, J., Schlomiuk, D. & Vulpe, N. [2020a] "Global topological configurations of singularities for the whole family of quadratic differential systems," *Qual. Theor. Dyn. Syst.* **19**, 32pp.

Artés, J.C., Llibre, J. & Vulpe, N. [2008] "Singular points of quadratic systems: a complete classification in the coefficient space $\mathbb{R}^{12}$," *Internat. J. Bifur. Chaos Appl. Sci. Engrg.* **18**, 313–362.

Artés, J.C., Mota, M.C. & Rezende, A.C. [2020b] "Quadratic differential systems with a finite saddle–node and an infinite saddle–node $(1,1)SN$ - (A)," *Internat. J. Bifur. Chaos Appl. Sci. Engrg.* **31**, 24pp.

Artés, J.C., Oliveira, R.D.S. & Rezende, A.C. [2020c] "Structurally unstable quadratic vector fields of codimension two: families possessing either a cusp point or two finite saddle–nodes," *J. Dyn. Diff. Equat.* , 43pp.

Artés, J.C., Rezende, A.C. & Oliveira, R.D.S. [2013b] "Global phase portraits of quadratic polynomial differential systems with a semi–elemental triple node," *Internat. J. Bifur. Chaos Appl. Sci. Engrg.* **23**, 21pp.

Artés, J.C., Rezende, A.C. & Oliveira, R.D.S. [2014] "The geometry of quadratic polynomial differential systems with a finite and an infinite saddle–node (A,B)," *Internat. J. Bifur. Chaos Appl. Sci. Engrg.* **24**, 30pp.

Artés, J.C., Rezende, A.C. & Oliveira, R.D.S. [2015] "The geometry of quadratic polynomial differential systems with a finite and an infinite saddle–node C," *Internat. J. Bifur. Chaos Appl. Sci. Engrg.* **25**, 111pp.

Bautin, N.N. [1954] "On periodic solutions of a system of differential equations," *Prikl. Mat. Meh.* **18**, 128.

Coll, B. & Llibre, J. [1988] "Limit cycles for a quadratic system with an invariant straight line

and some evolution of phase portraits," *Qualitative Theory of Differential Equations, Colloq. Math. Soc. János Bolyai, Bolyai Institut, Szeged, Hungria* **53**, 111–123.

Coppel, W.A. [1966] "A survey of quadratic systems," *J. Differential Equations* **2**, 293–304.

Dumortier, F., Llibre, J. & Artés, J.C. [2006] "Qualitative Theory of Planar Differential Systems," *Universitext, Springer–Verlag, New York–Berlin.*

Dumortier, F., Roussarie, R. & Rousseau, C. [1994] "Hilbert's 16th problem for quadratic vector fields," *J. Differential Equations* **110**, 66–133.

Jager, P. [1990] "Phase portraits for quadratics systems with a higher order singularity with two zero eigenvalues," *J. Diff. Eqns.* **87**, 169–204.

Li, C. [1986] "Non–existence of limit cycles around a weak focus of order three for any quadratic system," *Chinese Ann. Math. Series B* **7**, 174–190.

Schlomiuk, D. & Vulpe, N. [2004] "Planar quadratic vector fields with invariant lines of total multiplicity at least five," *Qualitative Theory of Dynamical Systems* **5**, 135–194.

Schlomiuk, D. & Vulpe, N. [2005] "Geometry of quadratic differential systems in the neighborhood of the infinity," *J. Differential Equations* **215**, 357–400.

Vulpe, N. [2011] "Characterization of the finite weak singularities of quadratic systems via invariant theory," *Nonlinear Anal.* **74**, 6553–6582.

Pingguang, Z. [2001] "Quadratic systems with a 3rd–order (or 2nd–order) weak focus," *Ann. Differential Equations* **17**, 287–294.